

MASTER

Glass panes stabilizing an in-plane loaded steel frame

annealed float and heat strengthened glass connected with an acrylic adhesive to a steel frame which is subjected to in-plane and indicative in- and out-of-plane loading

Bemelmans, M.H.J.

Award date:
2012

[Link to publication](#)

Disclaimer

This document contains a student thesis (bachelor's or master's), as authored by a student at Eindhoven University of Technology. Student theses are made available in the TU/e repository upon obtaining the required degree. The grade received is not published on the document as presented in the repository. The required complexity or quality of research of student theses may vary by program, and the required minimum study period may vary in duration.

General rights

Copyright and moral rights for the publications made accessible in the public portal are retained by the authors and/or other copyright owners and it is a condition of accessing publications that users recognise and abide by the legal requirements associated with these rights.

- Users may download and print one copy of any publication from the public portal for the purpose of private study or research.
- You may not further distribute the material or use it for any profit-making activity or commercial gain



structural design

E H U

Glass panes stabilizing an in-plane loaded steel frame

Annealed float and heat strengthened glass connected with an acrylic adhesive to a steel frame which is subjected to in-plane and indicative in- and out-of-plane loading

Marcel Bemelmans

A-2012.06

Master Thesis

Glass panes stabilizing an in-plane loaded steel frame

Annealed float and heat strengthened glass connected with an acrylic adhesive to a steel frame which is subjected to in-plane and indicative in- and out-of-plane loading

Author:

- M.H.J. Bemelmans -

Eindhoven University of Technology
Department of the Built Environment
Structural Design

Report
A-2012.06
O-2012.02

M.H.J. Bemelmans
Hoofdstraat 35A
6436 CB Amstenrade

Phone number: 06-25588811
Student number: 0655250
E-mailadress: m.h.j.bemelmans@student.tue.nl
Version: April 2012

Graduation committee:

Prof. Ir. H.H. Snijder (1st supervisor)
Dr. Ir. H. Hofmeyer (2nd supervisor)
Dr. Ir. E.M.P. Huveners (External expert)

Project Data

Educational institution: Eindhoven University Of Technology
Department of the Built Environment
Structural Design

Address: Den Dolech 2
5612 AZ Eindhoven
Postadres 513
5600 MB Eindhoven
The Netherlands

Telephone: +31-402479111

Project committee: Prof. ir. H.H. Snijder (1st supervisor)
Dr. ir. H. Hofmeyer (2nd supervisor)
Dr. ir. E.M.P. Huvener (External expert)

Name student: M.H.J. Bemelmans

Address: Hoofdstraat 35A
6436 CB Amstenrade
The Netherlands

Telephone: +31-625588811
E-mail: m.h.j.bemelmans@student.tue.nl
mhj.bemelmans@gmail.com

Acknowledgements

This master thesis is the product of one and a half year research on glass panes stabilizing an in-plane loaded steel frame. I would like to thank a few people who supported me along the development of this report.

I would like to express my gratitude to prof. ir. Bert Snijder and dr. ir. Herm Hofmeyer who supervised and supported this research. During the process they provided a lot of valuable advice and expertise. I enjoyed the constructive feedback and pleasant cooperation of my graduation period. I would like to thank dr. ir. Edwin Huvener of Volantis Maastricht for his guidance and support. His enthusiasm and knowledge about adhesive bonded glass structures encouraged and motivated me enormously.

Next I would like to thank the staff of the Pieter Van Musschenbroek laboratory of the Unit Structural Design, Department of the Built Environment. I am grateful to Hans Lamers who ensured materials and resources, Theo van der Loo and Toon van Alen who fabricated a lot of steel specimens needed for the experiments and Rien Canters who always had time to support me when necessary. In particular I would like to thank Martien Ceelen who taught me a lot about measuring, data acquisition and for being my help and stay during the experiments.

Further, I would like to express my gratitude to Victor Hofmans of Sika Netherlands in Utrecht and Joosten of Scheuten Glass Netherlands in Venlo for supplying the testing materials for this research.

I am very grateful to my parents, Léon Bemelmans and Mina Bemelmans-Melchers, who gave me a careless youth and the opportunity to develop my interests and ambitions. Finally I would like to thank my partner Jeanine Wrobel, for her understanding, support and pep talks during the master phase.

Marcel Bemelmans
Amstenrade, April 2012

Summary

Glass panes have the capacity to resist in-plane loads. This research is a continuation of the doctoral thesis of [Huvener 2009] on in-plane loaded glass panes. In the research in this master thesis, two types of glass were used, namely: annealed float glass and heat strengthened glass, which were adhesively bonded on both sides of the glass pane to a steel frame according to joint type 2. Joint type 2 was one of the three joint types investigated by [Huvener 2009], and had the best practical potency. The glass pane, the adhesive bonded joint and the steel frame together are called the system. Three experiments were carried out using annealed float glass and three experiments were carried out with heat strengthened glass, where the system was loaded by a gradual increase of the horizontal in-plane displacement at the right top corner of the system. Two indicative experiments were carried out where the system was loaded in- and out-of-plane, a situation which will occur if the stabilizing frame is placed in the façade of a building. The objectives of this research were finding a proper structural adhesive less stiff than epoxy and with the ability to account for material tolerances in the system, getting insight into the structural behavior where both annealed float glass and heat strengthened glass panes are applied, adjusting mechanical models which are able to describe the global behavior of the system and getting insight into the behavior of in- and out-of-plane loaded systems. The research methodology consisted of shear tests on adhesive bonded joints, full scale experiments on the system, finite element simulations of the system and adjust current mechanical models to predict the behavior of the system.

All experiments were carried out with glass panes with a nominal thickness of 12 mm. In-plane loaded systems based on joint type 2 with the acrylic adhesive have, compared to systems with the epoxy adhesive, a low in-plane stiffness and a moment of glass-steel contact at large horizontal in-plane displacements of the right top corner of the system. The large horizontal in-plane displacement after limited horizontal in-plane displacement and the increasing in-plane load give the system a good residual capacity before the moment of fracture. Moreover, at the moment of glass-steel contact annealed float glass panes failed almost immediately. Heat strengthened glass panes show more resistance at the moment of glass-steel contact. Systems which were loaded in-plane up to the serviceability limit state and then out-of-plane loaded up to glass failure show large capacity for out-of-plane loads. Both in-plane loaded systems and in- and out-of-plane loaded systems did not warn by visible and audible cracks before the glass panes of both types failed.

Simulations of the load-displacement diagram with the finite element model matched well with the results of the experiments up to the point where the adhesive bonded joints starts to fail. Sensitivity analyses showed that the position of the glass pane with reference to the centre of the system has a large influence on the moment of glass steel contact. The exceeding of the maximum principle (tension) stress in the right bottom corner of the glass pane showed not to be the failure mode of the system. First the adhesive bonded joint failed, followed by failure of the glass pane due to glass-steel contact.

Mechanical models are derived for predicting the global behavior of the system. The shear flexibility between the outside beam and the beadwork combined with the acrylic adhesive, in contrast with the epoxy adhesive, did not result in a complex stress distribution along the edges of the glass pane and in the adhesive bonded joint. Up to a horizontal in-plane displacement of 14 mm of the right top corner of the system, the mechanical model can be used to predict the global behavior of the system. After that point the behavior of the system is random, because of adhesive failure. The moment of glass-steel contact can still be predicted by the mechanical models.

In-plane loaded glass panes can be used in steel frames to substitute steel bracings in one storey buildings. Moreover, the applied acrylic adhesive behaves too weak and therefore a stiffer adhesive is recommended which has to result in failure of the glass pane in the right bottom corner of the system due to exceeding the maximum principle (tension) stress. This failure mode has to occur before the acrylic adhesive fails on cohesion, before glass-steel contact occurs and after the serviceability limit state has been exceeded and maintaining the adhesive bonded joint thickness of 3 mm to account for material tolerances. Exceeding the maximum principle (tension) stress attends with visible and audible cracks and the glass panes warn before failure of the system. Prior to practical application of the system, still a lot of research is needed. The adhesive has to withstand influences due to moisture, uv-light and temperature changes. Furthermore the influence on short term loading and unloading for a longer period has to be investigated.

Samenvatting

Glasplaten hebben capaciteit om weerstand te bieden tegen in het vlak belastingen. Dit onderzoek is een vervolgonderzoek op het promotieonderzoek naar belasting in het vlak van glasplaten [Huvener 2009]. In dit onderzoek is gebruik gemaakt van twee soorten glasplaten, namelijk: ongehard floatglas en thermisch versterkt glas, die volgens lijmnadtype twee aan beide zijden van de glasplaat op het stalen frame zijn verlijmd. Samen vormen de glasplaat, de lijmnad en het stalen frame het systeem. Drie proeven zijn uitgevoerd met floatglas en drie proeven zijn uitgevoerd met thermisch versterkt glas, waarbij het systeem in de rechter bovenhoek door een geleidelijke horizontale verplaatsing is belast. Daarnaast zijn twee indicatieve proeven uitgevoerd waarbij de glasplaat in het systeem zowel door een vlakbelasting als door een belasting loodrecht op het vlak is belast, een combinatie die kan optreden als het stabiliserende element in de façade geplaatst is. De doelstellingen van dit onderzoek zijn het vinden van een geschikte lijm die minder stijf is dan epoxy waarvan de toe te passen lijmdikte maattoleranties in het systeem kan opvangen, inzicht verkrijgen in het constructieve gedrag van het systeem waarbij beide glas typen zijn toegepast, het aanpassen van mechanicamodellen die het globale gedrag van het systeem kunnen beschrijven en inzicht verkrijgen in systemen die zowel in als uit het vlak zijn belast. Het onderzoek bestond uit afschuifproeven van lijmverbindingen, experimenten met het systeem, eindige elementen simulaties van het systeem en het aanpassen van bestaande mechanica modellen om het gedrag van het systeem te kunnen beschrijven.

Alle experimenten zijn uitgevoerd met glasplaten met een nominale dikte van 12 mm. Een horizontale in het vlak belasting op het systeem gebaseerd op lijmnadtype 2 met de acrylaat heeft in verhouding met epoxy een lage stijfheid in het vlak en een moment van glas-staal contact bij een grotere horizontale verplaatsing in het vlak aan de rechter bovenzijde van het systeem. De grote horizontale verplaatsing na de horizontale gelimiteerde in het vlak verplaatsing kan worden gezien als restcapaciteit. Echter, op het moment van glas-staal contact bezweken float glasplaten vrijwel direct. Thermisch versterkte glas platen lieten meer weerstand zien bij glas staal contact. Systemen waarbij de glasplaten die in het vlak belast zijn tot de bruikbaarheids grenstoestand van het systeem (de horizontale scheefstand) en uit het vlak zijn belast tot bezwijken, lieten zien een grote capaciteit te hebben voor uit het vlak belastingen. Zowel bij systemen die alleen in het vlak en systemen die in en uit het vlak zijn belast, waarschuwde de constructie niet door zichtbare scheuren of door middel van geluiden voordat het glas bij beide glas soorten bezweek.

Simulaties met het eindige elementen model kwamen goed overeen met de experimenten tot op het punt waar de lijm in de lijmnad cohesief begon te bezwijken. Gevoeligheidsanalyses toonden aan dat de positie van de glasplaat ten opzichte van het centrum van het systeem van grote invloed is op het moment van glas-staal contact. Een overschrijding van de hoofdtrekspanningen in de rechter onderhoek van de glasplaat bleek niet meer het bezwijkmechanisme te zijn van het systeem. Als eerste bezweek de lijm waarna de glasplaat bezweek door glas-staal contact.

De bestaande mechanicamodellen zijn aangepast en voorspellen het globale gedrag van het systeem. De niet-schuifvaste boutverbinding tussen de buitenste balk en het lijstwerk in combinatie met de acrylaatlijm leidde in tegenstelling tot de epoxy lijm niet tot een complexe spanningsverdeling in de randen van de glas plaat en in de lijmnad. Vanaf een horizontale verplaatsing in het vlak van 14 mm van de rechter bovenhoek is het mechanica model niet meer geldig om het globale gedrag van het systeem te voorspellen. Het gedrag van de experimenten reageren na dit punt random. Wel kan het moment van glas-staal contact bepaald worden.

Glazen platen als schorende elementen in stalen raamwerken kunnen stalen schoren vervangen in eenlaagse gebouwen. De toegepaste acrylaatlijm gedraagt zich echter te slap en daarom wordt er een lijm aanbevolen waarbij hoofdtrekspanningen in de rechter onderhoek van het glas in het systeem het bezwijken van de constructie inleiden. Dit bezwijkmechanisme moet optreden voordat de lijm bezwijkt, voordat glas staal contact optreedt en nadat de bruikbaarheids grenstoestand is overschreden met behoud van een lijmnad dikte van 3 mm om maattoleranties in de materialen te kunnen opvangen. Het overschrijden van de hoofdtrekspanningen zal gepaard gaan met het geleidelijk scheuren van het glas inclusief bijbehorende geluiden en waarschuwt dat de constructie gaat bezwijken. Voordat dit systeem in praktijk kan worden toegepast is er nog veel vervolgonderzoek nodig. De lijm moet bestand zijn tegen invloeden van weer en wind, waarbij gedacht moet worden aan vocht, uv-licht en temperatuursveranderingen. Daarnaast moet de invloed van een langdurig periode onderzocht worden, waarbij het systeem telkens kort wordt belast en ontlast.

Notations and abbreviations

Abbreviations

ANG	Annealed (Float) Glass
ADP	Acrylic Double Performance
FE	Finite Element
FTG	Fully tempered glass
HSG	Heat Strengthened Glass (Partly toughened glass)
LBC	Left Bottom Corner
LTC	Left Top Corner
LVDT	Linear Variable Displacement Transducer
MMA	Monomer Methyl Methacrylate
RBC	Right Bottom Corner
RTC	Right Top Corner

Notations

Latin capital letters

T_g	Glass transition temperature [$^{\circ}\text{C}$]
E_a	Young's modulus of the adhesive [N/mm^2] (section 5.3.2)
E_g	Young's modulus of glass [N/mm^2] (section 5.3.2)
E_s	Young's modulus of steel [N/mm^2] (section 5.3.2)
F_h	Horizontal in-plane load at the RTC of the system [kN]
$F_{h;1}$	Horizontal in-plane load at the RTC of the system at glass steel contact [kN]
$F_{h;LIM}$	Horizontal in-plane load at limited horizontal in-plane displacement of the RTC of the system [kN] (figures 4.9 and 4.15)
F_t	Tension force [kN] (equation 3.1)
F_w	Out-of-plane load (section 4.7 and 5.7.5)
G_a	Shear modulus of the adhesive [N/mm^2] (equation 3.5)
G_g	Shear modulus of glass [N/mm^2]
I	Moment of inertia [mm^4]
K_{1-4}	Discrete shear springs 1 to 4 in y-direction [kN/mm] (figure 6.6)
K_{7-10}	Discrete shear springs 7 to 10 in x-direction [kN/mm] (figure 6.6)
K_{5-6}	Discrete shear springs 5 and 6 in y-direction [kN/mm] (figure 6.6)
K_{11-12}	Discrete shear springs 11 and 12 in x-direction [kN/mm] (figure 6.6)
K_s	Horizontal in-plane stiffness of the system [kN/mm] (equation 4.2)
$K_{s;lim}$	Limited horizontal in-plane stiffness of the system [kN/mm] (table 6.1)
$K_{y;RBC}$	Vertical normal stiffness at the RBC of the system [kN/mm] (figure 6.1)
K_{φ}	In-plane rotation stiffness [kN/rad] (equation 7.10)

Latin lower case letters

$f_{mt;u;rep}$	Representative flexural tension strength [N/mm ²] (table 2.4)
h_g	Height of the glass pane [mm] (section 4.3.2)
h_{ob}	Height outside beam [mm] (section 4.3.1)
h_s	Height of the system [mm] (figure 4.2)
$k_{j;\eta}$	Shear stiffness of the adhesive bonded joint in longitudinal direction (section 5.3.2)
$k_{j;\zeta}$	Shear stiffness of the adhesive bonded joint in transversal direction (section 5.3.2)
$k_{b;\eta}$	Shear flexibility of the bolted connection between the outside beam and the beadwork [N/mm ³] (section 4.4.4.) (section 5.3.2)
$k_{b;\xi}$	Normal stiffness of the adhesive bonded joint [N/mm ³] (section 5.3.2)
$k_{j;\xi;ini}$	Initial normal stiffness of the adhesive bonded joint [N/mm ³]
n_g	Hardness according to Mohs's scale [Mohs] (section 5.3.2)
$t_{g;n}$	Nominal glass pane thickness [mm] (section 4.4.1)
$u_{j;\eta;rel}$	Relative horizontal in-plane displacement in longitudinal direction of the adhesive bonded joint [mm] (figure 6.2)
$u_{j;\zeta;rel}$	Relative horizontal in-plane displacement in transversal direction of the adhesive bonded joint [mm] (figure 6.2)
u_{LBC}	Horizontal in-plane displacement of the LBC [mm] (section 4.4.2)
$u_{MT;rel}$	Horizontal relative in-plane displacement in the middle of the top adhesive joint [mm] (section 4.4.2)
$u_{MB;rel}$	Horizontal relative in-plane displacement in the middle of the bottom adhesive joint [mm] (section 4.4.2)
u_{RBC}	Horizontal in-plane displacement of the RBC [mm] (section 4.4.2)
u_{RTC}	Horizontal in-plane displacement of the RTC [mm] (section 4.4.2)
$u_{RTC;lim}$	Limited horizontal in-plane displacement of the RTC [mm] (page 42)
$u_{RTC;s}$	Actual horizontal in-plane displacement of the RTC [mm] (equation 4.1)
$u_{RTC;t}$	Horizontal in-plane displacement of the RTC at glass-steel contact [mm] (section 6.2)
u_x	Translation variable of an element (section 5.2)
u_z	Translation variable of an element (section 5.2)
u_y	Translation variable of an element (section 5.2)
$v_{j;\eta;rel}$	Relative vertical in-plane displacement in longitudinal direction of the adhesive bonded joint [mm] (figure 6.2)
$v_{j;\zeta;rel}$	Relative vertical in-plane displacement in transversal direction of the adhesive bonded joint [mm] (figure 6.2)
v_{LBC}	Vertical in-plane displacement of the LBC [mm] (section 4.4.2)
v_{LTC}	Vertical in-plane displacement of the LTC [mm] (section 4.4.2)
$v_{ML;rel}$	Vertical relative in-plane displacement in the middle of the left adhesive joint [mm] (section 4.4.2)
$v_{MR;rel}$	Vertical relative in-plane displacement in the middle of the right adhesive joint [mm] (section 4.4.2)
v_{RBC}	Vertical in-plane displacement of the RBC [mm] (section 4.4.2)
v_{RTC}	Vertical in-plane displacement of the RTC [mm] (section 4.4.2)
w_{centre}	Out-of-plane displacement of the glass pane [mm] (section 4.4.2)
$w_{centre;cor}$	Corrected out-of-plane displacement of the glass pane [mm] (section 4.7 and 5.7.5)
w_g	Width of the glass pane [mm] (section 4.3.2)
w_{LTC}	Out-of-plane displacement of the LTC of the system [mm] (section 4.4.2)
w_{RTC}	Out-of-plane displacement of the RTC of the glass pane [mm] (section 4.4.2)
w_{ob}	Width outside beam [mm] (section 4.3.1)
w_s	Width of the system [mm] (figure 4.2)

Greek lower case letters

α_g	Thermal expansion coefficient [K^{-1}]
γ_{ave}	Average shear strain [rad] (equation 3.2)
Δl	Axial deformation (section 5.2)
ΔY	Shear deformation (section 5.2)
$\Delta \kappa$	Curvature (section 5.2)
$\Delta \phi$	Torsion (section 5.2)
ΔT	Difference in temperature [$^{\circ}C$]
ϵ_{xx}	Strain on the x plane along the x direction (section 5.2)
ϵ_{yy}	Strain on the y plane along the y direction (section 5.2)
ϵ_{zz}	Strain on the z plane along the z direction (section 5.2)
$\epsilon_{0^{\circ}}$	Horizontal strain (figure 4.11)
$\epsilon_{45^{\circ}}$	Strain at an angle of 45° (figure 4.11)
$\epsilon_{90^{\circ}}$	Vertical strain (figure 4.11)
ζ	Transversal direction
η	Longitudinal direction
Θ	Angle of the maximum principle stress to the horizontal [$^{\circ}C$]
μm	10^{-6} m
ξ	Normal directions
ρ_g	Density of glass [kg/m^3]
τ_{ave}	Average shear stress [N/mm^2] (equation 3.1)
$\tau_{j;\eta;x}$	Shear stress in longitudinal direction of the adhesive bonded joint in x-axis [N/mm^2] (figure 6.2)
$\tau_{j;\eta;y}$	Shear stress in longitudinal direction of the adhesive bonded joint in y-axis [N/mm^2] (figure 6.2)
$\tau_{j;\zeta;x}$	Shear stress in transversal direction of the adhesive bonded joint in x-axis [N/mm^2] (figure 6.2)
$\tau_{j;\zeta;y}$	Shear stress in transversal direction of the adhesive bonded joint in y-axis [N/mm^2] (figure 6.2)
σ_{xx}	Stress on the x plane along the x direction (section 5.2)
σ_{yy}	Stress on the y plane along the y direction (section 5.2)
σ_{zz}	Stress on the z plane along the z direction (section 5.2)
$\sigma_{g;1,max}$	Maximum principle stress in the glass pane [N/mm^2]
$\sigma_{g;2,min}$	Minimum principle stress in the glass pane [N/mm^2]
ν_g	Poisson's ratio of glass [-] (section 5.3.2)
ν_s	Poisson's ratio of steel [-] (section 5.3.2)
ϕ_x	Rotational degree of freedom (section 5.2)
ϕ_y	Rotational degree of freedom (section 5.2)
ϕ_z	Rotational degree of freedom (section 5.2)

Table of Contents

ACKNOWLEDGEMENTS.....	I
SUMMARY.....	III
SAMENVATTING	IV
NOTATIONS AND ABBREVIATIONS	V
1 INTRODUCTION	1
1.1 CIRCUMFERENTIALLY ADHESIVE BONDED GLASS PANES FOR BRACING STEEL FRAMES IN FAÇADES	1
1.2 PROBLEM DEFINITION	3
1.2.1 <i>Finding a proper structural adhesive</i>	3
1.2.2 <i>Different glass types</i>	5
1.2.3 <i>Loading mode</i>	5
1.3 RESEARCH OBJECTIVE.....	5
1.4 OUTLINE MASTER THESIS	6
2 LITERATURE REVIEW	7
2.1 GLUED CONNECTIONS	7
2.1.1 <i>What is bonding?</i>	7
2.1.2 <i>Strength of adhesives</i>	7
2.1.3 <i>Adhesion</i>	8
2.1.4 <i>Cohesion</i>	10
2.1.5 <i>Classification and structure of adhesives</i>	10
2.1.6 <i>Shear tests</i>	12
2.2 LITERATURE REVIEW ON GLASS	14
2.2.1 <i>Production of glass</i>	14
2.2.2 <i>Types of glass</i>	15
2.2.3 <i>Material properties</i>	17
2.3 LITERATURE REVIEW ON IN-PLANE LOADED GLASS.....	18
2.3.1 <i>German research: Nutzung der Verglasung zur Aussteifung von Gebäudehüllen</i>	18
2.3.2 <i>Glass panel under shear loading – use of glass envelopes in building stabilization</i>	19
2.3.3 <i>Buckling of flat laminated glass panels under in-plane compression or shear</i>	20
2.3.4 <i>Stability of glued and embedded glass panes: Dunkerley straight line as a conservative estimate of superimposed buckling coefficients</i>	21
3 EXPERIMENTS SHEAR STIFFNESS ACRYLIC ADHESIVE.....	22
3.1 PRELIMINARY RESEARCH: APPLIED ACRYLIC ADHESIVE	22
3.1.1 <i>Test methods and previous research</i>	23
3.1.2 <i>Specimens</i>	24
3.1.3 <i>Calculation</i>	26
3.1.4 <i>Average shear properties per batch</i>	28
3.1.5 <i>Discussion of the results</i>	30
3.1.6 <i>Conclusions</i>	31
3.2 COMPLEMENTARY SHEAR TESTS	32
3.2.1 <i>Specimens</i>	32
3.2.2 <i>Average shear properties</i>	33
3.2.3 <i>Conclusions</i>	34
4 EXPERIMENTS IN- AND INDICATIVE OUT-OF-PLANE LOADED GLASS.....	35

4.1	INTRODUCTION	35
4.2	TEST RIG	35
4.3	SYSTEM	36
4.3.1	<i>Steel frame</i>	36
4.3.2	<i>Glass pane</i>	37
4.3.3	<i>Adhesive bonded joint</i>	38
4.4	MEASUREMENTS	38
4.4.1	<i>Geometry of the glass pane</i>	38
4.4.2	<i>Response of the system</i>	39
4.4.3	<i>Boundary conditions of the supporting structures</i>	40
4.4.4	<i>Behavior of the bolted connection between the outside beam and the beadwork</i>	41
4.5	MEASUREMENTS BASICS.....	42
4.5.1	<i>In-plane stiffness of the system</i>	42
4.5.2	<i>Principle stresses</i>	42
4.6	RESULTS IN-PLANE LOADED GLASS	43
4.6.1	<i>Annealed float glass</i>	43
4.6.2	<i>Heat strengthened glass</i>	46
4.6.3	<i>Discussion of the results of in-plane loaded glass</i>	49
4.7	RESULTS IN- & OUT-OF-PLANE LOADED GLASS	52
4.7.1	<i>Annealed float glass</i>	53
4.7.2	<i>Heat strengthened glass</i>	55
4.7.3	<i>Discussion of the results of in-plane and out-of-plane loaded glass</i>	56
4.8	CONCLUSIONS.....	57
4.8.1	<i>In-plane loaded glass panes:</i>	57
4.8.2	<i>In- and out-of-plane loaded glass panes:</i>	57
5	FINITE ELEMENT ANALYSES.....	58
5.1	GEOMETRY.....	58
5.2	ELEMENTS.....	61
5.2.1	<i>Modeling the steel frame</i>	61
5.2.2	<i>Modeling the glass pane</i>	62
5.2.3	<i>Modeling the adhesive bonded joint</i>	63
5.2.4	<i>Vertical spring at the RBC of the frame</i>	64
5.2.5	<i>Overview elements</i>	65
5.3	MATERIAL INPUT	65
5.3.1	<i>Material input for interfaces</i>	65
5.3.2	<i>Linear and non-linear material behavior</i>	66
5.4	MESH DENSITY	67
5.5	GEOMETRICAL IMPERFECTIONS	68
5.6	SOLUTION STRATEGY	68
5.7	CALIBRATION	68
5.7.1	<i>Calibration of the global behavior of the system</i>	69
5.7.2	<i>In-plane loaded system with joint type 2</i>	70
5.7.3	<i>Sensitivity analyses</i>	73
5.7.4	<i>Distribution of longitudinal and transversal shear stresses in the adhesive bonded joint</i>	75
5.7.5	<i>In- & out-of-plane loaded system with joint type 2</i>	79
5.8	DISCUSSION OF THE RESULTS.....	80
5.9	CONCLUSION	82
5.9.1	<i>In-plane loaded glass panes:</i>	82
5.9.2	<i>In- and out-of-plane loaded glass panes:</i>	82

6	MECHANICAL MODELS	83
6.1	BASIC PRINCIPLES OF MECHANICAL MODELS	83
6.2	MECHANICAL MODELS AT GLASS STEEL CONTACT	91
6.3	MECHANICAL MODELS VERSUS FEM	92
6.4	DISCUSSION OF THE RESULTS	93
6.5	CONCLUSIONS	94
7	DISCUSSION	95
8	CONCLUSIONS	97
9	RECOMMENDATIONS	99
9.1	GLAZING	99
9.2	LOADING.....	99
9.3	ADHESIVES	99
	LITERATURE	100
	APPENDIX A DETERMINATION OF MECHANICAL PROPERTIES OF THE ADHESIVE	103
A.1	PREPARATION BONDED JOINT	103
A.2	STORING SPECIMENS	104
A.3	TESTING CONDITIONS	104
A.4	CODING SPECIMENS	104
A.5	OVERSIGHT SPECIMENS	105
A.6	MEASURING VALUES.....	106
A.7	RESULTS.....	107
A.8	GEOMETRY OF THE BONDED JOINT.....	114
A.9	SIKAFAST 5215 TECHNICAL DATASHEET.....	118
A.10	SIKA ADPREP TECHNICAL DATASHEET	120
A.11	PROPOSITION NEW SHEAR TESTS	122
	APPENDIX B SUPPLEMENTARY DATA FOR THE EXPERIMENT	123
B.1	DIMENSIONS OF THE STEEL FRAME	123
B.2	HIGH-SPEED CAMERA	127
B.3	ACTUAL GEOMETRY OF THE GLASS PANE	127
B.4	APPLICATION OF THE ADHESIVE AND PREPARATION OF THE EXPERIMENT	129
B.5	PRINCIPLES STRESSES IN THE GLASS PANE	131
	APPENDIX C EXAMPLE INPUT IDIANA	133

1 Introduction

1.1 Circumferentially adhesive bonded glass panes for bracing steel frames in façades

The ability of circumferentially adhesive bonded glass panes for bracing steel frames in façades has been investigated by e.g. [Huveners 2009]. Glass is used at a large scale in buildings and most of the time they are loaded out-of-plane. Few buildings are designed where glass is loaded in-plane. These buildings have been designed using laboratory research and experiences from previous projects. The problem is that no standards and guidelines are available for local authorities to check whether the glass structure fulfils the requirements.

No design rules are available in literature and standards for circumferentially adhesive bonded glass panes in steel frames acting as a vertical stability system for e.g. one-storey buildings. Strength and in-plane stiffness of vertical stability systems cannot be predicted.

Huveners divided a façade of a one-storey building into square hinged connected boxes (figure 1.1). Each box consists of steel transoms and mullions. The mullion and transom are respectively the vertical and horizontal frame members supporting the edges of the glass element. Boxes of stabilizing bays are provided with circumferentially adhesive bonded glass panes. One stabilizing box was isolated and used in the research project (figure 1.2).

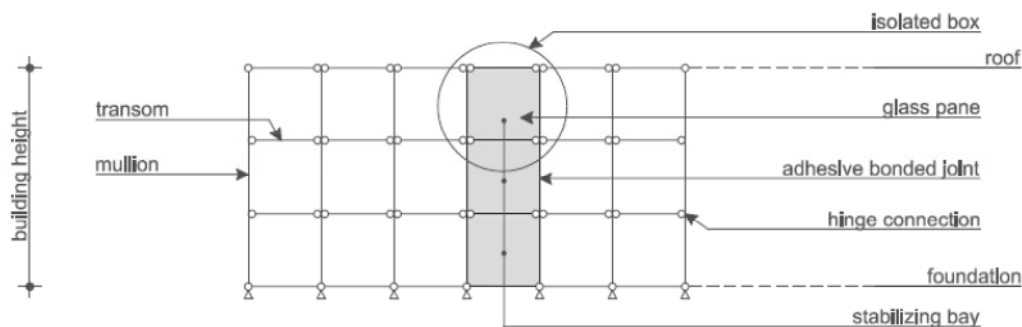


Figure 1.1 Vertical stability system of the building for transferring horizontal loads.

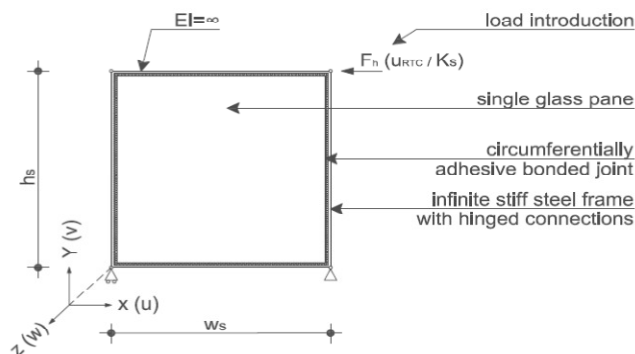


Figure 1.2 Isolated box from a stabilizing bay, called the system.

In figure 1.3, the system as presented in figure 1.2, is further specified. Square glass panes of annealed float glass, with sizes of 1.0 meter and a nominal glass pane thickness of 12 mm, were used and tested on three different joint types (figure 1.4). The mid-plane of the glass pane lines up with the centre of the beadwork and the outside beam. The displacement velocity of the right top corner, where the horizontal in-plane load is introduced, was 1 mm/min.

The objectives of the research of Huveners were:

- To get more insight into the structural behavior;
- To set-up mechanical models and possibly design rules for the prediction of the strength and the in-plane stiffness of the system.

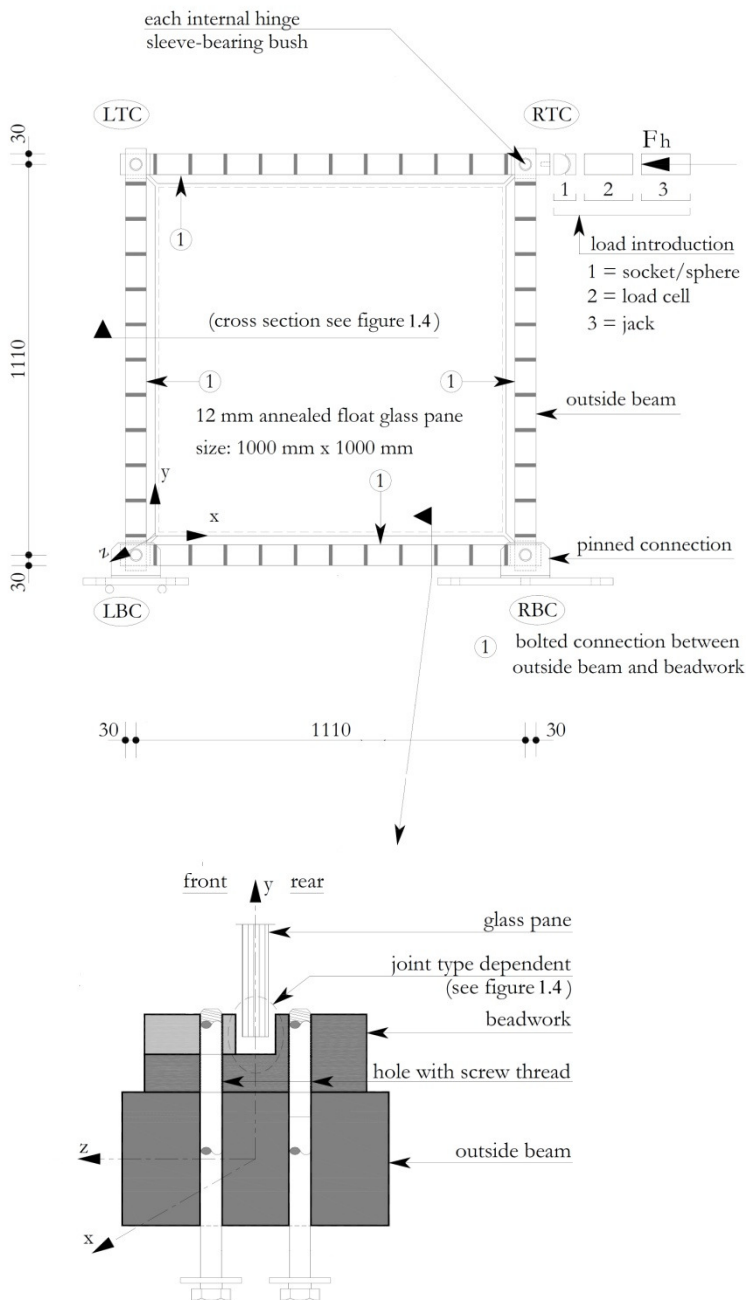


Figure 1.3 Specification of the system [Huvener 2009].

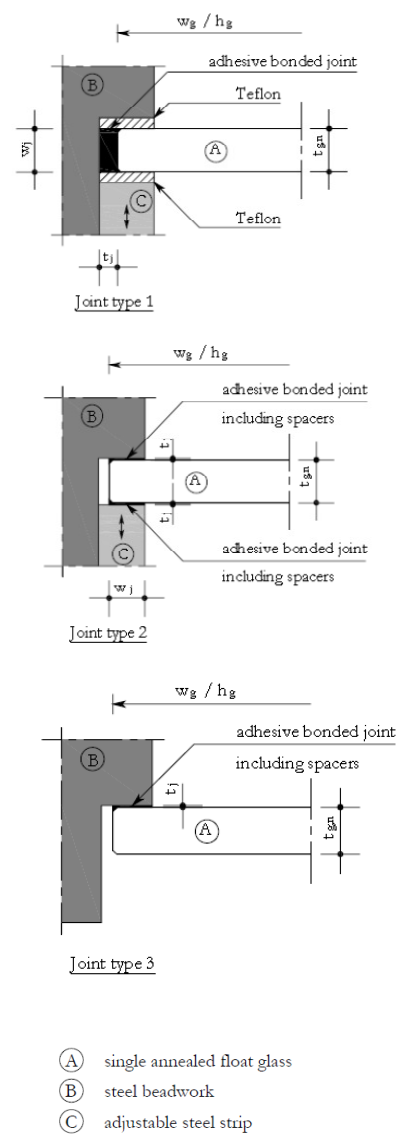


Figure 1.4 Joint types tested [Huvener 2009].

1.2 Problem definition

1.2.1 Finding a proper structural adhesive

In section 1.1 an introduction of the subject is given. Three different joint types were used but systems with joint type two, presented in figure 1.4, had the best in-plane stiffness and residual capacity. The in-plane load kept increasing after the first and following cracks appeared in the glass panes.

Figure 1.5 shows the relation between the horizontal in-plane load (F_h), the in-plane stiffness of the system (K_s), the largest maximum principle stress at the right bottom corner of the glass pane ($\sigma_{g;1;max}$) and varying shear stiffness of the adhesive bonded joint for a horizontal in-plane displacement (u_{RTC}) at the right top corner of the system of 1.02 mm. At a horizontal in-plane displacement (u_{RTC}) of 1.02 mm of the RTC of the system, the first cracks in the RBC of the glass pane occur in experiments for systems with joint type 2. The varying shear stiffness of the adhesive bonded joint was assumed by [Huveners 2009] because there was no other adhesive available with different stiffness's to compare the behavior of the system with. The varying shear stiffness is obtained by adjusting the relation between the average shear stress and the average relative in-plane displacement of the adhesive bonded joint, where the relative in-plane displacements kept the same values as in the point of origin.

The values in figure 1.5 are adopted from finite element simulations. The vertical green dashed line represents the shear stiffness of the epoxy joint applied by Huveners and the horizontal dashed green lines represent the matching horizontal in-plane load, in-plane stiffness and the largest maximum principle stresses at the right bottom corner of the glass pane.

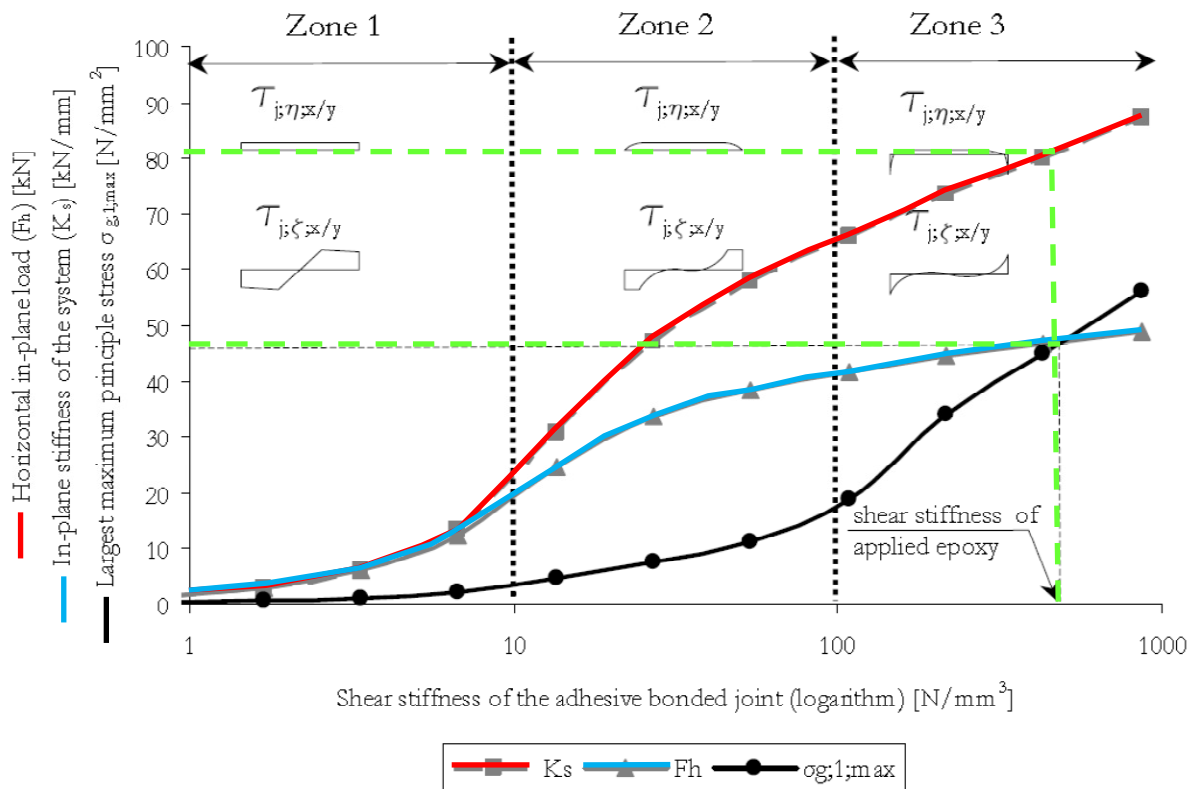


Figure 1.5 Relations between the horizontal in-plane load (F_h), the in-plane stiffness of the system (K_s), the largest maximum principle stress at the right bottom corner of the glass pane ($\sigma_{g;1;max}$) and varying shear stiffness of the adhesive bonded joint [Huveners 2009].

In zone 1 in figure 1.5, a small stiffness of the adhesive bonded joint results in a small horizontal in-plane stiffness and in a small maximum principle stress. The distribution of the shear stresses in the adhesive bonded joint in longitudinal direction ($T_{j;\eta;x/y}$) is uniform and the distribution in transversal direction ($T_{j;\zeta;x/y}$) corresponds to the multi-linear graph in figure 1.6, where the non-linear relation between the average shear stresses and the average relative in-plane displacements for epoxy is presented.

In zone 2 the shear stiffness of the adhesive bonded joint lies between 10 and 100 N/mm³. The in-plane stiffness increases and the maximum principle stress in the right bottom corner of the glass pane increases a little bit. The distribution of the shear stresses in the adhesive bonded joint in longitudinal direction ($T_{j;\eta;x/y}$) is uniform and decreases to zero at the ends of the adhesive bonded joint. The distribution in transversal direction ($T_{j;\zeta;x/y}$) is uniform at the ends and fluctuates around zero at the middle of the adhesive bonded joint. According to [Huvener 2009] the difference in the shear distribution is caused by bending of the steel frame.

In zone 3 the shear stiffness of the adhesive bonded joint is between 100 and 1000 N/mm³. In this zone the stiffness of the system still increases. Striking is the increase of the maximum principle (tensile) stresses in the right bottom corner of the glass pane. The distribution of the shear stresses in the adhesive bonded joint in longitudinal direction ($T_{j;\eta;x/y}$) is uniform except at the vicinity of the ends, where the shear stresses decrease to zero, switch sign, and rapidly increase. The distribution in transversal direction ($T_{j;\zeta;x/y}$) fluctuates around zero except at the ends of the adhesive bonded joint. At the vicinity of the ends, the shear stresses in transversal direction increase to a maximum. Here, the irregular stress distribution in the adhesive bonded joint introduces peak stresses in the RBC of the glass pane which causes the glass pane to crack. At this point the ultimate flexural tension strength of the glass pane has been exceeded. According to [Huvener 2009], the rapidly increasing shear stresses at the vicinity of the ends of the adhesive bonded joint are caused by the small shear flexibility of the bolted connection between the outside beam and the beadwork (figure 1.7). This results in an unfavorable distribution of the principle stresses in the right bottom corner of the glass pane.

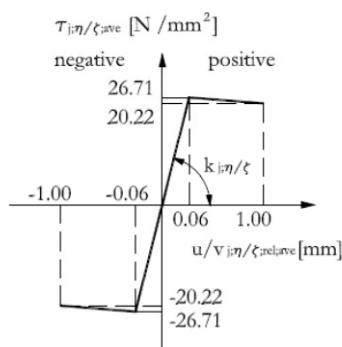


Figure 1.6 Non-linear relation between the average shear stresses and the average relative in-plane displacements for epoxy [Huvener 2009].

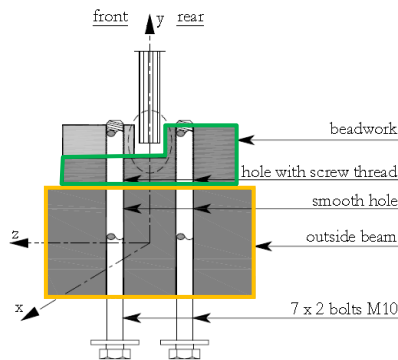


Figure 1.7 Shear flexibility of the bolted connection between the outside beam (orange) and the beadwork (green) [Huvener 2009].

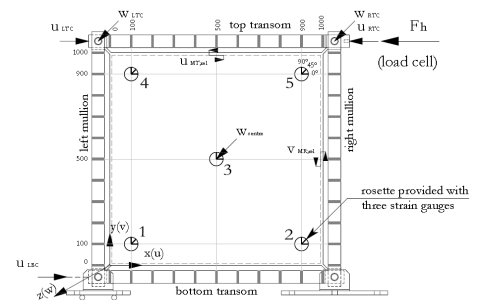


Figure 1.8 Unfavorable distribution of the principle stresses in the right Bottom corner (purple circle) [Huvener 2009].

The applied Epoxy is a very stiff adhesive and due to the small shear flexibility of the bolted connection between the outside beam and the beadwork (figure 1.7), an unfavorable distribution of the principle stresses occurred in the right bottom corner of the glass pane (figure 1.8). By using an adhesive with a shear stiffness corresponding to zone 2, peak stresses in the right corner of the glass pane will most likely not occur. Most likely, the point where the first cracks in the glass pane appear will be postponed and the capacity of the system will increase.

Besides the shear stiffness of the adhesive bonded joint, also the tolerances of the glass pane and the steel frame have to be taken into account. The epoxy Huvener applied, had a bonded joint thickness of 0.5 mm. There was no room to take care of tolerances necessary for the steel frame and the glass pane.

Finding a proper structural adhesive, less stiff and thicker than the epoxy was recommended by [Huvener 2009], and is necessary to eliminate the unfavorable peak stresses and account for tolerances of the applied materials.

1.2.2 Different glass types

Just like annealed float glass, heat-strengthened glass has a favorable crack pattern needed for the residual capacity after breakage. This means that after the first crack in the glass pane appeared, the pane still can resist in-plane loads. Heat-strengthened glass is originated from a follow-up treatment of normal float glass. The purpose of this follow-up treatment is to introduce compression stresses in the glass faces to suppress the surface flaws. This increases the representative flexural tension strength ($f_{mt,u,rep}$) of the glass and the resistance against change of temperature (figure 1.9). By choosing this glass type, the capacity of the system will become larger and a comparison with annealed float glass, used by Huveners, can be made.

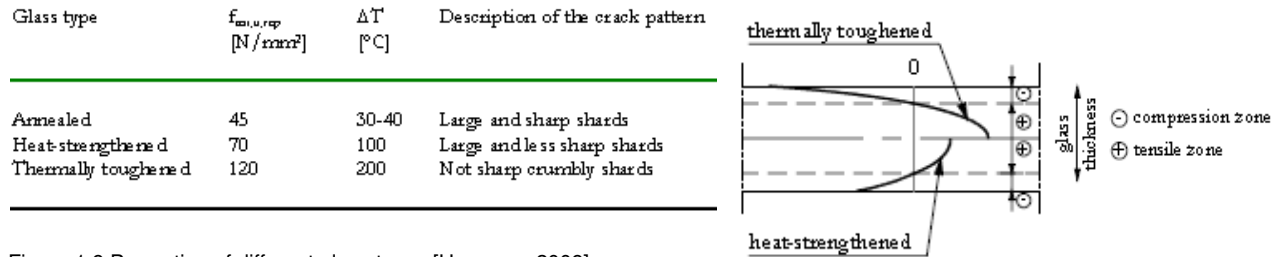


Figure 1.9 Properties of different glass types [Huveners 2009].

1.2.3 Loading mode

Stability elements are often placed as far as possible to the side of a building to prevent rotation (figure 1.10). The wind load (red) at the right side of the building will be collected by the stability elements in the length direction of the building. Due to this wind load, wind suction on the left, the front, and the rear façade of the building occurs. Besides an in-plane load, glass panes in façades used as a stability element will also be exposed to an out-of-plane load (figures 1.10 and 1.11). The interaction between the out-of-plane load and the in-plane load will affect the capacity of the stabilizing element and the residual capacity after breakage.

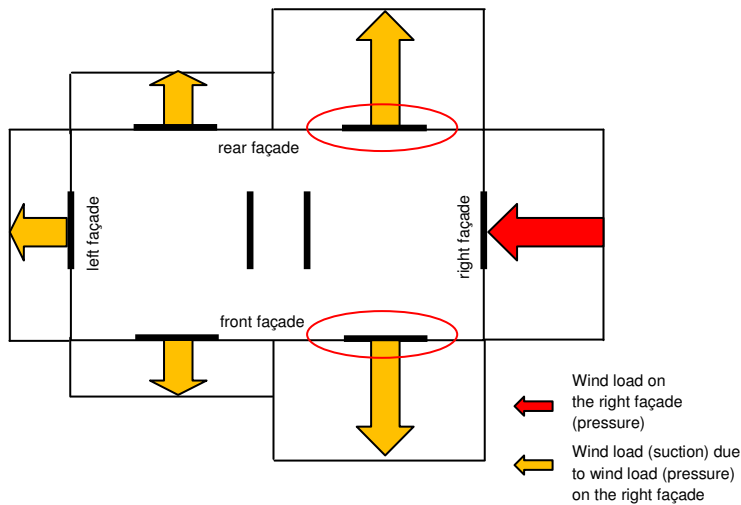


Figure 1.10 Example floor plan of in-plane and out-of-plane loaded stability elements in buildings adapted from [NEN 6702:2007].

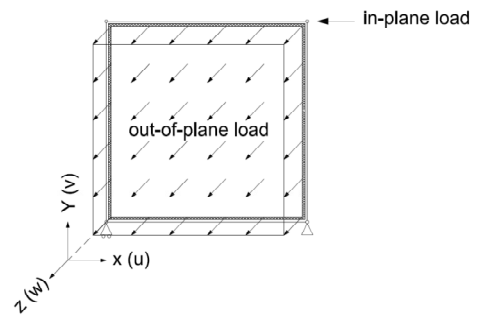


Figure 1.11 In-plane and out of plane loaded glass pane.

1.3 Research objective

It can be concluded that both the adhesive and the glass type may influence the behavior of the system. The research objective can now be phrased:

The objectives of this research are:

- finding a proper structural adhesive and getting insight into the in-plane structural behavior using both annealed float glass and heat strengthened glass;
- adjusting current mechanical models and predicting the strength and in-plane stiffness of circumferentially adhesive bonded glass panes;
- getting indicative insight into the behavior of in- and out-of-plane loaded glass panes.

1.4 Outline master thesis

Figure 1.12 presents the outline of this master thesis. In this section, chapters 2 to 9 are summarized.

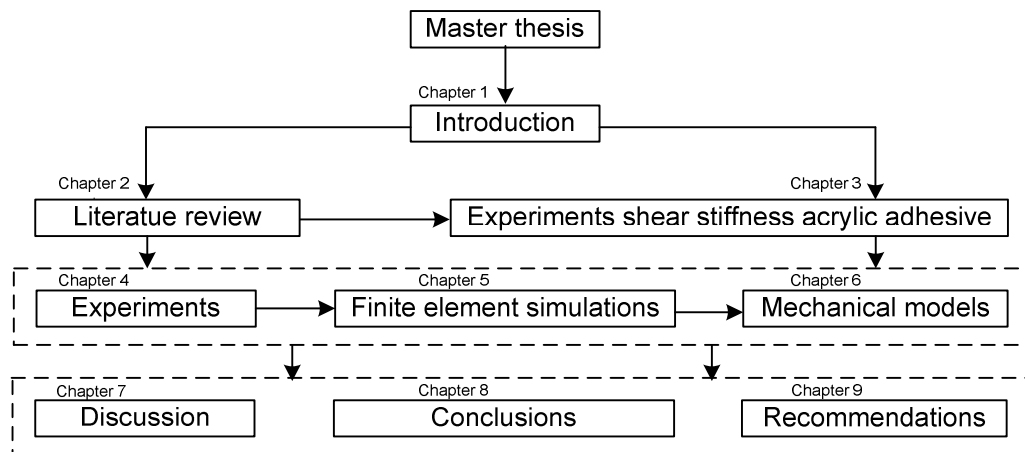


Figure 1.12 Outline of the master thesis.

Chapter 2, Literature review

Chapter 2 presents a literature review on glued connections, glass and in-plane loaded glass. In section 2.1 glued connections, basics of adhesives and how the strength of adhesives is influenced are discussed. Section 2.2 information about the production of glass and types of glass are presented. Also mechanical and chemical properties of glass are given. Section 2.3 gives an overview of glass used as a structural material and reviews relevant research projects of in-plane loaded glass structures.

Chapter 3, Experiments shear stiffness acrylic adhesive

In chapter 3 the shear properties of the chosen acrylic adhesive are determined which are needed to simulate the experiments on in-plane loaded glass panes in a FE model.

Chapter 4, Experiments in- and out-of-plane loaded glass

Before the behavior of the system is discussed, the experimental test set-up, supplementary data like the actual geometry of the glass panes, the specification of the steel frame, the application of the adhesive, the conditions of the laboratory and the measurement equipment to be used during the experiments are reviewed.

Chapter 5, Finite element analyses

In chapter 5, the finite element model is used to predict the behavior of the system. Several sensitivity studies are carried out. The moment of failure of the glass pane (glass steel contact), and the influence of the shear stiffness of the adhesive bonded joint are investigated.

Chapter 6, Mechanical models

The behavior of the experiments is well predicted by the finite element model. The mechanical models determined by [Huveners 2009] are adjusted and can be used as a simple tool to predict the in-plane stiffness, the in-plane load, the relative in-plane displacements in longitudinal direction of the adhesive bonded joint and the moment of glass-steel contact of the system.

Chapter 7, Discussion

Chapter 7 gives an overall discussion of the experiments, finite element simulations and mechanical models.

Chapter 8, Conclusions

In chapter 8 the overall conclusions of the experiments, finite element simulations and mechanical models are given.

Chapter 9, Recommendations

Finally, in chapter 9 recommendations for further research on in-plane loaded glass panes are given.

2 Literature review

2.1 Glued connections

Adhesives provide new possibilities for structural connections (i.e. glass-to-glass or glass to another material) and may offer a solution for the two main disadvantages of mechanical connections discussed by [Weller and Tashe 2008]: the undesired visual impact of the mechanical fixings and the stress concentrations that occur due to the introduction of loads at discrete locations. Furthermore, glued connections have the opportunity to distribute loads in an uniform manner, which is an advantage in glass connections. Glass is a brittle material and very sensitive for stress concentrations.

Most engineers are relatively unfamiliar with adhesive technology and terminology. This section describes general principles of adhesive bonding.

2.1.1 What is bonding?

Bonding is a joining technique just like welding, bolting, soldering, and so on. Bonding can be described as the joining of two substrates using an adhesive [FEICA 2004]. According to [DIN EN 923] an adhesive is defined as:

- a non-metal;
- a binder that acts via adhesion and cohesion.

2.1.2 Strength of adhesives

An adhesive bonded joint consists of an adhesive and two different or similar types of material. The strength of the bonded joint is affected by two factors:

- Cohesion is the inner strength of a material, such as the adhesive in this case;
- Adhesion is the strength of the adherent to fasten the mating surfaces.

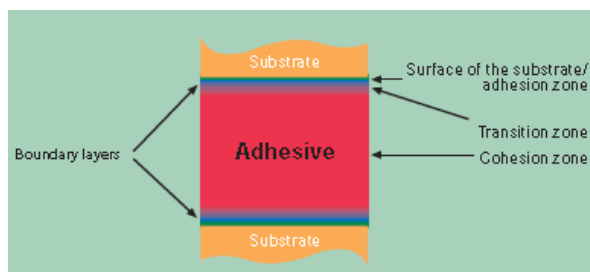


Figure 2.1 Cross section of a bond [FEICA 2004].

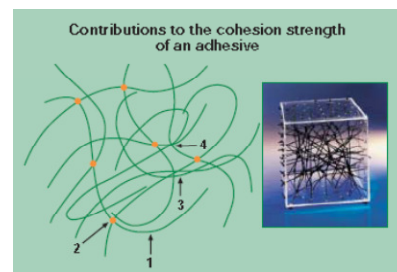


Figure 2.2 Contribution to the cohesion strength of an adhesive [FEICA 2004].

Besides choosing a proper adhesive, it is important that the adhesive is properly attached to the mating surfaces. Figure 2.1 shows that the interaction between the substrate and the adhesive do not only concern the actual area of contact (adhesion zone) of the adhesive and the substrate, but also the state of the surface of the substrate (transition zone) [FEICA 2004].

Adhesion zone

In this zone, the adhesive has a modified structure and composition due to its adhesion to the surface of the substrate. Adhesion consists of weak interactions between molecules of the substrate surface and the adhesive and strong chemical bonds. Long term stability of these bonds depends directly on their resistance against moisture and temperature.

Transition zone

In this zone, which varies in thickness between a few nanometers up to mm range, chemical, mechanical and optical properties are altered. The thickness depends on the nature of the adhesive, the substrate structure and the curing conditions.

Cohesive zone

The properties of non-cured adhesives, like the viscosity, are determined by the molecular forces in the adhesive zone (figure 2.2):

1. The chemical bonds within the adhesive polymers;
2. The chemical bonds resulting from cross-linking of the polymer;
3. The intermolecular interactions between the molecules in the adhesive;
4. The mechanical adhesion between various molecules in the adhesive.

To end paragraph 2.1.2 it can be mentioned that both adhesion, including the transition zone, and cohesion determine the strength of a bonded joint. Just like a chain, the weakest link in the bonded joint determines the ultimate strength [FEICA 2004]. Cohesive failure means that the inner strength of the adhesive has been exceeded and that the maximum load of a bonded joint has been reached i.e., the fracture is in the adhesive, and not in the adhesion zone between the substrate and the adhesive.

2.1.3 Adhesion

Adhesion has been studied for years and several theories have been proposed to provide an explanation for adhesion phenomena but none of them actually do in general. The bonding of an adhesive to an object or a surface is the sum of a number of mechanical, physical and chemical forces that overlap and influence one another [Kaasschieter et al. 2008]. Figure 2.3 shows the adhesion theory by [Brockmann et al. 2009] and is briefly explained in this section.

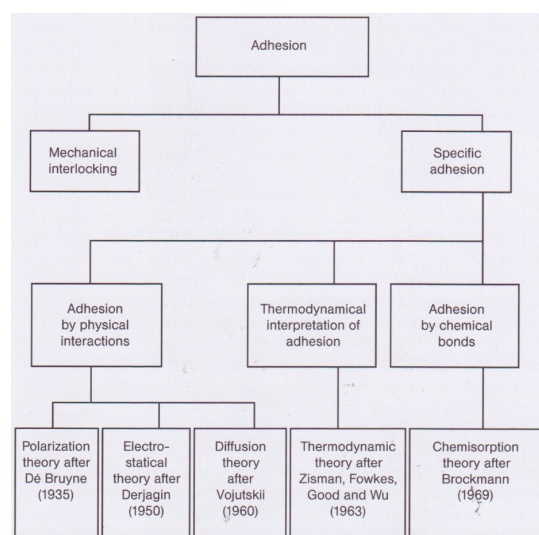


Figure 2.3 Adhesion theory [Brockmann et al. 2009]

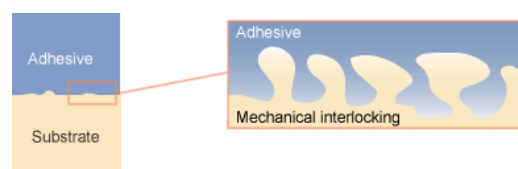


Figure 2.4 Mechanical interlocking [Specialchem 2010]

2.1.3.1 Mechanical Interlocking theory

Mechanical interlocking theory, also called 'mechanical theory' is the oldest and most dominant mechanism of adhesion between two materials according to [Fisher 2005]. When an adhesive penetrates into pores, holes, cracks and other irregularities of the adherent surface of a substrate, it locks mechanically to the substrate. According to [specialchem 2010] besides wetting the substrate, which is explained in paragraph 2.1.3.3., it has to have the right rheological¹ properties to penetrate pores and openings in a reasonable time. Higher viscosity improves the mechanical interlocking and the wettability.

Pretreatment methods applied on surfaces enhance adhesion. These pretreatments, especially plastic surface treatments, result in micro roughness on the adherent surface, which can improve bond strength and durability by providing mechanical interlocking. Generally this is only applicable to wood, paper and porous, swellable substances. Today it is well known that mechanical interlocking has no significance in the bonding of the majority of nonporous, technically used materials.

¹ Rheology is a part of science which investigates physical flow properties of materials. Rheology describes the relation of imposed forces executed on a material and the developed deformation or flow. Viscosity is the best known property of the rheology section and is a physical material property. Viscosity is a measurement of the resistance of a fluid which is being deformed by either shear stress or tensile stress.

2.1.3.2 Specific adhesion by adsorption

According to [Fisher 2005], the ability of a substrate and adhesive to come into intimate intermolecular contact is crucial to the success of an adhesive bond. The principle of wetting (section 2.1.3.3.) describes intermolecular contact. This intermolecular contact involves surface forces that develop between the atoms in the two surfaces. Adsorption is the adhesion or attachment of molecules to a surface. The molecules which are accumulating on the surface are collectively called as adsorbate and the surface on which these molecules are accumulated is called adsorbent. Adsorption can be classified as a surface phenomenon. The adsorption can be based on mainly two types, namely physical adsorption (physisorption) or chemical adsorption (chemisorptions). Figure 2.3 shows that there is also a thermodynamical interpretation of adhesion.

Physical adsorption

The physical adsorption (physisorption) is without any change in the chemical structure of the adsorbent and adsorbate. Physical adsorption is a phenomena which takes purely due the Van der Waals forces of attraction and is a reversible phenomena.

Chemical adsorption

Chemical adsorption is also called chemisorption. Here the surface layer molecules undergo chemical change after interaction with the adsorbate molecules. This irreversible process will improve the bonding strength in adhesives due to the chemical bonds (ionic, covalent and metallic).

Further information about bonding forces within adhesives is given in [Habernicht 2006], [Brockmann et al. 2009] and [Fisher 2005].

2.1.3.3 Principle of wetting

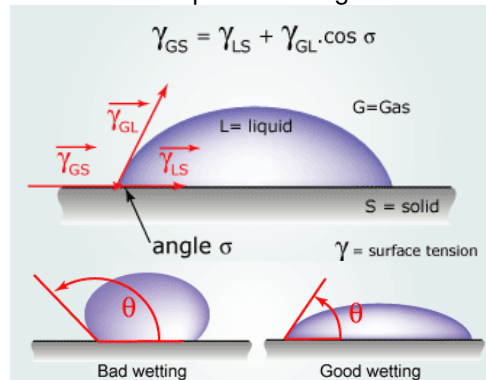


Figure 2.5 Angle of contact of a drop of liquid with the surface of a solid object. [Specialchem 2010]

Table 2.1. Properties of wettability.

Contact angle	Degree of wetting	Strength of:	
		Sol./Liq. interactions	Liq./Liq. interactions
$\theta = 0$	Perfect wetting	strong	weak
$0 < \theta < 90^\circ$	High wettability	strong	strong
$90^\circ \leq \theta < 180^\circ$	low wettability	weak	strong
$\theta = 180^\circ$	Perfectly non-wetting	weak	strong

The degree of wetting (wettability) is determined by a force balance between adhesive and cohesive forces (surface tension). Adhesive forces between a liquid and solid cause a liquid drop to spread across the surface. Cohesive forces within the liquid cause the drop to ball up and avoid contact with the surface. Regardless on the amount of wetting, the shape of a liquid drop on a rigid surface is roughly a truncated sphere. Table 2.1 shows at which contact angle, what the degree of wetting is and the strengths of the solid/liquid interactions and liquid/liquid interactions. See also figures 2.6 till 2.9.

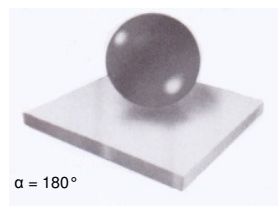


Figure 2.6 No Wetting [Brockmann et al. 2009]

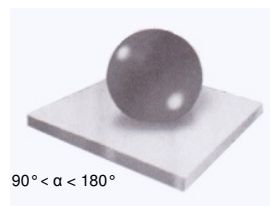


Figure 2.7 Minimal wetting [Brockmann et al. 2009]

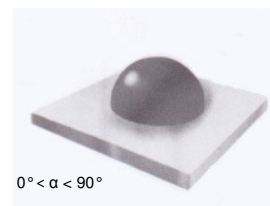


Figure 2.8 Medium wetting [Brockmann et al. 2009]

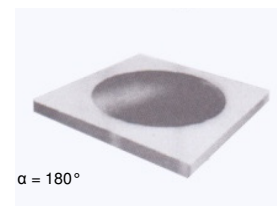


Figure 2.9 Good wetting [Brockmann et al. 2009]

2.1.4 Cohesion

Cohesion is based on molecular- and atomic forces within the adhesive. A good cohesion within the adhesive has to be developed after wetting occurs. In other words, the adhesive has to stitch to the substrate surface and is then allowed to cure. During the curing process it is important that internal stresses, due to shrink phenomena, appear as little as possible. The final joint strength will be influenced in a negative way if internal stresses are too high. Shrink phenomena occur due to curing of the adhesive (chemical contraction), evaporation of volatile adhesive components and due to differences in the coefficient of thermal expansion of the adhesive and the substrate.

2.1.5 Classification and structure of adhesives

According to [Habernicht 2006] classification of adhesives can be made on their chemical basis and by their curing mechanism. Figure 2.10 presents the classification on their chemical basis where the adhesives are split in organic and inorganic connections. The organic adhesive bonding can be divided on natural or synthetic basis. A few clear differences show a distinct division:

- The different ageing time resistances and bond strengths concerning synthetic adhesives in the organic bonding group have obvious higher values;
- The application and usage temperatures. Adhesive bonding on organic basis are in comparison to inorganic bonded adhesives applied with lower temperatures and have therefore also a lower thermal resistance.

Silicones have organic and inorganic bonding characteristics.

Besides classifying adhesives on their chemical basis (figure 2.10), adhesives can also be classified on their curing mechanism. Figure 2.11 gives an overview of the curing mechanisms.

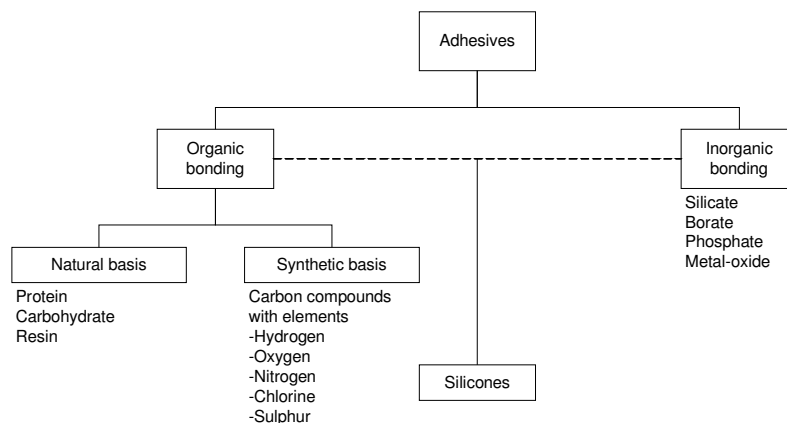


Figure 2.10 Classification of adhesives on chemical basis

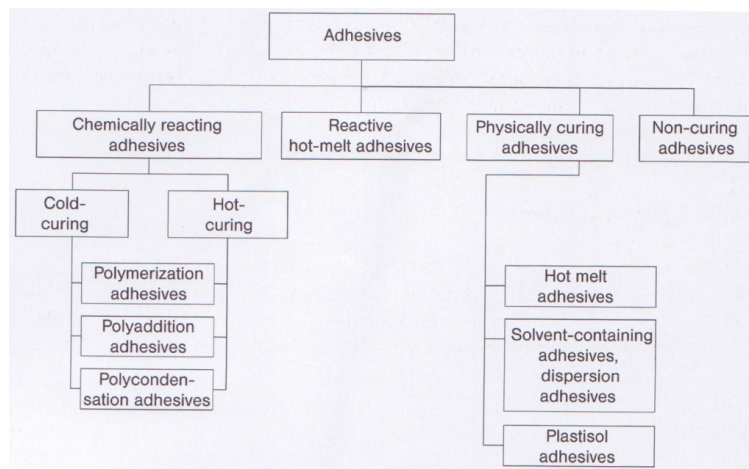


Figure 2.11 Curing mechanism of adhesives.

Adhesives are polymer materials that consist of simple monomer units recurrently chained to macromolecules. The macromolecules are physically or chemically bonded to each other and intertwining is inevitable [Haldimann et al. 2008]. Polymers can be classified according to their thermo-mechanical properties that are controlled by the molecular structure (figures 2.12 and 2.13).

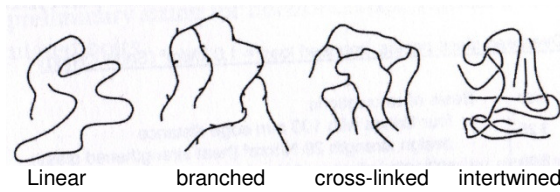


Figure 2.12 Molecular structure of polymers [Haldimann et al. 2008].

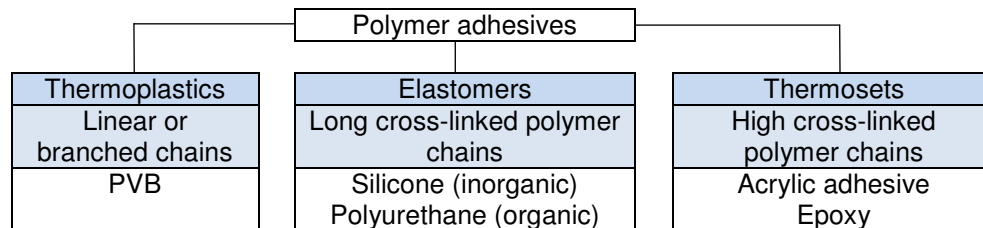


Figure 2.13 Classification of polymer adhesives.

Thermoplastics

Relatively weak intermolecular forces hold molecules together in a thermoplastic. When thermoplastics are heated the material softens, but when it is cooled it return to its original shape. Similar to metals, thermoplastic polymers can be repeatedly softened by heating and then solidified by cooling. Most linear and slightly branched polymers (figure 2.13) are thermoplastics and all the major thermoplastics are produced by chain polymerization.

Elastomers

Rubbery polymers can easily be stretched to several times of their own un-stretched length. When the applied stress is removed, the elastomer polymer rapidly returns back to its original shape. Elastomers are cross-linked (figure 2.13). Due to the low cross-link density, the polymer chains have still some freedom to move, but permanently movement relative to each other is not possible.

Thermosets

A thermosetting plastic, also known as a thermoset, is a polymer material that irreversible cures. Heating solidifies the polymers and further heating cannot reshape the material. Thermosets consist of three dimensional networked polymers with a high degree of cross-linking (figure 2.13) between polymer chains. The high density of the cross-links restricts the movement of the chains and leads to a rigid material.

2.1.6 Shear tests

A lot of adhesively bonded connections transmit loads through shear in the adhesive. Different codes can be used to determine the shear strength of an adhesive bonded joint. This section describes the (dis)advantages if specimens are made according to the [DIN 54 451:1978], the [NEN-EN 14869-2:2004] and the [ASTM D1002].

Specimens which are made according to the [DIN 54 451:1978] are cut from adhesively composed sheets (figure 2.14). According to [Kadioglu et al. 2002] bonding of two plates introduces a number of uncertainties into the specimen:

- The machining work needs to be done without coolant (to avoid any reactions with the adhesive), and the localized increase in temperature, that machining introduces, may affect the adhesive properties.
- The edge of the bonded joint is damaged when the slots are cut, or when a bar is cut from a sheet (figure 2.14).
- Irregular bar stock surfaces can lead to uncertain bonded joint thicknesses. The surface of bar stock is often bowed, such that the thickness of the bar is less at the edges than at the middle. This affects the measurement of the bonded joint thickness and in turn the calculation of the shear strain in the adhesive and it may also affect the mode of failure of the specimen.
- Test specimens cannot be reused. For testing in an industrial environment, the reuse of adherents plays an important part in the test procedure, especially if their manufacture is labor intensive and costly.

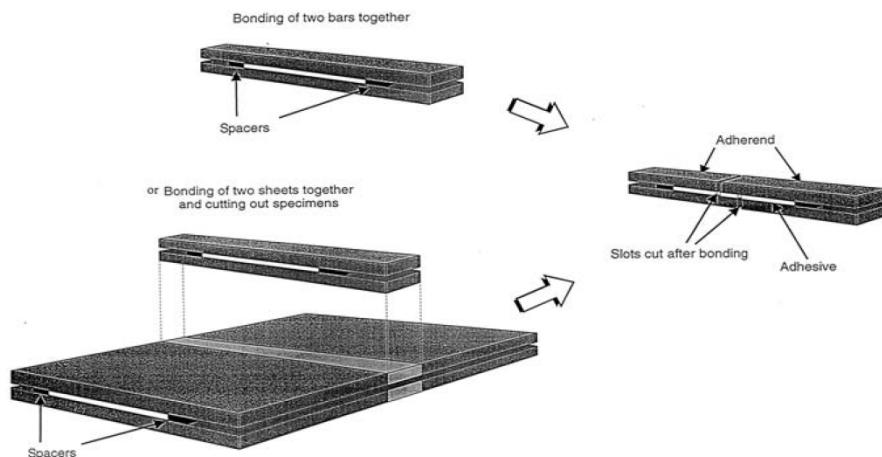


Figure 2.14 Specimen manufacture using bonded sheets [Kadioglu et al. 2002].

The alternative method to avoid all these uncertainties is to use two pre-shaped bonded bars like the [NEN-EN 14869-2:2004] and the research of [Huvener and Koggel 2006].

Through the years different researchers used either aluminum or steel for the adherents of test specimens. According to [Chiu and Jones 1992] pure shear in the adhesive layer can only be obtained if adherents with the highest stiffness are used. Therefore, steel is favored over aluminum as its elastic modulus is three times higher. Due to the higher elasticity modulus of the adherent, the stress variations in the overlap are reduced. [Chui and Jones 1992] showed this by using both aluminum and steel adherent materials for thick adherents shear test (TAST) joints. Shear tests carried out with aluminum specimens failed at a lower shear stress than steel specimens.

Beside the material, also the geometry of the adherents plays an important part in the behavior of the test results. A short overlap length and large thickness of the adherent reduces undesirable peel effects (figure 2.16) at the ends of the joint, when compared with a typical shear-lap specimen [Kadioglu et al. 2002], such as specified in [ASTM D1002] (figure 2.15). Due to the geometry of the specimen in figure 2.15, the application of the load is eccentric and the adherents rotate as a result of a bending moment. This rotation introduces adhesive peel stress in the vicinity of the joint edges [Brockmann et al. 2009]. The introduction of peel stresses decreases the capacity of the bonded joint, because it is not loaded in pure shear. The true shear strength of an adhesive can only be determined if normal stresses are entirely absent and therefore the best way to approach the true shear strength is to follow the code used in this research, [NEN-EN 14869-2:2004].

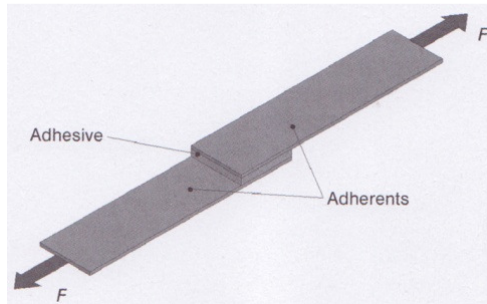


Figure 2.15 Shear lap specimen according to [ASTM D1002], sensitive to peel effects [Brockmann et al. 2009]

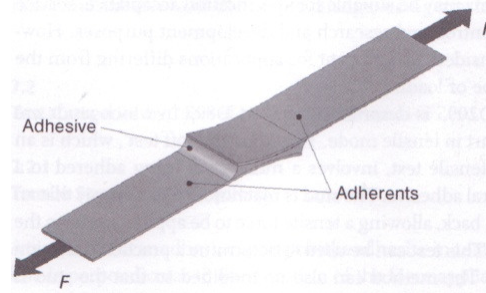


Figure 2.16 Peel effect, rotation due to bending moment [Brockmann et al. 2009].

Beside to the geometry of the adherents, the thickness of the adhesive bonded joint plays also an important role in the behavior of the test results. According to [Adams and Peppiatt 1974] cited in [Arenas et al. 2010], thicker bonded joints contain more defects such as air voids and micro cracks. The elastic analysis of [Crocombe 1989] shows that the stress distribution of a thin bonded joint is concentrated at the vicinity of the end of the bonded joint. Thicker bonded joints show a more uniform shear stress distribution. Thicker bonded joints have a larger average shear stress level compared to smaller bonded joints and peak stresses at the ends of the bonded joint are less high. This means that when yielding does occur in a thicker bonded joint, there is less elastic reserve to sustain further loading and thus yielding occurs more quickly. In a thin bonded joint the yield stress is reached at a lower load than in a thick bonded joint.

[Gleich et al. 2001] and [Da Silva et al. 2006] showed that interface peak stresses (peel and shear in point A, C, D and F of figure 2.18) for thicker bonded joints were higher and the average adhesive stresses (on line BE of figure 2.18) are shown to decrease with increasing bonded joint thickness (figure 2.17 and 2.18).

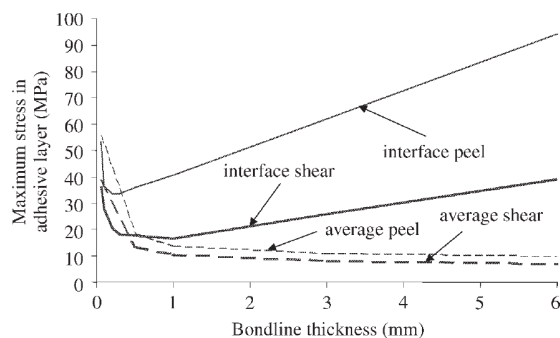


Figure 2.17 Maximum stress in relation to the bonded joint thickness [Gleich et al. 2001].

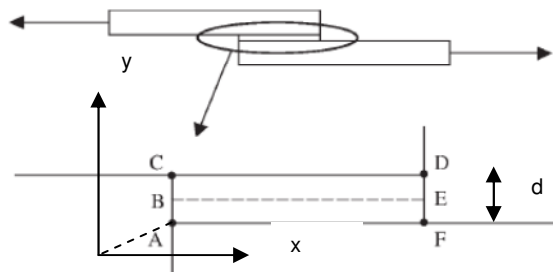


Figure 2.18 Location of the maximum (peak) stresses (points A, C, D, and F) and the average stresses (points B and E) in the adhesive bonded joint [Gleich et al. 2001].

[Grant et al. 2009] explained the influence of the adhesive thickness on the presence of bending moment. [Arenas et al. 2010] investigated the influence of the thickness of the adhesive on the mechanical performance of the joint. Using a statistical analysis based on Weibull distribution an optimum thickness of the adhesive, combining the best mechanical performance with reliability, is proposed.

2.2 Literature review on glass

2.2.1 Production of glass

In 1959 the Pilkington Brothers introduced a production process which accounts for about 90 percent of today's global flat glass production. According to [Haldimann et al. 2008] the advantages of the annealed float process are its low costs, superior optical quality and the large sizes of panes that can be produced.

The annealed float process is presented in figure 2.19. The raw material mix and the cullet, which consists of broken glass of the cutting section, are melted in a furnace at about 1500°C. The molten glass is then poured on a bath with molten tin. This is a continuous process at about 1100°C. In the enclosed box where the glass floats over the molten tin, an inert atmosphere consisting of hydrogen and nitrogen prevents the molten tin from oxidation. Tin has a large temperature range of its liquid state. It melts at 232°C, which is very low for metals, and starts boiling at 2270°C. Compared to glass tin has a high density. The molten glass floats over the molten tin and spreads outwards forming a smooth and plain layer with a thickness of 6 to 7 mm. The annealing lehr is a closed box where the glass is slowly cooled down starting at about 600°C to 100°C. This prevents the induction of residual stresses within the glass pane. The speed of the rollers whereon the glass is cooled and further transported determines the thickness of the glass within a range of 2 to 25 mm. A higher speed results in a decrease of the glass pane thickness and vice versa. When the glass leaves the annealing lehr, it is inspected by a machine. Visual defects and imperfections are marked and removed during cutting. In the cutting section, the glass ribbon is cut into standard sizes of 3.21 meter by 6.00 meter.

Producing glass according to this process, the glass pane will have two different faces. The bottom face is called the tin side. This side contains some diffused tin molecules into the glass pane. Using ultraviolet radiation the tin side of the glass pane can be detected and will bluish fluorescence. The upper face is often called the atmospheric side of the glass pane.

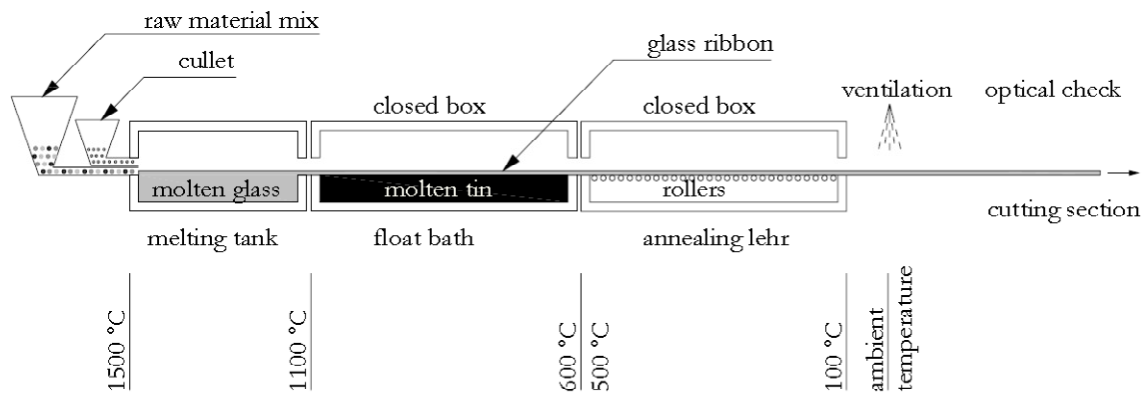


Figure 2.19 Production process of annealed float glass [Huvener 2009]

2.2.2 Types of glass

After manufacturing annealed float glass, it will be further processed to produce glass products with different kinds of shape, performance and appearance that are required to meet particular needs. According to [Haldimann et al. 2008] a wide variety of treatments of secondary processing are available in which edge working, hole drilling, tempering and laminating are the most important for structural applications [Luible, 2004]. In this section only tempering and laminating will be discussed as the other treatments are not relevant for this research.

2.2.2.1 Tempering of glass

Thermally or chemically tempering of glass is a follow-up treatment and increases the strength of glass (section 1.2.2). The purpose of a follow-up treatment is to introduce tensile stresses in the core of the glass pane and compression stresses on or near the surface (figure 2.20). The core of the glass pane does not contain flaws and is therefore able to resist tensile stresses. The surface of the glass pane does contain flaws and these flaws will become bigger when for example the glass pane is exposed to bending. If the residual compression stress due to the follow-up treatment is larger than the tensile stress due to action, the flaws will not grow and the glass will not break (figure 2.21). Follow-up treatments for glass can be compared to pre-tensioned concrete by steel reinforcements. Pre-tensioning of the concrete part causes a higher resistance to tensile stress. The strength of glass increases against mechanical loadings and change of temperature (figure 1.9).

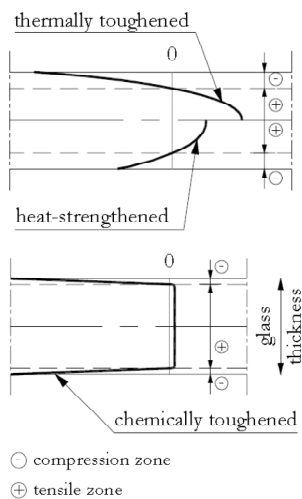


Figure 2.20 Residual stress distributions of fully tempered (thermally toughened), heat-strengthened and chemically toughened glass [Huvener 2009]

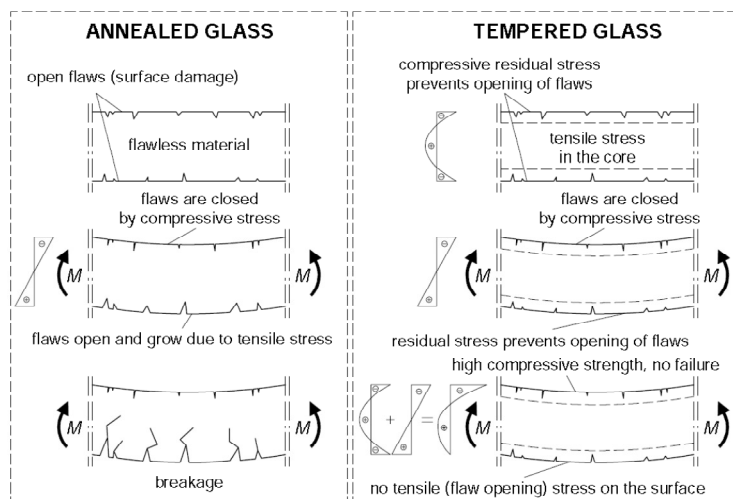


Figure 2.21 Principle of glass tempering [Haldimann et al. 2008]

The fracture pattern is a function of the energy stored in the glass, i.e. of the residual stress and the stress due to loads. We can distinguish the following glass types (table 2.2): annealed float glass (ANG), heat strengthened glass (HSG) and fully tempered glass (FTG, thermally toughened glass) but on international level no specific terminology for the different glass types has been universal accepted [Haldimann et al. 2008]. Figure 2.22 presents the crack patterns of ANG, HSG and FTG.

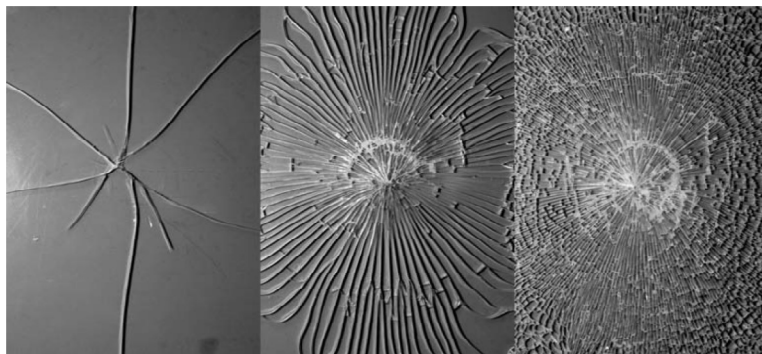


Figure 2.22 Fracture pattern of annealed float glass (left), heat strengthened glass (middle) and fully tempered glass (right) [Haldimann et al. 2008].

Table 2.2 Glass type terminology

Level of residual surface compression	Terminology used in master thesis	Other frequently used terms
(almost) none	Annealed glass (ANG)	Float glass
Medium	Heat-strengthened glass (HSG)	Partly toughened glass
High	Fully tempered glass (FTG)	Tempered glass, (thermally) toughened glass
Unspecified	Heat-treated glass	

Note. The terminology presented in this table is adapted from [Haldimann et al. 2008].

2.2.2.2 Fully tempered glass & heat strengthened glass

Fully tempered and heat strengthened glass can be made by heating annealed float glass in a furnace to approximately 620-675°C (approximately 100°C above the glass transition temperature), and then rapidly cooling down with a specific speed by jets of cold air (quenching). The tempering process is presented in figure 2.23. Within the first seconds, the cooling process results in tensile stresses on the surface and compressive stresses in the interior. Due to the viscous state of the glass in this temperature range, the tensile stresses can relax rapidly. As soon as the temperature on the glass falls below the transition temperature (T_g) (approximately 525°C), the glass solidifies and relaxation stops immediately. The temperature distribution is approximately parabolic. At the moment when the surface solidifies, the temperature of the core is still above the transition temperature. When the temperature of the core drops below the transition temperature, thermal shrinkage is resisted by the already solidified surface which leads to the residual stress distribution presented in figure 2.24. The faster the cooling down process, the larger the internal residual stresses (figure 2.20). The core of the glass pane has tensile stresses which are in equilibrium with the compression stresses at the surface. Glass cannot be cut, ground or drilled after tempering. If the equilibrium state of this glass type is disturbed the pane will crack immediately. The larger the residual stress, the smaller the fragments if the glass pane cracks (figure 2.22).

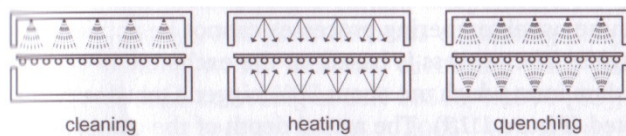


Figure 2.23 Tempering process [Haldimann et al. 2008].

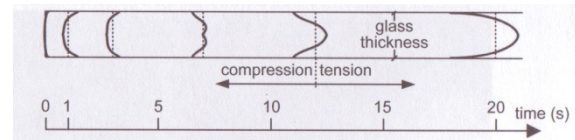


Figure 2.24 Residual stress distribution during the tempering process [Haldimann et al. 2008].

A fully tempered glass element can fail spontaneously within a few years of production. The small but not negligible risk of failure is caused by nickel sulfide (NiS) inclusions that cannot be avoided during production (figure 2.25). If such an inclusion of nickel sulfide is influenced by temperature, the NiS particles increase about 4% in volume due to a phase change. The expansion of these particles combined with high tensile stresses in the core of the glass due to tempering can cause spontaneous failure. The heat-soak test is able to eliminate almost all risk of spontaneous failure. During this test, the glass is slowly heated up to about 290°C and this temperature is maintained for several hours. The phase change is accelerated and most glass elements containing dangerous inclusion will fail during the test.

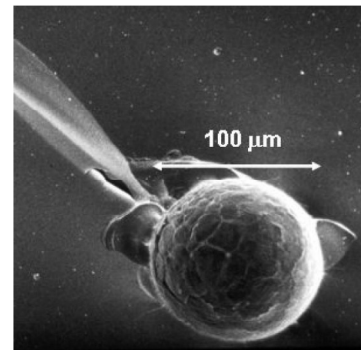


Figure 2.25 Nickel sulfide (NiS) inclusion [Haldimann et al. 2008]

2.2.2.3 Chemically toughened glass

Chemically toughened glass panes are hardly used in structural applications. Chemical toughening is an alternative tempering process without any thermal interaction. It is used for special geometries i.e. strongly curved glass panes where other tempering processes cannot be applied. The process is based on the exchange of sodium ions in the glass surface by potassium ions, which are about 30% bigger. Only a very thin layer of the glass surface is affected and the actual depth of the compression zone is time dependant (about 20 μm in 24 hours). The residual stress state is thus different from thermal tempering (figure 2.20). If the surface flaws are deeper than the depth of the compression zone, the tip lies in the tensile zone and subcritical crack growth without external loading occurs resulting in spontaneous failure. This is called self-fatigue. According to [Haldimann et al. 2008] cutting or drilling remains possible after tempering.

2.2.2.4 Laminated glass

Laminated glass is of major interest in structural applications. Tempering reduces the time dependence of the strength and improves the structural capacity of the glass. Glass is a brittle material and post-breakage performance is of great importance with respect to safety. Lamination of a transparent plastic film between two or more flat glass panes enables improvement in the post-breakage behavior. After breakage the glass fragments adhere to the film and obtain a certain remaining structural capacity as the glass fragments 'arch' or lock in place. This capacity is dependent on the fragmentation of the glass. Bigger shards result in better structural capacity after breakage, but the structural performance decreases (figure 2.26). Besides the glass type that is used, the post-breakage behavior is also dependent on the applied interlayer material. The most common interlayer material is polyvinyl butyral (PVB), also called UV-protection foil because it blocks almost completely UV radiation. PVB is a viscoelastic material, i.e. its physical properties depend strongly on the temperature and the load duration.

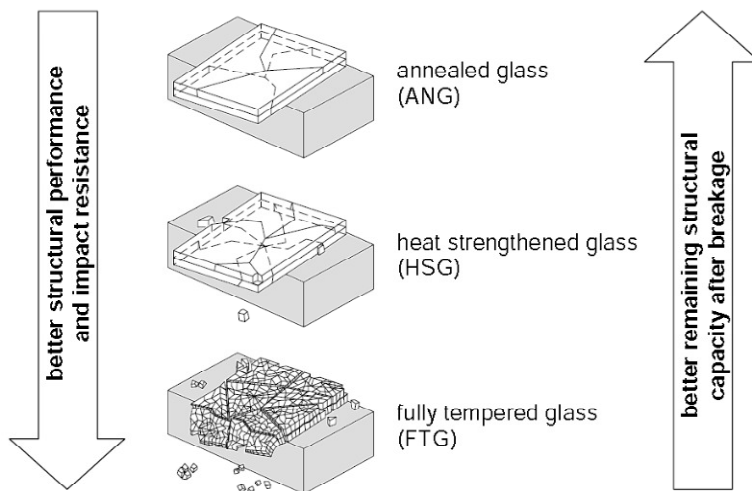


Figure 2.26 Post-breakage behavior of laminated glass with different glass types [Sedlacek et al. 1999].

2.2.3 Material properties

2.2.3.1 Chemical properties

Standard soda lime silica glass [Haldimann 2006] is commonly used in buildings. The main chemical composition includes silica sand, lime (calcium oxide) and soda. Additives like magnesia, alumina, iron and some other elements are present in a very small amount. For special applications, borosilicate glass is used. It has a larger resistance to change of temperature and acids than soda lime glass. The main chemical composition includes silica sand, boron oxide and additives like soda, potassium oxide, alumina and some other elements in a very small amount. In the experiments in this research standard soda lime silica glass is used.

Glass is an inorganic product (no carbon present) of fusion which is cooled down to a rigid state without crystallization [Wigginton 1996, Hess 2004]. The velocity of cooling down in the vicinity of the glass transition temperature (T_g) plays an important role in preventing crystals. The liquid becomes too viscous, and therefore complex chains of bonds between the glass molecules during cooling down is not able to transit from an unarranged to a arranged structure. Glass is an inert material which does not react with other chemicals. This makes glass a durable building material with great possibilities.

2.2.3.2 Mechanical properties

Glass is an isotropic material with perfect linear elastic behavior without any plastic behavior. According to [Schuler et al. 2004] glass fails if the local peak stress exceeds the tension strength of glass. In literature different values for the young's modulus (E_g) can be found ranging between 70000 and 74000 N/mm². The Young's modulus prescribed in [EN 572-1 2004] is 70000 N/mm² and is used in this research. Just as the values for the Young's Modulus, values for Poisson's ratio (ν_g) of glass differ in literature between 0.20 up to 0.24. [EN 572-1 2004] prescribes a Poisson's ratio 0.20, but in many researches 0.23 is used. Table 2.3 gives the relevant mechanical properties of soda silica glass used in this research.

Table 2.3 Properties of soda lime silica glass

Properties	Symbol	Unity	Value
Density	ρ_g	kg/m ³	2500
Young's modulus	E_g	N/mm ²	70000
Shear modulus	G_g	N/mm ²	28455
Poisson's ratio	ν_g	[-]	0.23
Thermal expansion coefficient	α_g	K ⁻¹	9x10 ⁻⁶
Hardness according to Mohs scale	n_g	Mohs	6

Table 2.4 gives an overview of the representative flexural tension strength for short term loading [NEN 2608-2 2007], maximum change of temperature and crack patterns of annealed, heat-strengthened and thermally toughened glass.

Table 2.4 Overview of the representative flexural tension strength for short term loading and maximum change of temperature belonging to different types of glass.

Glass type	$f_{mt;u;rep}$ [N/mm ²]	ΔT [°C]	Description of the crack pattern
Annealed	45	30-40	Large and sharp shards
Heat-strengthened	70	100	Large and less sharp shards
Fully tempered glass	120	200	Not sharp crumbled shards

2.3 Literature review on in-plane loaded glass

In this section research projects on in-plane loaded glass panes are highlighted. Table 2.5 gives an overview of the reviewed researches. The majority of the research projects on in-plane loaded glass panes focus on the stability of the glass pane.

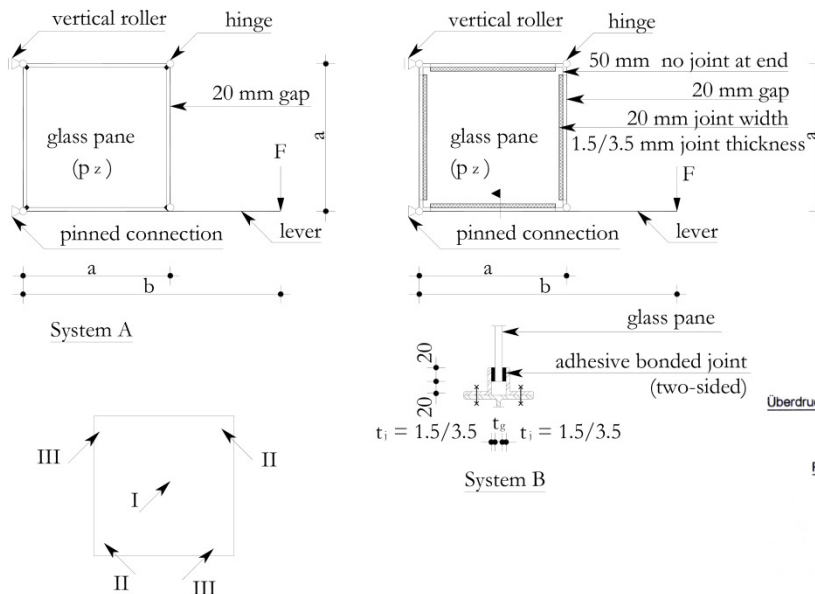
Table 2.5 Research projects on in-plane loaded glass

Research project	Authors	Section
Circumferentially adhesive bonded glass panes bracing steel frames in façades.	[Huveners 2009]	1.1
Nutzung der Verglasung zur Aussteifung von Gebäudehüllen.	Frank Wellershof (2006)	2.3.1
Glass panel under shear loading – use of glass envelopes in building stabilization	Danijel Mocibob (2008)	2.3.2
Buckling of flat laminated glass panels under in-plane compression or shear	Chiara Bedon, Claudio Amadio (2012)	2.3.3
Stability of glued and embedded glass panes: Dunkerley straight line as a conservative estimate of superimposed buckling coefficients.	Anton Arnold, Lukas Neumann and Werner Hochhauser (2012)	2.3.4

2.3.1 German research: Nutzung der Verglasung zur Aussteifung von Gebäudehüllen

In the research of [Wellershoff 2006] two systems were tested and analyzed by numerical analytical models. In system A (figure 2.27) the glass pane has symmetrical countersinks at each corner of the glass pane and the connections to the steel structure at these corners are provided with and without mortar. System B (figure 2.27) consisted of a circumferentially two-sided adhesive bonded glass pane to a steel frame. In the corners of the glass pane, the adhesive is not connected to the steel frame. This systems act like a pure shear wall. Experiments on the adhesive bonded glass pane were carried out on square glass panes of 1200 mm and 1600 mm. Not only single heat strengthened glass panes were tested but also laminated heat strengthened glass panes and a combination of a laminated heat strengthened glass pane and a fully tempered glass pane with in between an air chamber to apply a uniform distributed out-of-plane load on the laminated heat strengthened glass pane (figure 2.28). The applied adhesives consisted of an acrylate with a bonded joint thickness of 1.5 mm and two types of polyurethane adhesive with a thickness of 3.5 mm. Experiments on point supported glass panes were carried out on square laminated heat strengthened glass panes of 1200 mm and 1600 mm and with different glass pane thicknesses.

The behavior of the system of the glass pane in System A with counterstrikes and mortar show large influence of the applied mortar. Systems with counterstrikes and large facets which are connected at the corner of the steel frame without mortar, showed clear less load carrying capacity. The circumferentially adhesive bonded joint activated tension diagonals. Three positions with large surface tension stress concentrations were determined namely, at the centre of the glass pane at the front side along the tension diagonal by the out-of-plane displacements (I), in the corners of the glass pane at the rear side along the compression diagonal by the out-of-plane displacements (II) and in the corners of the tension diagonal at the front side in the adhesive bonded joint (III). The buckling load of the single and laminated glass panes are numerical and analytical analyzed. Analytical analyses by the linear buckling theory gives good results for the in-plane loaded of circumferentially adhesive bonded single and laminated glass panes. For laminated glass panes a correction factor was needed because of the effect of the PVB foil on the shear stiffness between the two glass panes.



Positions with large surface tension stress concentrations

Figure 2.27 Research project Wellershof [Huvener 2009].

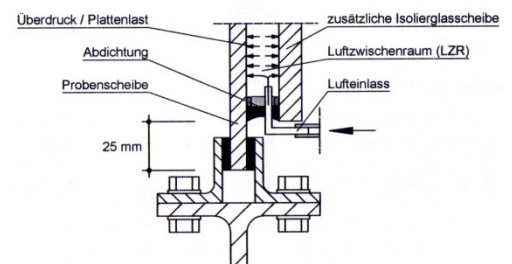


Figure 2.28 Isolation glass pane to apply an uniform distributed out-of-plane load [Wellershoff 2006].

2.3.2 Glass panel under shear loading – use of glass envelopes in building stabilization

When a fully transparent pavilion has to be designed, the glass panes in the façade are subjected to in-plane shear loads (lateral wind), in-plane compression loads (self weight roof structure, snow) and out-of-plane bending (wind load perpendicular to the glass pane). Important is the connection system of the glass panes and the development of a suitable connection system was the point of interest [Mocibob 2008]. In this research the local and global behavior of the structure was investigated for two structural concepts. The two connection systems were the point supported and the two-sided flexible linear supported glass panes (figure 2.29). For the point supported system, three different connections were tested, namely an eccentric rigid connection, an eccentric pinned connection and the axial rigid connection presented in figure 2.29.

The width of the glass panel is 1200 mm and the height of the glass pane is 3500 mm. The thickness of the laminated glass panel is built up two heat strengthened glass panes of 8 mm with a PVB interlayer of 1.52 mm. The point supported glass panel was provided with four drilling holes. The area around the bolt was filled up with an injection mortar which formed a non metallic layer to transfer the load via the bolt onto the glass pane and vice versa. The linear supported glass panel was realized with a structural silicone adhesive and applied with a thickness of 9.5 mm. The setting blocks transferred the vertical in-plane loads in the glass panel. Both systems were experimentally tested in flat position instead of the up-right position and were loaded in-plane and out-of-plane.

Experiments on point supported glass panel showed small horizontal in-plane displacement and small out-of-plane displacement of the glass panel. Failure of the glass panel was introduced in the compression diagonal at the drilling hole. Experiments on linear supported glass panel showed large horizontal in-plane displacement and large out-of-plane displacement of the glass panel. Failure of the glass panel was introduced in the compression diagonal at the setting block. For both systems, parametric study showed that the in-plane stiffness of the systems increase with increasing thickness of the glass panels.

For point loaded systems, in-plane normal compressive loads significantly decrease the shear buckling resistance. This is not the case for additional out-of-plane distributed loads and is verified by [Arnold, Neumann & Hochhauser 2012]. For linear loaded systems, in-plane normal compressive loads decrease the shear buckling resistance as well as out-of-plane loads due to the large out-of-plane displacements of the glass panel (small deformation theory / linear theory cannot be used). Because of the large horizontal in-plane displacement and out-of-plane displacement of linear supported panels, this system has limited potential to be used as a load bearing structure. The point supported system has a large potential to be used as a bearing structure.

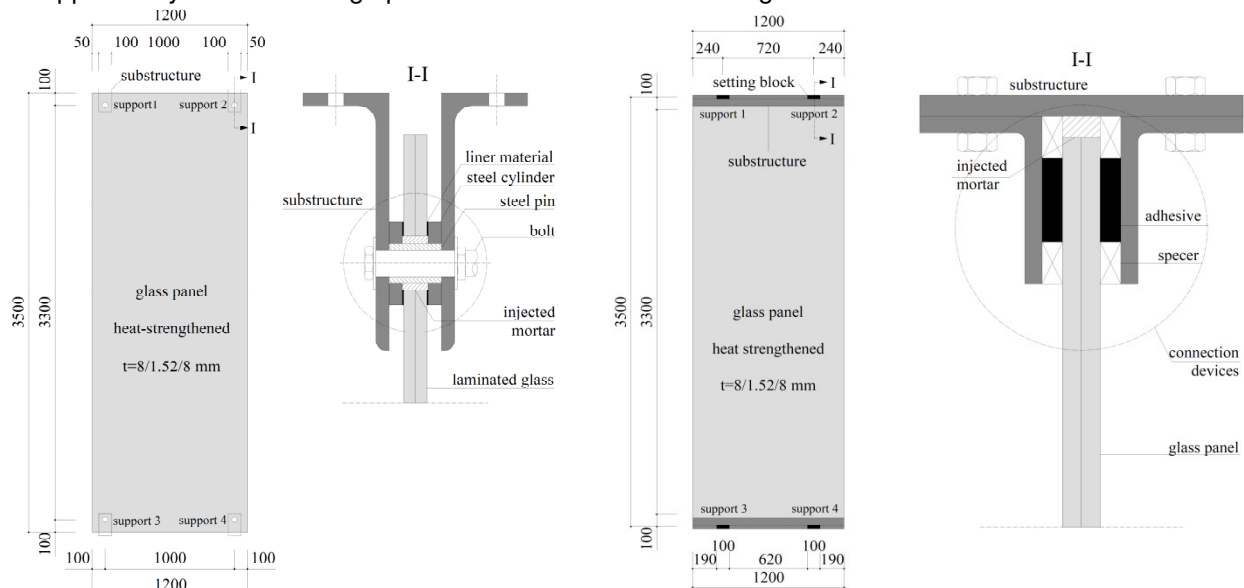


Figure 2.29 Point supported glass panel (left) and linear supported panel (right) [Mocibob 2008].

2.3.3 Buckling of flat laminated glass panels under in-plane compression or shear

To obtain insight in the behavior of in-plane loaded glass panes by compression or shear loads, a lot of research has been done by investigation of one single glass pane. However in practice, glass used as a structural material will always be laminated due to the higher residual capacity compared to single glass panes. The stability of in-plane loaded glass panes is of great importance, as glass panes have a slender geometry and are therefore susceptible to buckling. According to [Bedon and Amadio 2012], the existing methods for the buckling verification of structural elements, single or sandwich panels, applied with traditional material i.e., steel, concrete or wood, is widely available in literature, but cannot be applied to laminated glass panes. The influence of production tolerances, initial imperfections, the brittle behavior of the glass pane and viscoelastic behavior of thermoplastic interlayer's are not taken into account and therefore the methods describing buckling response of single plates cannot be used. The research focused on a proposal of an analytical formulation for the estimation of the buckling resistance of laminated glass panels subjected to in-plane compression and in-plane shear applicable at different boundary conditions and taking into account the influence of temperature and load duration of on the level of connection between the glass panes.

Finite element simulations showed that the proposed analytical model, based on the concept of equivalent thickness makes it possible to evaluate the buckling load of in-plane and shear loaded laminated glass panels. The proposed analytical method is also able to describe the relation between the load and out-of-plane displacement of the laminated glass panel taking into account the effective level of connection between the glass panes offered by the interlayer.

2.3.4 Stability of glued and embedded glass panes: Dunkerley straight line as a conservative estimate of superimposed buckling coefficients.

According to [Arnold, Neumann and Hochhauser 2012], timber glass hybrid elements meet modern architecture's demand and can help increase the use of timber and glass panes in structural applications. In their research the stability of a rectangular glass pane as a part of a stiffening and force transmitting timber –glass composed building element is investigated for width-to height ratios of 1:1 to 4:1. The glass pane is assumed to be circumferentially bonded and embedded into a timber structure via block setting. This enables load transfer of horizontal forces via shear and compression diagonals within the glass pane (figure 2.30). The stability of the glass pane has been investigated by determination of the buckling coefficient. Due to superposition of to load types onto the glass pane, the buckling coefficients have to superimpose as well. The stress tensor within the glass pane is a linear combination of the two loads, the buckling coefficients and therefore the buckling load is not a linear function of the critical compression load and the critical shear load (figure 2.31). This non-linear relation has been investigated by a numerical model for different combinations of each load. Next the superimposed buckling coefficients are approximated by the Dunkerley straight line. This method is a conservative way of predicting the critical compression load and the critical shear load. Only extremely material optimization makes finite element simulations worthwhile. Furthermore the research showed that when linear and small deformation theories are considered, that additional out-of-plane load due to wind or isochoric pressure within insulated glass does not affect the critical buckling load of stiffening glass panes.

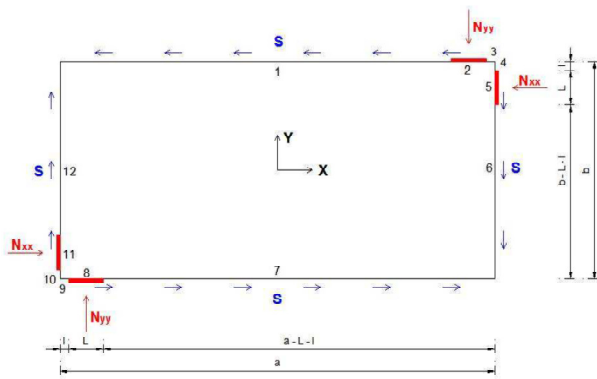


Figure 2.30 Load transfer timber-glass composed building element [Arnold, Neumann & Hochhauser 2012].

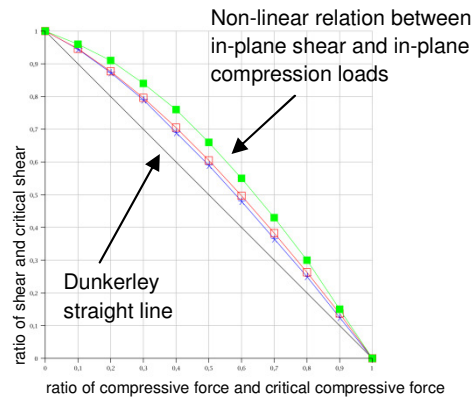


Figure 2.31 Dunkerley straight line [Arnold, Neumann & Hochhauser 2012].

3 Experiments shear stiffness acrylic adhesive

Generally, two types of glued connections are used for glass applications:

- Soft elastic adhesive connections (i.e. structural-silicone-sealant connections),
- Rigid adhesive connection (i.e. acrylic adhesives, epoxy adhesives and polyester resin).

The adhesive had to fulfill two requirements, namely: the shear stiffness had to be between 10 N/mm³ and 100 N/mm³ (zone 2) and the thickness had to be as large as possible to account for tolerances in the applied materials (section 1.2.1). Based on these two requirements different adhesive manufacturers were contacted and the proposal of the manufacturer of the applied adhesive was adopted. The applied acrylic adhesive was at the execution of the shear tests the most proper adhesive available on the market.

In section 3.1 the applied adhesive, the geometry and preliminary treatment of the test specimens are described followed by the methodology of measuring and calculation. The results are discussed and the section ends with conclusions. In section 3.2 the test results of complementary shear tests are reviewed. The objective of these experiments was to obtain the influence on the relation between the average shear stress and relative average displacement of the adhesive if the area of the loaded adhesive is enlarged.

3.1 Preliminary research: applied acrylic adhesive

The applied adhesive in this research concerned a two-component ADP (Acrylic Double Performance) Acryl known as SikaFast®-5215. The supplier and manufacturer is Sika division Industry. Adhesives based on the ADP technology are fast curing flexible adhesives with a sufficient open time. The curing mechanism is based on polymerization² (figure 2.11), but can also be classified as thermoset (figure 2.13).

Component A contains the reactive monomer and component B acts as initiator. Mixing with a ratio 10:1 using a static mixer, starts the polymerization reaction. The acrylic adhesive offers a relatively long open time followed by fast curing which results in an optimal relation between application time and strength development to reach handling strength.

The consistency of the adhesive is a thixotropic³ paste and can be processed between +10°C and +40°C. The service temperature lies between -40°C and +80°C. The curing time is dependent on the ambient temperature. The ambient temperature in the laboratory is 23°C. At this temperature the open time is about 5 minutes and after approximately 15 minutes 80% of the final strength is reached. The glass transition temperature⁴ (T_g) is roughly +52°C and therefore the bond has a stiff and brittle behavior. The acrylic adhesive can be used as substitute for welding, riveting, and other, mechanical fastening techniques. Suitable for structural and semi-structural bonding on a wide range of substrates for high strength fastening of concealed joints on different types of substrates including glass, top coats, plastics. The above data [SikaFast-5215 2006] is based on the technical data sheet of Sika Nederland B.V, version 4/2006 and presented in Appendix A.9.

Before the adhesive was applied, the surface of the adherent was prepared using [Sika®ADPrep-5901]. This is the general surface preparation agent for adhesively bonded systems with Sika. The application method consists of wiping the bonding area with a clean lint-free cloth or absorbent paper towel sparingly moistened with the preparation agent. Wiping the surface once was sufficient. The drying time is temperature dependant and for temperatures above 15°C it is approximate 1 minute. The open time is as long as 24 hours and during this time the bonding area is protected from dust and

² Polymerization is a process of reacting monomer molecules together in a chemical reaction to form three-dimensional networks or polymer chains. Each identical (basis) monomer molecule contains a double (internal) bond which is able to break and link up with other monomers to form a repeating chain (polymer).

³ Thixotropy is the property of certain gels or fluids that are thick (viscous) under normal conditions, but flow (become thin, less viscous) over time when shaken, agitated, or otherwise stressed.

⁴ The glass transition temperature is the temperature at which a material becomes soft upon heating or brittle upon cooling.

dirt. However, within two hours after every surface preparation, the adhesive was applied. The above data [Sika®ADPrep-5901] is based on the technical data sheet of Sika Nederland B.V, version 3/2006 and presented in Appendix A.10.

3.1.1 Test methods and previous research

There are different test methods to determine the behavior of the shear stiffness of structural bonds. Each method is described in codes. Below two relevant codes are listed.

[DIN 54 451:1978] Testing of adhesives for metals of bonded joints; tensile shear test for the determination of the shear stress-strain diagram of an adhesive in a bonded joint.

[NEN-EN 14869-2:2004] Structural adhesives - Determination of shear behavior of structural bonds – Part 2: Thick adherents shear test (TAST).

There are a few differences in test specimens. Specimens according the [DIN 54 451:1978] are produced out of two composed adhesively bonded steel plates. After the adhesive has cured, slots are cut in the steel plates. The dimensions of the specimens are presented in figure 3.1. Huveners and Koggel used this code in 2006 but due to the disadvantages of production, described by [Kadioglu et al. 2002] in section 2.1.6, each part of the specimen was produced in one piece (figure 3.2). In the [NEN-EN 14869-2:2004] the researcher is able to choose between the two production methods. Besides this, the material that is used is also an important point. In the DIN aluminum specimens are prescribed, but in the NEN-EN steel specimens where chosen (section 2.1.6).

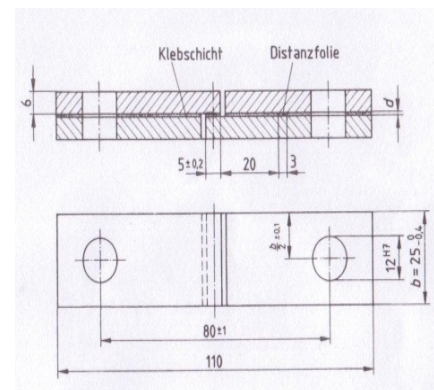


Figure 3.1 Dimensions of aluminum specimens according to [DIN 54 451:1978]

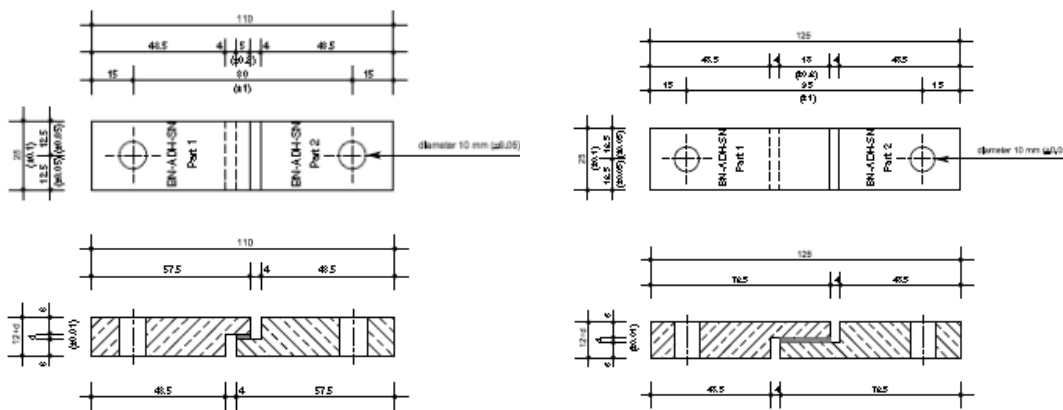


Figure 3.2 Aluminum specimens used by [Huveners and Koggel 2006]. Type of adhesive: on the left Epoxy, on the right polyurethane/silicone and putty.

3.1.2 Specimens

The specimens are made in accordance with [NEN-EN 14869-2:2004] but deviate slightly from this code. Below, all tested batches are reported with their specific properties. The tests are split in different batches. Between the batches each time only one parameter is changed, to be able to compare the results to each other (table 3.1).

- Batch 1: Aluminum specimens with a bond width of 10 mm and 2.5 mm/min displacement velocity. The bonded joint thickness is 3 mm and is prepared with the preparation agent recommended by the manufacturer (Appendix A.10). By testing these specimens a comparison with the results of [Huveners and Koggel 2006] can be made.
- Batch 2: Aluminum specimens with a bond width of 10 mm and 0.5 mm/min displacement velocity. The bonded joint thickness is 3 mm and is prepared with the preparation agent recommended by the manufacturer (Appendix A.10). By testing this batch, the influence of the displacement velocity can be verified. A lower displacement velocity is expected to lead to lower maximum shear stress.
- Batch 3: Steel specimens with a bond width of 10 mm and 0.5 mm/min displacement velocity. The bonded joint thickness is 3 mm and is prepared with the preparation agent recommended by the manufacturer (Appendix A.10). By testing this batch, the influence of the applied material can be verified. According to [Chiu and Jones 1992] shear tests using aluminum specimens will fail at a lower shear stress than steel specimens.

The overlap of the specimens in batch 1 up to 3 is 5 mm longer than prescribed in [NEN-EN 14869-2:2004]. [Huveners and Koggel 2006] decided to extend the overlap with 5 mm due to the expected sealant-like behaviour of the adhesive, based on polyurethane. Besides this, the bonded joint width in the in-plane load glass panes experiments is also 10 mm.

- Batch 4: Steel specimens with a bond width of 5 mm and 0.5 mm/min displacement velocity. The bonded joint thickness is 3 mm and is prepared with the preparation agent recommended by the manufacturer (Appendix A.10). By testing this batch, the influence of the bond width can be observed. The width of the bonded joint of 5 mm is in accordance with [NEN-EN 14869-2:2004].
- Batch 5: Steel specimens with a bond width of 5 mm and 0.5 mm/min displacement velocity. The bonded joint thickness is 3 mm and is prepared with acetone, which is the difference between batch 4 and 5. By testing this batch, the influence of the bonded joint preparation can be observed.
- Batch 6: Steel specimens with a bond width of 5 mm and 0.5 mm/min displacement velocity. The bonded joint thickness is 2 mm and is prepared with the preparation agent recommended by the manufacturer (Appendix A.10). Testing this batch the influence of the bonded joint thickness is exposed.

Figure 3.3 and 3.4 illustrate the test specimens with their dimensions of the different batches.

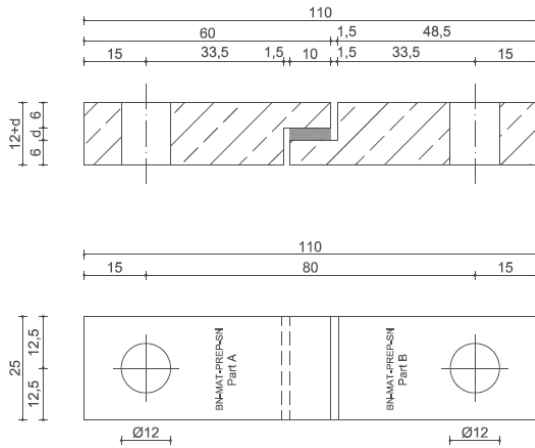


Figure 3.3 Specimens used for batches 1 up to 3.

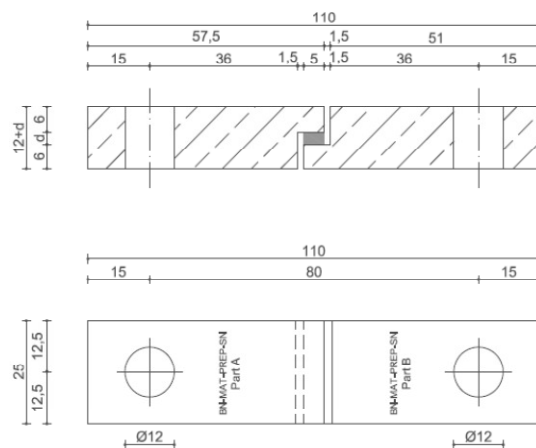


Figure 3.4 Specimens used for batches 4 up to 6.

Dimensions batch 1 to 6 (figure 3.3 and 3.4):

- L_j [mm] is the length of the bonded joint, in this case 25 mm (deviation is ± 0.5 mm);
- w_j [mm] is the width of the bonded joint, 10 mm and 5 mm respectively (deviation is ± 0.1 mm);
- t_j [mm] is the thickness of the bonded joint, 3 mm and 2 mm respectively (deviation is ± 0.01 mm).

Table 3.1 Overview of the properties of batch 1 to batch 6.

Test Code	Material specimens	Type of Adhesive	w_j [mm]	t_j [mm]	RH [%]	T_0 [°C]	T_t [°C]	DV [mm/min]
Batch 1	Aluminum	Acrylic	10	3	60	23	23	2.5
Batch 2	Aluminum	Acrylic	10	3	60	23	23	0.5
Batch 3	Steel	Acrylic	10	3	60	23	23	0.5
Batch 4	Steel	Acrylic	5	3	60	23	23	0.5
Batch 5	Steel	Acrylic	5	3	60	23	23	0.5
Batch 6	Steel	Acrylic	5	2	60	23	23	0.5

A milling-machine with different milling tools is used to prepare the shape of the aluminium and steel specimens. The steel specimens (steel grade: S235JR), made of normal structural steel, and aluminium specimens, are fastened in a fixing mechanism of the tensile bench, using a hole of 10 mm in diameter at both ends. A forklike structure will ensure a cardanic supporting structure at each end of the part (figure 3.5), so the specimen is able to rotate freely in two directions. This is important because presence of bending must be minimized as much as possible to ensure that only shear occurs in the bonded area. This method is in accordance with previous research [Huvener and Koggel 2006].

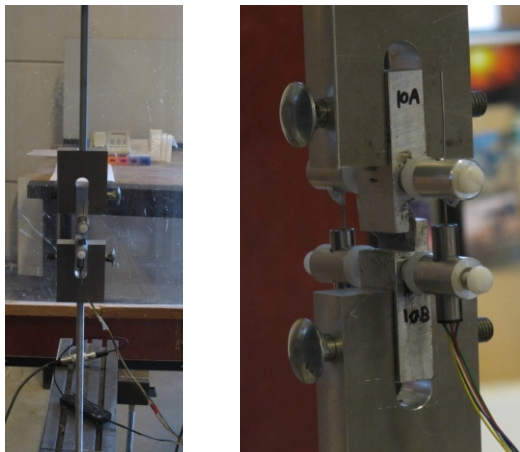


Figure 3.5 Cardanic supporting structure as applied in tensile bench.

3.1.3 Calculation

To discuss the shear behavior of each batch, the relation between the shear stress and the shear strain of each specimen will be determined. The average shear stress (τ_{ave}) in the adhesive, presented in equation (3.1), is the load (F_t) applied to the specimen divided by the bonded area ($l_j \cdot w_j$).

$$\tau_{ave} = \frac{F_t}{l_j \cdot w_j} \quad (3.1)$$

In which:

τ_{ave} [N/mm^2] is the calculated average shear stress in the adhesive;
 F_t [N] is the force applied to the specimen;
 l_j [mm] is the length of the bonded joint;
 w_j [mm] is the width of the bond joint.

The average shear strain is calculated according to the procedure followed by [Huvener and Koggel 2006], to be able to compare the results. The shear strain is the tangent of a quotient and is given in equation (3.2). This equation is based on the theory of large deformations, because of the proportional large deformations of the bonded joint (figure 3.6).

$$\tan \gamma_{ave} = \left(\frac{u_{ave}}{t_j} \right) \rightarrow \gamma_{ave} = \tan^{-1} \left(\frac{u_{ave}}{t_j} \right) \quad (3.2)$$

In which:

γ_{ave} [-] is the average relative shear strain;
 u_{ave} [mm] is the average relative shear deformation;
 t_j [mm] is the thickness of the bonded joint.

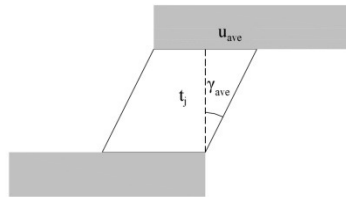


Figure 3.6 Large deformation and rotation of the bonded joint. [Huvener and Koggel 2006]

The average shear stress (τ_{ave}) and the average shear strain (γ_{ave}) of each tested specimen can be plotted in a relation to each other (figure 3.7).

For each specimen a polynomial approximation formula is determined. All these formulae per batch are used to determine an average formula based on discrete points (with steps of 0.05 [rad] for γ_{ave}). A normal polynomial function representing the relation between (τ_{ave}) and (γ_{ave}) can be described by equation (3.3).

$$\tau_{ave} = a_0 + a_1 \gamma_{ave} + a_2 \gamma_{ave}^2 + \dots + a_n \gamma_{ave}^n \quad (3.3)$$

In which:

τ_{ave} [N/mm^2] is the average shear stress per batch;
 γ_{ave} [rad] is the average relative shear strain per batch;
 a_i is a constant value;
 n is a natural number.

The average shear stresses per discrete point of ($\tau_{ave;i}$) in figure 3.7 can be calculated by equation (3.4).

$$\tau_{ave;i} = \frac{\sum \tau_i}{m} \quad (3.4)$$

In which:

$\tau_{ave;total}$ [N/mm²] is the total average shear stress;
 $\sum \tau_{ave;i}$ [N/mm²] is the sum of all average shear stresses per batch;
 m is the number of experiments per batch.

The average shear stresses of all these discrete points are used to determine an average equation also based on polynomial approximation.

The average shear modulus [G_a] is the quotient of the average shear stress divided by the average relative shear strain, given in equation (3.5).

$$G_a = \frac{\tau_{ave}}{\gamma_{ave}} \quad (3.5)$$

This equation is only valid for a linear relationship between the average shear stress and the average relative shear strain. For a low average shear stress and a low average relative shear strain value in a non linear relationship, equation 3.5 still can be used. A continuous function of the relation between the shear stress and shear angle will be represented by a polynomial approximation, based on discrete (experimentally determined) points.

Example BN-MAT-PREP-SN

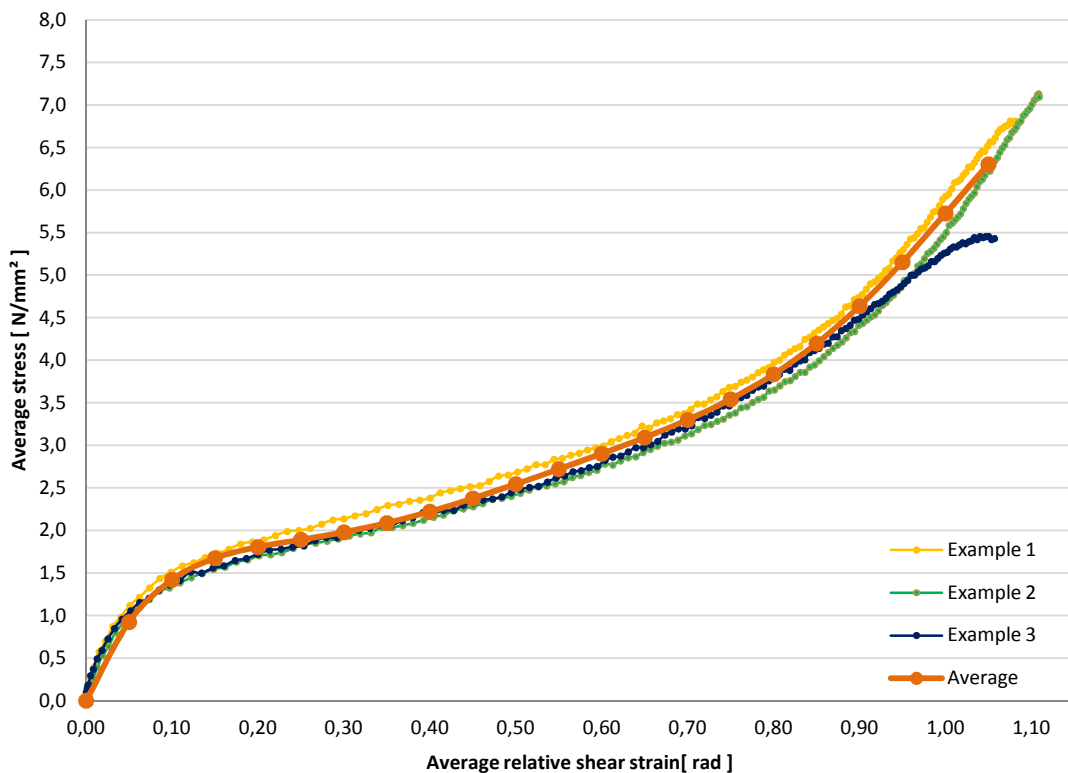


Figure 3.7 Relation of the average shear stress – average shear strain diagram (example).

3.1.4 Average shear properties per batch

In this section all average shear properties of each batch are discussed (figure 3.8). The average relation between the average shear stress (vertical axis) and the average relative shear strain (horizontal axis) per batch are calculated as explained in section 3.1.3. The test results of each batch are given in appendix A.7. The properties of each batch are presented in section 3.1.2 and appendix A.5.

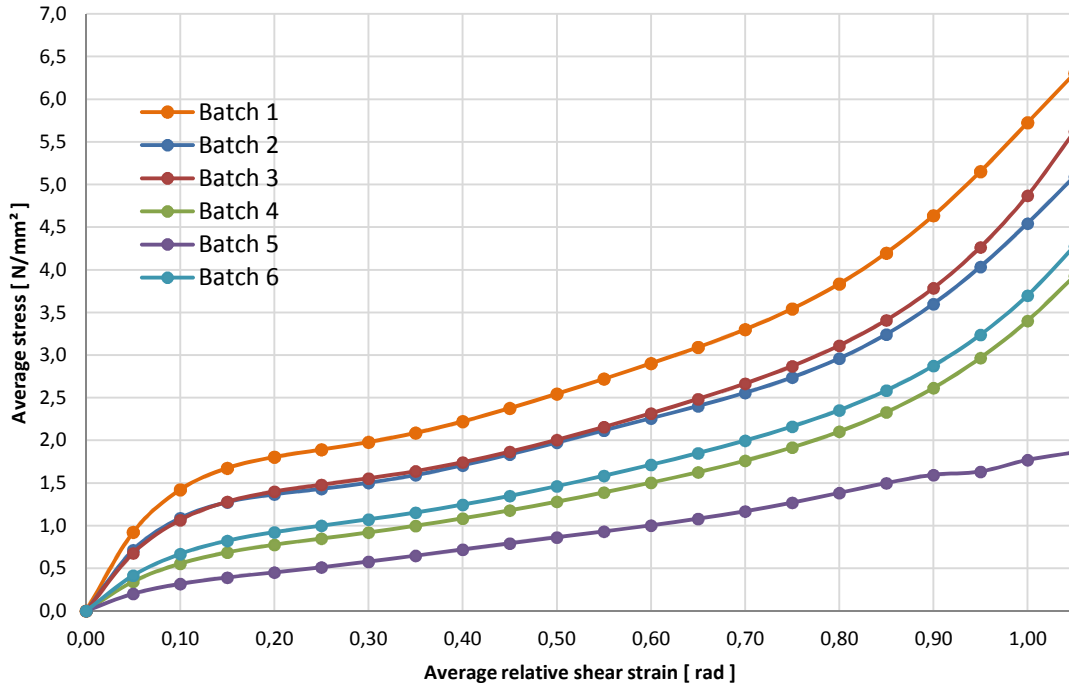


Figure 3.8 Average shear properties per batch.

The shear stiffness of the bonded joint ($k_{j;\eta/\zeta}$) is derived according to equations 3.5 and 3.6 from the linear stage of the shear stress-strain relation of adhesive shear experiments (table 3.2 and figure 3.8).

$$k_{j;\eta/\zeta} = \frac{G_a}{t_j} \quad (\text{Equation 3.6})$$

Table 3.2 Assumed linear behavior of the adhesive bonded joint of batch 3 in the first stage.

γ_{ave} [-]	τ_{ave} [N/mm ²]	G_a [N/mm ²]	t_j [mm]	$k_{j;\eta/\zeta}$ [N/mm ³]
0.05	0.68	13.53	3.0	4.51

Batch 1 versus batch 2

The difference between batch 1 and batch 2 is the displacement velocity, 2.5 mm/min and 0.5 mm/min respectively. If batch 1 is 100%, Batch 2 is on average 77.3% of batch 1. The average percentage is calculated by adding the percentages of each point divided by the total number of points $\left[\left(\sum_{i=0.05}^{1.05} \frac{\text{batch 2}}{\text{batch 1}} \times 100\% \right) / 21 \right]$.

The average lower curve of batch 2 can be explained by molecular relaxation of the polymer chains within the adhesive according to [Habernicht 2006] and [Chalkley and Chiu 1993]. Due to the lower displacement velocity, relaxation by re-storage of the molecules is possible and a new equilibrium will be found. At larger velocity, the molecules of the polymer chains have less time to align and the re-storage is more prevented than at a lower velocity, which results in a higher stress-strain relation (figure 3.9).

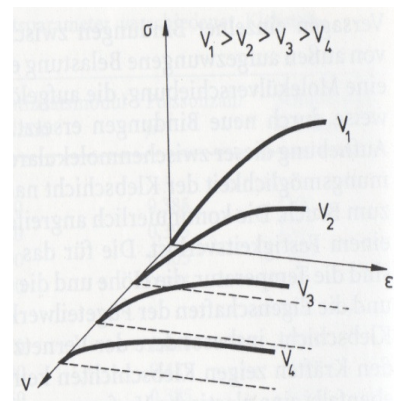


Figure 3.9 Influence displacement velocity on stress-strain relation [Habernicht 2006].

The stress-strain relation of batch 1 can be compared to the results of [Huvener and Koggel 2006]. In those experiments three different adhesives were tested with a displacement velocity of 2.5 mm/min. The results of the epoxy, polyurethane and silicone adhesive are also approximated according to the polynomial equation 3.3 of section 3.1.3, which makes it possible to plot the results in figure 3.10. It can be concluded that the acrylic adhesive has a higher stiffness than polyurethane and silicone, but a much lower stiffness compared to epoxy.

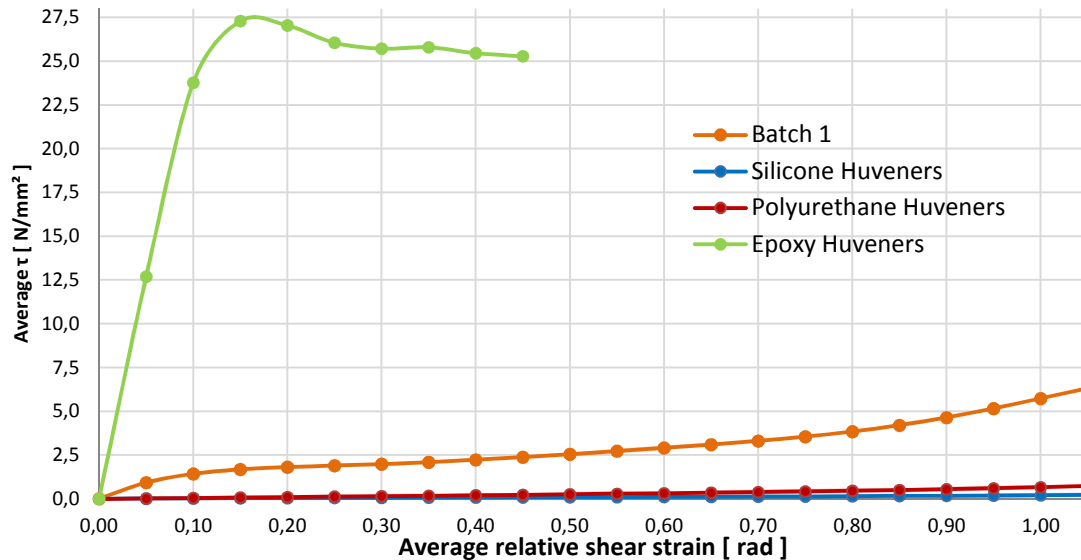


Figure 3.10 Comparison between stress-shear relation of silicone, polyurethane, acrylic and epoxy adhesive.

Batch 2 versus batch 3

The difference between batch 2 and batch 3 is the applied material of the specimen. Specimens of batch 2 are made of aluminum and specimens of batch 3 are made of steel. If batch 2 is 100%, batch 3 is on average 103.2% of batch 2. The experiences of [Chiu and Jones 1992] that shear tests using aluminum specimens will fail slightly at a lower shear stress than steel specimens can be confirmed by viewing the failure levels of the specimens of batch 2 and batch 3 in appendix A.7.

Batch 3 versus batch 4

The difference between batch 3 and batch 4 is the bond width, 10 mm and 5 mm respectively. If the stress-strain relation of batch 3 is 100%, the stress-strain relation of batch 4 is on average 63.9% of batch 3. The bond width in the experiments with glass is 10 mm but according to [NEN-EN 14869-2:2004], the shear properties of an adhesive have to be determined with a bond width of 5 mm.

Batch 5 versus batch 4

The difference between batch 5 and batch 4 is the preparation of the bonded joint. Batch 4 is prepared with the preparation agent recommended by the manufacturer (appendix A.10) and batch 5 is prepared with acetone. The technical datasheet of the preparation agent of the acrylic adhesive is presented in appendix A.10. It can be concluded that the preparation of the bonded joint is of great influence on the shear strength. If the stress-strain relation of batch 4 is 100%, the stress-strain relation of batch 5 is on average 61.6% of batch 3. When only acetone is used, adhesion is the failure mode of the bonded joint. All specimens prepared with the preparation agent recommended by the manufacturer (appendix A.10) fail cohesively. Failure in the adhesion zone means that the maximum strength of the adhesive has not been reached (section 2.1.2).

Batch 6 versus batch 4

The difference between batch 6 and batch 4 is the thickness of the bonded joint. The bonded joint of batch 4 has a thickness of 3 mm and the bonded joint thickness of batch 6 is 2 mm. If the stress-strain relation of batch 4 is 100%, the stress-strain relation of batch 6 is on average 144.4% of batch 4.

According to [Arenas et al. 2010] the effect of the adhesive thickness on the bond strength of single-lap adhesive joints is still not perfectly understood. Experiments show that the shear strength decreases as the adhesive becomes thicker, and vice versa [Habernicht 2006]. This is explained by various theories (section 2.1.6).

3.1.5 Discussion of the results

The objective was finding a proper structural adhesive, less stiff and thicker than the epoxy applied by Huvener. This should result in a reduction of unfavorable peak stresses and account for tolerances of the applied materials for systems with in-plane loaded adhesively bonded glass panes (section 1.2.1). Six batches were used for shear tests and between the batches each time only one parameter was changed, to be able to compare the results to each other (section 3.1.2).

The aluminum specimens of batch 1 were tested with a displacement velocity of 2.5 mm/min and the aluminum specimens of batch 2 with a displacement velocity of 0.5 mm/min. Due to the lower displacement velocity, relaxation by re-storage of the molecules is possible. At larger velocity, the molecules of the polymer chains have less time to align and re-storage is more prevented than at a lower velocity, which results in a higher stress-strain relation.

Comparison of the shear properties of the steel specimens of batch 3 to the aluminum specimens of batch 2 show that aluminum specimens fail at a lower stress level than specimens of steel. Adherents with a higher (bending) stiffness will reduce the operating peel stresses and take care of a more evenly distributed shear stress in the adhesive (section 2.1.6).

According to [NEN-EN 14869-2:2004], shear tests have to be prepared with an overlap width of 5 mm. Comparison of the acrylic adhesive to future adhesives will be easier if tests are carried out with an overlap of 5 mm. The overlap width of specimens of batch 4 was reduced from 10 mm to 5 mm. Because the loaded area had become less, the adhesive acted as expected less stiff.

Batch 5 was prepared with acetone (appendix A.1). Different from specimens prepared with the preparation agent recommended by the manufacturer (appendix A.10), shear tests with specimens prepared with acetone fail on adhesion (section 2.1.2). This means that the maximum shear strength of the adhesive has not been reached and therefore the shear stiffness is much lower than specimens of batch 4.

Finally the influence of the bonded joint thickness has been reviewed. The bonded joint thickness of batch 6 had been reduced from 3 mm to 2 mm. Although the effect of the adhesive thickness on the bond strength still is not perfectly understood by experts (section 2.1.6), the stiffness of batch 6 is higher compared to the stiffness of batch 4.

As mentioned before, the first batch was executed with a displacement velocity of 2.5 mm/min and could therefore be compared to shear tests done by Huvener. The acrylic adhesive is much less stiff than epoxy, but stiffer than polyurethane and silicone adhesives. The objective of finding a proper structural adhesive with a smaller shear stiffness has only partly been achieved. Two requirements had to be fulfilled, namely: the shear stiffness had to be between 10 N/mm³ and 100 N/mm³ (zone 2) and the thickness had to be as large as possible (section 1.2.1). Based on these two requirements the adhesive manufacturer advised the acrylic adhesive which was at the execution of the shear tests the most proper adhesive available on the market.

To apply for tolerances, the maximum thickness allowed of 3 mm was used in the experiments. The non-linear shear stiffness was much less than the linear stiffness of the epoxy (zone 3) and belongs to zone 1. In the first stage of the relation between the average shear stress and average relative shear strain, the stiffness of the adhesive ($k_{j;\eta/\zeta}$) is 4.51 N/mm³ (table 3.2). The advantage of an adhesive in zone 1 is the uniform shear stress distribution in longitudinal direction ($T_{j;\eta;x/y}$) along the bonded joint and the shear stress distribution in transversal direction ($T_{j;\zeta;x/y}$). This corresponds to the non-linear graph of batch 3 in figure 3.8, where the non-linear relation between the average shear stresses and the average shear strain for the acrylic adhesive is presented. A disadvantage could be that during the experiments on in-plane loaded glass, the adhesive will fail earlier than the glass pane.

3.1.6 Conclusions

Below, the conclusions of the shear tests with the recommended acrylic adhesive are given, which was at the time of the tests the most proper adhesive on the market:

- The average shear stiffness of batch 1 is higher than the average shear stiffness of batch 2. A lower displacement velocity results in a lower stiffness of the adhesive.
- The average shear stiffness of batch 2 is slightly lower than the average shear stiffness of batch 3. Materials of specimens with a larger E-modulus reduce undesirable peel stresses in the adhesive.
- The average shear stiffness of batch 3 is larger than the average shear stiffness of batch 4. A reduction of the bonded joint area reduces the average stiffness of the adhesive bonded joint.
- The average shear stiffness of batch 4 is larger than the average shear stiffness of batch 5. Preparation of the adhesive bonded joint with the preparation agent recommended by the manufacturer of the adhesive, results in a larger average stiffness of the adhesive compared to specimens which were prepared with acetone.
- The average shear stiffness of batch 4 is smaller than the average shear stiffness of batch 6. A reduction of the bonded joint thickness from 3 mm to 2 mm results in a higher stiffness of the adhesive bonded joint.

The objective of finding a proper structural adhesive with a smaller shear stiffness than the epoxy adhesive has only partly been achieved. Two requirements had to be fulfilled, namely: the shear stiffness had to be between 10 N/mm^3 and 100 N/mm^3 (zone 2 in figure 1.5) and the thickness had to be as large as possible (section 1.2.1). The shear stiffness of the adhesive bonded joint (batch 3) which will be applied in the in-plane loaded systems is only 4.51 N/mm^3 (table 3.2). The maximum allowable thickness of the acrylic adhesive is 3 mm and is much better able to account for tolerances of the applied materials when compared to epoxy with a bonded joint thickness of 0.5 mm.

3.2 Complementary shear tests

In this section the influence on the relation between the average shear stress and the relative average displacement of the adhesive is obtained by loading a larger area of the adhesive. The adhesive used for the complementary shear tests is the same acrylic adhesive as described in section 3.1 and appendix A.9. The tests were prepared using the preparation agent (appendix A.10) as recommended by the adhesive manufacturer and tested under the same conditions as described in section 3.1.

3.2.1 Specimens

The complementary shear tests were carried out three times for each batch. Figure 3.11, 3.12 and table 3.2 present the test specimens and their dimensions.

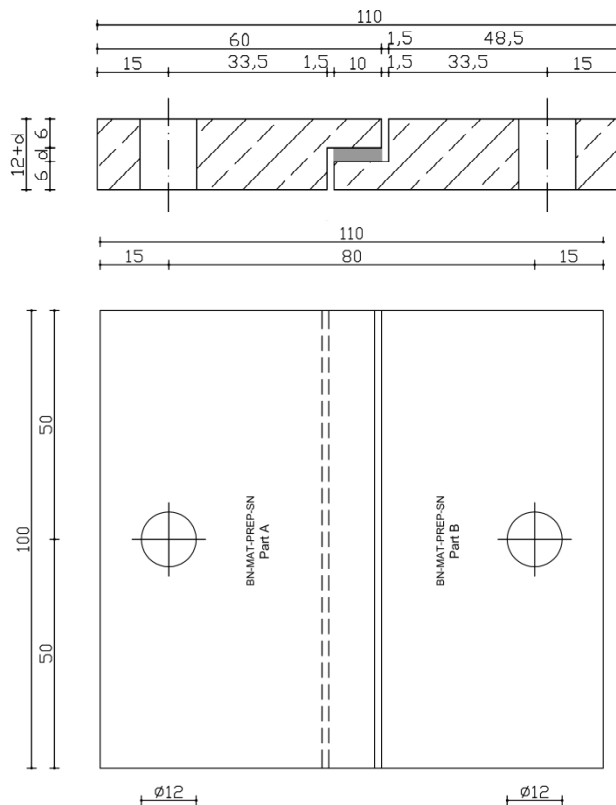


Figure 3.11 Batch 100x10 mm.

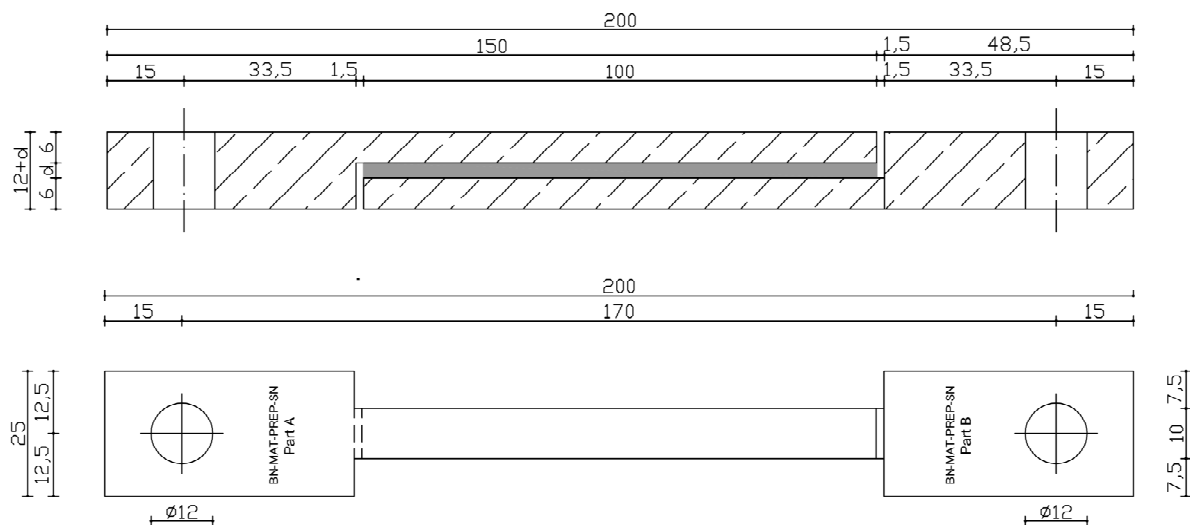


Figure 3.12 Batch 10x100 mm.

Dimensions of the batches:

- L_j [mm] is the length of the bonded joint, in this case 25, 100 mm respectively (deviation is ± 0.5 mm);
- w_j [mm] is the width of the bonded joint, 10 mm and 100 mm respectively (deviation is ± 0.1 mm);
- d_j [mm] is the thickness of the bonded joint, 3 mm (deviation is ± 0.01 mm).

Table 3.2 Overview of properties of the complementary shear tests.

Test Code	Material specimens	Type of Adhesive	W_i [mm]	l_j [mm]	t_j [mm]	RH [%]	T_0 [°C]	T_t [°C]	DV [mm/min]
25x10 (Batch 3)	Steel	Acrylic	10	25	3	60	23	23	0.5
100x10	Steel	Acrylic	10	100	3	60	23	23	0.5
10x100	Steel	Acrylic	100	10	3	60	23	23	0.5

3.2.2 Average shear properties

The relation between the average shear stress and the average relative displacement is obtained using the same procedure as described in section 3.1.3 where the relation of the average shear stress and average shear strain has been deducted. Figures 3.13 and 3.14 present the relation between the average shear stress and the average relative displacement of batch 100x10 and 10x100 respectively. In figure 3.15 the shear properties of the different batches are compared to each other.

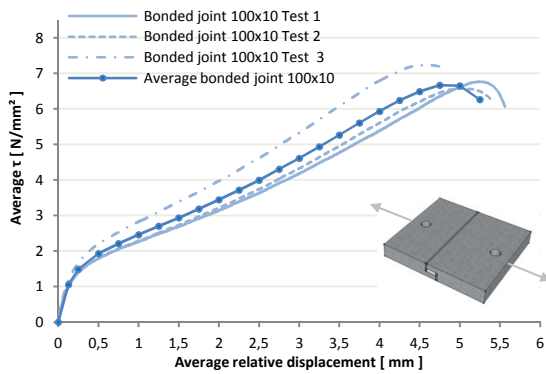


Figure 3.13 Shear properties batch 100x10.

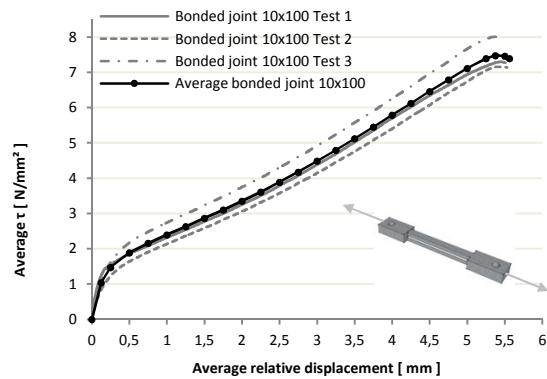


Figure 3.14 Shear properties batch 10x100.

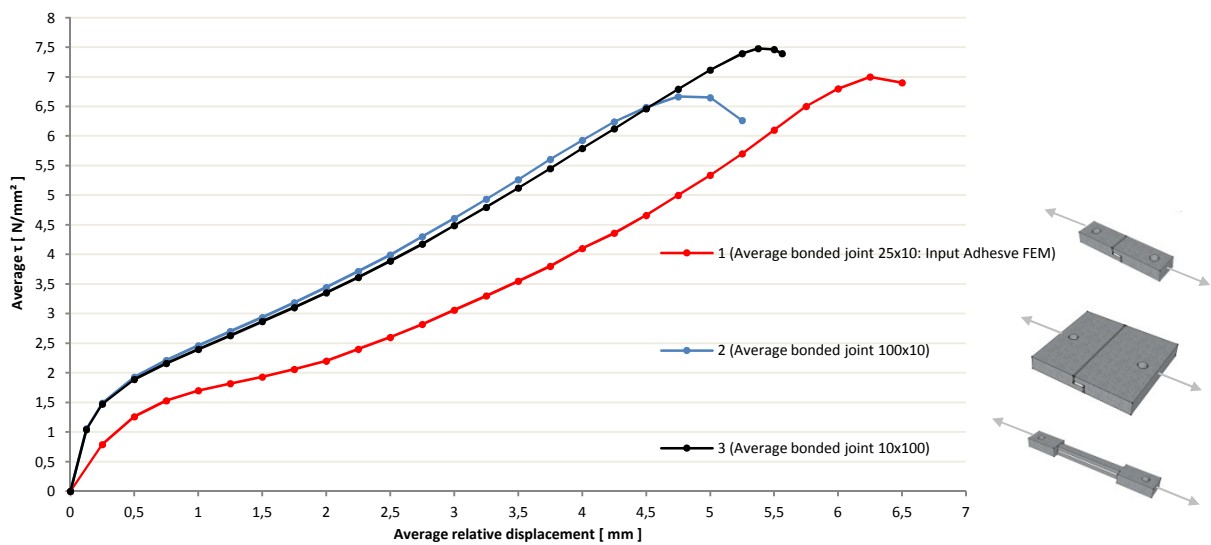


Figure 3.15 Comparison of shear properties.

3.2.3 Conclusions

There are a few differences between the batches:

- The maximum average shear stress of batch 10x100 lays at a higher level than batch 100x10.
- According to figure 3.15 batch 100x10 fails at a smaller value of the average relative displacement than batch 10x100. However this conclusion cannot be made. Test 2 of batch 100x10 strongly influences the average curve (figure 3.13). A larger amount of shear tests are needed to confirm or decline this hypothesis.
- The average relative displacement belonging to the maximum shear stress of the complementary batches is obvious less comparing to batch 25x10 (batch 3). It can be concluded that an adhesive bonded joint with a larger area fails at a smaller value for the average relative displacement.

4 Experiments in- and indicative out-of-plane loaded glass

Eight full-scale experiments have been carried out to explore the behavior of the system. In this chapter these experiments are discussed. Section 4.1 starts to introduce the experiments. Section 4.2 describes the composition of the test rig which enclosed the system. The system, consisting of a steel frame with a two-sided circumferentially adhesive bonded glass pane is described in section 4.3. The measurement technique and test program are presented in section 4.4 and 4.5 followed by the results, which are presented and discussed in section 4.6 for in-plane loaded glass panes and in 4.7 for in- and out-of-plane loaded glass panes. Finally in section 4.8, the conclusions are summed up.

4.1 Introduction

Experiments give valuable information about complex structures and light up important phenomena. Imperfect material behavior can influence the outcome of the experiments and therefore deviate from the expected behavior.

4.2 Test rig

The test rig presented in figure 4.1 was used to enclose the system. The test rig was composed of nine standard wide flange steel HEB 300 members of different lengths, provided with a regular pattern of holes ($\varnothing 26$) in the web and flanges. First two cross beams were placed on the floor of the laboratory and connected to the horizontal bottom beam. These cross beams provided lateral stability of the test rig. The second step consisted of connecting one vertical member on the left on top of the bottom beam. The bottom of this member was provided with a special angled member, to ensure in-plane lateral stability of the test rig. Next two vertical members were connected on both sides of the bottom beam onto the right cross beam. An extra cross member, provided with two angled members, was used to couple the two vertical members directly onto the bottom beam. Also on top of the two vertical members, a cross beam was placed and connected to each other. The last step to complete the test rig was connecting the top horizontal member on top of the left vertical member, and below the top cross member on the right. Because of the higher expected in-plane capacity of the system, a different load jack (600 kN static, 400 kN dynamic), was chosen than used by [Huvener 2009] and connected on the test rig. Between the flanges of the two vertical members where the load jack was connected, thick horizontal lateral buckling bracings were placed, to activate the web and thus protecting the flanges of the members against bending. The centre of the load jack corresponded with the centre line of the load cell and the hinged connections to the left bottom corner (LTC) and right bottom corner (RTC) of the system. All connections between the members of the test rig were made with M24 (10.9) bolts.

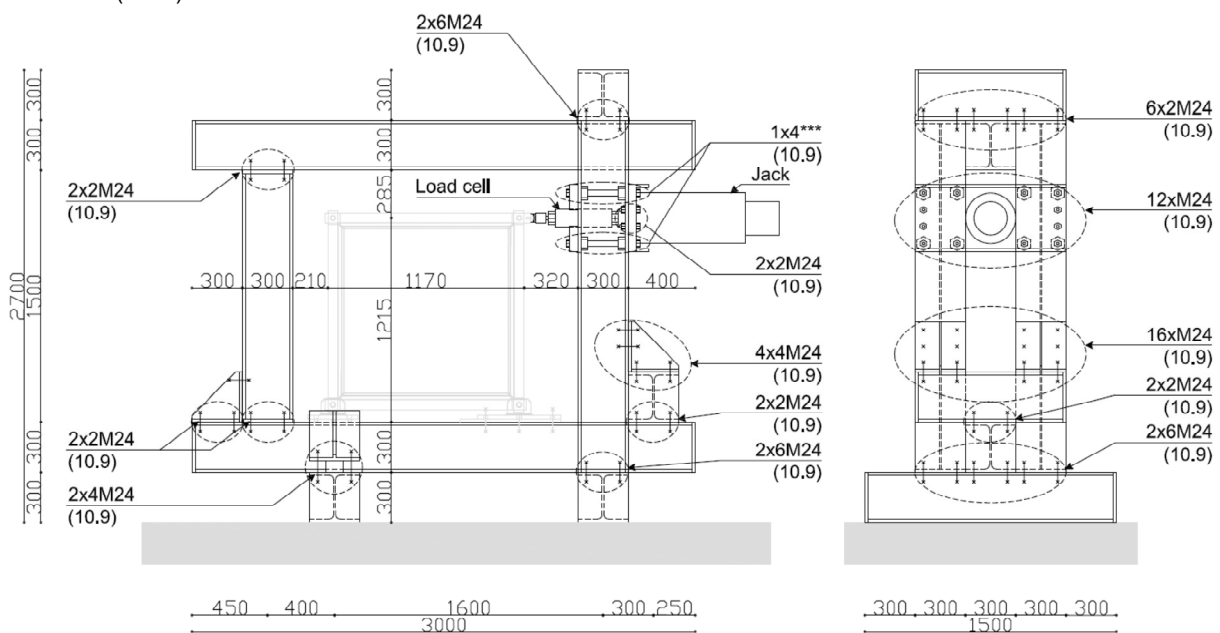


Figure 4.1 Front view (left) and side view (right) of the test rig including the system

4.3 System

Figure 4.2 presents the set-up of the system. The system was loaded horizontally in-plane at the RTC, and supported at the LBC and RBC on the test rig. This section describes the set-up of the system and the method how the glass pane adhesively is bonded to the steel frame.

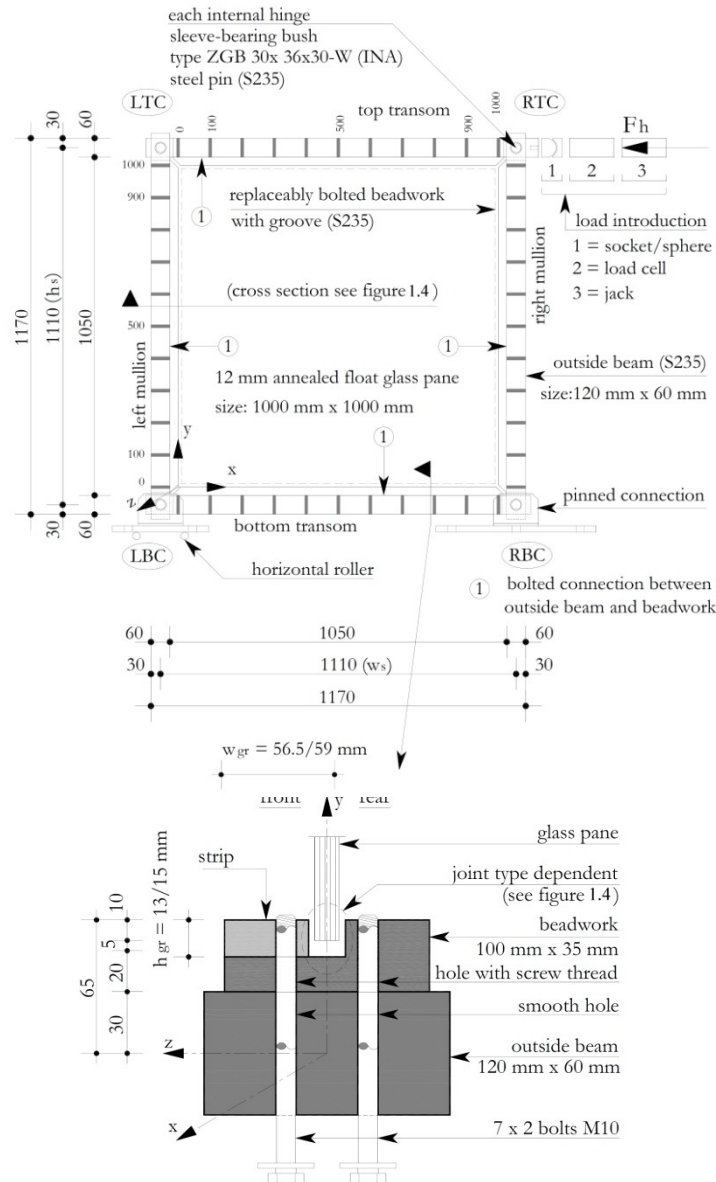


Figure 4.2 Set-up of the system (upper part) and a section of the bottom transom (below) [Huvener 2009].

4.3.1 Steel frame

The steel frame, presented in figure 4.2, is an important part of the system. The in-plane load was introduced by a jack, on an extended pen of the outside beam of the top transom, at the RTC and via the adhesive bonded joint transferred into the glass pane. A socket and sphere were placed on the extended pen for a centric in-plane load introduction. Steel is a ductile material which redistributes stress concentrations at the load introduction, at the supporting structures and at the bolted connection between the outside beam and the beadwork. The steel frame consists of two transoms and two mullions and each of these parts is built up of two components, the outside beam and the replaceable beadwork (figure 4.2). The properties of these components are discussed below and in appendix B.1 the applied components of the steel frame are specified in detail.

Outside beam

The rectangular outside beam has a width $w_{ob} = 120$ mm, a height $h_{ob} = 60$ mm, and is provided with 7x2 smooth holes of 10 mm in diameter for connection with the replaceable beadwork. The outside beams of the transoms are provided with a pin, a round hole and a sleeve-bearing bush at both ends. A sleeve-bearing bush reduces friction under contact pressure. The outside beams of the mullions are provided with a groove and a round hole on both ends. The outside beams of the transoms and mullions are mutual hinged connected with a round pin of 30 mm in diameter. The hinged connection at the RBC and the horizontal roller connection at the LBC are also connected to these pins and support the system to the test rig. The pinned connection was bolted with 4 M24 (10.9) and 2 M10 (10.9) to the test rig. The horizontal roller connection is prepared using three round bars 20 mm in diameter.

Beadwork

The beadwork was provided with 7x2 holes with screw thread and connected with M10 (10.9) bolts via the outside beam. The strips, provided with slotted holes, on the front of the beadwork were also connected with M10 (10.9) bolts to the beadwork. The edges of the beadwork, including the strips, were provided with a mitre and a small seam between the ends of the beadwork was made to avoid steel-steel contact (figure B.5). To ensure that all bolts were evenly tightened, a torque wrench was used. The beadwork was made replaceable for two reasons. The first reason was that the groove of the beadwork in [Huvener 2009] was joint type dependent (figure 1.4). The second reason had to do with safety aspects. After each test the beadwork was removed to be able to burn the adhesive from the beadwork in a well ventilated environment with reference to noxious fumes.

4.3.2 Glass pane

Both annealed float and heat strengthened glass panes were tested. The square glass panes had a height of $h_g = 1.0$ m and a width $w_g = 1.0$ m and the nominal glass pane thickness $t_{g;n}$ was 12 mm. The parameter study of [Huvener 2009] showed that square ANG panes with a width and height of 1.0 m and a nominal thickness of 12 mm are less susceptible for out-of-plane displacements (figure 4.3). The out-of-plane displacements (w_{centre}) of thinner glass panes, rectangular glass panes and square glass panes with a larger geometry become larger.

The glass panes were provided with facets on both sides with an angle about 45° in the factory of the glass supplier. ANG has a lower strength compared to HSG, but when laminated it has a favorable crack pattern needed for residual capacity (figure 2.26).

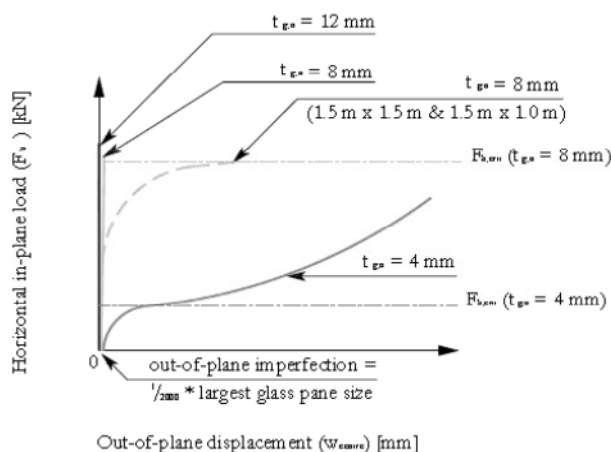


Figure 4.3 Relation of horizontal in-plane load and out-of-plane displacement for different glass pane sizes [Huvener 2009].

4.3.3 Adhesive bonded joint

According to [Huveners 2009] an adhesive bonded joint is a proper joining technique for glass structures, in spite of well known disadvantages e.g. aging. Main benefits of adhesive bonded joints are uniform in-plane load introduction in the glass pane and to avoid direct glass steel contact. Huveners recommended a structural adhesive less stiff than epoxy to eliminate the unfavorable peak stresses, and a thicker adhesive bonded joint to account for tolerances of the glass pane and steel frame (section 1.2.1). In chapter 3 the shear properties of the acrylic adhesive were reported and the test results are discussed. A basic assumption in the research of Huveners was that the geometry of the adhesive bonded joint was kept as small as possible for the benefit of maximum transparency. To compare the results to each other only the thickness of the adhesive is adjusted according to joint type 2 (figure 1.4).

4.4 Measurements

4.4.1 Geometry of the glass pane

The thickness of the glass pane is measured at eight points, presented in figure 4.4. Beside the thickness of the glass pane, also the height, width and the out-of-plane imperfection of the glass pane is measured at certain points. The procedure how the out-of-plane imperfection is measured and remaining data are presented in appendix B.3.

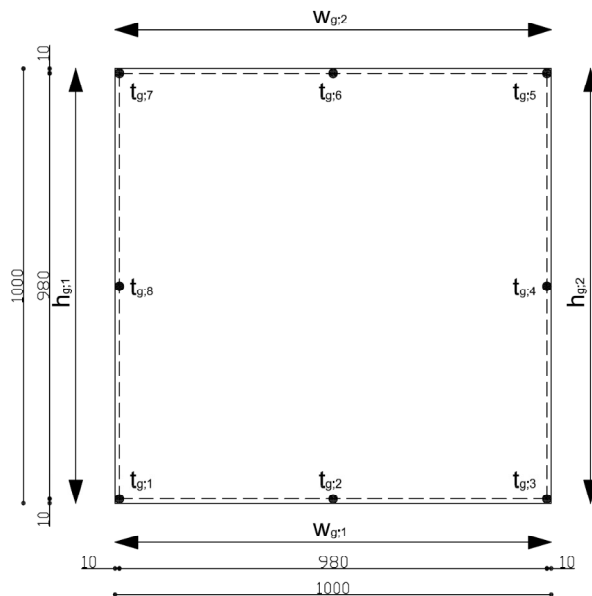


Figure 4.4 Measurement of actual glass thickness at point 1 to 8 and the actual glass pane size.

4.4.2 Response of the system

The jack at the RTC of the system was displaced with a speed of 1 mm/min. The response of the system was monitored using several measuring equipment (figure 4.5). Displacement gauges (linear variable displacement transducers, LVDT's) were used to measure the vertical and horizontal in-plane movement of the system (V_{RTC} , V_{LTC} , V_{RBC} , V_{LBC} , U_{RBC} and U_{LBC}) and the out-of-plane displacements (W_{RTC} , W_{LTC} , W_{CENTRE}). In the middle of each transom and mullion, the relative displacement between the glass and the strip of the beadwork and the beadwork itself and the relative displacement between the outside beam and the beadwork ($V_{MR,rel}$, $V_{ML,rel}$, $U_{MT,rel}$ and $U_{MB,rel}$) were also measured using LVDT's. Strain gauges were applied on the points 1 to 5 (figure 4.5) to measure the strain level during the experiments. At these points, the influence of the shear flexibility of the steel frame and the adhesive bonded joint on the principle stress distribution is minimized and has a two-dimensional stress state [Huvener 2009]. The electrical signals of the strain gauges were corrected by a K-factor given by the supplier of the strain gauges. The horizontal in-plane force was measured with a load cell.

The analogue signals from the different measurement equipment were processed by a data acquisition unit which communicated with a personal computer. The measurements were taken at an interval of 1.5 seconds. All data was then assembled in an ASCII output file.

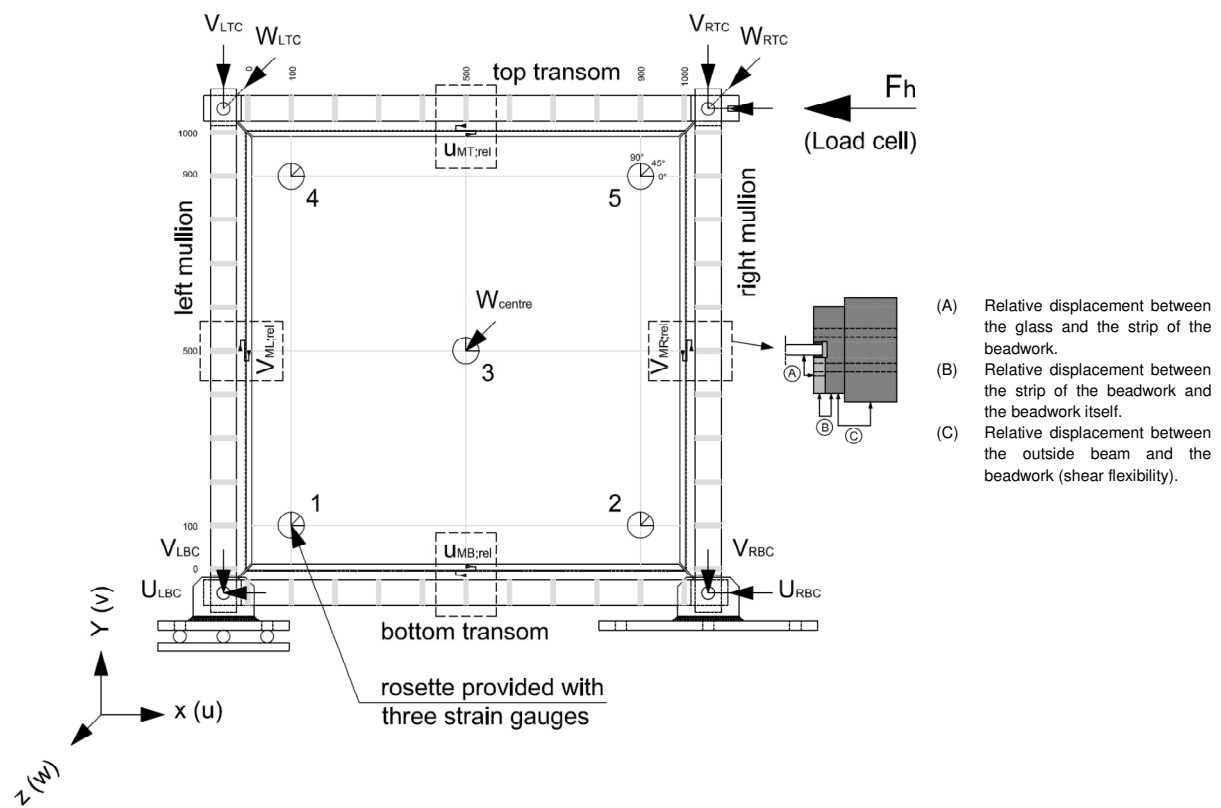


Figure 4.5 Response of the system measured at the several points of interest.

4.4.3 Boundary conditions of the supporting structures

The boundary conditions of the system can be influenced by the supporting structure. During the experiments the movements of several points of interest were measured. Figure 4.6 shows the vertical displacements of the horizontal roller (LBC) and the pinned connection (RBC). The positive vertical displacement of the RBC due to loading at the RTC causes the entire system to rotate in the direction of the load (to the left). This enlarges the horizontal displacement of the RTC of the system and cannot be neglected.

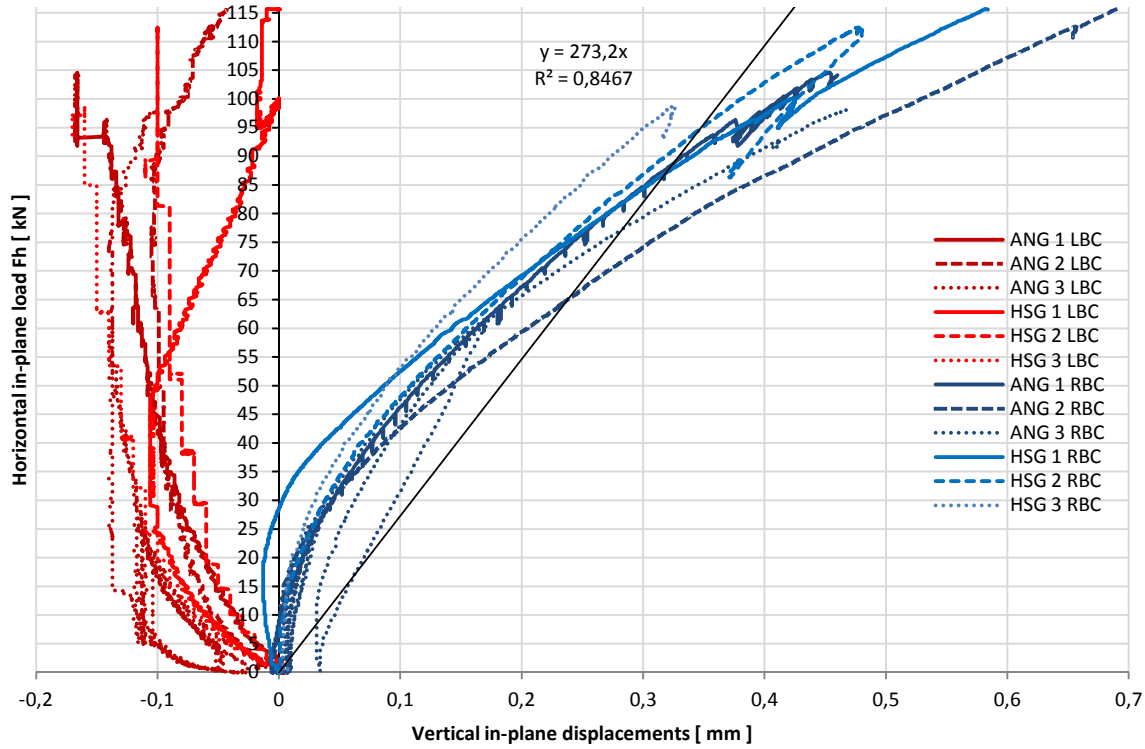


Figure 4.6 Relation between the in-plane load at the RTC and the vertical displacements of the horizontal roller (LBC) and the pinned connection (RBC) (a negative displacement means a movement downwards and a positive displacement means a movement upwards of the measured point).

To eliminate the rotation caused by the vertical displacement at the RBC equation 4.1 can be used. The non linear relation between the horizontal in-plane load and the vertical displacement of the RBC is translated into a linear spring stiffness. A linear trend line was applied in the non-linear relation between the horizontal in-plane load and the vertical in-plane displacement of the RBC of the first ANG pane experiment (ANG 1 RBC), which is according to figure 4.6 about the average of all experiments.

The linear spring stiffness is obtained by the formulae of the trend line in figure 4.6 ($K_{y;RBC} = 2.73 \times 10^5 \text{ kN/mm}$), and is used in FE simulations (section 5.3.2).

$$u_{RTC;s} = u_{RTC} - \frac{F_h}{K_{y;RBC}} \left(\frac{h_s}{w_s} \right)^2 \quad (\text{Equation 4.1})$$

Where:

- $u_{RTC;s}$ is the horizontal displacement of the RTC;
- u_{RTC} is the horizontal displacement of the RTC including the effect of the vertical displacement of the RBC caused by the rotation of the system;
- F_h is the horizontal in-plane load;
- $K_{y;RBC}$ is the linear spring stiffness accounting for the vertical displacement of the RBC (figure 4.6);
- h_s is the height of the system;
- w_s is the width of the system.

4.4.4 Behavior of the bolted connection between the outside beam and the beadwork.

The transoms and mullions of the steel frame were built up of an outside beam and a beadwork connected with bolts (section 4.3.1). The bolted connection consists of 14 bolts M10 which are placed in slightly larger holes of the outside beam (figures A.1 up to A.3) and is screwed in the beadwork. This means that every bolt has a small clearance which makes a small sliding between the outside beam and the beadwork possible.

During the experiments the relative displacement between the outside beam and the beadwork is measured at four points, each in the middle of the transom or mullion (figure 4.5). The relative displacement between the outside beam and the beadwork during the experiments never exceeded 0.7 mm. This is also applicable to the relative displacement between the strip of the beadwork and the beadwork itself.

The response of the bolted connection was checked by [Huvener 2009] with a four-point bending test (figure 4.7) and confirmed that there is shear flexibility between the outside beam and the beadwork due to the clearance in the holes, which reduces the flexural stiffness of the transom and mullions. A FE model, corresponding to the properties of the four-point bending test, was used to find the shear flexibility (try and error, figures 4.8 to 4.10) and was applied in the FE model for the simulations of the system ($k_{b,\eta} = 10 \frac{N}{mm^3}$).

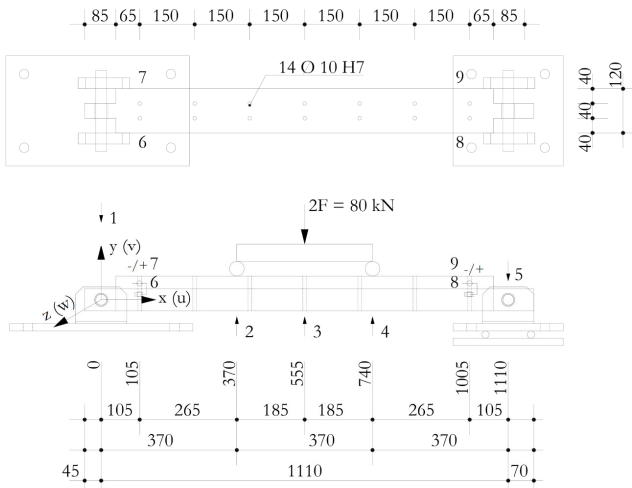


Figure 4.7 Four point bending test for the determination of the flexural stiffness of the transoms and mullions [Huvener 2009].

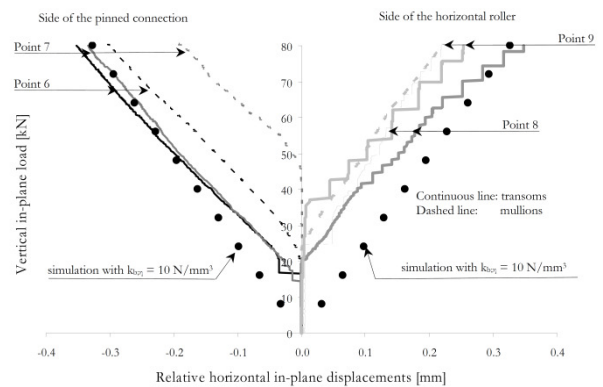


Figure 4.8 Relation between the vertical in-plane load and the relative horizontal in-plane displacements between the outside beam and the beadwork at points 6 to 9 [Huvener 2009].

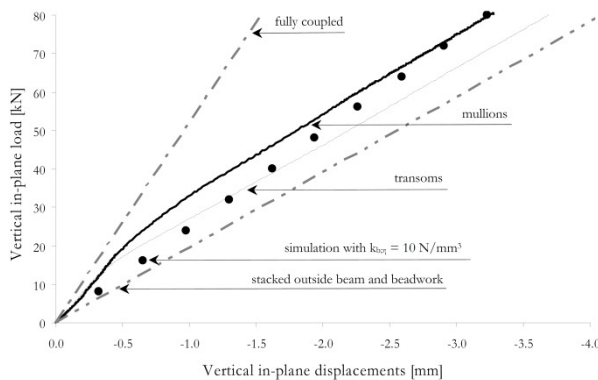


Figure 4.9 Relation between vertical in-plane load and the vertical the vertical displacement at point 3 [Huvener 2009].

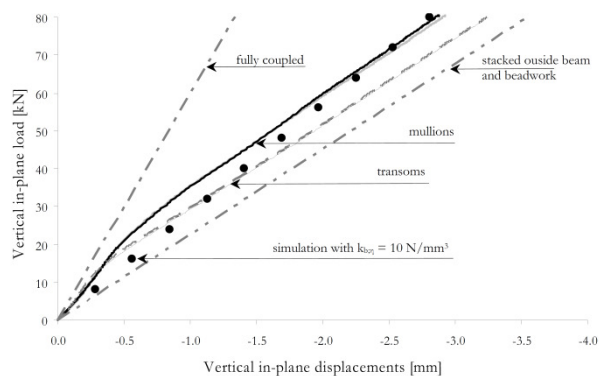


Figure 4.10 Relation between vertical in-plane load and displacement at points 2 and 4 [Huvener 2009].

4.5 Measurements basics

4.5.1 In-plane stiffness of the system

The in-plane stiffness of the system can be determined using equation 4.2. The In-plane stiffness of stabilizing elements is an important factor to calculate the stability of a building and in chapter 6 the in-plane stiffness of the system is calculated using mechanical models.

$$K_s = \frac{F_h}{u_{RTC;s}} \quad (\text{Equation 4.2})$$

Where:

K_s is the in-plane stiffness of the system;
 F_h is the horizontal in-plane load;
 $u_{RTC;s}$ is the horizontal displacement of the RTC.

4.5.2 Principle stresses

For a brittle material as glass the failure criterion is the maximum principle (tension) stress (section 2.2.3). To determine the principle stresses at several points in the glass pane, strain gauge rosettes were used.

To be able to compare the principle stresses to the experiments of [Huvener 2009] the rosettes are placed at the same points. The rosettes at points 1 to 5, presented in figure 4.5, measured the horizontal strain (ε_{0°), the vertical strain (ε_{90°) and the strain at an angle of 45° (ε_{45°) (figure 4.11). The strain gauges are placed on a sufficient distance with respect from the edges of the glass pane and therefore it can be considered as a two-dimensional strain/stress state. Equation 4.3 can be used to calculate the maximum principle stress ($\sigma_{g;1}$) and the minimal principle stress ($\sigma_{g;2}$). Equation 4.4 gives the angle (θ) of the maximum principle stress with the horizontal.

$$\sigma_{g;1,2} = \frac{E_g}{2(1-\nu_g)} \left[(\varepsilon_{0^\circ} + \varepsilon_{90^\circ}) + \sqrt{2(\varepsilon_{90^\circ} - \varepsilon_{45^\circ})^2 + 2(\varepsilon_{0^\circ} - \varepsilon_{45^\circ})^2} \right] \quad (\text{Equation 4.3})$$

$$\tan 2\theta = \frac{(2\varepsilon_{45^\circ}) - \varepsilon_{90^\circ} - \varepsilon_{0^\circ}}{(\varepsilon_{0^\circ} - \varepsilon_{90^\circ})} \quad (\text{Equation 4.4})$$

The Young's modulus (E_g) and the Poisson's ratio (ν_g) of the glass were not measured during the experiments. The values assumed are given in table 2.3.

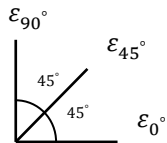


Figure 4.11 Rosette with strain gauges in three directions

4.6 Results in-plane loaded glass

4.6.1 Annealed float glass

Three experiments were carried out with annealed float glass. Figure 4.12 shows the relation between the horizontal in-plane load and the horizontal in-plane displacement of the RTC.

In the first two experiments the system was loaded till the glass pane failed. The line describing the test result of the first experiment is a bit nervous. By adjusting the setup of the PID controller (section 4.4.2) the lines of the following tests were much smoother. The behavior of the system due to loading and unloading was obtained during the third experiment. The system was loaded till a displacement of the RTC of 1 mm and then unloaded till the in-plane load dropped to zero. Next the system was again loaded till a displacement of the RTC of 2 mm and then unloaded till the in-plane load dropped to zero. This procedure was repeated 3 times at a displacement of the RTC of 3 mm and once at a displacement of the RTC of 5 mm. Finally the system was loaded till failure of the glass pane.

The loop which occurs during loading and unloading is a phenomenon called elastic hysteresis or damping. The area of this hysteresis loop represents the energy that dissipates per cycle, and is a measure of the damping properties of the applied adhesive. The effect of hysteresis due to loading and unloading on the behavior of the system is not further investigated in this thesis.

In the first stage of the test the relation between the horizontal in-plane load and the horizontal in-plane displacement of the RTC is non-linear. Next the stiffness of the system drops but the relation of the horizontal in-plane load and the horizontal in-plane displacement at the RTC becomes linear. Finally the glass pane fails due to glass steel contact at the RTC of the system. Figure 4.13 shows the moment before fracture of the glass pane recorded by a high speed camera. Within four thousands of a second the crack grows from its origin at the RTC and disperses to the LBC (figure 4.14). This behavior is representative for all experiments with ANG panes.

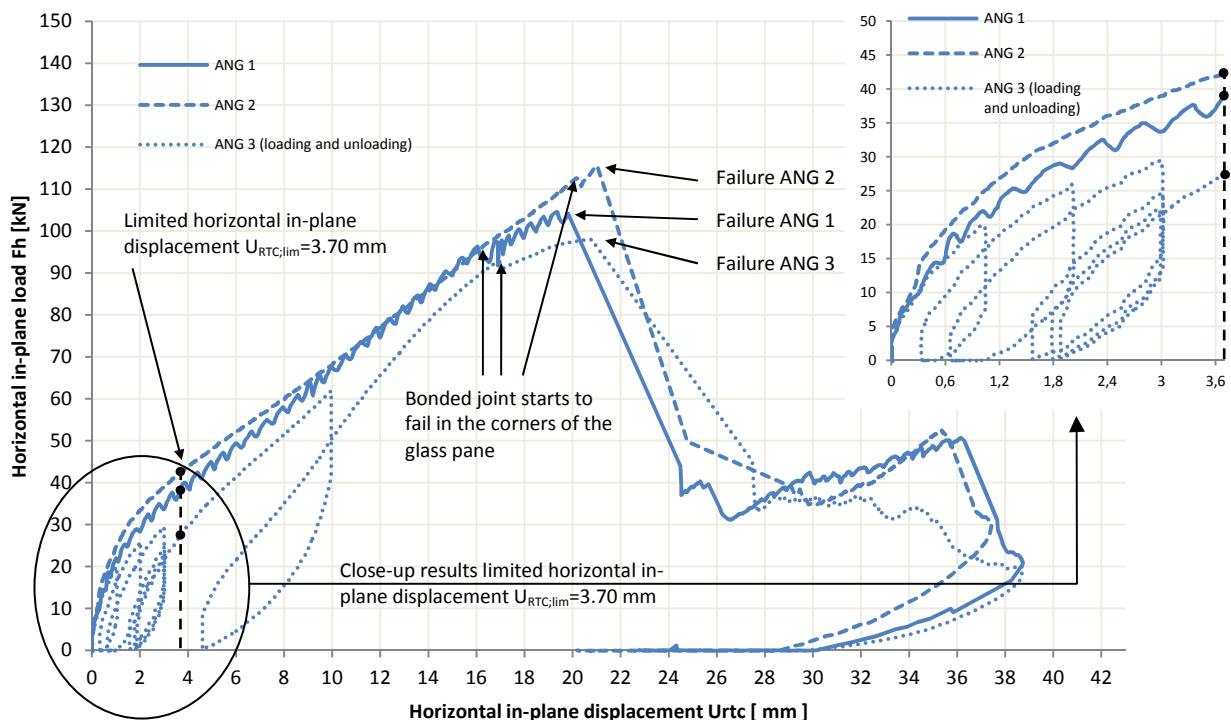


Figure 4.12 The relation between the horizontal in-plane load and the horizontal in-plane displacement u_{RTC} of ANG panes.

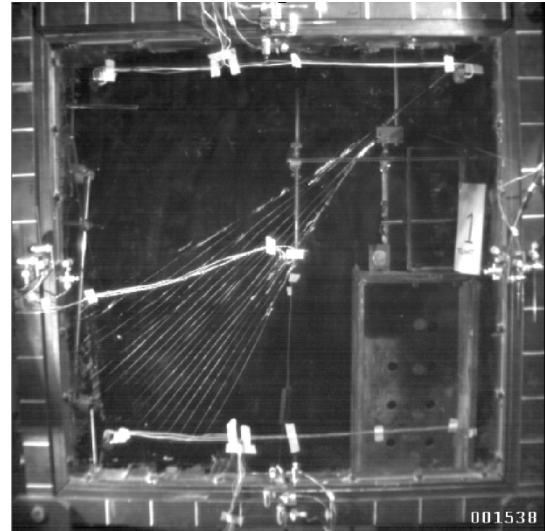
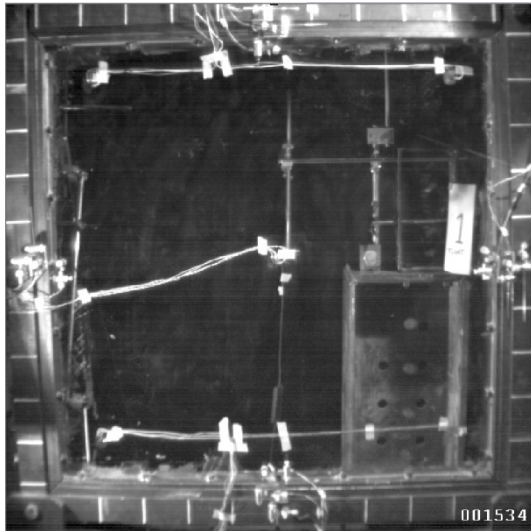


Figure 4.13 (left) Un-cracked glass pane one four thousand of a second before moment of fracture.

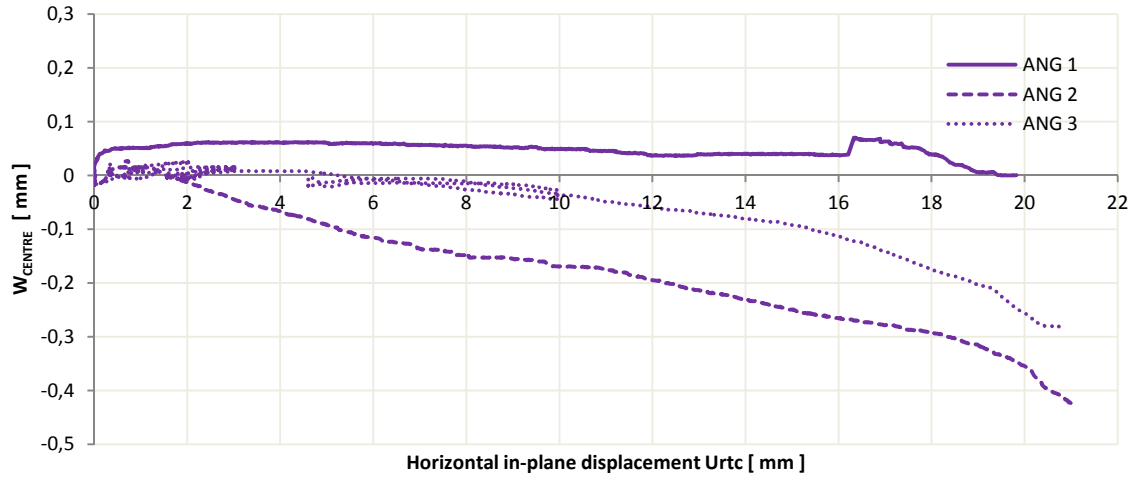
Figure 4.14 (right) Failure of the glass pane of test 1 due to glass steel contact at the right top corner of the glass pane.

For square systems with glass panes of one by one meter, the horizontal in-plane displacement of the RTC of the system has to be limited, because of service life restrictions according to [NEN 6702:2007]. The limited horizontal in-plane displacement of the RTC of the system is $\frac{1}{300}$ of the height of the system ($u_{RTC;lim} = 3.70 \text{ mm}$).

In table 4.1 an overview of the measured results at limited and maximum horizontal in-plane displacement at the RTC of the system (u_{RTC}) are given. As explained in section 4.4.3 u_{RTC} is the horizontal displacement of the RTC including the effect of the vertical displacement of the RBC caused by the rotation of the system. This effect is eliminated in $u_{RTC;s}$. The stiffness K_s is the quotient of F_h and $u_{RTC;s}$. w_{centre} is the out of plane displacement of the glass pane and the development during the experiments is presented in figure 4.15. The relative displacements $u_{MT;rel}$, $u_{MB;rel}$, $u_{ML;rel}$ and $u_{MR;rel}$ are the relative displacements of the glass and the strip of the beadwork, the strip of the beadwork and the beadwork itself and the outside beam and the beadwork (figure 4.5). u_{LBC} is the horizontal in-plane displacement of the LBC (section 4.4.2). To clarify the response of the system, behind the displacements the direction of the displacements are given.

Table 4.1 Overview of measuring results of annealed float glass at limited and maximum u_{RTC} .

Test		ANG1		ANG2		ANG3	
Limited u_{RTC}	u_{RTC} [mm]	3,69	(left)	3,70	(left)	3,71	(left)
	F_h [kN]	38,84		42,34		27,47	
	$u_{RTC;s}$ [mm]	3,55	(left)	3,54	(left)	3,61	(left)
	K_s [kN/mm]	10.81		11.96		7.61	
	w_{centre} [mm]	0,06	(back)	0,06	(front)	0,01	(back)
	$u_{MT;rel}$ [mm]	1,21	(left)	1,03	(left)	1,14	(left)
	$u_{MB;rel}$ [mm]	0,88	(left)	0,68	(left)	0,79	(left)
	$u_{ML;rel}$ [mm]	0,90	(down)	0,88	(down)	0,99	(down)
	$u_{MR;rel}$ [mm]	0,85	(up)	0,82	(up)	0,85	(up)
u_{LBC} [mm]	0.04	(left)	0,04	(left)	0,04	(left)	
Maximum u_{RTC}	u_{RTC} [mm]	19,82	(left)	21,02	(left)	20,78	(left)
	F_h [kN]	104,12		115,56		98,05	
	$u_{RTC;s}$ [mm]	19,44	(left)	20.60	(left)	20.42	(left)
	K_s [kN/mm]	5.36		5.61		4.80	
	w_{centre} [mm]	0,00		0,43	(front)	0,28	(front)
	$u_{MT;rel}$ [mm]	x	(left)	5,67	(left)	5,39	(left)
	$u_{MB;rel}$ [mm]	x	(left)	4,71	(left)	5,11	(left)
	$u_{ML;rel}$ [mm]	x	(down)	5,32	(down)	5,67	(down)
	$u_{MR;rel}$ [mm]	5,02	(up)	5,07	(up)	x	(up)
u_{LBC} [mm]	0,6	(left)	1,16	(left)	0,08	(left)	



4.15 Development of out-of-plane displacements in the centre of the glass pane during experiments with annealed float glass.

Figure 4.16 shows the maximum principle stresses ($\sigma_{g,1}$), the minimum principle stresses ($\sigma_{g,2}$) and their direction (θ) at limited and maximum horizontal in-plane displacement of the RTC (u_{RTC}). The largest maximum and minimum principle stresses can be found at point 3 (centre), except for the largest minimum principle stress for test 2 at maximum horizontal in-plane displacement. The strain gauge at point 3 failed during the test and therefore no results are given at maximum u_{RTC} . A complete overview of the principle stress development per point can be found in appendix B.5.

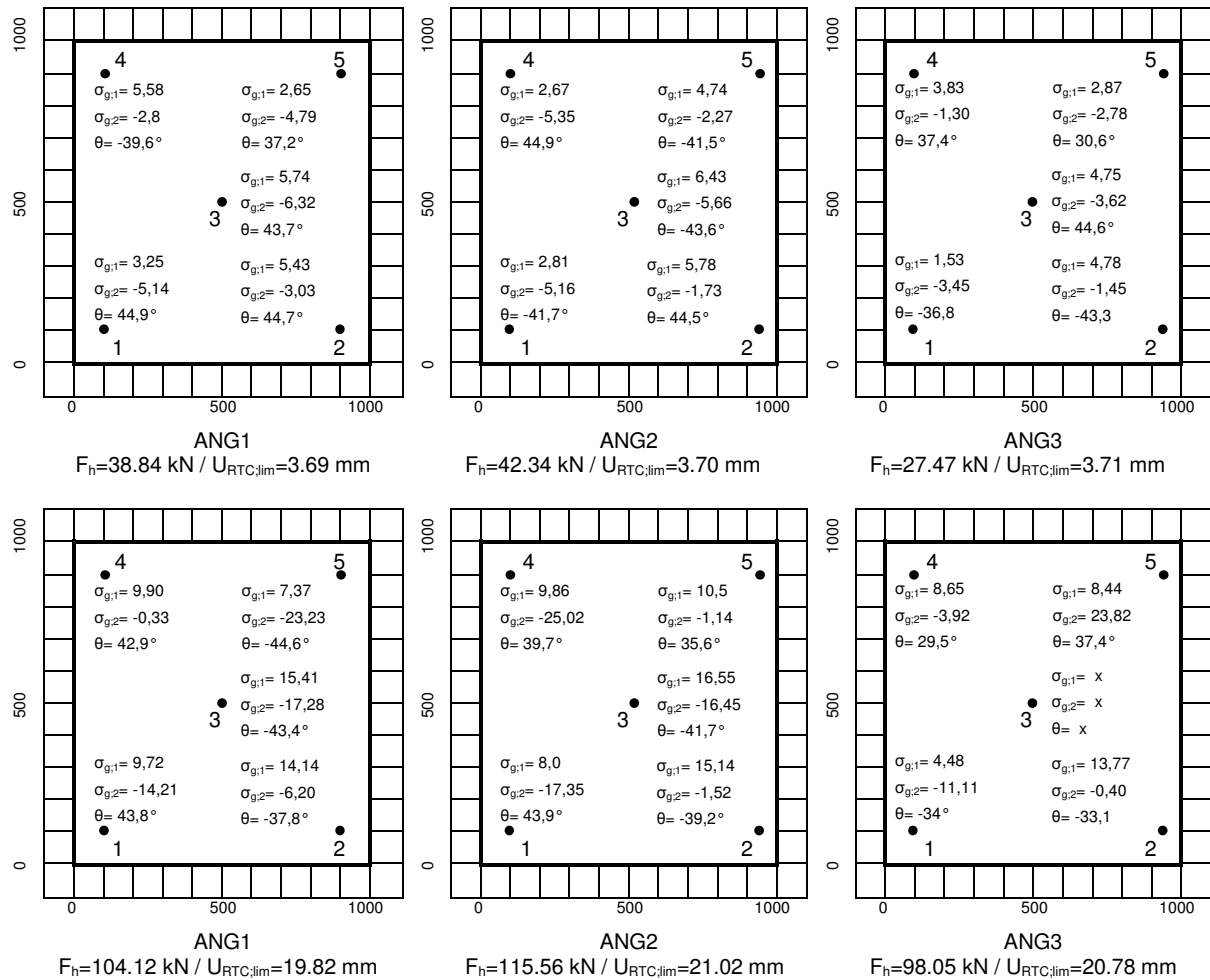


Figure 4.16 Overview of the principle stresses and their directions for ANG at limited u_{RTC} and just before the moment of failure.

4.6.2 Heat strengthened glass

Besides experiments with annealed float glass, also three experiments with heat strengthened glass have been carried out. Figure 4.17 shows the relation between the horizontal in-plane load (F_h) and the horizontal in-plane displacement of the RTC (u_{RTC}).

The system of each experiment was loaded till the glass pane failed. In the first stage of the tests the relation between the horizontal in-plane load and the horizontal in-plane displacement of the RTC is non-linear. Next the stiffness of the system drops but the relation of the horizontal in-plane load and the horizontal in-plane displacement at the RTC becomes linear. This behavior of systems with HSG is similar to ANG.

At a certain point the slope of the graph becomes horizontal and the glass pane shifts along the failed adhesive. Before the HSG pane fails due to glass steel contact at the RTC of the system, the negative or almost zero slope of the relation between the horizontal in-plane load and the horizontal in-plane displacement of the RTC, switches sign and becomes positive. This effect did not occur with ANG panes and can be explained referring to the higher representative flexural tension strength for HSG panes (section 2.2.3).

After the first crack had appeared in the glass pane, the crack grows within four thousands of a second from its origin at the RTC and disperses to the LBC (figures 4.18 to 4.20). The fracture pattern of HSG panes is different from ANG panes in the sense that HSG panes show smaller fracture fragments (section 2.2.2.1) and that the path of the fracture is curved instead of straight lines.

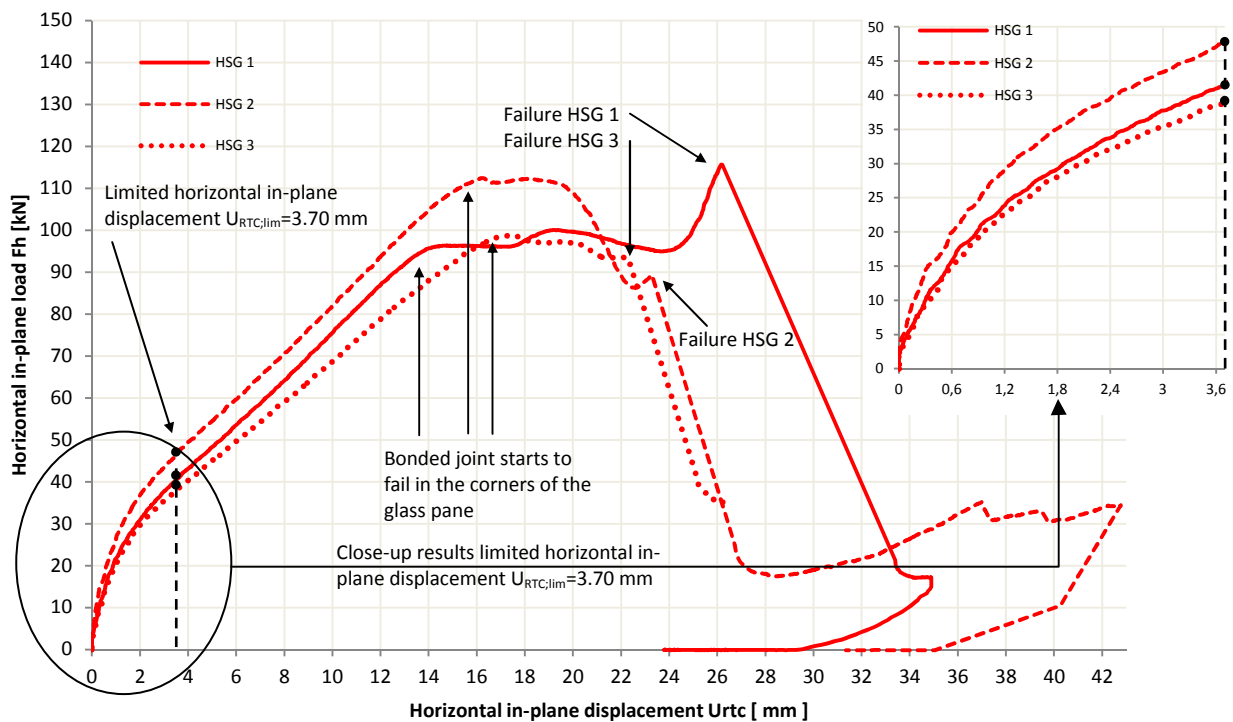


Figure 4.17 The relation between the horizontal in-plane load and the horizontal in-plane displacement u_{RTC} of HSG panes.

In table 4.2 an overview of the measured results at limited and maximum horizontal in-plane displacement at the RTC of the system (u_{RTC}) are given. As explained in section 4.4.3 u_{RTC} is the horizontal displacement of the RTC including the effect of the vertical displacement of the RBC caused by the rotation of the system. This effect is eliminated in $u_{RTC;s}$. The stiffness K_s is the quotient of F_h and $u_{RTC;s}$. W_{centre} is the out of plane displacement of the glass pane and the development during the experiments is presented in figure 4.21.

The relative displacements $u_{MT;rel}$, $u_{MB;rel}$, $u_{ML;rel}$ and $u_{MR;rel}$ are the relative displacements of the glass and the strip of the beadwork, the strip of the beadwork and the beadwork itself and the outside beam and the beadwork (figure 4.5). U_{LBC} is the horizontal in-plane displacement of the LBC (section 4.4.2). To clarify the response of the system, behind the displacements the direction of the displacements are given.

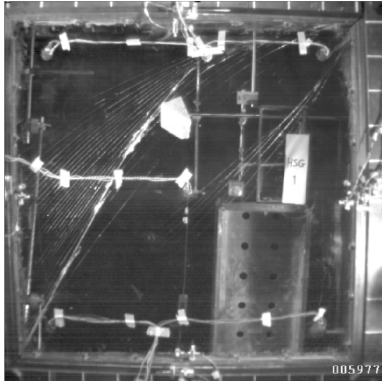


Figure 4.18 Fracture pattern experiment HSG 1

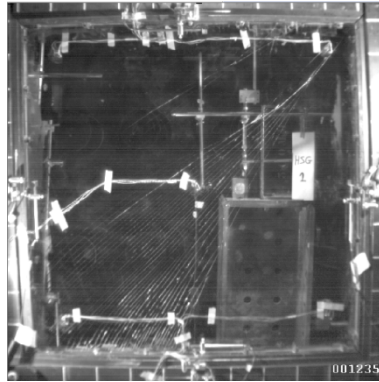


Figure 4.19 Fracture pattern experiment HSG 2

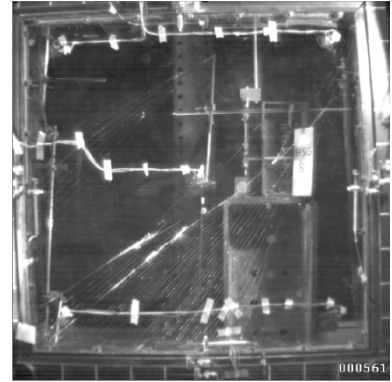
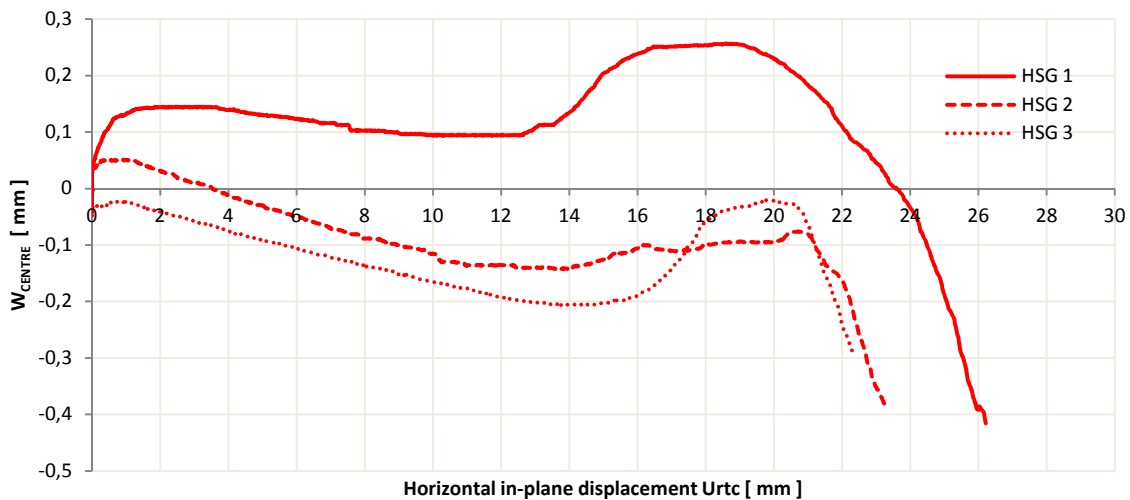


Figure 4.20 Fracture pattern experiment HSG 3

4.2 Overview of measuring results of heat strengthened glass at limited and maximum U_{RTC} .

Test		HSG1		HSG2		HSG3	
Limited U_{RTC}	U_{RTC} [mm]	3,70	(left)	3,71	(left)	3,70	(left)
	F_h [kN]	41,53		47,97		38,95	
	$U_{RTC;s}$ [mm]	3.55	(left)	3.53	(left)	3.56	(left)
	K_s [kN/mm]	11.7		13.59		10.94	
	w_{centre} [mm]	0,14	(back)	-0,01	(front)	0,07	(front)
	$u_{mT;rel}$ [mm]	1,04	(left)	1,09	(left)	1,22	(left)
	$u_{mB;rel}$ [mm]	0,76	(left)	0,95	(left)	0,69	(left)
	$u_{ML;rel}$ [mm]	0,91	(down)	0,97	(down)	0,85	(down)
Maximum U_{RTC}	U_{RTC} [mm]	26,22	(left)	23,28	(left)	22,30	(left)
	F_h [kN]	115,59		89,40		93,37	
	$U_{RTC;s}$ [mm]	25.80	(left)	22.95	(left)	21.96	(left)
	K_s [kN/mm]	4.48		3.90		4.25	
	w_{centre} [mm]	-0,42	(front)	0,39	(front)	0,29	(front)
	$u_{mT;rel}$ [mm]	5,41	(left)	x	(left)	x	(left)
	$u_{mB;rel}$ [mm]	5,57	(left)	5,73	(left)	5,51	(left)
	$u_{ML;rel}$ [mm]	5,48	(down)	6,57	(down)	5,73	(down)
	$u_{MR;rel}$ [mm]	5,31	(up)	6,96	(up)	6,88	(up)
	u_{LBC} [mm]	0,12	(left)	0,14	(left)	0,32	(left)



4.21 Development of the out-of-plane displacements in the centre of the glass pane during experiments with HSG.

Figure 4.22 shows the maximum principle stresses ($\sigma_{g,1}$), the minimum principle stresses ($\sigma_{g,2}$) and their direction (θ) at limited and maximum horizontal in-plane displacement of the RTC (u_{RTC}). The largest maximum principle stresses can be found at point 3 (centre), except for test 1 at maximum horizontal in-plane displacement and test 3 for both limited and maximum horizontal in-plane displacement. A complete overview of the principle stress development per point can be found in appendix B.5.

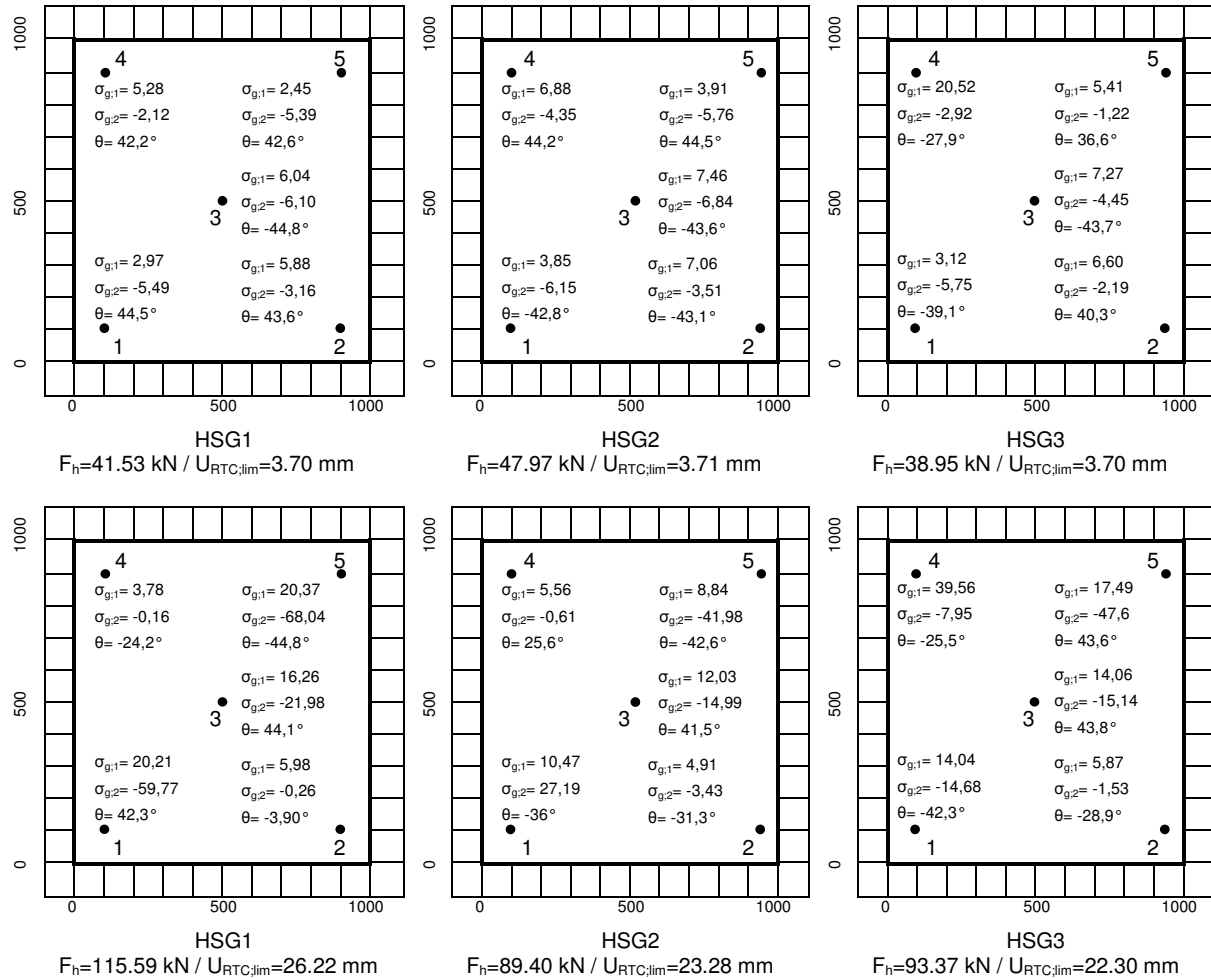


Figure 4.22 Overview of the principle stresses and their directions for HSG at limited u_{RTC} and just before the moment of failure.

4.6.3 Discussion of the results of in-plane loaded glass

Figure 4.23 presents the results of all six experiments of in-plane loaded glass. Up to the point where the slope of the results of heat strengthened glass becomes horizontal, the experiments show the same behavior with a certain spread.

HSG panes show more resistance at glass steel contact compared to ANG, which fail immediately. In [Huvener 2009] systems with ANG panes bonded to the steel frame with joint type one showed large resistance at glass steel contact (figure 4.28). Obviously, the polyurethane adhesive introduces the stresses more gradually into the glass pane at glass-steel contact. To enlarge the residual capacity of the system, joint type one and joint type two should be combined, using the polyurethane adhesive at the position like in joint type one and using the acrylic adhesive as applied (joint type two).

Remarkable is the point where the slope of the load-displacement curve of heat strengthened glass becomes horizontal. This only occurs when HSG panes are used. A plausible answer can explain this behavior, but cannot be confirmed experimentally. HSG panes are partly tempered ANG panes and compression stresses at the surface suppress the surface flaws (section 2.2.2.1). This process decreases the adhesion of the acrylic adhesive to the glass pane. In the corners of the bonded joint, the adhesive has suffered the largest relative in-plane displacement (section 5.7.1) and here the cohesive failure of the adhesive bonded joint starts. Locally, the bonded joint can also fail on adhesion.

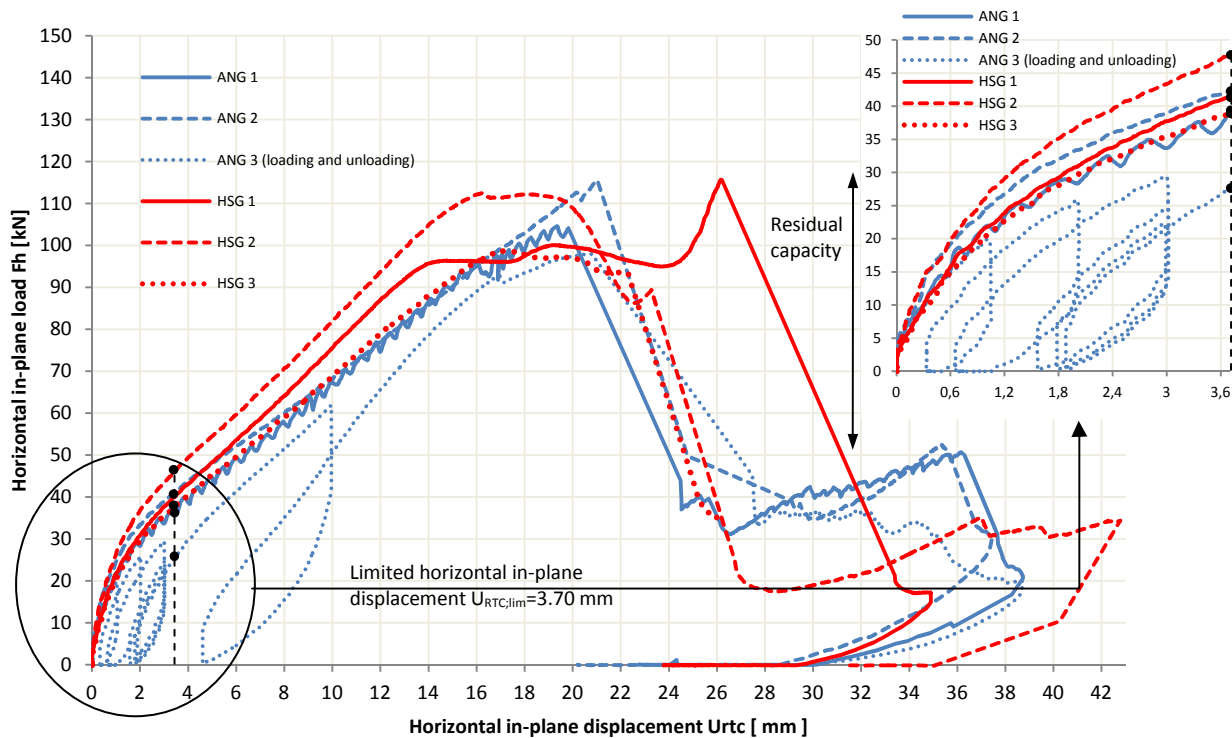


Figure 4.23 Relation between the horizontal in-plane load and the horizontal in-plane displacement u_{RTC} of all experiments.

When the bonded joint of the ANG pane starts to fail at the corners of the glass pane, the adhesive parts direct next to the failed adhesive stay intact and are locked in the surface flaws of the glass pane. This causes a small discontinuity in the load-displacement curve. Eventually the intact part of the adhesive direct next to the failed adhesive fails also when it has reached the maximum permitted relative in-plane displacement.

Moreover, if cohesive failure of the adhesive bonded joint has started at the corners of systems with HSG panes, the adhesive parts direct next to the failed adhesive also fail and rupture. Here, the adhesive is not locked in the surface flaws of the glass panes and a slow chain reaction causes a constant failure of the adhesive, resulting in a horizontal relation of the load displacement curve.

During experiment HSG 1, the surface of the front adhesive bonded joint in the RTC of the systems was monitored. Every 30 seconds a photograph was taken. Figure 4.24 shows the adhesive bonded joint before testing. Figure 4.25 shows the adhesive bonded joint just before failure of the glass pane and figures 4.26 and 4.27 show the adhesive bonded joint after failure. The adhesive shows clear curved cracks in normal direction of the adhesive bonded joint between the beadwork and the glass pane and therefore cohesive failure is plausible to be the failure mode of the adhesive bonded joint.

The out-of-plane displacements of the glass panes for both glass types are very small. [Huveners 2009] calculated the maximum principle stress for four-sided simply supported and four-sided clamped glass panes using formulae of [Wellershof 2006]. These values were much larger than the measured principle stresses in the glass panes for joint type two. Local exceeding of the strength of glass was the failure criterion and plate buckling did not occur. In the experiments of section 4.6.1 and 4.6.2 first adhesive failure occurred (adhesion and cohesion), followed by shifting of the glass pane along the failed adhesive up till the point of glass steel contact. Therefore, plate buckling is also here not a criterion.

The residual capacity is based on the limited horizontal in-plane displacement of the RTC. Up to the point of failure the system did not warn by visual or audible cracks. This means that the system does not warn before failure. Systems with joint type one [Huveners 2009] did warn before failure (figure 4.28) and therefore combining joint type one and two (figure 1.4) can improve the behavior of the system.



Figure 4.24 undamaged adhesive bonded joint. (HSG 1 before testing)

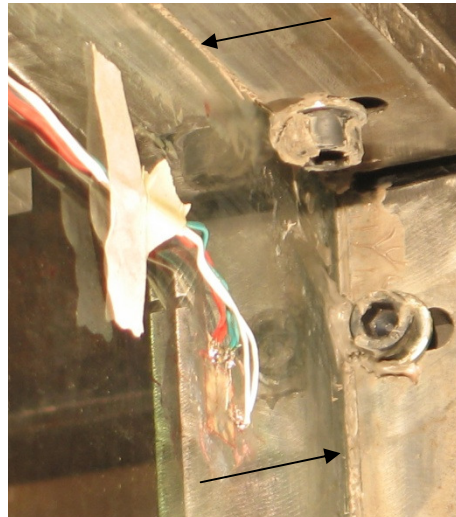


Figure 4.25 Damaged adhesive bonded joint (HSG 1 just before failure of the glass pane)



Figure 4.26 Close up adhesive joint RTC. (HSG 1 after glass pane failure)



Figure 4.27 Close up failed adhesive bonded joint. (HSG 1 after glass pane failure)

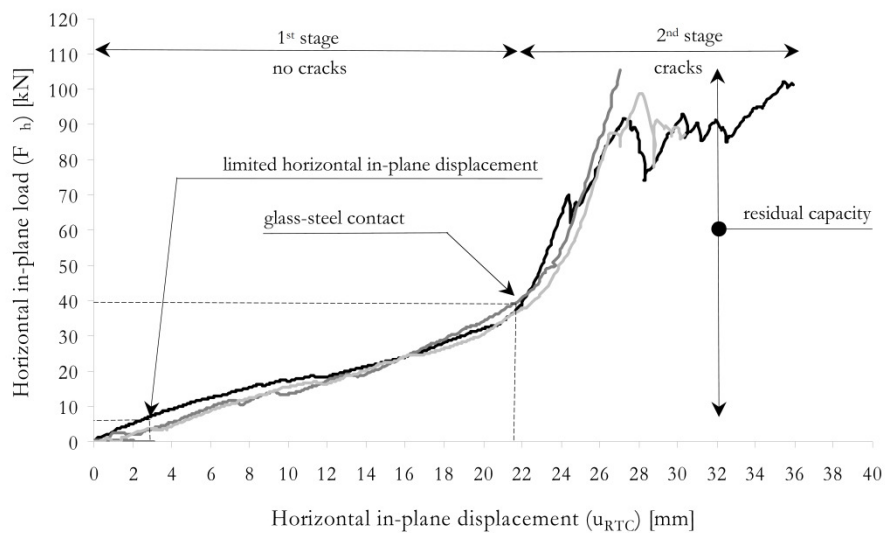


Figure 4.28 Load displacement curve joint type 1. [Huveners 2009]

4.7 Results in- & out-of-plane loaded glass

Two experiments were carried out where glass panes were loaded in- and out-of-plane. One experiment was carried out with ANG and one experiment was carried out with HSG. Figure 4.29 shows the relation between the horizontal in-plane load and the horizontal in-plane displacement of the RTC. The in-plane load due to a controlled displacement at the RTC of the system was applied with a speed of 1 mm/min. At the point where u_{RTC} reaches 3.7 mm, the in-plane load is stopped and the out-of-plane load with a speed of about 0.5 mm/min is introduced up to glass failure. The out-of-plane load introduced by a displacement was applied with a hand driven jack. In practice, the in-plane and out-of-plane load will act together but due to experimental practicability issues, the in-plane and out-of-plane load have been applied separately.

To introduce the out-of-plane load smoothly into the glass pane, a square piece of rubber is placed in front of the jack. The point of application of the rubber is in the centre of the glass pane and the area of the rubber was chosen to be $80 \times 80 \text{ mm}^2$, which corresponds with the mesh of the FEM (section 5.4). Figure 4.30 shows the un-cracked glass pane and figure 4.31 shows the cracked glass pane after failure. Within a second the crack grows from its origin in the centre of the glass pane to the corners of the glass pane.

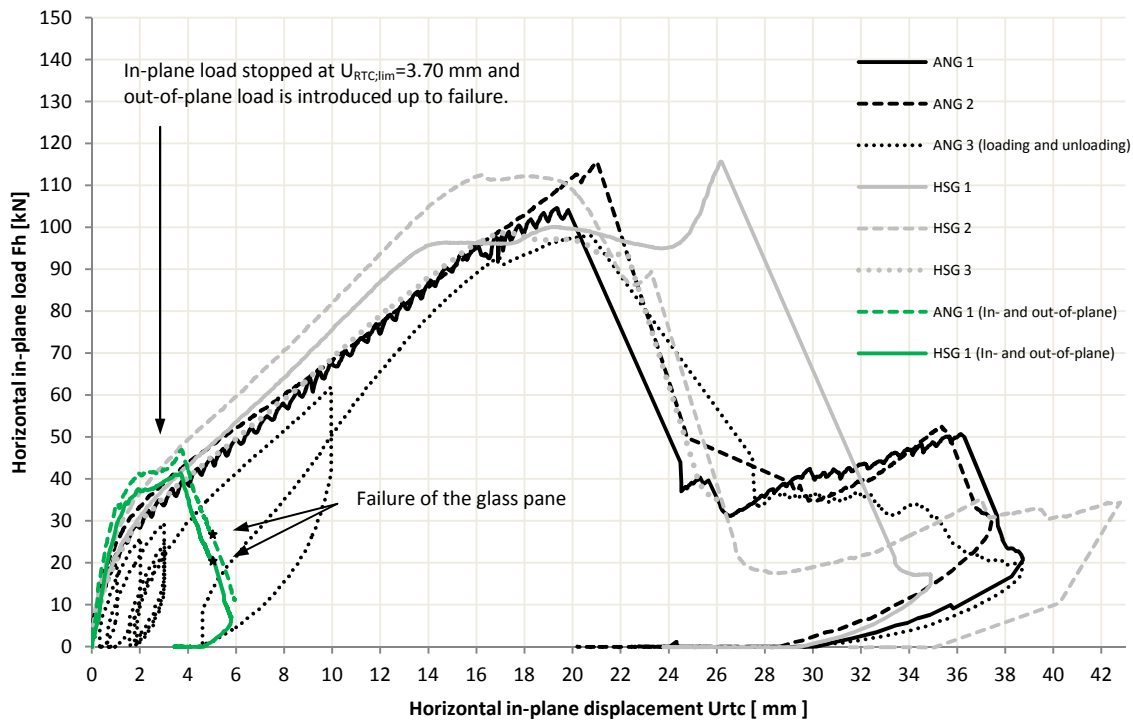


Figure 4.29 Relation between the horizontal in-plane load and the horizontal in-plane displacement u_{RTC} of all experiments.

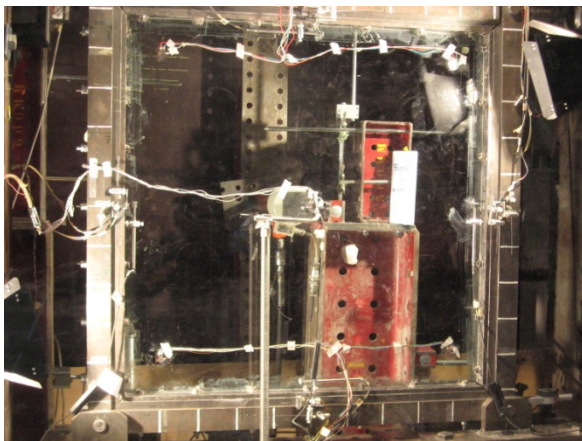


Figure 4.30 Un-cracked glass pane.



Figure 4.31 Cracked glass pane.

4.7.1 Annealed float glass

During the out-of-plane load, the system twisted in the direction of the load. This behavior occurred because the system was not supported at the LTC and RTC. The out-of-plane displacement of the LTC and RTC of the system in relation to the in-plane displacement of the RTC of the system are presented in figure 4.32. In figure 4.33 the twisted glass pane is visualized. The measured out-of-plane displacement in the middle of the glass pane is the out-of-plane displacement due to bending of the glass pane and due to twisting of the glass pane. To compare the out-of-plane displacement of the experiment to the FEM, the out-of-plane displacement due to twisting has to be subtracted from the total out-of-plane displacement of the centre of the glass pane. The total out-of-plane displacement and the corrected out-of-plane displacement in the middle of the glass pane are presented in figure 4.34.

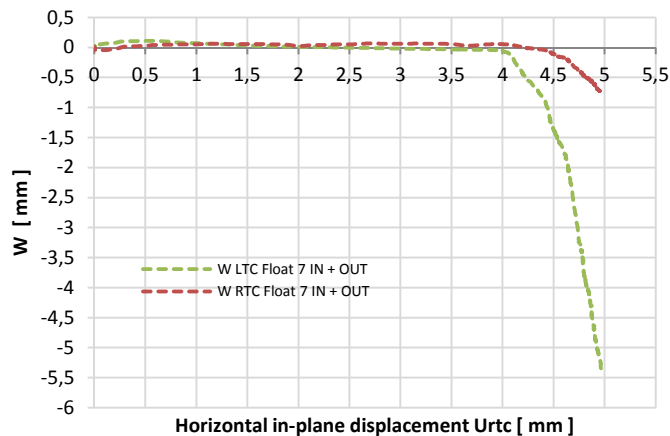


Figure 4.32 Out-of-plane displacements at the LTC and RTC in relation to the horizontal in-plane displacement of the RTC of the system.

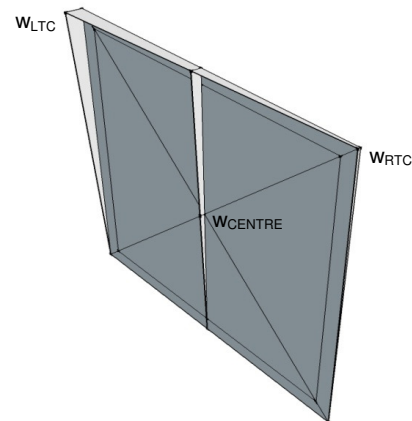


Figure 4.33 Twisted system due to an out-of-plane load.

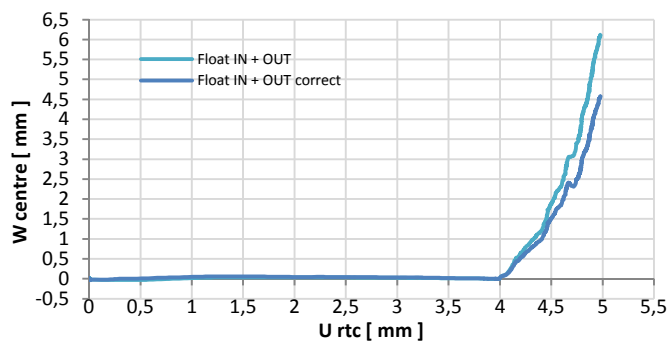


Figure 4.34 Total out-of-plane displacement and corrected out-of-plane displacement of the centre of the glass pane in relation to the in-plane displacement of the RTC of the system.

Figure 4.35 shows the relation between the out-of-plane load and the (corrected) out-of-plane displacement of the centre of the glass pane. During the experiment suddenly the centre of the glass pane stopped displacing out-of-plane, and the out-of-plane load kept increasing. At about an out-of-plane load of 3.5 kN the out-of-plane displacements continue to displace (figure 4.35). No plausible answer can be given for this behavior.

Figure 4.36 gives an overview of the maximum- and minimum principle stresses, measured during the experiment at points one to five just before the moment of failure. Figures 4.37 and 4.38 show the glass pane just before and after failure. Within two thousand of a second the crack grows from its origin at the centre of the glass pane and disperses to the corners of the glass pane.

From the point where the in-plane load is stopped ($u_{RTC}=3,7$ mm) and the out-of-plane load is introduced, the RTC of the system still displaces in-plane and the in-plane load decreases. Relaxation of the adhesive and twisting of the system is the cause of this behavior (figure 4.29).

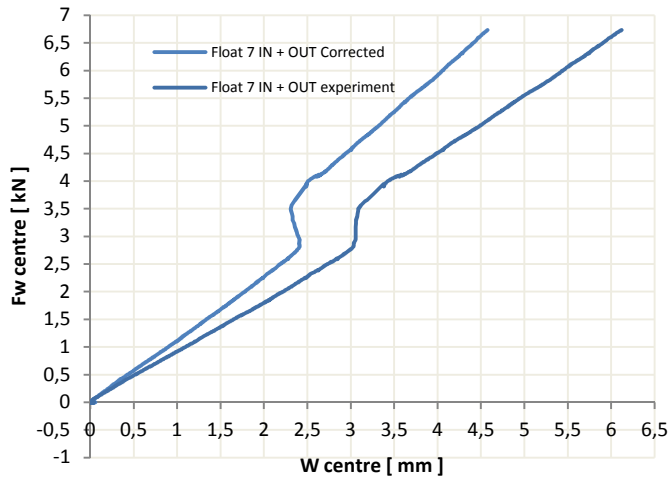
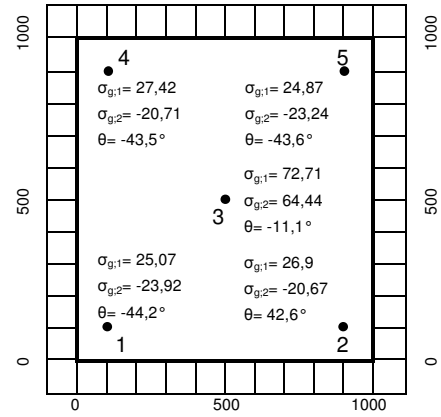


Figure 4.35 Relation between the out-of-plane load and the (corrected) out-of-plane displacement of the system .



ANG 4
 $F_h = 27.05 \text{ kN} / U_{RTC,lim} = 4.98 \text{ mm}$
 $F_w = 6.74 \text{ kN} / w_{Centre,cor.} = 4.58 \text{ mm}$

Figure 4.36 Overview of the principle stresses and their directions for ANG just before the moment of failure.



Figure 4.37 (left) Un-cracked glass pane one four thousand of a second before moment of fracture.

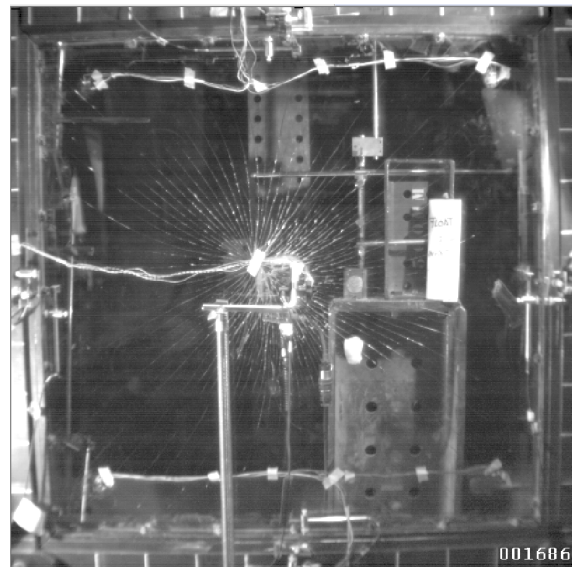


Figure 4.38 (right) Failure of the glass pane due to bending in the middle of the glass pane.

4.7.2 Heat strengthened glass

Just like the experiment with ANG, the system with HSG pane also twists when loaded out-of-plane. This behavior occurred because the system was not supported at the LTC and RTC. The out-of-plane displacement of the LTC and RTC of the system in relation to the in-plane displacement of the RTC of the system are presented in figure 4.39. Figure 4.40 shows the total and corrected out-of-plane displacement in the centre of the glass pane in relation to the in-plane displacement of the RTC of the system.

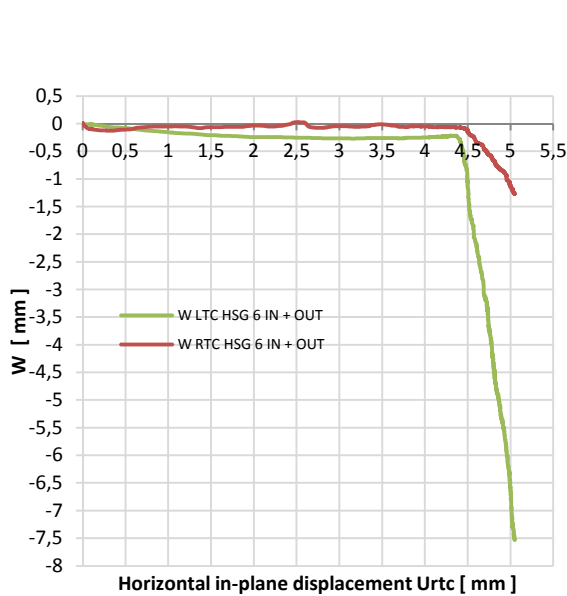


Figure 4.39 Out-of-plane displacements at the LTC and RTC in relation to the horizontal in-plane displacement of the RTC of the system.

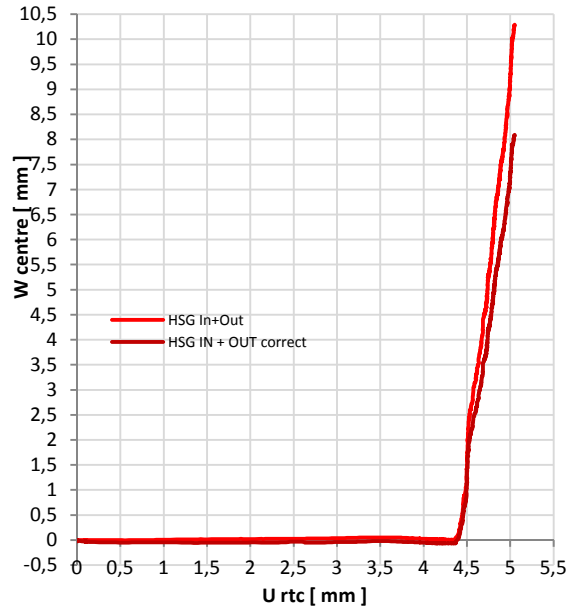


Figure 4.40 Total out-of-plane displacement and corrected out-of-plane displacement of the centre of the glass pane in relation to the in-plane displacement of the RTC of the system.

Figure 4.41 shows the relation between the out-of-plane load and the (corrected) out-of-plane displacement of the centre of the glass pane. Figure 4.42 gives an overview of the maximum- and minimum principle stresses, measured during the experiment at points one to five just before the moment of failure.

Figures 4.43 and 4.44 show the glass pane just before and after failure. Within two thousand of a second the crack grows from its origin at the centre of the glass pane and disperses to the corners of the glass pane.

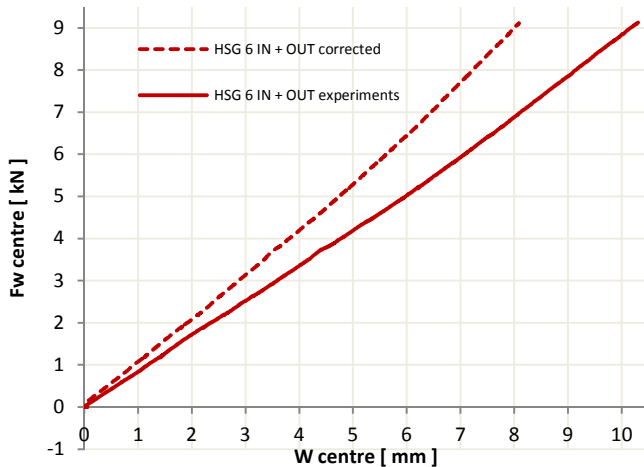


Figure 4.41 Relation between the out-of-plane load and the (corrected) out-of-plane displacement of the system .

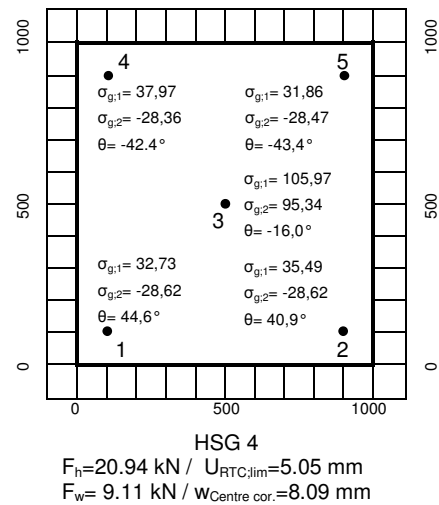


Figure 4.42 Overview of the principle stresses and their directions for ANG at limited U_{RTC} and just before the moment of failure.

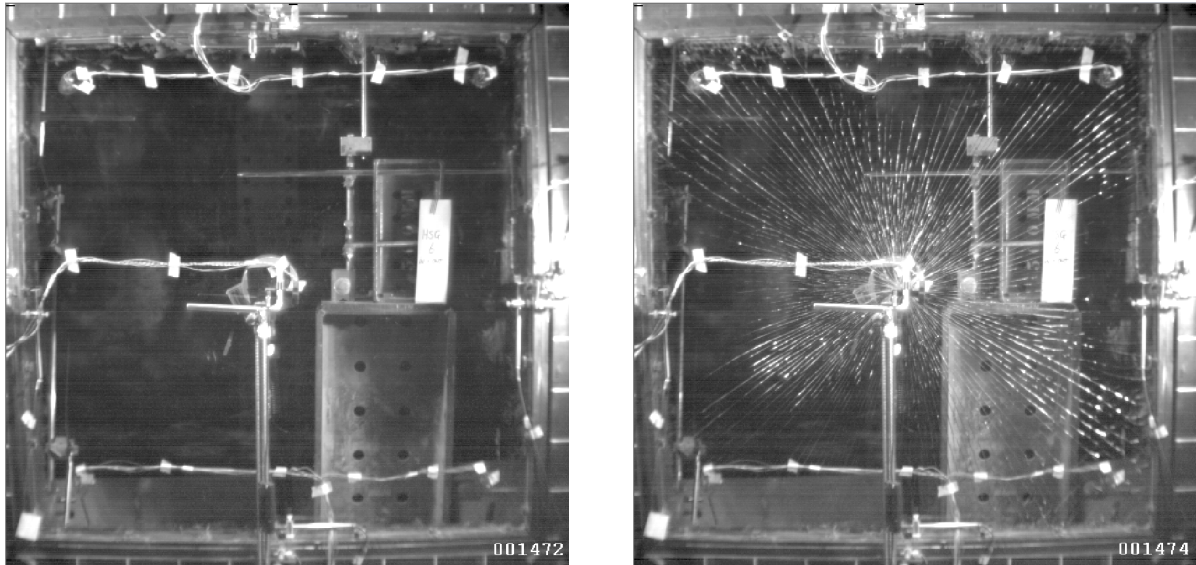


Figure 4.43 (left) Un-cracked glass pane one four thousand of a second before moment of fracture.
 Figure 4.44 (right) Failure of the glass pane due to bending in the middle of the glass pane.

4.7.3 Discussion of the results of in-plane and out-of-plane loaded glass

Two experiments were carried out where glass panes were loaded in- and out-of-plane. One experiment was carried out with ANG and one experiment was carried out with HSG. First, the system was loaded by an in-plane displacement at the RTC of the system with a speed of 1mm/min. At the point where the in-plane displacement of the RTC reached 3.7 mm, the in-plane load was stopped and the out-of-plane load was introduced with a speed of about 0.5 mm/min up to glass failure. The out-of-plane load, introduced by a displacement, was applied with a hand driven jack. In practice, the in-plane and out-of-plane load will act together but due to experimental practicability issues, the in-plane and out-of-plane load have been applied separately.

Due to an implementation fault in the set-up of system, the LTC and RTC were able to displace. To compare the results with the FEM, the total out-of-plane displacement in the centre of the glass pane had to be corrected i.e. the out-of-plane displacement due to twisting of the system had to be deducted from the total out-of-plane displacement (figures 4.34 and 4.40). The out-of-plane load was introduced in centre of the glass pane by a square rubber element ($80 \times 80 \text{ mm}^2$) with a thickness of 20 mm.

The ANG pane failed at a corrected out-of-plane displacement in the centre of the glass pane of 4.58 mm and an out-of-plane load of 6.74 kN. The HSG pane failed at a corrected out-of-plane displacement in the centre of the glass pane of 8.09 mm and an out-of-plane load of 9.11 kN. Due to the larger representative flexural tension strength, the HSG pane could handle a larger out-of-plane load and out-of-plane displacement in the centre of the glass pane. During the experiments no audible or visible cracks were determined and the glass pane did not warn before failure.

4.8 Conclusions

Section 4.8.1 presents the conclusions of experiments with in-plane loaded glass panes. In section 4.8.2, conclusions of experiments with in- and out-of-plane loaded glass panes are given.

4.8.1 In-plane loaded glass panes:

- During the experiments the pinned connection at the RBC displaced vertically and caused the system to rotate. The pinned connection behaved as a spring;
- Up to the point where the slope of the results of HSG panes became horizontal, the experiments of ANG and HSG showed the same behavior with a certain spread;
- Peak stresses in the glass panes, due to a sudden irregular stress distribution in the adhesive bonded joint because of the shear flexibility between the outside beam and the beadwork, did not occur;
- In-plane loaded systems with ANG panes and joint type 2 failed immediately when glass-steel contact occurred;
- In-plane loaded systems with ANG panes and joint type 1 (figure 1.4) in [Huveners 2009] showed more resistance when glass-steel contact occurred. Combining joint type 1 with a rubber like material and joint type 2 with the acrylic adhesive will enlarge the residual capacity of the system;
- In-plane loaded systems with HSG panes and joint type 2 showed more resistance when glass-steel contact occurred;
- The system did not warn by visual of audible cracks in the glass pane before failure;
- The point where the relation between the horizontal in-plane load and the horizontal in-plane displacement of the RTC of the system becomes horizontal, distinct systems with HSG panes from systems with ANG panes;
- In the corners of the glass pane, the adhesive bonded joint has the largest relative in-plane displacement and the adhesive displaces in longitudinal and transversal direction. Here cohesive failure of the adhesive bonded joints starts;
- During the experiments, the out-of-plane displacements of the glass panes for both glass types are very small;
- For systems with the acrylic adhesive and glass panes with a thickness of 12 mm as applied in this research, plate buckling is not a criterion for failure.

The conclusions below are based on the plausible theorem that the acrylic adhesive adheres better to ANG panes than to HSG panes. Moreover, this could not be confirmed experimentally.

- The adhesive is able to lock itself in the surface flaws of the ANG panes;
- In HSG panes, the surface flaws are suppressed by compression stresses and the adhesive is not able to lock itself;
- After the adhesive bonded joint of systems with ANG had failed, the intact adhesive parts direct next to the failed adhesive parts, continued to displace and eventually also failed on cohesion when the maximum permitted relative in-plane displacement of the adhesive had been exceeded;
- In systems with HSG panes, the intact adhesive parts next to the failed adhesive parts were not able to lock in the surface flaws. A slow chain reaction caused a continuous failure of the adhesive bonded joint resulting in a horizontal behavior of the relation between the horizontal in-plane load and the horizontal in-plane displacement at the RTC of the system.

4.8.2 In- and out-of-plane loaded glass panes:

- Results can only be used indicatively;
- Due to the out-of-plane load, both glass pane types failed through bending, e.g. the maximum flexural tension strength in the middle of the glass pane was exceeded.
- The system did not warn by visual of audible cracks in the glass pane before failure;
- The ANG pane and the HSG pane showed both a large capacity to account for in-plane and out-of-plane loads.

5 Finite element analyses

The finite element (FE) model that is used in the analyses to simulate the experiment of chapter 4, is based on the model of [Huvener 2009]. The FE model was able to simulate the experiments till glass steel contact for systems with joint type one, or up to the point where the first crack in the glass appeared for systems with joint type two and three. The model is sufficient to simulate the behavior of the system with a non-cracked glass pane.

5.1 Geometry

The geometry of the system, presented in figure 5.2, is built up of a steel frame which is supported at the test rig at the LBC and RBC. The in-plane load is introduced at the RTC of the system and the glass pane is adhesively bonded to the steel frame, based on joint type 2 (figure 1.4).

The FE-model of [Huvener 2009] had to fulfill the following eight requirements:

- the mid-plane of the glass pane lines up with the centre line of the outside beam;
- the outside beams of the transoms and mullions are coupled and released for rotation around the z-axis (internal hinge);
- the centre line of the outside beam of the transom and the mullion coincides with the centre of the internal hinge;
- the line of action of the horizontal in-plane load coincides with the centre line of the top outside beam;
- the centre of the roller at the LBC and centre of the pinned connection at the RBC coincide with the centre of the internal hinge;
- the centre line of the outside beam of the transom and the mullion has a distance to the edge of the glass pane (eccentricity);
- the pinned connection at the RBC behaves elastic in vertical direction (section 4.4.3);
- the shear flexibility of the bolted connection between the outside beam and the beadwork behaves elastic (section 4.4.4).

In figure 5.1 the composition of the FE-model is presented. In figure 5.2 the cross section of the bottom transom can be seen, which also represents the top transom and the mullions. The steel frame is divided into three parts, namely the outside beam, the beadwork and the bolted connection between the outside beam and the beadwork.

Outside Beam

The rectangular cross section of the outside beam is modeled for only the half height (h_2) with shell elements and completed with beam elements ($w_1 \times h_1$) in the centre line of the outside beam (figure 5.2).

Beadwork

The beadwork is modeled to a forked cross section to enclose the glass pane and the interfaces A to C (figure 5.2). The beadwork consists of the following parts:

- the height of the 'handle' of the forked cross section (h_4) is the distance between the bolted connection and the bottom of interface B;
- the width of the forked cross section (w_5) corresponds to the thickness of the glass pane (t_{10}) and the thicknesses of interface A (t_8) and interface C (t_9);
- the prong of the forked cross section (h_7) corresponds to the thickness of interface B (t_6) and the width of interfaces A and C (w_8, w_9).

The geometrical properties of the modeled cross section with shell elements meet the geometrical properties of the real outside beam and the real beadwork (appendix B.1 and table 5.1).

Bolted connection between outside beam and beadwork

The bolted connection between the outside beam and the beadwork (w_3, h_3) is modeled with two dimensional interface elements (figure 5.2).

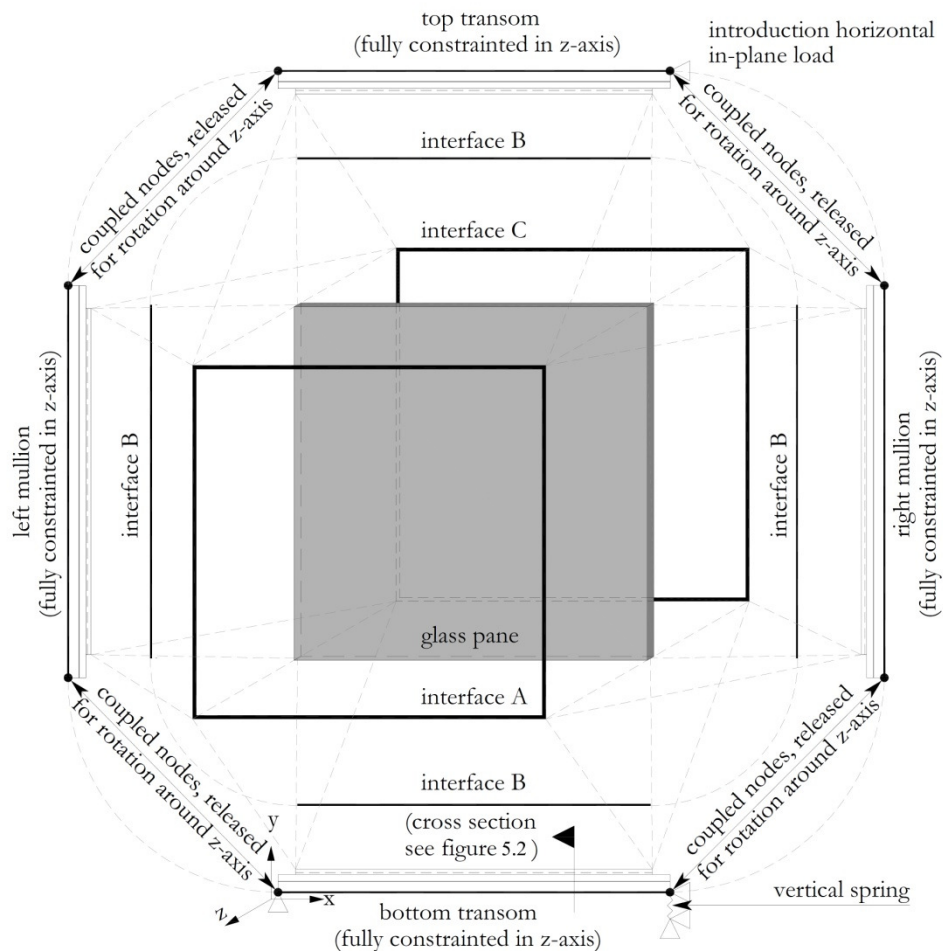


Figure 5.1 Composition of the FE-model [Huvener 2009].

Supports of the system

At the LBC the steel frame is supported with a horizontal in-plane roller at the intersection of the centre line of the outside beam of the bottom transom and the left mullion. The RBC of the steel frame is supported by a vertical in-plane roller at the intersection of the centre line of the outside beam of the bottom transom and the right mullion. A vertical spring (section 5.2.4) is placed between the vertical in-plane roller and the in-plane pin, due to the flexibility of the bottom plate which connects the system to the test rig (figure 4.6). The steel frame is fully supported in z-direction, because in the experiments the out-of-plane displacements of the LTC and the RTC of the system were negligible small (< 1 mm).

Interfaces A B, and C

The positions of the interfaces in the system are (figure 5.5):

- interface A is placed along the four edges of the glass pane between the prong of the forked cross section and the front of the glass pane;
- interface C is also placed along the four edges of the glass pane, but between the prong of the forked cross section and on the rear of the glass pane;
- interface B is placed between the glass pane and the bottom of the forked cross section;
- the length of interfaces A, B and C corresponds with the width (w_g) and the height of the glass pane (h_g);
- At the corners interfaces A and C have an overlap. Due to the overlap, unreal stresses in the glass pane at a premature end of the interface elements on the glass pane are avoided.

Glass pane

Due to eccentric load transfer in systems with joint type 3 (figure 1.4), the glass pane is modeled with solid elements. This improves the description of the three-dimensional stress distribution along the

edges of the glass pane. The edges of the glass pane are modeled without facets, which differs from the tested glass panes in the experiments.

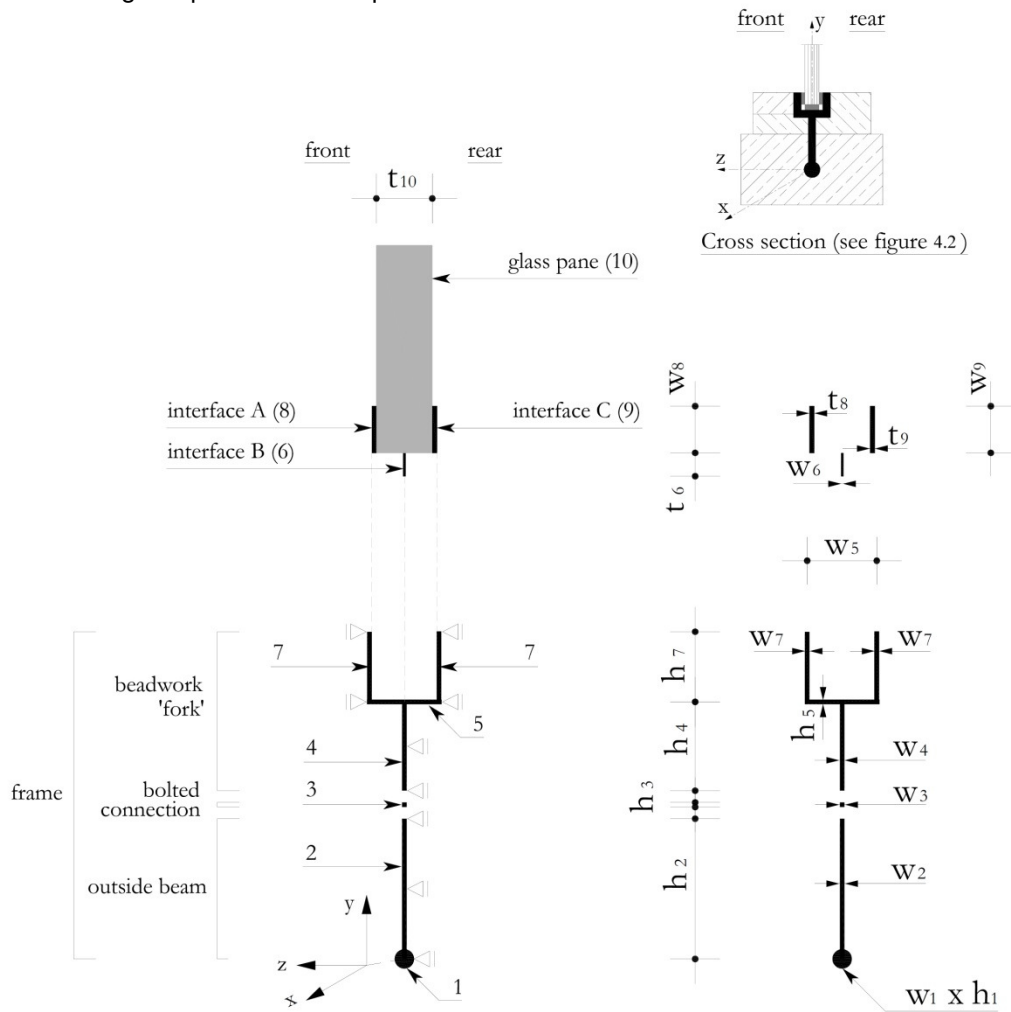


Figure 5.2 Modeled cross section of the steel frame, the interfaces and the glass pane [Huveners 2009].

At each corner, the transom and the mullion have an overlap with uncoupled nodes except the common node of the beam element (figure 5.3). This node is coupled and released for rotation around z-axis to simulate the internal hinge. Figure 5.4 shows the in-plane displacements of the steel frame only which correspond with the non-braced steel frame of the system. The ends of all beadworks are straight instead of a mitre (figure B.5) and it is a local simplification in the finite element model.

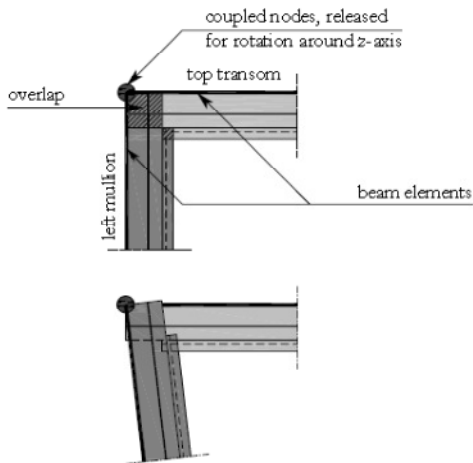


Figure 5.3 Simulation of the internal hinge at the LTC and the tilting mechanism of the non-braced steel frame [Huveners 2009].

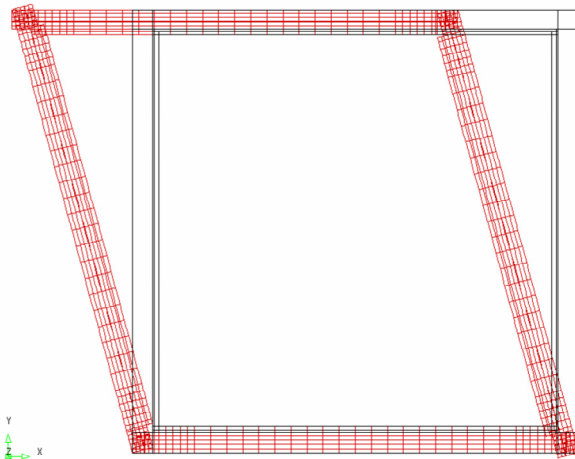


Figure 5.4 In-plane displacements of the non-braced steel frame (scale factor 10) [Huveners 2009].

Huveners implemented the geometry of systems with joint types 1 to 3 into one finite element model. The experiments described in chapter 4 are based on joint type two, so interfaces A and C (figure 5.5) will be used to apply the shear properties of batch 3 (section 3.1.4) of the acrylic adhesive into the model. During the FE calculations interface B will be inactive, except for determining when glass steel contact occurs. This is further explained in sections 5.7.3.1 and 5.7.3.2 where the sensitive analyses are reviewed.

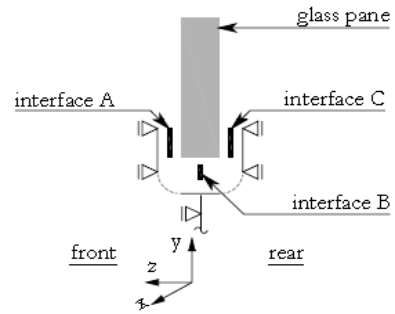


Figure 5.5 Interfaces A, B and C [Huveners 2009]

5.2 Elements

The descriptions of the elements that are used in the FE-model are based on the user manual of [TNO Diana 2010].

5.2.1 Modeling the steel frame

A part of the outside beam is represented by a line type element which longitudinal axis passes through the elastic neutral center of the steel member. Characteristic for a beam element is that the ratio between the dimensions d and the length of the bar axis perpendicular to it, must be very small (figure 5.6). Beam elements may have axial deformation Δl , shear deformation ΔY , curvature $\Delta \kappa$ and torsion $\Delta \phi$, and therefore they can describe axial force, shear force and bending moment.

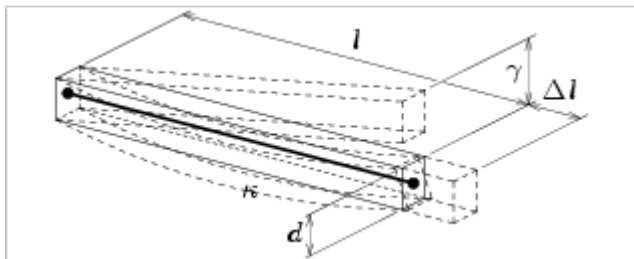


Figure 5.6 Characteristics beam elements

The L12BE element (figure 5.7) is a two-node, three-dimensional class-I beam element. This classical beam element with directly integrated cross-sections may be used in linear and in geometrical nonlinear analysis. Physic nonlinear analyses are limited to generalized stress-strain diagrams. By default Diana assumes that the cross-sections remain plane and perpendicular to the slope of the beam axis. Therefore these beam elements may be viewed as based on the Bernoulli theory.

Basic variables are the translations u_x , u_y and u_z , and the rotations ϕ_x , ϕ_y and ϕ_z in the nodes. The predefined rectangular cross-sectional shape of the beam is specified using the actual dimensions of the steel outside beam (height and thickness).

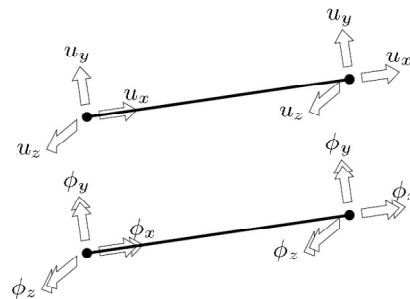
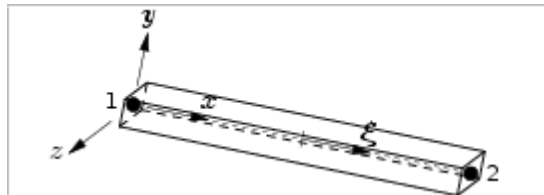


Figure 5.7 The L12BE element, a two-node three-dimensional line-type beam element based on the Bernoulli theory.

For the L12BE beam element, Diana performs by default a 2-point numerical Gauss integration in only the isoparametric ξ direction of the element which coincides with the bar axis (figure 5.8).

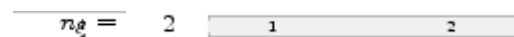


Figure 5.8 two-point Gauss integration scheme in ξ direction.

Element CQ40S has been used in a part of the outside beam and the entire forked cross section of the beadwork. CQ40S is a regular eight-node isoparametric quadrilateral curved shell element (figure 5.9). It is based on quadratic interpolation and Gauss integration over the $\xi \eta$ element area. The integration in ζ direction (thickness) may be Gauss or Simpson.

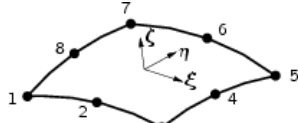


Figure 5.9 Element CQ40S

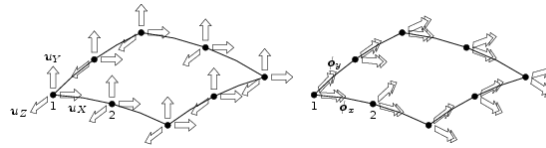


Figure 5.10 Variables are the translations and rotations of the eight-node shell element.

Basic variables are the translations u_x , u_y and u_z , and the rotations ϕ_y and ϕ_z in the nodes of the curved shell element (figure 5.10). The strains due to translations of the nodes is presented in figure 5.11 and for the rotations the strains are presented in figure 5.12.

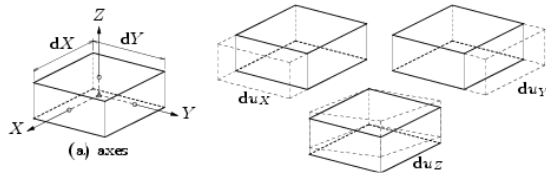
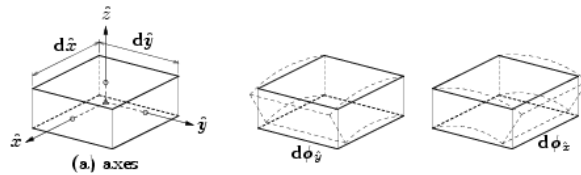


Figure 5.11 Strains derived from translations.



5.12 Strains derived from rotations.

The strain ϵ_{xx} , the curvature κ_{xx} , the moment m , the membrane force n_{xx} and the shear force q_{xz} vary linearly in x direction and quadratically in y direction. The strain ϵ_{yy} , the curvature κ_{yy} , the moment m , the membrane force n_{yy} and the shear force q_{yz} vary linearly in y direction and quadratically in x direction.

For element CQ40S two types of stresses can be derived: Cauchy stresses (figure 5.13) and generalized moments and forces (figure 5.14).

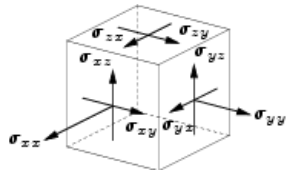
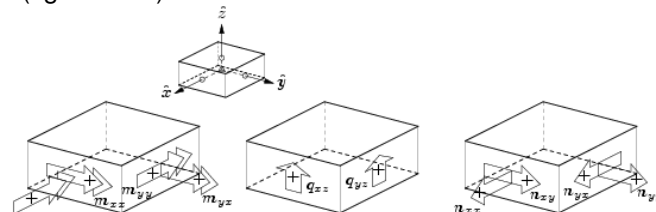


Figure 5.13 Cauchy stresses.



5.14 Generalized moments and forces.

5.2.2 Modeling the glass pane

Solid elements are usually applied when other elements are unsuitable or would produce inaccurate analysis results. The CHX60 element is a twenty-node isoparametric solid brick element and is based on quadratic interpolation and Gauss integration (figure 5.15). The basic variables in the nodes of solid elements are the translations u_x , u_y and u_z in the local element direction (figure 5.16)

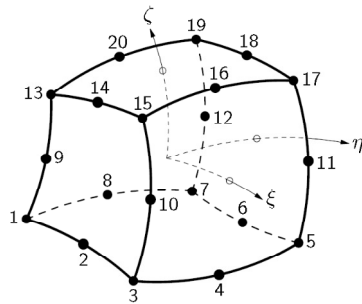


Figure 5.15 Twenty-node isoparametric solid brick element (CHX60).

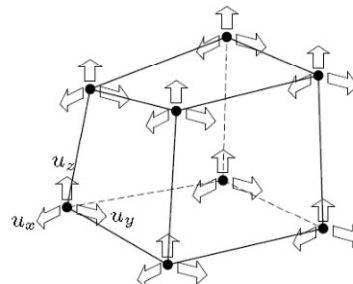


Figure 5.16 Variables are the translations of the nodes of the solid brick element.

An important factor in modeling the glass pane is the ability of calculating the principle stresses. In the twenty-node brick element these stresses are derived from the nodal displacements. The displacements in the nodes yield the deformations du_x , du_y and du_z of an infinitesimal part dx , dy and dz of the element (figure 5.17). From these deformations the Green-Lagrange strains are derived. These Green-Lagrange strains are derived for all integration points and may be extrapolated to the nodes. Diana applies by default a $3 \times 3 \times 3$ Gauss [$n_\xi = 3$, $n_\eta = 3$, $n_\zeta = 3$] integration scheme (figure 5.18). The strain ε_{xx} and stress σ_{xx} vary linearly in x direction and quadratically in y and z direction. The strain ε_{yy} and stress σ_{yy} vary linearly in y direction and quadratically in x and z direction. The strain ε_{zz} and stress σ_{zz} vary linearly in z direction and quadratically in x and y direction.

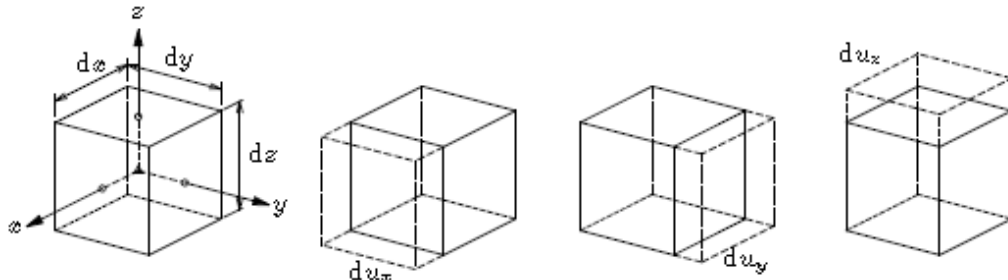


Figure 5.17 Green-Lagrange strains derived from nodal displacements.

If the strains are known, the Cauchy stresses can be derived. The accuracy of the results is very important because glass is a brittle material and will fail if the maximum principle stress is exceeded. The principle stresses are calculated using the results of the Cauchy stresses (figure 5.19).

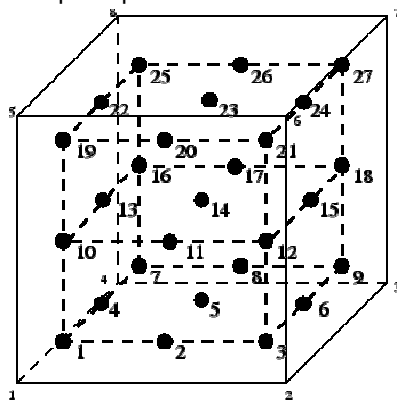


Figure 5.18 $3 \times 3 \times 3$ Gauss integration scheme twenty-node brick element [$n_\xi = 3$, $n_\eta = 3$, $n_\zeta = 3$]

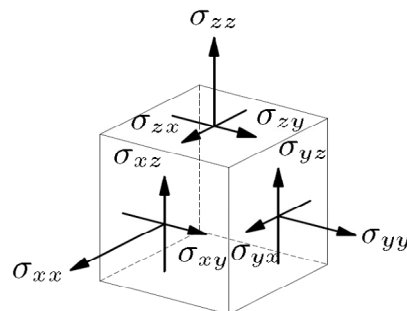


Figure 5.19 Cauchy stresses

5.2.3 Modeling the adhesive bonded joint

The adhesive bonded joint can be represented by structural interface elements. These elements are able to describe the interface behavior in terms of a relation between the normal- and shear traction and the normal- and shear relative displacements across the interface. Interfaces A and C in figure 5.5 are used to model the adhesive bonded joint. Interface element B is still very useful for analyzing the moment of glass steel contact. This is further explained in section 5.7.3.1 and 5.7.3.2.

5.2.3.1 Interface elements A and C

The elements which are needed for joint type two are the interface elements A and C and are described in section 5.1, where the geometry of the FE-model is presented.

The CQ48I element is an interface element between two planes in a three-dimensional configuration. The element has 8+8 nodes and is fully isoparametric, which means that the plane interface elements may be flat as well as curved (figure 5.20).

The basic variables for structural interfaces are the nodal displacements u_x , u_y and u_z (figure 5.21). The derived values are the relative displacements Δu_x , Δu_y , Δu_z and the tractions t_x , t_y and t_z . The normal traction t_x is perpendicular to the interface; the shear tractions t_y and t_z are tangential to the interface (figure 5.22). The element is based on quadratic interpolation and by default DIANA applies a 4×4 Newton-Cotes [$n_\xi = 4$, $n_\eta = 4$] integration scheme (5.23).

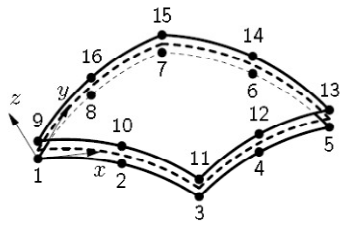


Figure 5.20 Eight plus eight-node isoparametric plane interface element

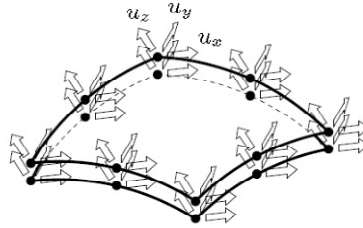
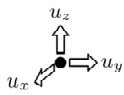
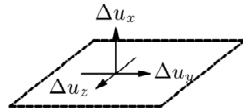


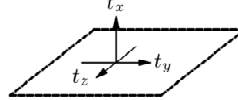
Figure 5.21 Variables are the translations of the nodes of element (CQ48).



(a)

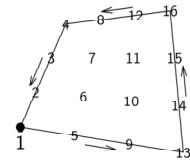


(b)



(c)

Figure 5.22 Nodal displacements (a), relative displacements (b), and tractions (c).



4 x 4

Figure 5.23 4 x 4 Newton-Cotes integration scheme [n ξ =4, n η =4]

5.2.3.2 Interface element B

The element which is needed for joint type one is the interface element B and is described in section 5.1, where the geometry of the FE-model is presented. As mentioned in the introduction of this section, interface B will not be used to model an adhesive bond, but is used to analyze the moment of glass steel contact. In section 5.7.3.1 and 5.7.3.2 this is further explained.

The CL12I element is placed between lines of solid- and shell elements in a two-dimensional configuration. The element has 3+3 nodes and is fully isoparametric, which means that the quadratic line interface elements may be straight as well as curved (figure 5.24).

The basic variables for this structural interface are the nodal displacements u_x and u_y (figure 5.25). The derived values are the relative displacements Δu_x , Δu_y ; and the tractions t_x , t_y . The normal traction t_x is perpendicular to the interface; the shear traction t_y is tangential to the interface (figure 5.26). The element is based on quadratic interpolation and by default DIANA applies a 4-point Newton-Cotes [n ξ =4] integration scheme (figure 5.27).

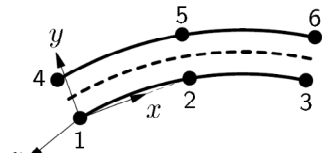


Figure 5.24 Three plus three-node isoparametric line interface element

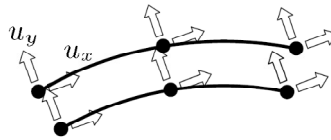
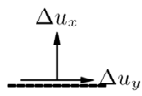


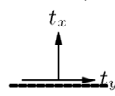
Figure 5.25 Variables are the translations of the nodes of element (CL12I).



(a)



(b)



(c)

Figure 5.26 Nodal displacements (a), relative displacements (b), and tractions (c).

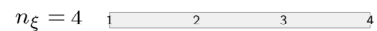


Figure 5.27 4-point Newton-Cotes integration scheme [n ξ =4]

5.2.4 Vertical spring at the RBC of the frame

Due to a horizontal in-plane load at the RTC of the system, the RBC displaces vertically. The vertical in-plane displacement of the RBC during testing has been discussed in section 4.4.3. Due to this displacement, the pinned connection at the RBC of the system behaves like a spring. Element SP2TR is a linear spring element and represents the non linear vertical in-plane displacement of the pinned connection at the RBC (figure 5.28 to 5.30).



Figure 5.28 Topology.



Figure 5.29 Displacement.

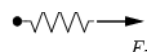


Figure 5.30 Stress.

5.2.5 Overview elements

In table 5.1 an overview of the element types applied in the FE-model are presented, including the geometrical data input.

Table 5.1 Element types as applied in finite element analyses and geometrical data input

Part	Number	Element name	Element type	Width [mm]	Height [mm]	Thickness [mm]
Outside beam	1	Bending beam	L12BE	-	118	60
	2	Quadrilateral curved shell	CQ40S	-	3	30
Bolted connection Beadwork	3	Line interface	CL12I	-	15	1
	4	Quadrilateral curved shell	CQ40S	-	98	19
	5	Quadrilateral curved shell	CQ40S	-	18	15
	7	Quadrilateral curved shell	CQ40S	-	19	15
Vertical spring at the RBC of the frame	-	Translation spring/dashpot	SP2TR	-	-	-
Glass pane	10	Solid brick	CHX60	12	-	-
Adhesive bonded joint	8/9	Quadrilateral interface	CQ48I	3	-	-
	6	Line interface	CL12I	12	-	-

5.3 Material input

5.3.1 Material input for interfaces

Figure 5.31 presents the definition of the directions for interface elements A to C and the bolted connection between the outside beam and the beadwork. The indices in figure 5.31 are frequently used in this chapter.

The normal stiffness of the adhesive for interface elements is assumed to be linear and for non-linear material behavior of the interface elements, a multiple linear relation between the shear stresses in longitudinal / transversal direction and the relative in-plane displacements in longitudinal / transversal direction is used (section 5.3.2).

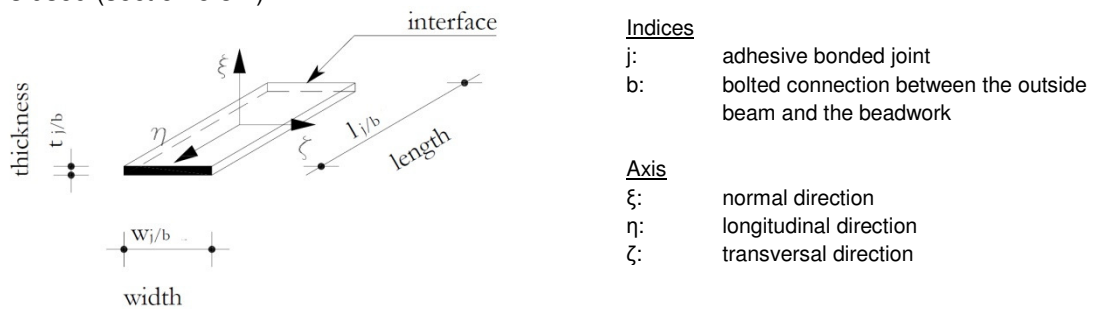


Figure 5.31 Definition of the directions for interface elements A to C and the bolted connection between the outside beam and the beadwork [Huvener 2009].

For two and three dimensional interface elements the normal direction, longitudinal and transversal direction are not coupled. This means that normal stresses have no influence on the shear stress in longitudinal or transversal direction and vice versa. Also the shear stresses in longitudinal and transversal direction are not coupled. Section 5.3.2 presents the material properties with physical linear material and non-linear properties.

5.3.2 Linear and non-linear material behavior

In this section the linear and non-linear material behavior of the materials applied to the elements in the FE model are presented. Table 5.3 presents the physical linear material behavior. The material properties of glass and steel are adopted from the Dutch design codes [NEN 2608-2:2007 nl] and [NEN 6770:1997 nl – TGB 1990] respectively. It is assumed that the steel frame has no imperfections and behaves isotropic and linear elastic. The glass pane in the FE model has an imperfection of 0.5 mm in the centre (section 6.5) and is assumed to behave linear elastic and isotropic.

The vertical spring stiffness at the RBC of the system was determined during the experiments (section 4.4.3). The shear flexibility of the bolted connection between the outside beam and the beadwork was determined by [Huvener 2009] and described in section 4.4.4. The shear flexibility ($k_{b,\eta}$) simulates the in-plane sliding and contact friction of the bolted connection and is assumed to be linear. The normal stiffness ($k_{b,\xi}$) of the steel beams is assumed to be very large. Furthermore, it is assumed that local yielding of the steel frame, e.g. around the bolted connection between the outside beam and the beadwork has no influence on the global behavior of the system.

The initial normal stiffness of the bonded joint ($k_{j,\xi,ini}$) is derived according to equations 5.1 to 5.4 from the (first) linear stage of the shear stress-strain relation of adhesive shear experiments (table 5.2 and figure 5.32). The shear stiffness of the acrylic adhesive shows a non-linear behavior but the normal shear stiffness is assumed to be linear and has no material imperfections i.e., no varying Young's modulus or geometrical imperfections (no varying joint thickness or joint width) during all stages. This assumption can be made, because the in-plane load transfers via shear (in η and ζ direction) through the adhesive bonded joint. When interface element B is inactivated, the element has a very small normal stiffness, so no in-plane loads can be transferred through this element.

$$G_{a,ini} = \frac{\tau_{ave,ini}}{\gamma_{ave,ini}} \quad (\text{Equation 5.1})$$

$$E_{a,ini} = 2G_{a,ini}(1 + \nu_a) \quad (\text{Poisson's constant is assumed to be 0.5}) \quad (\text{Equation 5.2})$$

$$k_{j,\xi,ini} = \frac{E_{a,ini}}{t_j} \quad (\text{Equation 5.3})$$

$$k_{j,\eta/\zeta} = \frac{G_{a,ini}}{t_j} \quad (\text{Equation 5.4})$$

Table 5.2 Overview of assumed linear behavior of the adhesive bonded joint in the first stage.

γ_{ave} [-]	τ_{ave} [N/mm ²]	$G_{a,ini}$ [N/mm ²]	t_j [mm]	$k_{j,\eta/\zeta}$ [N/mm ³]	$E_{a,ini}$ [N/mm ²]	$k_{j,\xi,ini}$ [N/mm ³]
0.05	0.68	13.53	3.0	4.51	40.58	13.53

Table 5.3 Material properties with physically linear material behavior

Material / component	Properties	Comments
Glass	E_g [N/mm ²]	70000 [NEN 2608-2:2007 nl]
	ν_g [-]	0.23 [Haldimann et al. 2008]
Steel	E_s [N/mm ²]	210000 [NEN 6770:1997 nl – TGB 1990]
	ν_s [-]	0.3 [NEN 6770:1997 nl – TGB 1990]
Vertical spring stiffness at the RBC of the system	$K_{y,RBC}$ [N/mm]	2.73×10^5 Determined during experiments (section 4.4.3)
Bolted connection between the outside beam and the beadwork	$k_{b,\xi}$ [N/mm ³]	10^6 Large normal stiffness (assumed) [Huvener 2009]
	$k_{b,\eta}$ [N/mm ³]	10 Determined during experiments (section 4.4.4) [Huvener 2009]
Initial normal stiffness of the bonded joint (interfaces A and C)	$k_{j,\xi,ini}$ [N/mm ³]	13.53 Derived from first linear stage of the stress-strain relation
Inactivated interface B	$k_{j,\eta/\zeta}$ [N/mm ³]	10^{-9} Very small normal stiffness

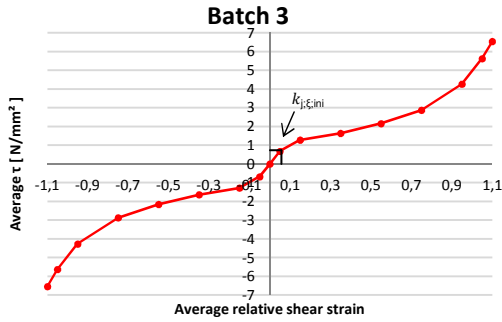


Figure 5.32 Relation of the average shear stress and average shear strain in longitudinal / transversal direction.

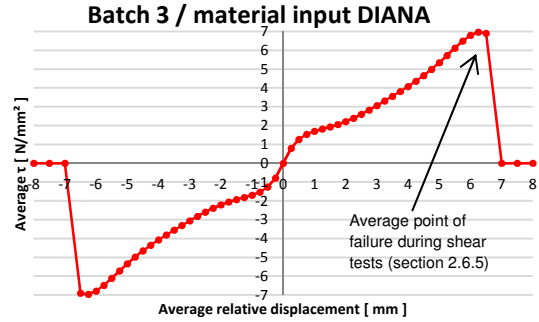


Figure 5.33 Relation of the average shear stress and average relative in-plane displacement in longitudinal / transversal direction with joint thickness of 3 mm.

Figure 5.33 shows the input of the non linear material behavior of the acrylic adhesive for interface elements A and C. On the vertical axis the average stress is presented and on the horizontal axis the average relative in-plane displacement is given.

5.4 Mesh density

Figure 5.34 shows the mesh density of one fourth of the glass pane (nominal thickness 12 mm) applied for FE simulations with squared glass panes of 1000 mm. The mesh density depends on the strain gradient in the glass pane and was refined along the edges because of the crack initiation at the vicinity of the corners of the glass pane in the experiments. However, the fine mesh along the edges of the glass is still not sufficient to describe the strain gradient well (discretisation fault). The element sizes used by Huvener and the element sizes used in this research are presented in table 5.4.

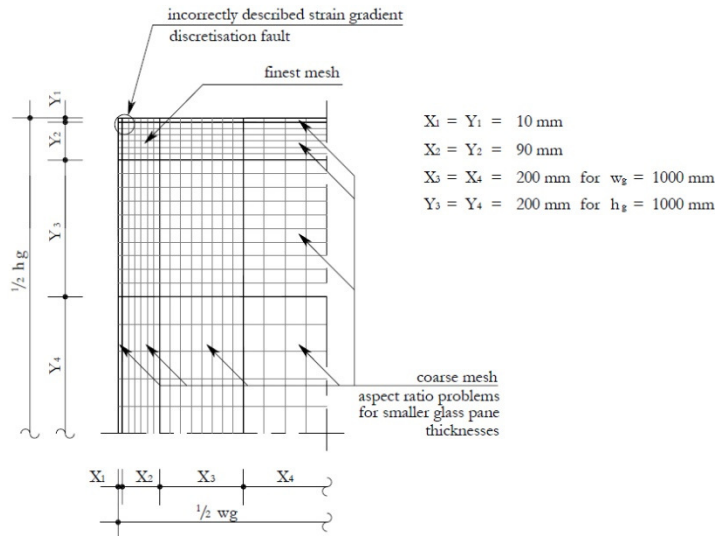


Figure 5.34 Mesh density of one fourth of the glass pane [Huvener 2009]

Table 5.4 Element sizes (figure 6.28) of the glass pane (nominal thickness 12 mm).

$w_g \times h_g$ [m]	X_1 [mm]	X_2 [mm]	X_3 [mm]	X_4 [mm]	Y_1 [mm]	Y_2 [mm]	Y_3 [mm]	Y_4 [mm]
1.0x1.0	10 (1x)	18 (15x)	40 (5x)	40 (5x)	10 (1x)	18 (15x)	40 (5x)	40 (5x)

5.5 Geometrical imperfections

Geometrical imperfections can have a large influence on the behavior of in-plane loaded structures. Out-of-plane curvature and varying thickness are common imperfections for glass panes. The thickness tolerance of the glass pane is influenced by the float process and has an upper- and lower limit. These values are prescribed in [EN 572-8 2004]. The nominal glass pane thickness used in the experiments is 12 mm. Appendix B.3 shows the measured thicknesses for ANG and HSG panes. In the FE calculation the applied glass panes thickness for ANG is 12.06 mm and for HSG 11.91 mm. Follow-up treatments to increase the glass strength as described in section 2.2.2.1 causes the out-of-plane imperfection of the glass pane. According to [Luible 2004] the maximum out-of-plane imperfection at the centre of the glass pane is the largest value of the length or the width of the glass pane divided by 2000. This value $\frac{1000}{2000} = 0.5$ mm is also used in the FE model (section 5.6). In appendix B.3, the measurements for the out-of-plane imperfections of each glass pane are given. The out-of-plane imperfections in the experiments were very small. In slender glass panes with a larger height and a smaller thickness these imperfections will increase (section 4.3.2.).

5.6 Solution strategy

The solution strategy consisted of two analyses. In first analysis the out-of-plane imperfection had to be applied on the glass pane, using a geometrical and physical linear calculation. This was done by applying an out-of-plane load onto the perfect flat glass pane. After an out-of-plane displacement of 0.5 mm was reached in the centre of the glass pane (section 4.4.2), all element coordinates of the displaced glass pane were read and applied in a new FE model. The new FE model consisted of a glass pane with an out-of-plane imperfection without any pre-stress and is used in the second analysis.

The second analysis is used to simulate the in-plane behavior of the system. In this analysis a geometrical and physical non linear calculation was needed, due to out-of-plane displacements of the glass pane with an initial out-of-plane imperfection and the physical non linear behavior of the applied adhesive when the system was exposed to an in-plane load. Starting point for non linear calculations was the regular Newton-Raphson iteration scheme (figure 5.35), i.e. the tangential stiffness matrix was set up before each iteration. To stabilize the convergence and to increase its speed, a line search algorithm was applied. The geometrical non linear calculation was done using the Total Lagrange formulation (i.e. strain and stress values are defined with reference to the un-deformed geometry). For the physical non linear calculation, only the option interface non linear behavior was applied. Additional information can be found in [TNO DIANA 2010].

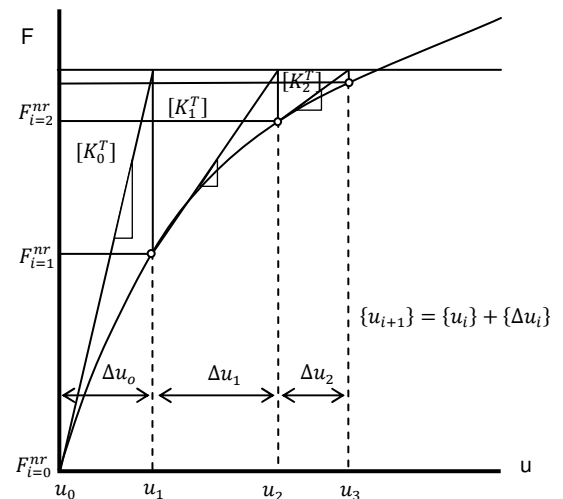


Figure 5.35 Newton Raphson procedure.

After checking the influence of smaller and larger load step sizes, the load step size in general was chosen to be 0.6 mm ($\frac{1}{50}$ of 30 mm), to obtain smooth graphs. Each calculation took about 50 minutes. The horizontal in-plane load (F_h) was displacement controlled and centrally introduced in the negative x-direction at the right side of the outside beam of the top transom (figure 4.1 and 4.2). An example of the input file used in the FE simulations can be found in appendix C.

5.7 Calibration

Section 5.7.1 starts with the calibration of the global behavior of the system implemented by [Huvener 2009]. In section 5.7.2, the simulation of the in-plane loaded system is calibrated and several sensitive studies (section 5.7.3) are carried out. In the sensitive studies the moment of glass-steel contact for a perfect system and for systems where the glass pane is not placed exactly in the middle of the system is determined. The distribution of longitudinal and transversal shear stress in the adhesive bonded joint is investigated in section 5.7.4 and in section 5.7.5 the simulation of the in-and out-of-plane loaded system is calibrated.

5.7.1 Calibration of the global behavior of the system

The FE model was calibrated for joint types 1 to 3 [Huvener 2009]. Several sensitive studies were carried out to investigate the influence of the vertical spring at the RBC of the system (section 4.4.3) and the shear flexibility ($k_{b,\eta}$) of the bolted connection between the outside beam and the beadwork (section 4.4.4) on the global behavior (F_h , $u_{RTC;s}$ and K_s) of all systems. Table 5.5 shows an overview of the global behavior of systems with joint types 1 to 3 at four different combination of the vertical spring stiffness at the RBC of the system and the shear flexibility of the bolted connection between the outside beam and the beadwork compared with the behavior found in experiments [Huvener 2009].

The influence of the shear flexibility between the outside beam and the beadwork on the global behavior of the systems is showed in column I and II. The shear flexibility results in relative horizontal and vertical in-plane displacements between the outside beam and the beadwork and reduces the flexural stiffness of the mullions and transoms. This behavior results in a reduction of the horizontal in-plane loads (column II).

The vertical in-plane loaded spring in the RBC of the systems displaces vertically and causes rotation in the system. Rotation of the systems reduces the in-plane loads (column III).

If the shear flexibility between the outside beam and the beadwork and the vertical spring stiffness of the RBC of the system interact together, a larger reduction on the horizontal in-plane load has to be taken into account (column IV). These results correspond well to the experiments (column V and VI).

Table 5.5 Overview global behavior of systems 1 to 3 [Huvener 2009]

		I	II	III	IV	V	VI
	$K_{y;RBC}$ [N/mm]	10^{20}	10^{20}	1.03×10^5	1.03×10^5	Exp.	Dev.
	$k_{b,\eta}$ [N/mm ³]	10^6	10	10^6	10		[%]
System 1	u_{RTC} [mm]	3.69	3.69	3.69	3.69	3.69	0.00
	F_h [kN]	4.37	4.33	4.30	4.27	4.42	-3.40
	$u_{RTC;s}$ [mm]	3.69	3.69	3.65	3.65	3.65	0.00
	K_s [kN/mm]	1.18	1.17	1.18	1.17	1.21	-3.30
	u_{RTC} [mm]	23.40	23.40	23.40	23.40	21.84	7.14
	F_h [kN]	39.10	37.20	36.70	37.70	36.87	2.25
	$u_{RTC;s}$ [mm]	23.01	23.03	23.03	23.02	21.13	8.96
System 2	u_{RTC} [mm]	1.02	1.02	1.02	1.02	1.02	0.00
	F_h [kN]	249.33	82.62	72.31	45.56	45.89	-0.72
	$u_{RTC;s}$ [mm]	1.02	1.02	0.30	0.56	0.56	0.00
	K_s [kN/mm]	239.65	79.41	243.56	80.72	81.79	-1.30
System 3	u_{RTC} [mm]	0.81	0.81	0.81	0.81	0.81	0.00
	F_h [kN]	182.52	55.80	58.21	33.80	31.43	7.54
	$u_{RTC;s}$ [mm]	0.81	0.81	0.23	0.47	0.50	-6.00
	K_s [kN/mm]	225.33	68.89	253.09	71.91	65.39	9.97

In this research the shear flexibility ($k_{b,\eta} = 10$) and the vertical spring stiffness ($K_{y;RBC} = 2.73 \times 10^5$) obtained in the experiments is used in the FE simulation of systems with joint type 2 (section 5.3.2).

5.7.2 In-plane loaded system with joint type 2

Figure 5.36 shows the comparison between the experiments and the FE simulation for the horizontal in-plane loads and the horizontal in-plane displacement of the RTC. The out-of-plane imperfection at the centre of the glass pane is -0.5 mm (section 5.5). Up to an in-plane displacement of the RTC of 14 mm, the FE simulation corresponds to the experiments. Beyond this point, the relation between the horizontal in-plane load and the horizontal in-plane displacement of the RTC of the FE model deviates from the experiments. The elements in the FE model representing the adhesive bonded joint, only describe the uni-axial shear behavior of the acrylic adhesive. However, this is only true if the middle of the glass pane is observed. From the middle to the corners of the glass pane, the adhesive bonded joint displaces in two directions (figure 5.37 and 5.38). Bi-axial shear behavior is not implemented in the FE model.

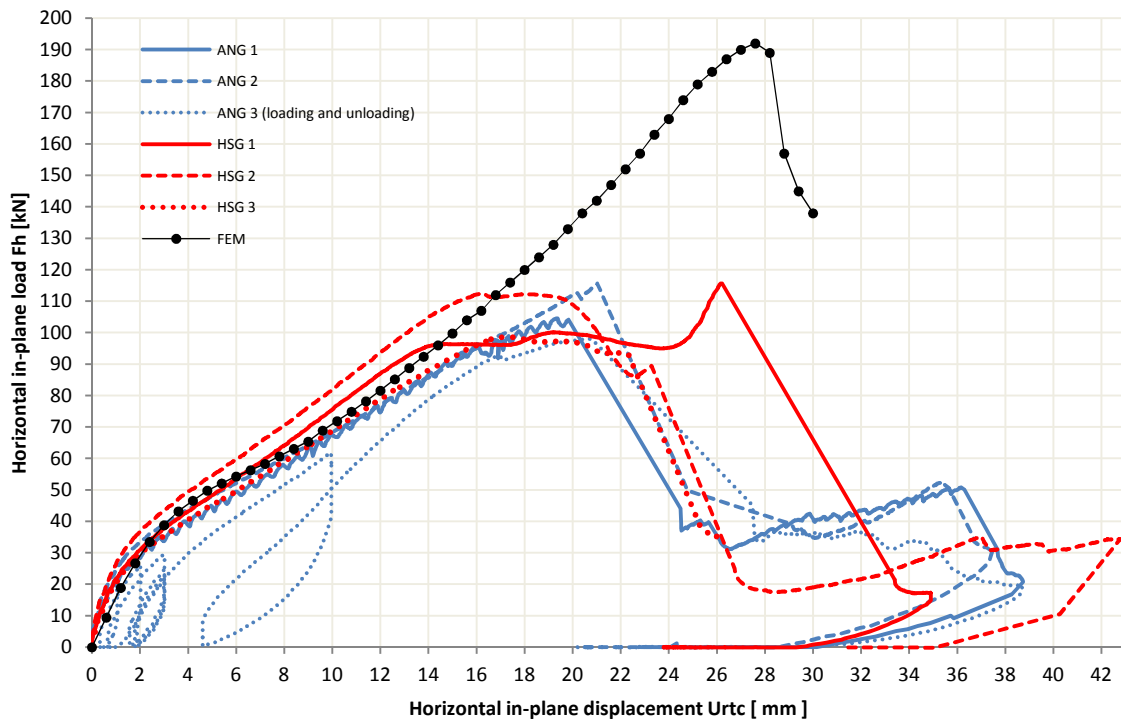


Figure 5.36 Comparison of the relation between the horizontal in-plane load and the horizontal in-plane displacement of the RTC of the FE simulation (black bolt dots) and the experiments (continuous, dashed and dotted red and blue lines).

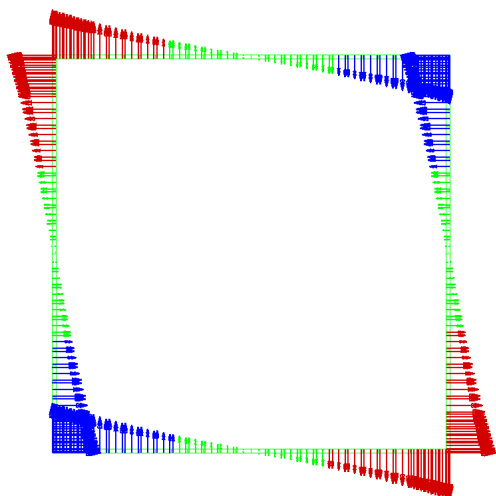


Figure 5.37 Relative displacement of the adhesive bonded joint in transversal direction ($u_{j;\zeta;rel}$ and $v_{j;\zeta;rel}$).

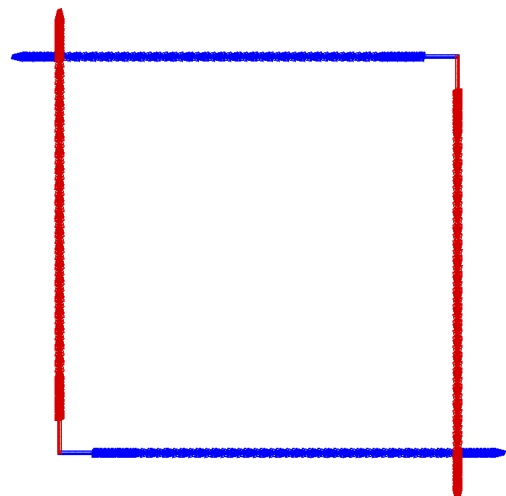


Figure 5.38 Relative displacement of the adhesive bonded joint in longitudinal direction ($u_{j;\eta;rel}$ and $v_{j;\eta;rel}$).

In figure 5.39 the comparison of the relation between the out-of-plane displacement of the centre of the glass pane and the in-plane displacement at the RTC of the system for the experiments and the FE simulation is presented. The simulation of the out-of-plane displacements of the centre of the glass pane is incorrectly described by the FE model.

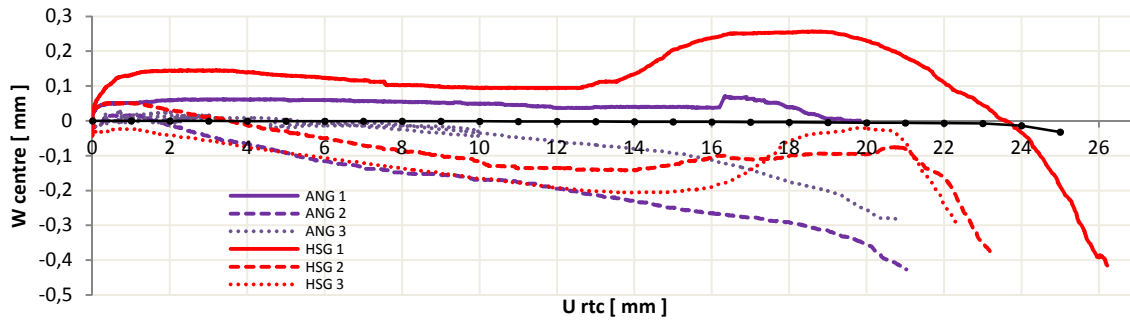


Figure 5.39 Comparison of the relation between the out-of-plane displacement of the centre of the glass pane and the horizontal in-plane displacement of the RTC of the FE simulation (black bolt dots) and the experiments (continuous, dashed and dotted red and purple lines).

In figure 5.40 and 5.41 for position 2 and position 5 respectively, the relation between the principle stresses and the in-plane displacement of the RTC are compared for the experiments and the FE simulation. The minimum principle stresses are compression stresses and the maximum principle stresses are tension stresses. Remarkable is the fact that the principle stresses are only well described in the dominant direction of the stresses. No plausible explanation can be given for this behavior. In the compression zone (position 1, 3 and 5, section 4.4.2) the minimum principle stresses are well simulated by the FE model. For position 1 and position 5 the maximum principle stresses are incorrectly described. In the tension zone (position 2, 3, and 4, section 4.4.2) the maximum principle stresses are well simulated by the FE model. The minimum principle stresses in position 2 and position 4 are incorrectly described. Position 3 is situated in the centre of the glass pane. In this point the minimum- and maximum principle stresses are correctly described. An overview of the development of the principle stresses in position 1 to 5 can be found in appendix B.5. Figure 5.43 shows the principle stresses and the stress angle at limited horizontal in-plane displacement of the RTC of the system. The maximum principle stress can be found in the RBC of the glass pane according to figure 5.42.

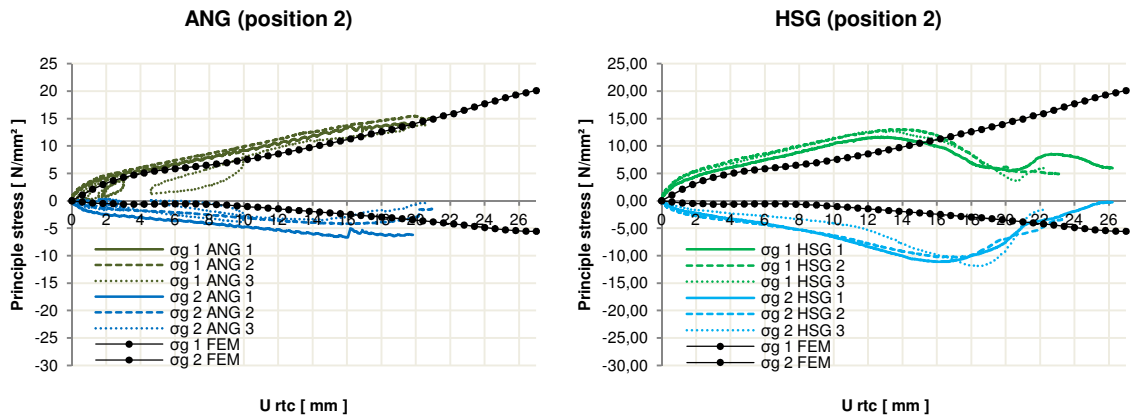


Figure 5.40 (ANG left and HSG right) Comparison of the relation between the principle stress at position 2 and the horizontal in-plane displacement of the RTC of the FE simulation (black bolt dots) and the experiments (continuous, dashed and dotted green and blue lines).

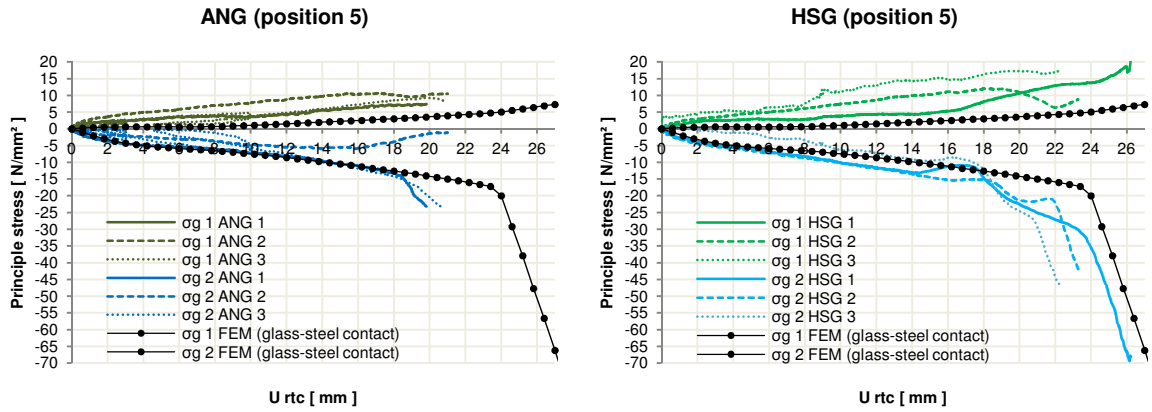


Figure 5.41 (ANG left and HSG right) Comparison of the relation between the principle stress at position 5 and the horizontal in-plane displacement of the RTC of the FE simulation (black bolt dots) and the experiments (continuous, dashed and dotted green and blue lines).

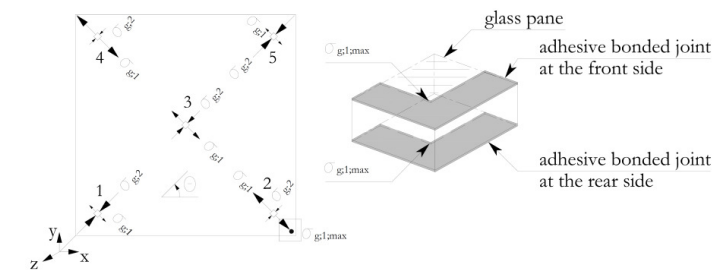


Figure 5.42 Location of the maximum principle stress for joint type two according to the FE model [Huvener 2009].

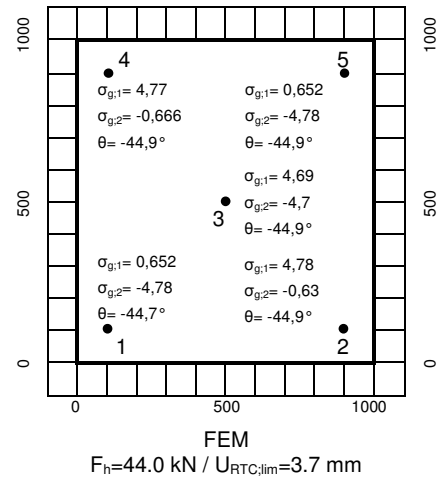


Figure 5.43 Principle stress distribution according to FEM.

5.7.3 Sensitivity analyses

Figure 4.14 (section 4.6.1) shows the fracture pattern which is representative for each in-plane loaded ANG pane and figures 4.18 up to 4.20 show the fracture patterns of in-plane loaded HSG pane. It is assumed that the sudden failure of the glass panes is caused by glass-steel contact. To (in)validate this assumption the FE model is used.

5.7.3.1 Glass - steel contact

In section 5.2.3.2 the working procedure of interface element B, which was used for simulations of systems with joint type one by Huveners (figure 1.4), is described. Here, interface element B has been used to analyze when and if glass-steel contact occurs. The free space around the glass pane in perfect position of the glass pane is 5 mm (figure 5.44). When the system is loaded in-plane, the free space around the glass pane at the LTC and RBC becomes larger. At the RTC and LBC the free space becomes less and eventually glass steel contact occurs. Interface element B is programmed to give almost no stiffness to the system when the space between the glass pane and the steel transom or mullion becomes larger (positive direction of the element). If the space between the glass pane and the steel transom or mullion becomes less (negative direction of the element), interface element B gives almost no stiffness up to the point of 5 mm relative in-plane displacement. When the relative in-plane displacement of interface element B becomes 5 mm, interface element B will behave very stiff (figure 5.45). The slope of the load displacement curve of the RTC will become larger and the point of glass-steel contact in terms of horizontal in-plane displacement (u_{rtc}) can be determined (figure 5.46).

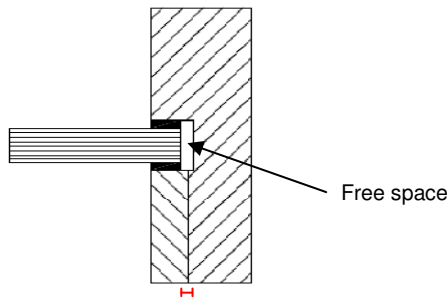


Figure 5.44 The free space around glass pane is 5 mm (perfect position of the glass pane).

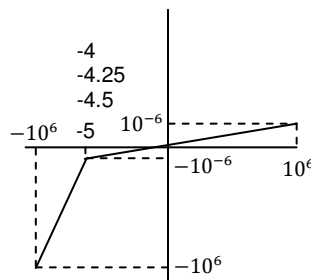


Figure 5.45 Stiffness properties of interface element B.

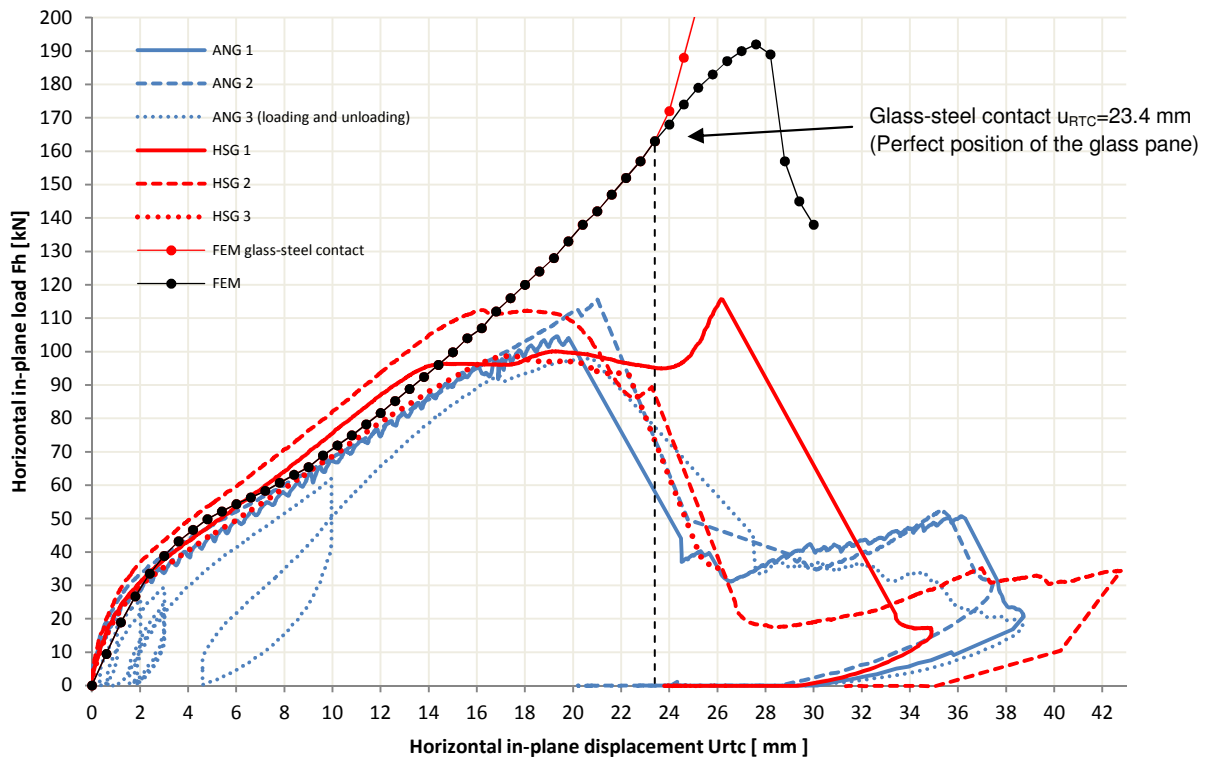


Figure 5.46 Determination moment of glass steel contact: 23.4 mm horizontal in-plane displacement RTC.

Now the moment of glass steel contact of a perfect positioned glass pane is known, an explanation for the failure at different horizontal in-plane displacement of the RTC has to be found. In section 5.7.3.2, glass-steel contact and the influence of the position of the glass pane has been discussed.

5.7.3.2 Glass - steel contact & the position of the glass pane

Each glass pane of ANG or HSG failed at different horizontal in-plane load or horizontal in-plane displacement. In this section the influence of the position of the glass pane is reviewed. It is very likely that the glass pane is not positioned perfect in the centre of the system, such that the space around the glass pane is 5 mm at each point. Figure 5.47 shows the influence on the moment of glass-steel contact when the free space around the perfect positioned glass pane is declined with respectively 0.5, 0.75 and 1 mm. In the FE model, the glass pane is still in perfect position. In practice the glass pane is not position perfect in the middle of the system and the free space around the glass pane is not equal on each side.

The objective of this analysis, by declining the free space around the glass pane, is to determine the influence on the moment of glass-steel contact if the position of the glass pane is not perfect in the centre of the system and moved 1 mm to the right. The result of this analysis is a simplification of the real behavior and overestimates the real influence of the position of the glass pane.

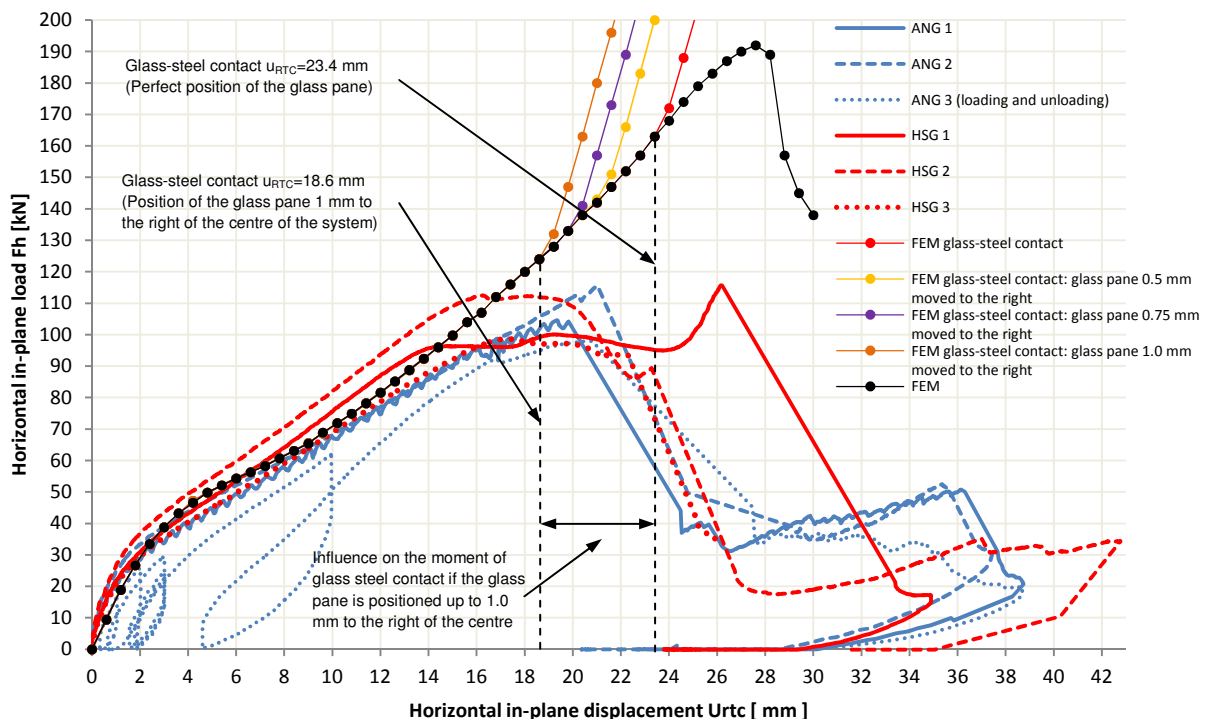


Figure 5.47 Moment of glass steel contact if the glass pane is not perfectly positioned in the centre of the system.

If the free space around the glass pane is 4 mm, the moment of glass-steel contact occurs at a horizontal in-plane displacement of the RTC of 18.6 mm. It can be concluded that the position of the glass pane has a large influence on the moment of glass-steel contact. The assumption that the failure of the glass pane is caused by glass-steel contact is now validated.

5.7.4 Distribution of longitudinal and transversal shear stresses in the adhesive bonded joint

The adhesive bonded joint can reveal a lot of information about the behavior of the system. In section 4.6 possible failure of the adhesive bonded joint and failure of the glass pane have been pointed out for each experiment. In section 5.7.3 glass-steel contact has been verified to be the failure mode of the glass pane. In this section failure of the adhesive bonded joint is reviewed using the relative displacements of the adhesive bonded joint of each in-plane loaded experiment, except for experiment ANG 3. In experiment ANG 3, the system has been loaded and unloaded, which influences the behavior of the adhesive bonded joint. Therefore this experiment cannot be compared to the other in-plane loaded glass panes.

Figures 5.48 and 5.49 represent the relation between the relative displacement of the adhesive and the horizontal in-plane displacement of the RTC of the system in the middle of the left- and right mullion and in the middle of the top- and bottom transom for in-plane loaded glass panes.

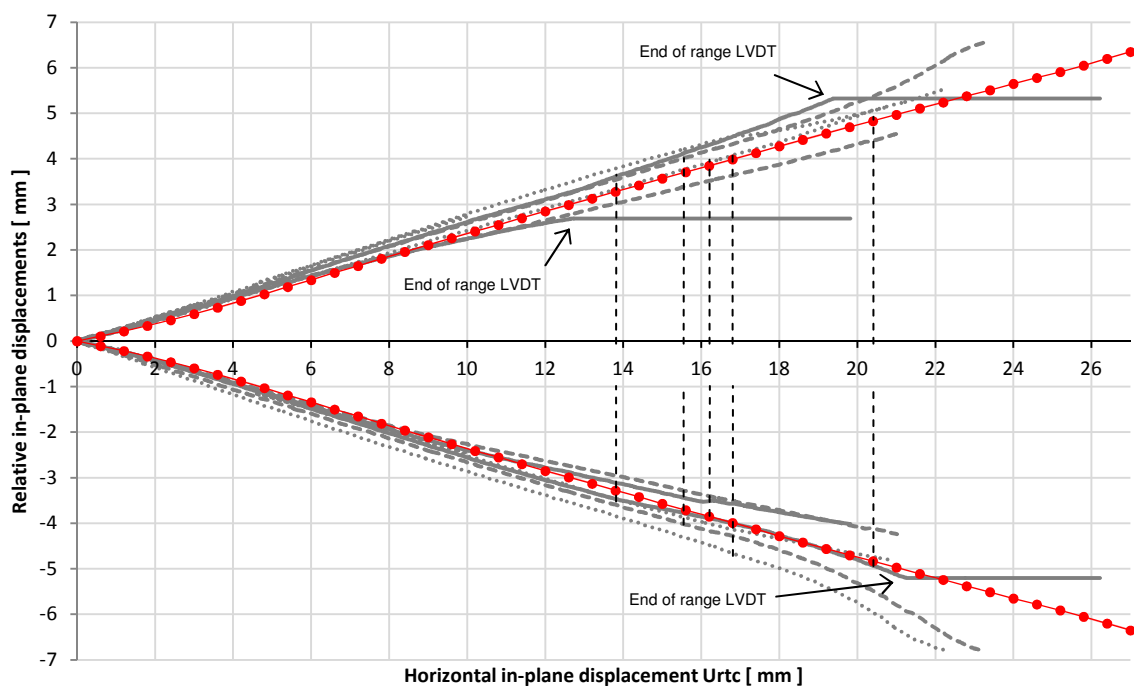


Figure 5.48 Relation between the relative displacement of the adhesive in longitudinal direction in the middle of the left and right mullion, and the horizontal in-plane displacement of the RTC.

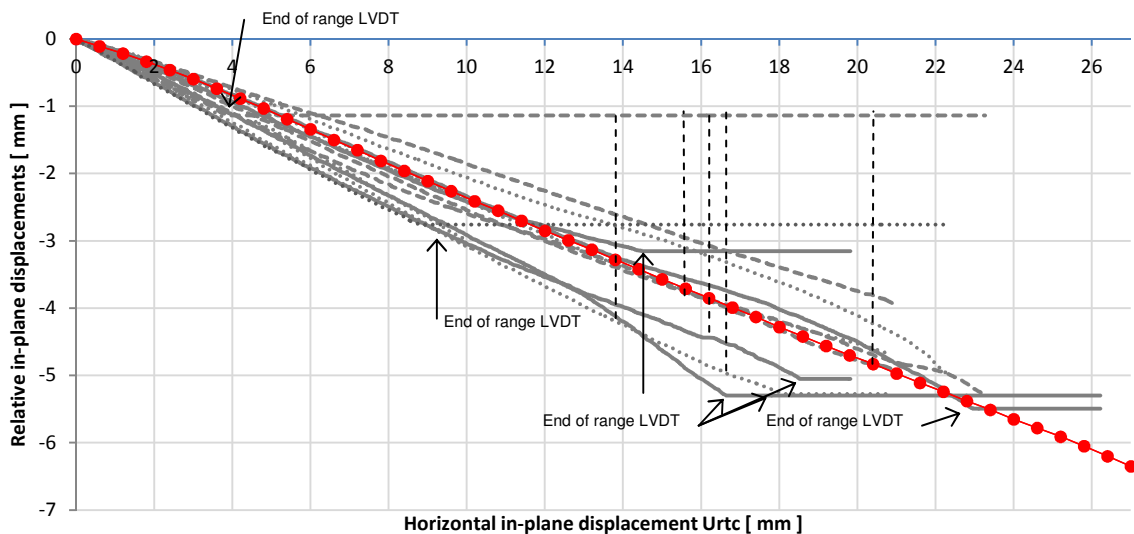


Figure 5.49 Relation between the relative displacement of the adhesive in longitudinal direction in the middle of the bottom and top transom, and the horizontal in-plane displacement of the RTC.

To check if the adhesive bonded joint fails, the relative displacements measured during in-plane loaded experiments are reviewed at the moment where the slope of the load-displacement curve of the system (suddenly) decreases.

The relation of the in-plane load and the horizontal in-plane displacement of the RTC of the system in experiment HSG 1, becomes horizontal at a horizontal in-plane displacement of the RTC of about 13.8 mm. For experiment 2 and 3 with HSG, the horizontal in-plane displacements of the RTC are about 15.6 and 16.8 mm. For experiments 1 and 2 with ANG the in-plane displacements of the RTC of the system are 16.2 and 20.4 mm. The relative displacement of the bonded joint for the experiments is highlighted in figure 5.48 and figure 5.49.

Figures 5.50 and 5.52 give an overview of the relative displacements of the adhesive bonded joint in longitudinal and transversal direction according to the FEM. The green dots represent the middle of the bonded joint and at these points the relative transversal displacement of the bonded joint is zero. In the experiments the relative displacement in longitudinal direction is measured (section 4.4.2) and is compared to the results of the FEM in tables 5.6 and 5.7. At the red dots, the adhesive bonded joint displaces in longitudinal- and in transversal direction. The maximum relative displacements per bonded joint can be found in these points and are equal to the sum of the vectors of the relative displacements in transversal and longitudinal direction.

According to the FEM, the relative transversal displacement of the adhesive bonded joint is about 90 percent of the relative longitudinal displacement for each corner of the bonded joint. To estimate the relative transversal displacement in the corner of the adhesive bonded joint in the experiments, the maximum relative longitudinal displacement of the experiment is multiplied with 0,9. The reduction on the transversal displacement is caused by the shear deformation of the glass pane. Adding up the vectors of the relative transversal- and longitudinal displacement of the adhesive bonded joint gives the maximum relative displacement in the corner of the adhesive bonded joint (tables 5.6 and 5.7).

For almost all experiments, one of the four relative displacements in the middle of the adhesive bonded joint exceeded the predicted value by the FEM. This means that the maximum relative displacement in at least one of the four corners of the adhesive bonded joint is also higher than the predicted value by the FEM. Figures 5.51 and 5.53 compare the relative displacement in the leading corner of the adhesive bonded joint between experiments and FEM at different horizontal in-plane displacements of the RTC.

The maximum relative displacement in the leading corner of the adhesive bonded joint in the experiments is, except for experiment ANG 2, larger than the maximum relative displacement in the LBC of the system for the FEM. The maximum relative displacements in experiments HSG 1, HSG 2 and ANG 1 lay before of near the maximum allowable relative displacement, the point where the adhesive fails on cohesion. For experiments HSG 3 and ANG 2, the relative maximum displacement in the corner of the adhesive bonded joint lays at or behind the maximum allowable relative displacement. The maximum allowable relative displacement is based on experiments in the preliminary research (batch 3, section 3.1).

To get more information about the behavior of the adhesive bonded joint during experiments, complementary shear tests were carried out (section 3.2). Here, the area of the bonded joint was multiplied by four, compared to batch 3 of the preliminary research. The geometry of the adhesive bonded joints of batch 3 in the preliminary research were $10 \times 25 \text{ mm}^2$, and the geometry of the adhesive bonded joints in the complementary research were $10 \times 100 \text{ mm}^2$ and $100 \times 10 \text{ mm}^2$.

The adhesive bonded joints with a larger area fail at a smaller value for the relative displacement of the adhesive (section 3.2.3). This means that it is very plausible that the adhesive in the full scale experiments fail also at lower values for the relative displacement, for both ANG and HSG panes (figures 5.51 and 5.53).

When the bonded joint of the ANG pane starts to fail at the corners of the glass pane, the adhesive parts direct next to the failed adhesive stays intact and are locked in the surface flaws of the glass pane. This causes a small discontinuity in the load-displacement curve. Eventually the intact part of the adhesive direct next to the failed adhesive fails also when it has reached the maximum permitted relative in-plane displacement.

Moreover, if cohesive failure of the adhesive bonded joint has started at the corners of systems with HSG panes, the adhesive parts direct next to the failed adhesive also fail and rupture. Here, the adhesive is not locked in the surface flaws of the glass panes and a slow chain reaction causes a constant failure of the adhesive, resulting in a horizontal relation of the load displacement curve.

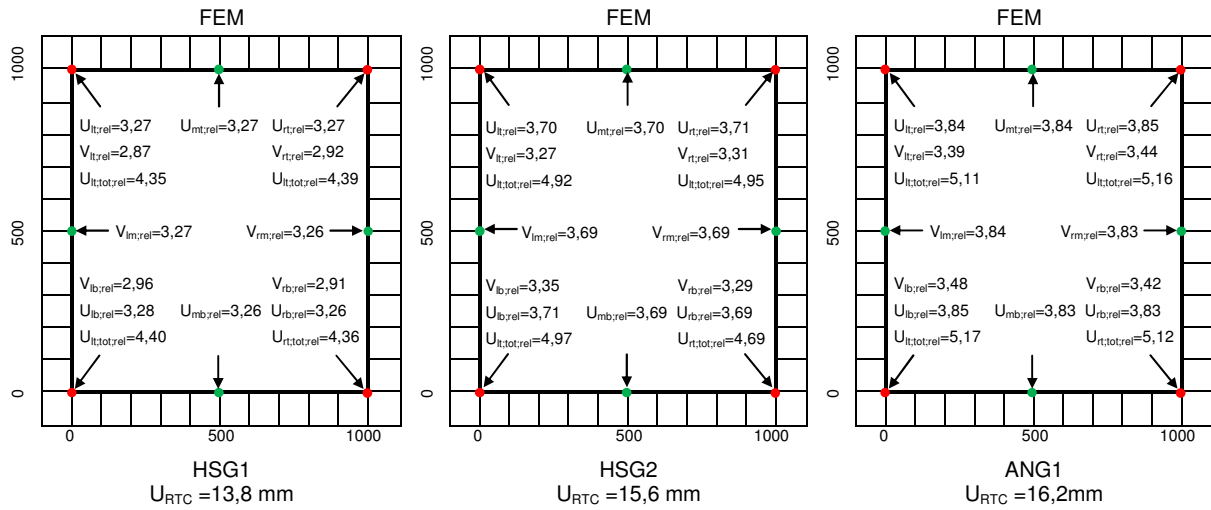


Figure 5.50 Relative displacements of the adhesive bonded joint in longitudinal and transversal direction, adopted from the FEM for experiments HSG1 ($U_{RTC} = 13,8 \text{ mm}$) and HSG2 ($U_{RTC} = 15,6 \text{ mm}$) and ANG1 ($U_{RTC} = 16,2 \text{ mm}$).

Table 5.6 Estimation of the maximum relative displacements in the corner of the adhesive bonded joint.

	HSG 1 $U_{RTC} = 13,8 \text{ mm}$	FEM	HSG 2 $U_{RTC} = 15,6 \text{ mm}$	FEM	ANG 1 $U_{RTC} = 16,2 \text{ mm}$	FEM
$U_{mt,rel}$ [mm]	4,12	3,27	3,76	3,70	4,44	3,84
$U_{mr,rel}$ [mm]	3,47	3,26	4,03	3,69	3,52	3,83
$U_{mb,rel}$ [mm]	3,24	3,26	X	3,69	X	3,83
$U_{ml,rel}$ [mm]	3,61	3,27	4,03	3,70	X	3,84
	$V_{max,rel; HSG1} \approx 0,90 \times 4,12$	$\frac{V_{max,rel; FEM}}{U_{max,rel; FEM}} \approx 0,90$	$V_{max,rel; HSG2} \approx 0,90 \times 4,03$	$\frac{V_{max,rel; FEM}}{U_{max,rel; FEM}} \approx 0,90$	$V_{max,rel; ANG1} \approx 0,90 \times 4,44$	$\frac{V_{max,rel; FEM}}{U_{max,rel; FEM}} \approx 0,90$
$U_{max,rel}$ [mm]	4,12	3,28 (LBC)	4,03	3,71 (LBC)	4,44	3,85 (LBC)
$V_{max,rel}$ [mm]	3,71	2,96 (LBC)	3,63	3,35 (LBC)	4,00	3,48 (LBC)
$U_{tot,rel}$ [mm]	5,54	4,40	5,42	4,97	5,97	5,17
$\tau_{tot,rel}$ [N/mm ²]	6,17	4,54	5,99	5,32	6,75	5,60

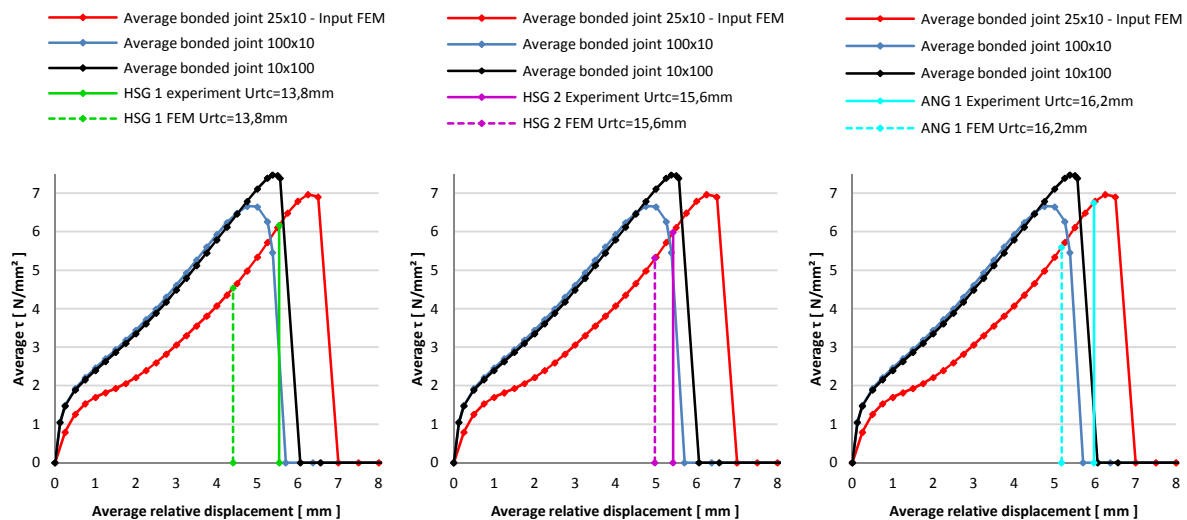


Figure 5.51 Comparison of the vector of the relative displacement in the leading corner of the adhesive bonded joint between experiments and FEM for experiments HSG1 ($U_{RTC} = 13,8 \text{ mm}$) and HSG2 ($U_{RTC} = 15,6 \text{ mm}$) and ANG1 ($U_{RTC} = 16,2 \text{ mm}$).

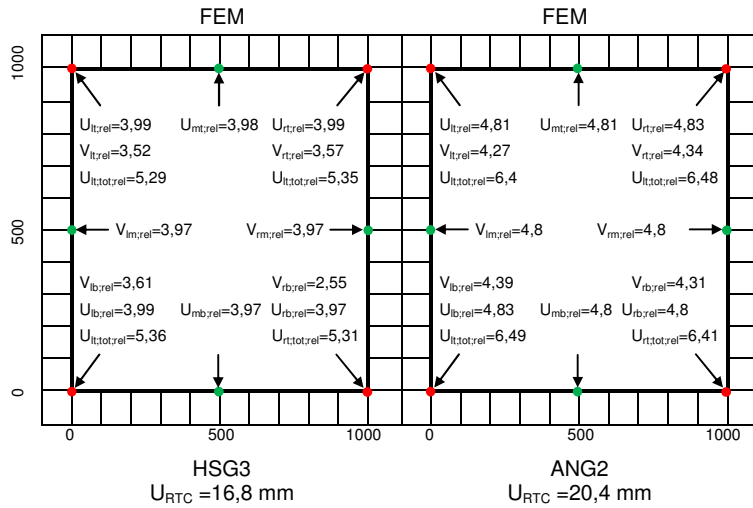


Figure 5.52 Relative in-plane displacements of the adhesive bonded joint in longitudinal and transversal direction, adopted from the FEM for experiments HSG3 ($U_{RTC} = 16,8 \text{ mm}$) and ANG2 ($U_{RTC} = 20,4 \text{ mm}$).

Table 5.7 Estimation of the maximum horizontal displacement (addition of vectors) in the LBC of the system.

	HSG 3 $U_{RTC} = 13,8 \text{ mm}$	FEM	ANG 2 $U_{RTC} = 20,4 \text{ mm}$	FEM
$U_{mt,rel} [\text{mm}]$	3,35	3,98	4,82	4,81
$U_{mr,rel} [\text{mm}]$	4,66	3,97	4,11	4,8
$U_{mb,rel} [\text{mm}]$	2,76	3,97	3,81	4,8
$U_{ml,rel} [\text{mm}]$	4,08	3,97	4,39	4,8
	$V_{max,rel; HSG3} \approx 0,90 \times 4,66$	$V_{max,rel; FEM} \approx U_{max,rel; FEM} \approx 0,90$	$V_{max,rel; ANG1} \approx 0,90 \times 4,82$	$V_{max,rel; FEM} \approx U_{max,rel; FEM} \approx 0,90$
$U_{max,rel} [\text{mm}]$	4,66	3,99 (LBC)	4,82	4,83 (LBC)
$V_{max,rel} [\text{mm}]$	4,19	3,61 (LBC)	4,34	4,39 (LBC)
$U_{tot,rel} [\text{mm}]$	6,27	5,36	6,48	6,49
$\tau_{tot,rel} [\text{N/mm}^2]$	6,96	5,89	6,91	6,90

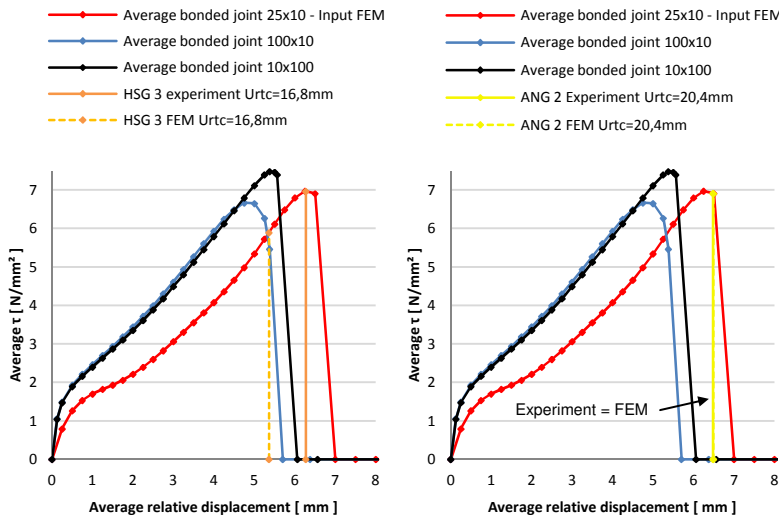


Figure 5.53 Comparison of the vector of the relative displacements in the leading corner of the adhesive bonded joint between experiments and FEM for experiments HSG3 ($U_{RTC} = 16,8 \text{ mm}$) and ANG2 ($U_{RTC} = 20,4 \text{ mm}$).

5.7.5 In- & out-of-plane loaded system with joint type 2

Before the experiments are compared to the FE simulation, the differences in basic assumptions have been given:

FEM:

- The LTC and RTC of the system are supported and cannot displace out-of-plane;
- The in-plane displacement of 3.7 mm and the out-of-plane load are simultaneously applied and distributed in 25 steps;
- The glass pane has an out-of-plane imperfection of -0.5 mm (section 5.5).

Experiments:

- The LTC and RTC of the system are not supported and can displace out-of-plane;
- First the system has been displaced up to $u_{RTC}=3.7\text{mm}$. Next the out-of-plane load is introduced up to glass failure;
- The out-of-plane imperfection is less than 0.5 mm (Appendix B.5)

In the experiments the out-of-plane load is applied through a 20 mm thick square rubber element of $80\times 80\text{ mm}^2$ and in the FEM the load is applied on four elements of $40\times 40\text{ mm}^2$, according to the mesh density in the centre of the glass pane (section 5.4).

Figure 5.54 shows the comparison between the experiments and the FE simulation for the out-of-plane load and the out-of-plane displacement of the centre of the glass pane. The corrected out-of-plane displacement of the centre of the glass pane for the system with ANG and the corresponding out-of-plane load deviates a lot when compared to the out-of-plane displacement of the FEM with its corresponding out-of-plane load. The sudden inexplicable increase in the load-displacement curve causes the divergence. The corrected out-of-plane displacement of the centre of the glass pane for the system with HSG and the corresponding out-of-plane load is well described by the FE model.

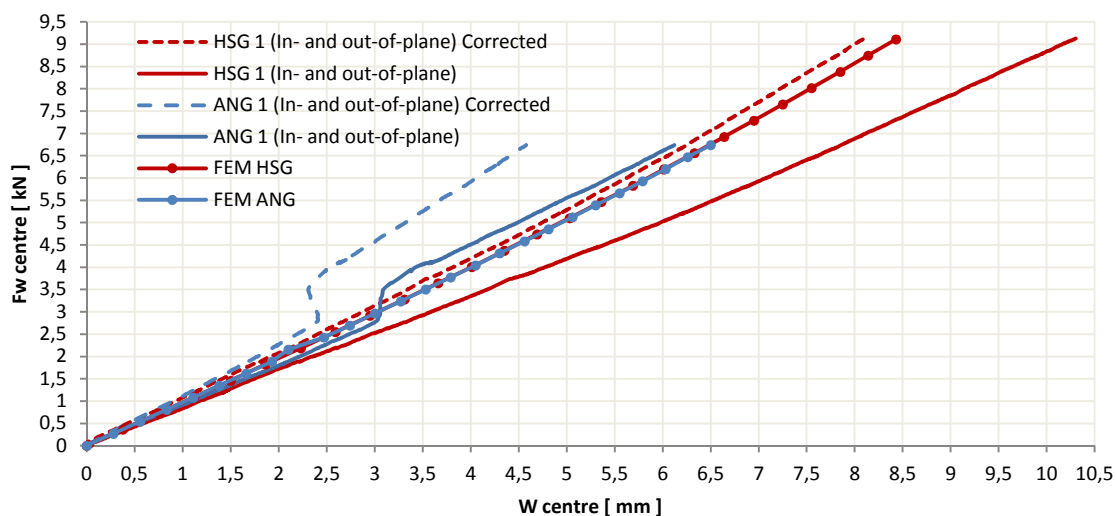


Figure 5.54 Relation between the out-of-plane load and the (corrected) out-of-plane displacement of the experiments compared to the FE simulation.

Figure 5.55 presents the relation between the out-of-plane load and the maximum principle stress in the centre of the glass pane for experiments and the FE simulation. Possibly, due to stress relaxation in the adhesive bonded joint the maximum principle stress in the centre of the glass pane for the experiments have a smaller value comparing to the FE simulation. This behavior has not been taken into account in the FEM.

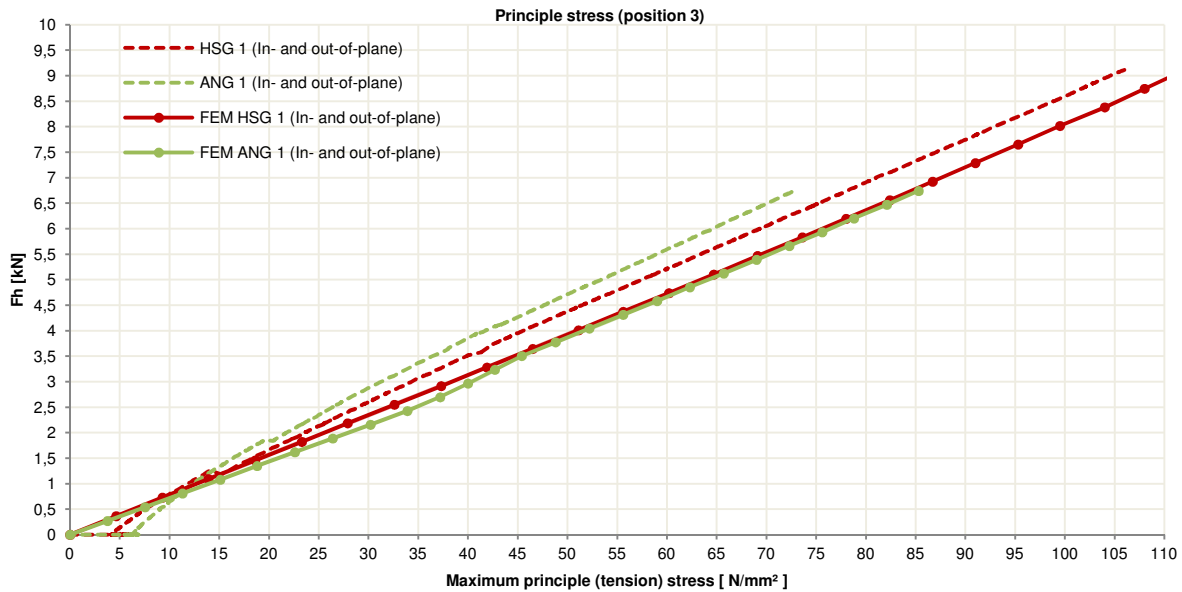


Figure 5.55 Relation between the out-of-plane load and the maximum principle stress of the experiments compared to the FE simulation.

The out-of-plane point load applied in the FE simulation corresponds with the out-of-plane point load in the experiments. However, a wind load is uniform distributed and therefore a uniform distributed load has been determined corresponding to the out of-plane displacement of the out-of-plane point load by the FE simulation for both ANG and HSG panes (table 5.8). To get an idea of the maximum representative out-of-plane wind load for one-storey buildings an ordinary calculation determining the wind loads according to the [NEN 6702:2007] has been made (equation 5.5).

$$Q_{\text{wind}} = (\text{internal} + \text{external surface pressure coefficient}) \times P_w \times C_{\text{dim}} \quad (\text{equation 5.5})$$

where:

P_w	0.73	Wind pressure (uncultivated);
C_{dim}	1.0	Dimension factor not allowed to be used for local calculation;
C_{pi}	0.3	(internal positive surface pressure coefficient);
C_{pe}	0.8	(external negative surface pressure coefficient).

$$Q_{\text{wind}} = (0.8+0.3) \times 1.0 \times 0.73 = 0.80 \text{ [kN/m}^2\text{]}$$

In-plane loaded glass panes up to limited horizontal in-plane displacement of the have a large capacity to be loaded out-of-plane by an uniform distributed wind load.

Table 5.8 Out-of-plane uniform distributed loads and point loads for both ANG and HSG in experiments and FE simulations.

	Experiments ANG Point load	FEM ANG Point load	FEM ANG Uniform load	Experiments HSG Point load	FEM HSG Point load	FEM HSG Uniform load
Corrected out-of-plane displacement (W_{CENTRE})	4.58 [mm]	6.50 [mm]	6.51 [mm]	8.09 [mm]	8.43 [mm]	8.41 [mm]
Out-of-plane load	6.74 [kN]	6.74 [kN]	18.57 [kN/m ²]	9.11 [kN]	9.11 [kN]	25.6 [kN/m ²]

5.8 Discussion of the results

Up to 14 mm horizontal in-plane displacement of the RTC, the FE model is representative for the behavior of the system with the acrylic adhesive. At that point the load-displacement curve of the experiments diverges from the FE model.

The out-of-plane displacements due to an in-plane load are not well described. No plausible answer can be given for this behavior.

The principle stresses at points 1 to 5 (section 4.4.2) are only well described in the dominant direction of the stresses. In the compression zone (position 1, 3 and 5) the minimum principle stresses are well simulated by the FE model. For position 1 and position 5 the maximum principle stresses are incorrectly described. In the tension zone (position 2, 3, and 4) the maximum principle stresses are well simulated by the FE model. The minimum principle stresses in position 2 and position 4 are incorrectly described. Position 3 is situated in the centre of the glass pane. In this point the minimum- and maximum principle stresses are correctly described. No plausible answer can be given for this behavior. The maximum principle stress can be found in the RBC of the glass pane (figure 5.42), but is not a criterion.

The FE model shows that glass-steel contact in a perfect system occurs at a horizontal in-plane displacement of the RTC of 23.4 mm, including the effect of the vertical spring at the RBC (section 5.7.3.1). In practice the glass pane will not be perfect in position. Sensitivity analysis showed that if the free space around the glass pane is declined to 4 mm, glass-steel contact occurs at a horizontal in-plane displacement of the RTC of 18.6 mm (5.7.3.2). It can be concluded that the position of the glass pane in the steel frame has a large influence on the moment of glass-steel contact. Glass-steel contact is the failure mode of all in-plane loaded experiments.

The maximum longitudinal and transversal relative displacements and shear stresses are located at the corners of the adhesive bonded joint (section 5.7.4). According to the FE simulation, the relative displacements in transversal direction in the corners of the adhesive bonded joint can be estimated about 90% of the relative displacements in longitudinal direction. The reduction on the relative transversal displacement is caused by the shear deformation of the glass pane. The vectors of the longitudinal and transversal displacements at the corners of the adhesive bonded joints are according to the experiments at least in one corner larger than simulated by the FE model (tables 5.6 and 5.7). In the FE model, the glass pane is positioned perfectly in the centre of the system while the glass pane in the experiments is likely to be positioned slightly out of the centre of the system. This causes larger longitudinal and transversal in-plane displacements in at least one corner of the adhesive bonded joint.

According to preliminary shear tests, the vector of the relative in-plane displacement at the corner of the adhesive bonded joint is less or near the maximum allowable relative in-plane displacement (figures 5.51 and 5.53). Moreover, complementary shear tests (section 3.2) showed that if the area of the adhesive bonded joints is multiplied by four ($100 \times 10 \text{ mm}^2$ or $10 \times 100 \text{ mm}^2$ instead of $25 \times 10 \text{ mm}^2$) cohesive failure of the adhesive bonded starts at less relative in-plane displacement of the adhesive bonded joint. This means that at the points where the load-displacement curve of the experiments show a discontinuity or becomes horizontal (figures 4.12 and 4.17), the adhesive has started to fail on cohesion in the corners of the adhesive bonded joint (figures 5.51 and 5.53).

FE simulation on in- and out-of-plane loaded glass panes (section 5.7.5) were carried out and compared to the experiments. The out-of-plane displacement in the centre of the glass pane is well described by the FE model for the system with the HSG pane. Due to a sudden inexplicable increase in the load-displacement curve in the experiment of the system with the ANG pane, the FE model deviates a lot compared to the experiment (figure 5.54).

The maximum principle stress in the centre of the glass pane in the FE simulation corresponds quite well to the experiments but the maximum principle stress in the centre of the glass pane in the experiments is less than simulated by the FE model (figure 5.55). The small deviation is likely caused by stress relaxation in the adhesive bonded joint. This behavior has not been taken into account in the FEM.

An uniform distributed out-of-plane load has been determined which gives the same out-of-plane displacement due to the out-of-plane point load in the centre of the glass pane. The ultimate uniform out-of-plane load which causes the glass pane to crack is very large and out-of-plane wind loads for one-storey buildings can easily be supported (table 5.8).

5.9 Conclusion

Section 5.9.1 presents the conclusions of the FE simulations with in-plane loaded glass panes. In section 5.6.2, conclusions of FE simulations with in- and out-of-plane loaded glass panes are given.

5.9.1 In-plane loaded glass panes:

- Simulations are carried out with an initial out-of-plane displacement of the centre of the glass pane of 0.5 mm;
- The FE model is representative for the global behavior (F_h , $u_{RTC;s}$ and K_s) of the system and simulates the experiments well up to 14 mm horizontal in-plane displacement of the RTC of the system;
- Out-of-plane displacements of the centre of the glass pane are not correctly described by the FE model;
- The principle stresses are only well described in the dominant direction of the stresses;
- The maximum principle stress in the RBC of the glass pane is not a failure criterion;
- Glass-steel contact is the failure mode of the system;
- For perfect systems, glass-steel contact occurs at 23.4 mm horizontal in-plane displacement of the RTC of the system;
- For glass panes with a free space of 4 mm around the glass pane, glass-steel contact occurs at 18.6 mm in-plane displacement of the RTC of the system;
- The position of the glass pane in the steel frame has a large influence on the moment of glass-steel contact;
- In the corners of the adhesive bonded joints, the adhesive failed on cohesion before the point of glass-steel contact was reached;
- The relative displacement in transversal direction in the corners of the adhesive bonded joint is about 90% of the relative displacement in longitudinal direction;
- The vector of the relative displacement in transversal- and longitudinal direction in the corners of the adhesive bonded joint for experiments is at least in one corner of the adhesive bonded joint larger than the simulated by the FE model;
- Complementary shear tests showed cohesive failure of the adhesive bonded joints at less relative in-plane displacement of the adhesive. At points where the load-displacement curve of the system in experiments showed a discontinuity (ANG panes) or became horizontal (HSG panes), the adhesive in the corners of the adhesive bonded joint had started to fail on cohesion.

5.9.2 In- and out-of-plane loaded glass panes:

- Results can only be used indicatively;
- The maximum principle stresses in the centre of the glass pane in experiments are quite well described by the FE model. The small deviation is possibly caused by stress relaxation of the adhesive bonded joint, which has not been taken into account in the FE model;
- In-plane loaded glass panes up to limited horizontal in-plane displacement have a large capacity to account for out-of-plane wind loads.

6 Mechanical models

In this chapter mechanical models are derived for systems with square circumferentially adhesive bonded glass panes to a steel frame. The mechanical models for joint type 1 (figure 1.4), applied with polyurethane, derived by [Huvener 2009] are adapted to joint type 2, applied with an acrylic.

6.1 Basic principles of mechanical models

Figure 6.1 presents the relation of the horizontal in-plane displacement (u_{RTC}) and the horizontal in-plane load (kN) for experiments and finite element analyses. The mechanical models are based on the FE model (chapter 5) but can only be used to describe the in-plane load transfer for non-cracked glass panes and a non-failed adhesive bonded joint. This means that the mechanical model can only be used up to a horizontal in-plane displacement of the RTC of 14 mm. The moment of glass-steel contact still can be predicted in section 6.2. The partial factor approach for the ultimate and serviceability limit state is not taken into account.

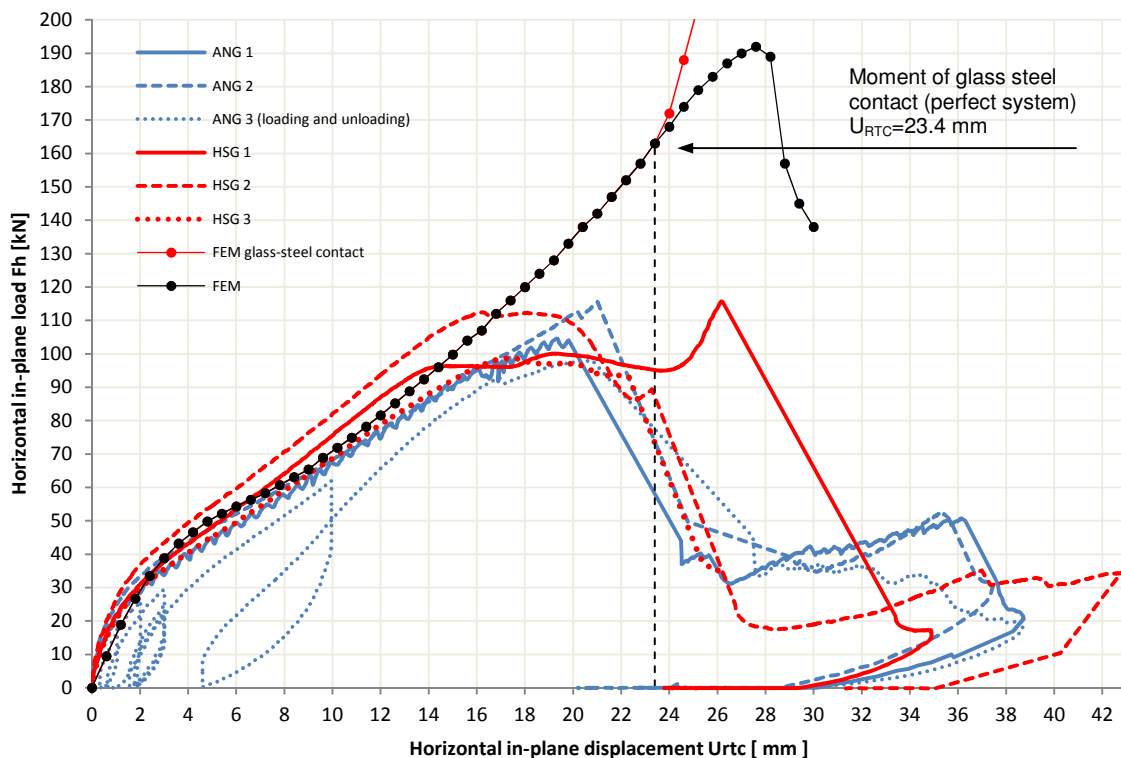


Figure 6.1 Relation of the horizontal in-plane displacement (u_{RTC}) and the horizontal in-plane load (kN) for experiments and finite element analyses.

In figure 6.2 the distribution of the relative horizontal and vertical in-plane displacements in longitudinal ($u_{j;\eta;rel} / v_{j;\eta;rel}$) and transversal direction ($u_{j;\zeta;rel} / v_{j;\zeta;rel}$) and the shear stresses in longitudinal ($\tau_{j;\eta;x} / \tau_{j;\eta;y}$) and transversal direction ($\tau_{j;\zeta;x} / \tau_{j;\zeta;y}$) are given. The distribution is representative for the adhesive bonded joints on both sides of the glass pane (section 5.7.3). The maximum principle stress in the glass pane which occurs in the RBC of the system has not been taken into account in the mechanical models, because it is not a failure criterion of the system with the acrylic adhesive.

For square glass panes, bonded with the acrylic used in this research (appendix A.9) there are two points of interest in predicting the behavior of the system. The limited horizontal in-plane displacement (table 6.1, because of serviceability of a building and the moment of glass-steel contact (table 6.2) are important to predict.

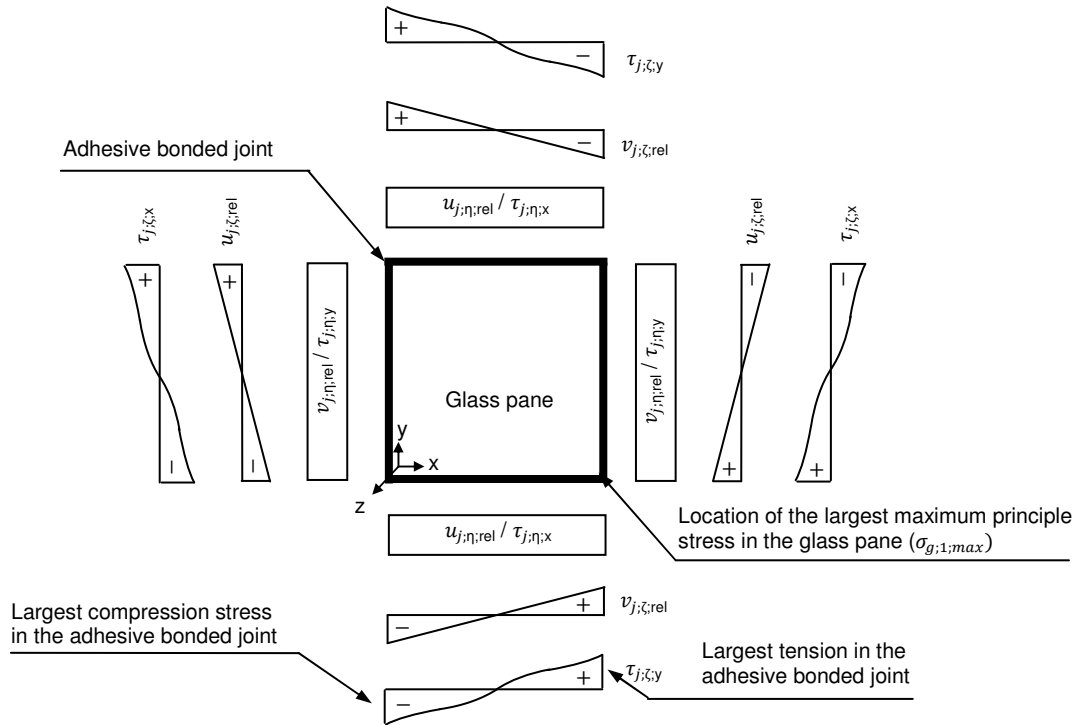


Figure 6.2 Distribution of the relative horizontal and vertical in-plane displacements in longitudinal ($u_{j,\eta;rel} / v_{j,\eta;rel}$) and transversal direction ($u_{j,\zeta;rel} / v_{j,\zeta;rel}$) and the shear stresses in longitudinal ($\tau_{j,\eta;x} / \tau_{j,\eta;y}$) and transversal direction ($\tau_{j,\zeta;x} / \tau_{j,\zeta;y}$) representative for the adhesive bonded joints on both sides of the glass pane.

Table 6.1 To be predicted in mechanical models at limited horizontal in-plane displacement at the RTC.

At limited horizontal in-plane displacement at the RTC of the system, the mechanical models have to predict:

- the in-plane stiffness of the system ($K_{s,lim}$);
- the horizontal in-plane load ($F_{h,lim}$);
- the maximum relative horizontal and vertical in-plane displacement in transversal direction of the adhesive bonded joint ($u_{j,\zeta;rel,max}$ and $v_{j,\zeta;rel,max}$);
- the maximum transversal shear stress in x- and y- direction ($\tau_{j,\zeta;x,max}$ and $\tau_{j,\zeta;y,max}$);
- the maximum relative horizontal and vertical in-plane displacement in longitudinal direction of the adhesive bonded joint ($u_{j,\eta;rel,max}$ and $v_{j,\eta;rel,max}$);
- the maximum longitudinal shear stress in x- and y- direction ($\tau_{j,\eta;x,max}$ and $\tau_{j,\eta;y,max}$);

Table 6.2 To be predicted in mechanical models at glass-steel contact.

At glass-steel contact, the mechanical models have to predict:

- the horizontal in-plane load ($F_{h,1}$);
- the horizontal in-plane displacement at the RTC of the system ($U_{RTC,1}$).

The geometrical parameters of the system are presented in table 6.3 and at the left top of figure 6.4. The coordinate system of interface elements A, B and C differ in direction (figure 6.3). For joint type 2, the relative horizontal- and vertical displacement ($u_{j,\xi;rel,max} / v_{j,\xi;rel,max}$) in figure 6.4 based on joint type 1, have to be read as ($u_{j,\zeta;rel,max} / v_{j,\zeta;rel,max}$).

Table 6.3 The geometric parameters of the system are:

Geometric parameters:	[mm]
- the nominal glass thickness (t_g)	12
- the glass pane width (w_g)	1000
- the glass pane height (h_g)	1000
- the system width (w_s)	1110
- the system height (h_s)	1110
- the thickness of the steel frame (t_f)	80
- the joint thickness ($t_{j;A/C}$)	3
- the joint thickness ($t_{j;B}$)	5
- the joint width (w_j)	10

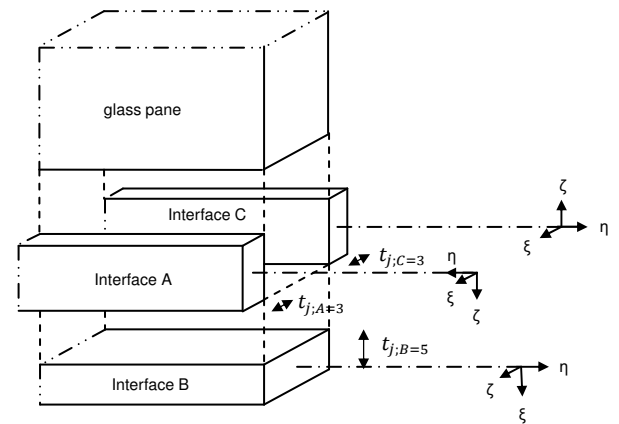


Figure 6.3 Direction of the coordinate system of the interfaces A,B and C.

The centre of the glass pane is coupled to the middle of a construction line (d_s) from the hinge at the LBC to the hinge of the RTC of the system. The parameters in figure 6.4 at the right top that go with in-plane displacements of the RTC are presented in table 6.4. Figure 6.4 at the bottom shows an enlarged view of the RBC of the system.

Table 6.4 The parameters that go with in-plane displacements at RTC:

- the horizontal in-plane load (F_h)
- the horizontal in-plane displacement at the RTC of the system (u_{RTC})
- the in-plane rotation of the right mullion around the internal hinge at the RBC (β)
- the in-plane rotation of the glass pane around its centre (φ)
- the relative horizontal and vertical in-plane displacement in longitudinal and transversal direction ($u_{j;\eta/\zeta;rel}$ and $v_{j;\eta/\zeta;rel}$)
- the additionally relative horizontal and vertical in-plane displacement in longitudinal and transversal direction ($\Delta u_{j;\eta/\zeta;rel}$ and $\Delta v_{j;\eta/\zeta;rel}$)

Basic assumptions for the mechanical models are:

- no initial out-of-plane displacements of the glass pane;
- the glass pane acts rigid in-plane;
- the centre of the horizontally in-plane displaced glass pane is thought to coincide with the middle of the construction line;
- no deformation in axial direction of the steel mullions and transoms;
- no vertical in-plane displacements of the transoms and mullions;
- no bending of the steel transoms and mullions;
- no shear deformation of the bolted connection between the beadwork and the outside beam;
- linear distribution of the relative in-plane displacements in transversal direction (section 5.7.2);
- multi-linear distribution of the transversal shear stresses of the adhesive bonded joint corresponding with the assumed relation between the shear stress and relative in-plane displacement;
- uniform distribution of the relative in-plane displacements in longitudinal direction (section 5.7.2);
- uniform distribution of the longitudinal shear stresses of the adhesive bonded joint;
- equal diagonals of the horizontally in-plane displaced steel frame (parallelogram) at limited horizontal in-plane displacement at the RTC of the system.

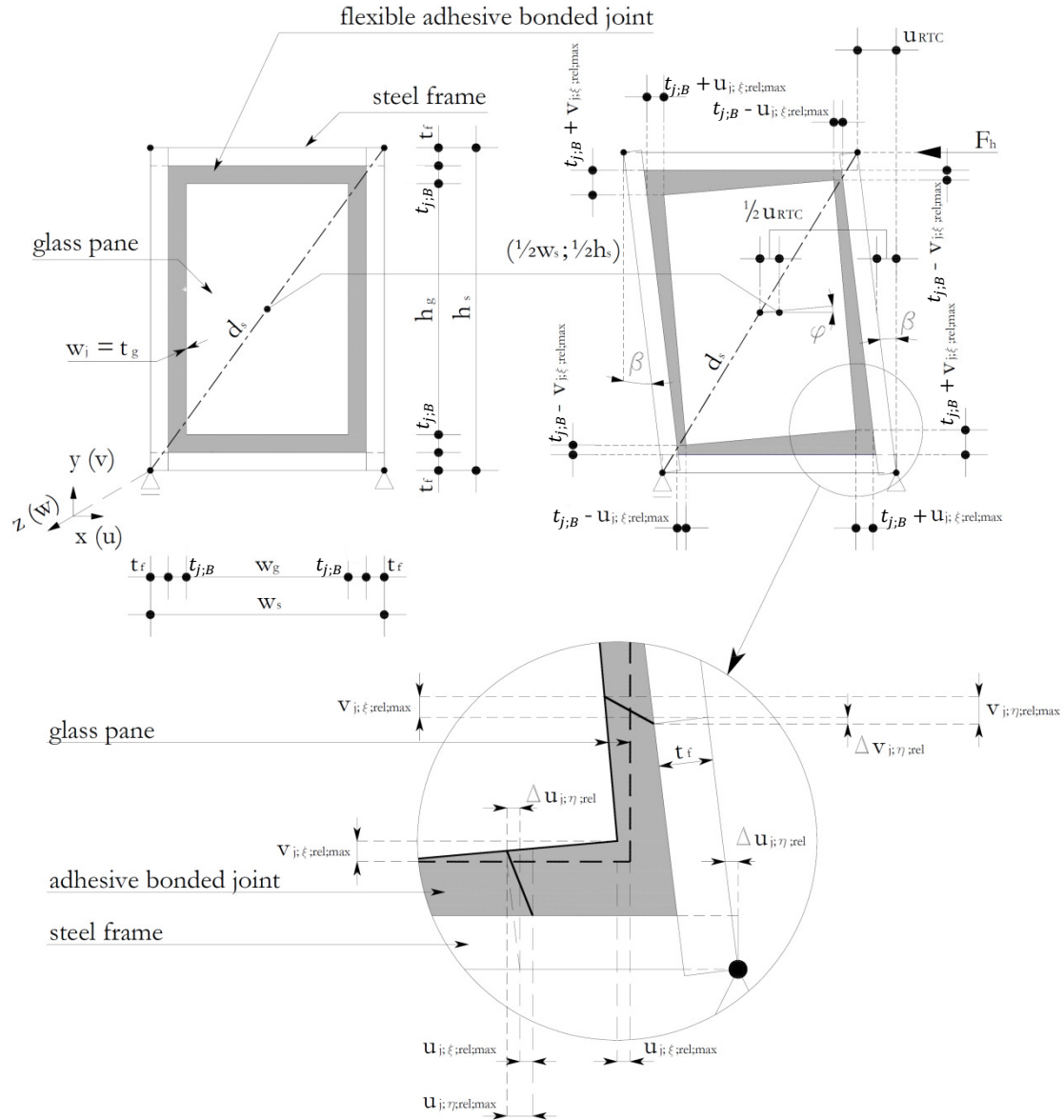


Figure 6.4 Geometry of the system (left top), a displaced situation of the system at limited horizontal in-plane displacement at the RTC of the system (right top) and an enlarged view of the RBC of the system.

For linear behavior of the adhesive bonded joint, the shear stiffness ($k_{j;\eta/\zeta}$) is the quotient of the shear modulus of the adhesive (G_a) and the joint thickness (t_j) represented in equation 6.1a. For non-linear behavior of the adhesive, equations 6.1b and 6.1c are more suitable [Habenicht 2006]. The shear stiffness for the non-linear adhesive is the quotient of the shear stress and the relative in-plane displacement in longitudinal or transversal direction. The data needed to use equation 6.1a-c is obtained from shear tests presented in chapter 3 and section 5.3.2.

$$k_{j;\eta/\zeta} = \frac{G_a}{t_j} \quad (a) \qquad k_{j;\eta/\zeta;x} = \frac{\tau_{j;\eta/\zeta;x}}{u_{j;\eta/\zeta;rel}} \quad (b) \qquad k_{j;\eta/\zeta;y} = \frac{\tau_{j;\eta/\zeta;y}}{v_{j;\eta/\zeta;rel}} \quad (c) \qquad \text{(Equation 6.1a-c)}$$

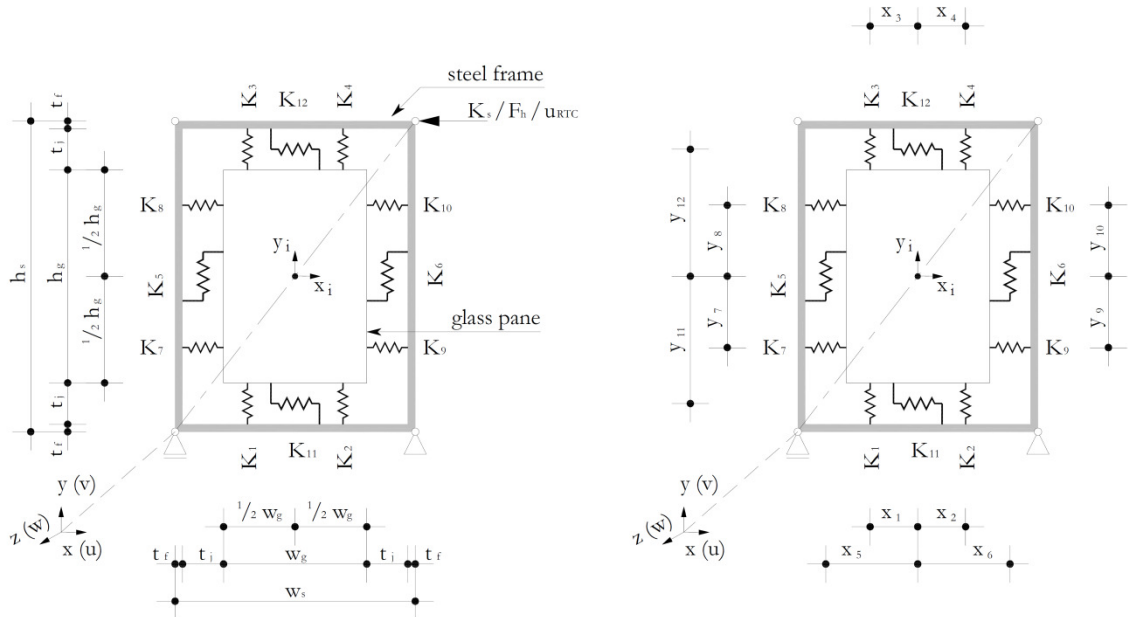


Figure 6.6 System with twelve discrete springs representing the circumferentially adhesive bonded joint (left) and their positions in relation to the centre of the glass pane (right) [Huveners 2009].

$$K_1 = K_2 = K_3 = K_4 = \frac{6}{8} k_{j;\zeta;y} t_g w_g \quad (\text{Equation 6.2})$$

$$K_7 = K_8 = K_9 = K_{10} = \frac{6}{8} k_{j;\zeta;x} t_g h_g \quad (\text{Equation 6.3})$$

$$K_5 = K_6 = 2k_{j;\eta;y} t_g h_g \quad (\text{Equation 6.4})$$

$$K_{11} = K_{12} = 2k_{j;\eta;x} t_g w_g \quad (\text{Equation 6.5})$$

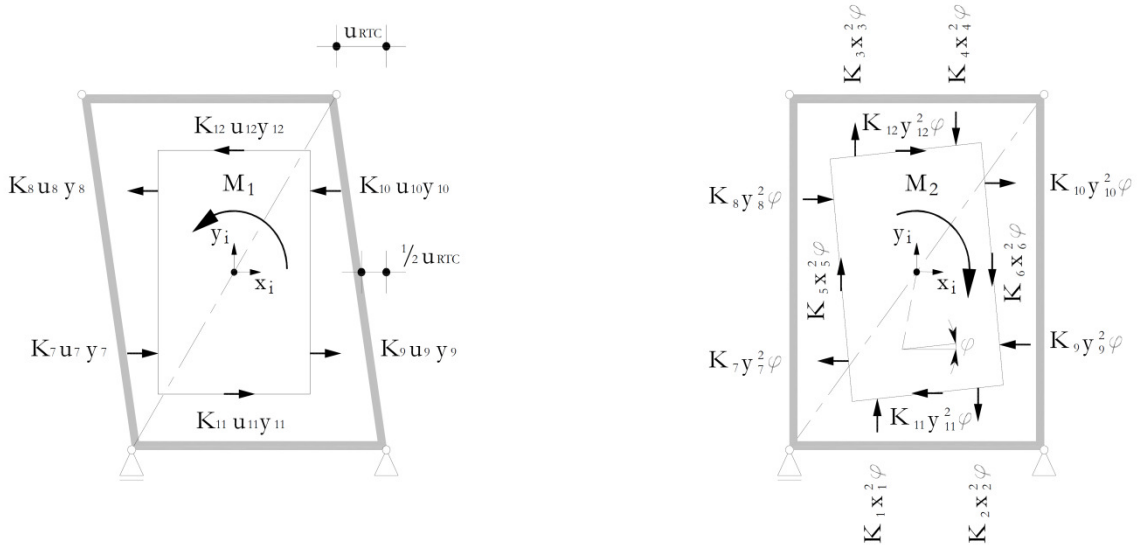


Figure 6.7 Horizontal in-plane loads imposed by the horizontal in-plane displacements at the RTC of the system (left) and all in-plane loads imposed by the in-plane rotation of the glass pane (right) [Huveners 2009].

The horizontal in-plane displacements (\$y_7\$ to \$y_{12}\$) are the difference between the horizontal in-plane displacements of the glass pane and the steel frame at the location of the discrete springs 7 to 12.

$$u_i = \frac{y_i u_{rtc}}{h_s} \quad (\text{Equation 6.6})$$

The in-plane moment (M_1) is the sum of the product of the discrete springs (K_7 to K_{12}), the horizontal in-plane displacements (u_7 to u_{12}) and the vertical levers (y_7 to y_{12}). Substitution of equation 6.6 in the formulae for the in-plane moment (M_1) results in equation 6.7.

$$M_1 = \sum_{i=7}^{12} K_{x,i} u_i y_i = \frac{u_{rtc}}{h_s} \sum_{i=7}^{12} K_{x,i} y_i^2 \quad (\text{Equation 6.7})$$

The in-plane moment (M_2) is the sum of the product of the stiffness of the discrete springs (K_1 to K_{12}), the in-plane displacements of the discrete springs derived from the in-plane rotation ($x_1 \varphi$ to $x_6 \varphi$ and $y_7 \varphi$ to $y_{12} \varphi$) and their levers (x_1 to x_6 and y_7 to y_{12}). This results in equation 6.8.

$$M_2 = \varphi \left(\sum_{i=1}^6 K_{y,i} x_i^2 + \sum_{i=7}^{12} K_{x,i} y_i^2 \right) \quad (\text{Equation 6.8})$$

After equating the in-plane moments of equations 6.7 and 6.8, the in-plane rotation of the glass pane can be derived and is presented in equation 6.9.

$$\varphi = K_\varphi \frac{u_{rtc}}{h_s} \quad (\text{Equation 6.9})$$

In equation 6.9 the in-plane rotation stiffness (K_φ) is introduced and represented in equation 6.10. The in-plane rotation stiffness is a system constant which depends on the stiffness of the discrete springs and their positions.

$$K_\varphi = \frac{\sum_{i=7}^{12} K_{x,i} y_i^2}{\left(\sum_{i=1}^6 K_{y,i} x_i^2 + \sum_{i=7}^{12} K_{x,i} y_i^2 \right)} \quad (\text{Equation 6.10})$$

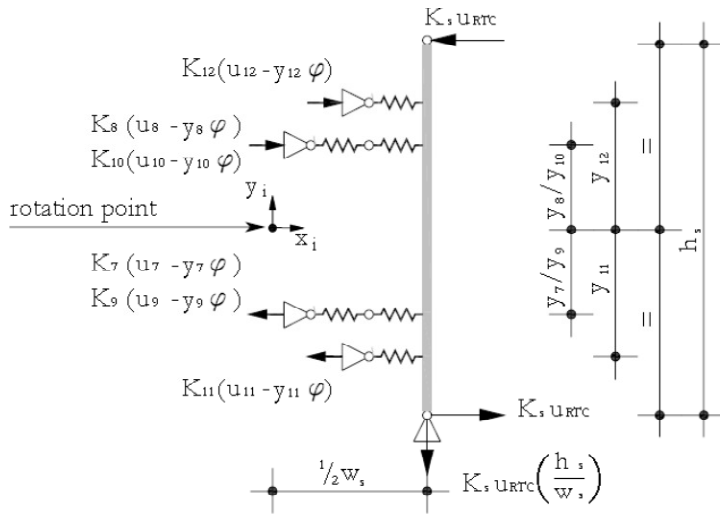


Figure 6.8 Determination of the in-plane stiffness of the system represented by a vertical member supported by horizontal discrete springs K_7 to K_{12} [Huvener 2009].

In figure 6.8 a vertical member provided with horizontal discrete springs (K_7 to K_{12}) is in equilibrium and represents the system in equilibrium. The discrete springs are needed to predict the in-plane stiffness of the system. The in-plane stiffness of the system is the result of the sum of the moment around the centre of the glass pane and is represented in equation 6.11.

$$K_s = \frac{(1-K_\varphi)}{h_s^2} \sum_{i=7}^{12} K_{x,i} y_i^2 \quad (\text{Equation 6.11})$$

The prediction of the horizontal in-plane load, presented in equation 6.12, is the product of the in-plane stiffness of the system (equation 6.11) and the horizontal in-plane displacement at the RTC of the system. For linear relation of the in-plane stiffness of the system, determined by the adhesive equation 6.12 is suitable.

$$F_h = K_s u_{rtc} \quad (\text{Equation 6.12})$$

The maximum relative horizontal in-plane displacements in transversal direction of the left and right adhesive bonded joint are located at the corners of the glass pane and can be calculated with equation 6.13.

$$u_{j;\zeta;rel,max} = \frac{1}{2}\beta h_g - \frac{1}{2}\varphi h_g = \frac{(1-K\varphi)h_g u_{RTC}}{2h_s} \quad (\text{Equation 6.13})$$

In which:

- β is the ratio between the horizontal in-plane displacement at the RTC of the system (u_{RTC}) and the height of the system (h_s);
- φ is the rotation of the system;

The second part of equation 6.13 can be obtained by substitution of equation 6.9 for the in-plane rotation of the system (φ).

The maximum relative horizontal in-plane displacements in transversal direction of the top and bottom adhesive bonded joint are also located at the corners of the glass pane and can be calculated with equation 6.14.

$$v_{j;\zeta;rel,max} = \frac{1}{2}w_g\varphi = \frac{w_g K\varphi u_{RTC}}{2h_s} \quad (\text{Equation 6.14})$$

The maximum relative in-plane displacements in transversal direction on the adhesive in the corners of the glass pane correspond to the relative in-plane displacements in longitudinal direction of the adhesive.

The second part of equation 6.14 can be obtained by substitution of equation 6.9 for the in-plane rotation of the system (φ). For circumferentially adhesive squared bonded glass panes, equation 6.13 and 6.14 lead to the same results.

Batch 3

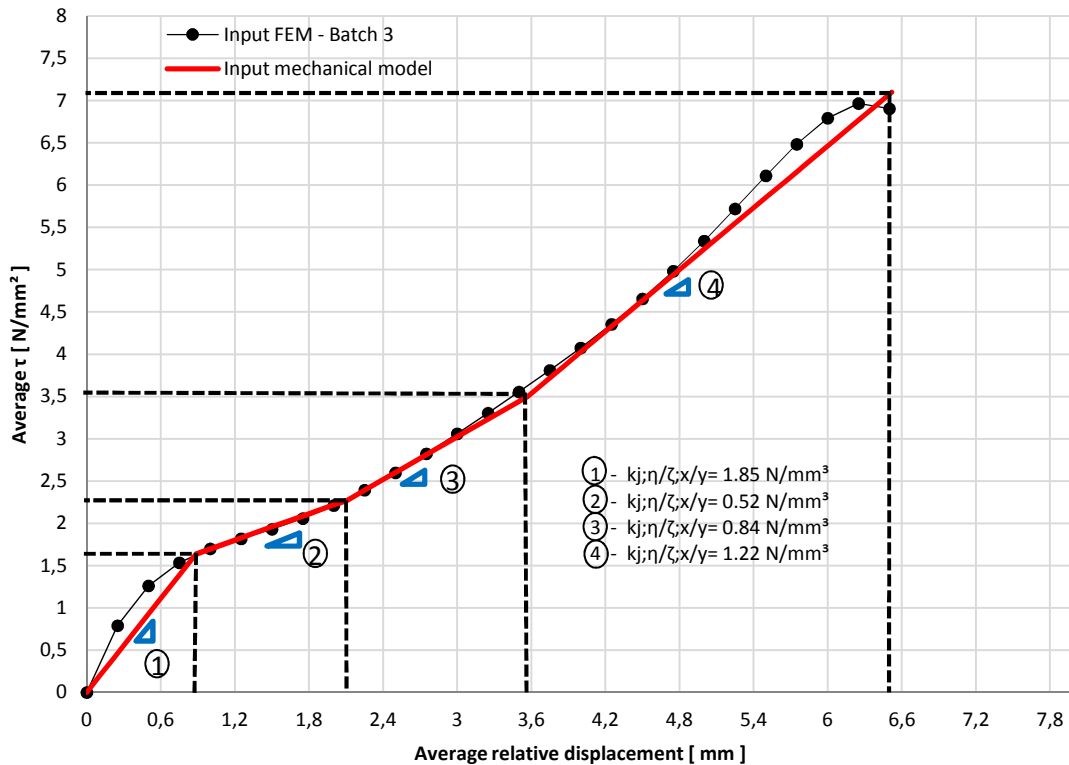


Figure 6.9 Shear properties of the applied adhesive (black line), and the tri-linear simplification of the shear properties, including the stiffness of the adhesive in three zones, to be used in mechanical models (red line).

The applied adhesive does not have a linear relation between the average shear stress (τ) and the average relative displacement ($u_{,rel}$) (figure 6.9). Different values for stiffness of the adhesive bond have to be considered, to describe the behavior of the system with an acrylic adhesive.

For displacements of the RTC of the system up to the maximum displacement in zone 1 ($u_{rtc;1,max} = 4.2 \text{ mm}$), equation 6.15 is able to describe the behavior of the system (zone 1). If the in-plane load is requested for a displacement ($u_{rtc;2}$) of the RTC of the system in zone 2, equation 6.16 has to be used. In the first part of the formula, the stiffness in zone 1 and the maximum displacement of the RTC of zone 1 ($u_{rtc;1,max} = 4.2 \text{ mm}$) has to be used. In the second part, the stiffness of zone 2, the displacement of the RTC of the system and the maximum displacement of zone 1 have to be used. For the behavior of the system in zone 3, equation 6.14 is extended to equation 6.17 where the first part accounts for zone 1, the second part for zone 2 and the last part accounts for zone 3. The behavior of the system in zone 4, equation 6.15 is extended to equation 6.18 where the first part accounts for zone 1, the second part for zone 2, the third part for zone 3 and the last part accounts for zone 4.

$$\text{Zone 1: } F_h = K_{s;1} u_{rtc} \quad (\text{Equation 6.15})$$

$$\text{Zone 2: } F_h = K_{s;1} u_{rtc;1,max} + K_{s;2} (u_{rtc;2} - u_{rtc;1,max}) \quad (\text{Equation 6.16})$$

$$\text{Zone 3: } F_h = K_{s;1} u_{rtc;1,max} + K_{s;2} (u_{rtc;2,max} - u_{rtc;1,max}) + K_{s;3} (u_{rtc;3} - u_{rtc;2,max}) \quad (\text{Equation 6.17})$$

$$\text{Zone 4: } F_h = K_{s;1} u_{rtc;1,max} + K_{s;2} (u_{rtc;2,max} - u_{rtc;1,max}) + K_{s;3} (u_{rtc;3} - u_{rtc;2,max}) + K_{s;4} (u_{rtc;4,max} - u_{rtc;3,max}) \quad (\text{Equation 6.18})$$

Where:

$$\begin{aligned} u_{rtc;1,max} &= 4.2 \text{ mm} & \text{and} & & K_{s;1} &= 12.102 \text{ kN/mm} \\ u_{rtc;2,max} &= 9 \text{ mm} & \text{and} & & K_{s;2} &= 3.402 \text{ kN/mm} \\ u_{rtc;3,max} &= 15 \text{ mm} & \text{and} & & K_{s;3} &= 5.495 \text{ kN/mm} \\ u_{rtc;4,max} &= 22.2 \text{ mm} & \text{and} & & K_{s;4} &= 7.981 \text{ kN/mm} \end{aligned}$$

In figure 6.10 the behavior of the system according to FE simulation, can be compared to the prediction of the system using mechanical models.

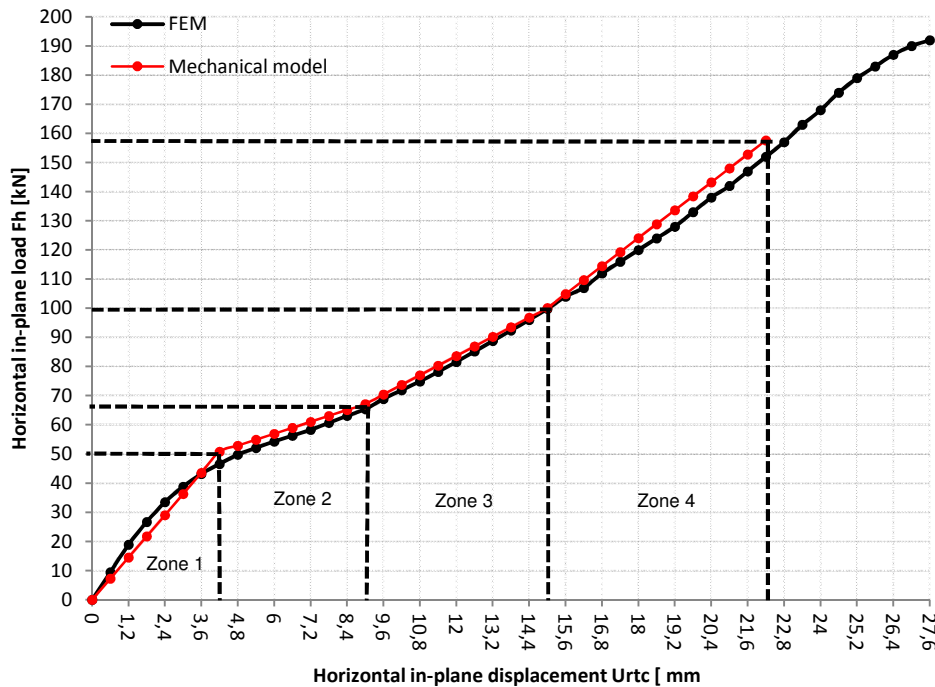


Figure 6.10 The behavior of the system according to FE simulation and using the mechanical model.

6.2 Mechanical models at glass steel contact

The geometry of the system determines the moment of glass-steel contact (section 5.7.3.1). The in-plane rotation stiffness of the system (equation 6.10) is used with the assumption that the system behaves linearly up till the point of glass-steel contact. Glass-steel contact in a perfect system will occur if $v_{j;\zeta;rel,max}$ and $u_{j;\zeta;rel,max}$ have reached $t_{j;B} = 5$ mm (section 5.7.3.1).

To predict the moment of glass-steel contact in a perfect system, equation 6.14 is adjusted to equation 6.19.

$$u_{RTC;1} = \frac{2t_{j;B}h_s}{w_g K_\varphi} \quad (\text{Equation 6.19})$$

Figure 6.11 gives the moment of glass-steel contact for a perfect system according to FE analyses ($u_{RTC;1}=23.4$ mm) and according to the mechanical model ($u_{RTC;1}=22.2$ mm).

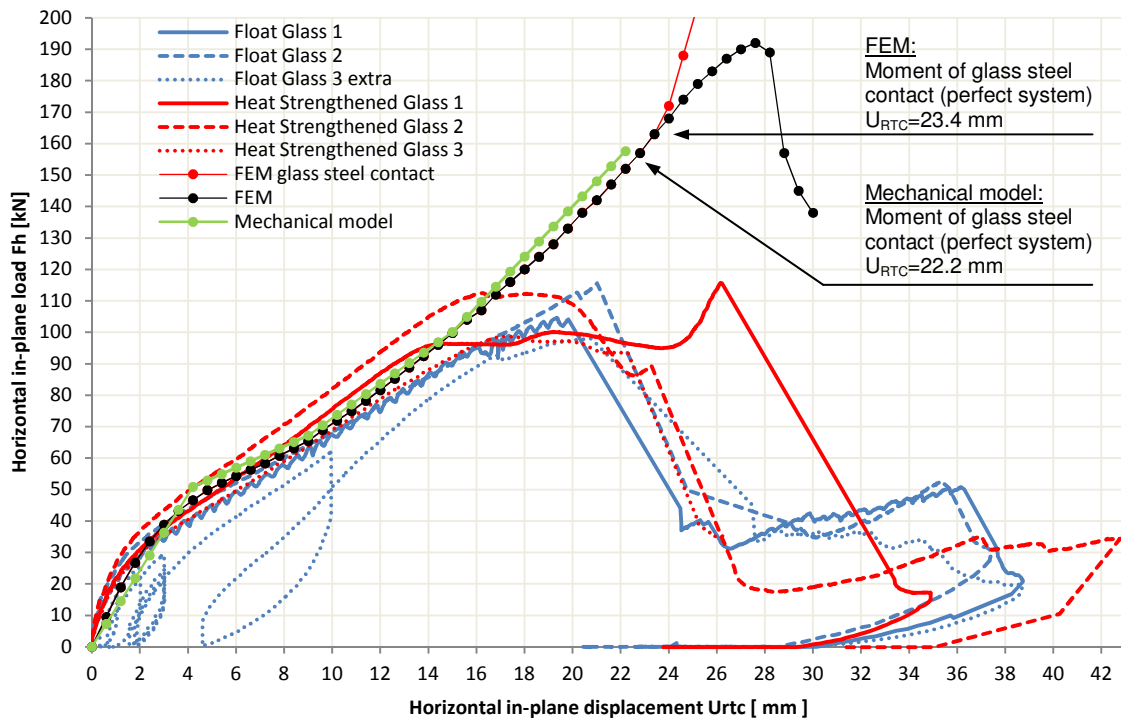


Figure 6.11 Moment of glass-steel contact for FE analyses and the mechanical model.

6.3 Mechanical models versus FEM

Table 6.5 gives an overview of the prediction by mechanical models and FE analyses (figure 6.11) for the horizontal in-plane load (F_h), the in-plane stiffness of the system (K_s), the relative displacement of the adhesive in transversal direction and is only valid for square glass panes of 1 by 1 m with a nominal thickness of 12 mm.

Table 6.5 Comparison of the horizontal in-plane load (F_h) and in-plane stiffness (K_s) among the mechanical model and the FEM.

u_{RTC} [mm]	F_h [kN] Mechanical Model	F_h [kN] FEM	ΔF_h in %	K_s [kN/mm] Mechanical Model	K_s [kN/mm] FEM	ΔK_s in %	$u_{j,\eta;rel,max}$ / $v_{j,\eta;rel,max}$ [mm] FEM (LBC/RTC)	$u_{j,\zeta;rel,max}$ / $v_{j,\zeta;rel,max}$ [mm] Mechanical Model (LBC/RTC)	$\Delta u / v$ in %
0	0	0	0,0				0,00	0,00	0,0
0,6	7,3	9,45	-23,2				0,11	0,14	25,1
1,2	14,5	18,9	-23,2				0,22	0,27	25,7
1,8	21,8	26,7	-18,4				0,34	0,41	21,0
2,4	29,0	33,5	-13,3				0,46	0,54	17,5
3	36,3	38,8	-6,4				0,60	0,68	13,6
3,6	43,6	43,2	0,9				0,74	0,81	10,2
4,2	50,8	46,6	9,1	12,102	11,1	9,1	0,88	0,95	7,0
4,8	52,9	49,8	6,2				1,03	1,08	5,0
5,4	54,9	52,1	5,4				1,19	1,22	2,2
6	57,0	54,3	4,9				1,34	1,35	0,8
6,6	59,0	56,3	4,8				1,50	1,49	-0,9
7,2	61,0	58,3	4,7				1,65	1,62	-1,7
7,8	63,1	60,7	3,9				1,81	1,76	-2,9
8,4	65,1	63,1	3,2				1,96	1,89	-3,5
9	67,2	65,4	2,7	3,402	3,9	-13,1	2,11	2,03	-3,9
9,6	70,5	68,9	2,3				2,26	2,16	-4,3
10,2	73,8	71,9	2,6				2,41	2,30	-4,7
10,8	77,0	74,9	2,9				2,55	2,43	-4,6
11,4	80,3	78,2	2,7				2,70	2,57	-4,9
12	83,6	81,6	2,5				2,85	2,70	-5,2
12,6	86,9	85,2	2,0				2,99	2,84	-5,1
13,2	90,2	88,8	1,6				3,13	2,97	-5,0
13,8	93,5	92,4	1,2				3,28	3,11	-5,2
14,4	96,8	96	0,9				3,42	3,24	-5,2
15	100,1	99,8	0,3	5,495	5,7	-4,2	3,57	3,38	-5,4
15,6	104,9	104	0,9				3,71	3,51	-5,3
16,2	109,7	107	2,5				3,85	3,65	-5,2
16,8	114,5	112	2,2				3,99	3,78	-5,2
17,4	119,3	116	2,8				4,13	3,92	-5,1
18	124,1	120	3,4				4,28	4,05	-5,3
18,6	128,9	124	3,9				4,42	4,19	-5,2
19,2	133,6	128	4,4				4,56	4,32	-5,2
19,8	138,4	133	4,1				4,70	4,46	-5,1
20,4	143,2	138	3,8				4,83	4,59	-4,9
21	148,0	142	4,2				4,97	4,73	-4,8
21,6	152,8	147	3,9				5,11	4,86	-4,8
22,2	157,6	152	3,7	7,981	7,3	10,1	5,24	5,00	-4,6

Table 6.6 gives an overview of the prediction by mechanical models and FE analyses (figure 6.11) for the limited horizontal in-plane load ($F_{h;lim}$), the limited in-plane stiffness of the system ($K_{s;lim}$) and the moment of glass-steel contact ($u_{RTC;1}$). These values are only valid for square glass panes of 1 by 1 m with a nominal thickness of 12 mm.

Table 6.6 Comparison of the horizontal in-plane load (F_h) and in-plane stiffness (K_s), moment of glass-steel contact between the mechanical model and the FEM.

$u_{RTC;lim}$ [mm]	$F_{h;lim}$ [kN] Mechanical model	$F_{h;lim}$ [kN] FEM	$\Delta F_{h;lim}$ in %	$K_{s;lim}$ [kN/mm] Mechanical model	$K_{s;lim}$ [kN/mm] FEM	$\Delta K_{s;lim}$ in %	$u_{RTC;1}$ [mm] Mechanical Model	$u_{RTC;1}$ [mm] FEM	$\Delta u_{RTC;1}$ in %
3,7	44,8	44	1,8	12,102	12,430	-2,6	22,2	23,4	-5,1

6.4 Discussion of the results

The mechanical models as described in this chapter are derived by [Huvener 2009] for a bonded joint with a polyurethane adhesive according to joint type 1 and are adapted to joint type 2 (figure 1.4) for a bonded joint with an acrylic adhesive.

As the applied adhesive does not have a linear relation between the average shear stress (τ_{ave}) and the average relative displacement ($u_{,ave;rel}$), different values for the stiffness of the adhesive bond have been considered. Therefore the relation between the average shear stress and the average relative displacement has been divided into four zones (figure 6.9). To apply the different shear stiffness of the adhesive in the mechanical model, the relation between the in-plane load and the in-plane displacement of the RTC of the system has also been divided into four zones (figure 6.10).

Up to 14 mm horizontal in-plane displacement of the RTC, the mechanical model is representative for the behavior of the system with the acrylic adhesive. At that point the load-displacement curve of the experiments diverges from the mechanical model, due to failure of the adhesive bonded joint. Just as in the FE model, the mechanical model only takes into account the relative displacements of the adhesive in one direction.

The prediction of the in-plane stiffness of the system by the mechanical model is influenced by the presumed shear stiffness of the adhesive bonded joint in figure 6.9. To keep the mechanical models uncomplicated, the shear stiffness of the adhesive is divided into four zones. Applying more zones, will enlarge the similarity with the FE simulation, but makes the calculation unnecessary complicated.

Except for the first part of the load displacement curve, the mechanical model slightly overestimates the FE model (figures 6.10, 6.11 and table 6.5). Mainly this is the result of the presumed shear stiffness of the adhesive (figure 6.9). Besides this, there are a few presumptions in the mechanical model, which do not apply for the FE model. In the mechanical model, the glass pane acts rigid in-plane and has no initial out-of-plane displacement of the glass pane. Also no deformation in axial direction, no bending and no vertical in-plane displacements in the steel mullions and transoms are taken into account.

The maximum relative horizontal in-plane displacement in transversal direction of the top and bottom adhesive bonded joint, and for the left and right adhesive bonded joint are located at the corners of the glass pane and yield similar results for square glass panes. The maximum relative horizontal in-plane displacement in transversal direction described by equation 6.13 and 6.14 underestimate the relative longitudinal in-plane displacement of the adhesive bonded joint by the FE simulation (table 6.5). This is caused by the presumption that the glass pane acts infinite stiff in the mechanical model. Due to shear deformation of the glass pane, the relative displacements in longitudinal direction increase.

According to the mechanical model the moment of glass-steel contact occurs at an in-plane displacement of the RTC of 22.2 mm. The FE simulation yields a value of 23.4 mm. The smaller value for the moment of glass-steel contact is caused by the presumption as discussed above.

6.5 Conclusions

The mechanical models are based on square glass panes of 1 by 1 meter, a thickness of 12 mm and a shear stiffness of the adhesive obtained by shear tests. The relation between the average relative shear stress and the average relative displacement of the adhesive is divided in four zones to account for non-linear behavior.

- The mechanical models describe the behavior of to the FE simulation quite well. Due to the deviation of the experimental results, the mechanical models can only be used up to 14 mm in-plane displacement of the RTC of the system to predict the in-plane stiffness and in-plane load at the RTC of the system (figure 6.11);
- The prediction of the in-plane stiffness of the system at limited horizontal in-plane displacement at the RTC of the system slightly yields a smaller value than obtain by the FE simulation (table 6.6);
- The prediction of the in-plane load of the system at limited horizontal in-plane displacement at the RTC of the system slightly yields a larger value than obtain by the FE simulation (table 6.6);
- The maximum relative horizontal in-plane displacement in transversal direction of the adhesive bonded joint occurs in the corners of the glass pane and slightly underestimates the values obtained by the FE simulation for the longitudinal relative in-plane displacements of the adhesive;
- The prediction of the horizontal in-plane displacement at glass-steel contact yields a smaller value than obtained by the FE simulation for a perfect system.

7 Discussion

This research focused on a square steel frame with infinite stiff transoms and mullions with a two sided circumferentially adhesive bonded glass pane. Eight full-scale experiments were carried out. For the in-plane behavior of the system, three experiments were carried out with annealed float glass panes and three experiments with heat strengthened glass panes. To get an impression of the behavior of in- and out-of-plane loaded systems, one experiment with annealed float glass and one experiment with heat strengthened glass was carried out.

All experiments were carried out with an acrylic adhesive according to joint type two (figure 1.4). The shear stiffness of the acrylic adhesive is larger than polyurethane but much less than epoxy (section 3.1.4). To take material imperfections into account the applied thickness of the adhesive bonded joint was 3 mm.

For square in-plane loaded glass panes, the LBC and RTC of the glass panes simultaneously make contact with the steel system. All in-plane loaded glass panes fail at the RTC of the system due to glass-steel contact, where the in-plane load is introduced. Up to this point no cracks were visible in the glass pane. FE simulations showed that the position of the glass pane with respect to the centre of the system has large influence on the moment of glass-steel contact. The FE simulations are valid up to an in-plane displacement of the RTC of 14 mm. After this point the adhesive bonded joint starts to fail on cohesion and the behavior of each system is random (section 5.7.4). Due to the lower shear stiffness of the acrylic adhesive bonded joint, glass-steel contact is the failure criterion instead of exceeding the maximum principle (tension) in the RBC of the system.

Except for the out-of-plane displacement in the centre of the glass pane and the principle stresses in the non dominant stress direction in the glass pane (section 5.7.2), the FE model simulates well the behavior of the system for in-plane loaded systems.

The relative in-plane displacement in the middle of the adhesive bonded joint, measured in the experiments, is compared to the results of the FE simulations. FE simulations showed that the relative in-plane displacement in longitudinal direction in the middle of the adhesive bonded is equal to the longitudinal relative in-plane displacement in the corners of the adhesive bonded joint and that the transversal in-plane displacement in the corner of the adhesive bonded joint is about 90% of the longitudinal relative in-plane displacement. According to preliminary shear tests, the vector of the relative in-plane displacement at the corner of the adhesive bonded joint is less or near the maximum allowable relative in-plane displacement (figures 5.51 and 5.53). Complementary shear test showed that a larger area of the adhesive bonded joint results in cohesive failure of the adhesive bonded joint at less relative in-plane displacement (section 3.2). The random behavior of the system after an in-plane displacement of the RTC of the system of 14 mm is therefore verified to be caused by cohesive failure of the adhesive bonded joint.

The adhesion of the acrylic adhesive on HSG panes is different compared to ANG panes. A plausible answer can explain this behavior, but cannot be confirmed experimentally. HSG panes are partly tempered ANG panes and compression stresses at the surface suppress the surface flaws (section 2.2.2.1). The adhesive is, when applied to ANG panes, able to lock itself in the surface flaws and for HSG panes this is not possible, because the surface flaws are closed.

The existing mechanical model is adjusted and it represents well the behavior of the FE model. Just like the FE simulations, the mechanical model is only valid up to a horizontal in-plane displacement of the RTC of the system of 14 mm. After this point experiments deviate from the FE simulations.

Indicative in- and out-of-plane loaded glass panes failed due to bending in the centre of the glass pane and showed large resistance against out-of-plane loads for systems with square glass panes and a nominal glass pane thickness of 12 mm. The system was first in-plane loaded up to limited horizontal in-plane displacement of the RTC and then loaded out-of-plane up to failure of the glass pane. Both glass panes failed without any visible or audible warnings by the glass pane.

The stiffness of the adhesive bonded joint is less than expected. The adhesive bonded joint with the acrylic adhesive had a stiffness of 4.51 N/mm^3 . FE simulations showed that the system has an in-

plane stiffness of 12.43 kN/mm and resisted an in-plane load of 44 kN. Figure 7.1 shows the results of FE simulations by [Huvener 2009] where the relation between the horizontal in-plane load, the in-plane stiffness of the system, the largest maximum principle (tension) stress in the RBC of the system and varying shear stiffness of the adhesive bonded joint is shown for an in-plane displacement of the RTC of 1.02 mm. At this horizontal in-plane displacement of the RTC, the first cracks in the RBC of the glass pane appeared due to exceeding the maximum principle (tension) stress.

The behavior of the system with the acrylic adhesive is also plotted in figure 7.1 and is located in zone 1 (orange dashed line). In this zone, the stress distribution of the acrylic adhesive bonded joint in longitudinal direction is equal to the stress distribution of the epoxy adhesive. The stress distribution of the acrylic adhesive in transversal direction is different from the epoxy adhesive (zone 1, figure 7.1). The shear flexibility between the outside beam and the beadwork had no influence on the stress distribution of the adhesive bonded joint and the principle stress distribution in the glass pane and therefore only the horizontal in-plane stiffness and the horizontal in-plane load are presented.

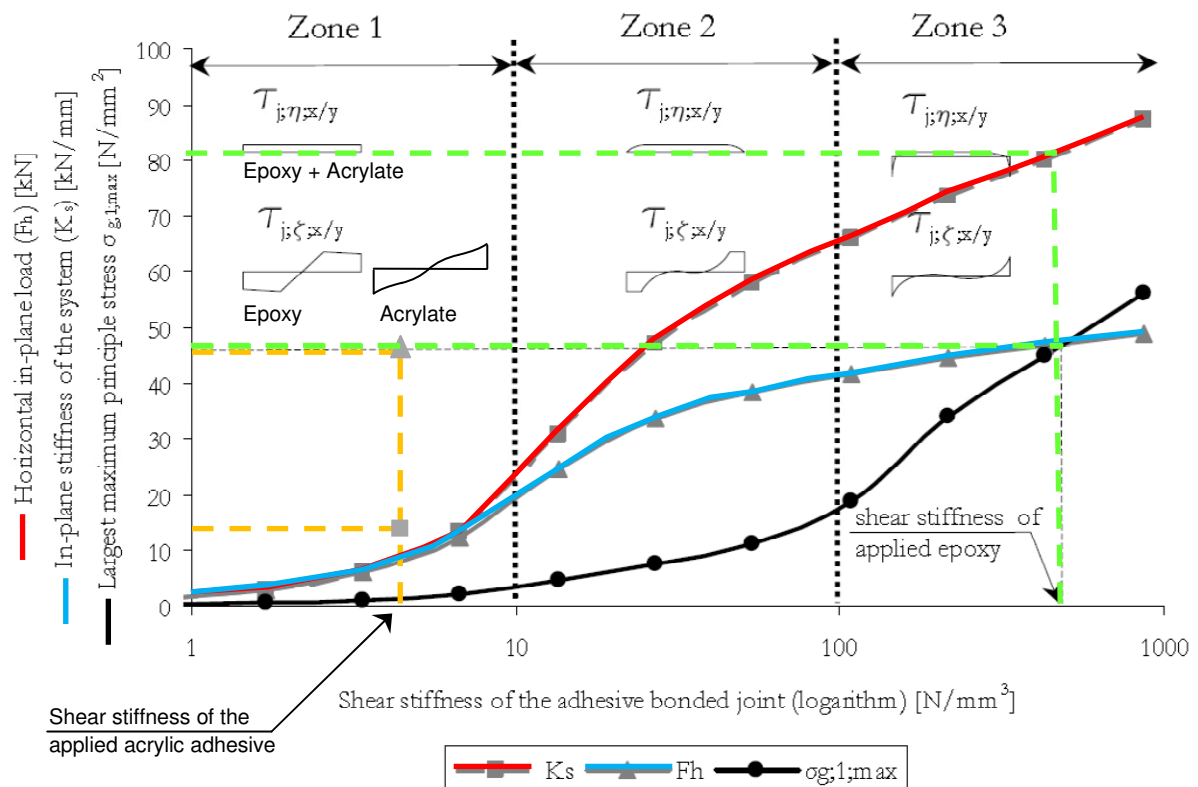


Figure 7.1 Comparison of the global behavior of systems with an epoxy adhesive bonded joint and the acrylic adhesive bonded joint as applied in experiments in this research.

8 Conclusions

The main conclusions of the experiments, finite element simulations and the mechanical model of the system based on joint type 2 with an acrylic adhesive are given below.

Experiments:

- The relation between the horizontal in-plane load and the horizontal in-plane displacement of the right top corner of the system is non-linear, just like the relation between the shear stress and the average relative displacement of the adhesive;
- The serviceability limit state (horizontal in-plane displacement of the right top corner) is the design criterion;
- The in-plane stiffness of the adhesive is small (zone 1);
- The shear stiffness of the adhesive bonded joint determines the in-plane stiffness of the system;
- The shear flexibility of the bolted connection between the outside beam and the beadwork has no influence on the shear stress distribution of the adhesive bonded joint;
- The maximum principle stress in the right bottom corner of the system is not a criterion;
- At larger horizontal in-plane displacement, the acrylic adhesive fails cohesively. Glass-steel contact is the failure mode of the system;
- Square glass panes have only one moment of glass-steel contact at larger in-plane displacement of the right top corner of the system;
- At the moment of glass-steel contact, in-plane loaded systems with annealed float glass panes fail almost immediately;
- In-plane loaded systems with heat strengthened glass panes show more resistance at glass-steel contact;
- In-plane loaded systems with a horizontal in-plane displacement up to the serviceability limit state and out-of-plane loaded up to failure showed large resistance;
- Residual capacity of the system based on the limited horizontal in-plane displacement of the right top corner of the system is good. Large in-plane displacement of the right top corner is possible with increasing in-plane load;
- Residual capacity based on the first crack in the glass pane is very poor. Both in-plane loaded systems and in- and out-of-plane loaded systems fail without audible or visible warnings.

Finite element simulations:

- The finite element model describes the behavior of the experiment very well up to an in-plane displacement of the right top corner of the system of about 14 mm. After that point, the behavior of the systems is random due to cohesive failure of the adhesive bonded joint;
- The relative displacements of the adhesive bonded joint in transversal and longitudinal direction are not coupled. The adhesive bonded joint in the FE simulation fails when the uni-axial maximum relative displacement of the adhesive bonded joint has been reached instead of the maximum bi-axial relative displacement of the adhesive bonded joint;
- The position of the centre of the glass pane with reference to the centre of the system has a large influence on the moment of glass-steel contact;
- The out-of-plane displacement of the glass pane due to an in-plane load of the system simulated by the FE model, is smaller than found in the experiments;
- The principle stresses in points 1 to 5 describe only the dominant direction of the stresses well;
- In-plane loaded systems up to limited horizontal in plane displacement have large capacity to account for uniform distributed out-of-plane wind loads.

Mechanical model:

- The mechanical models for systems with joint type 1 based on the polyurethane adhesive are adapted for systems with joint type 2 based on the acrylic adhesive.
- The mechanical models can be used up to a horizontal in-plane displacement of the right top corner of the system of 14 mm. After that point, the behavior of the systems is random due to cohesive failure of the adhesive bonded joint;
- The in-plane stiffness, the in-plane load, the maximum relative displacement in longitudinal direction of the adhesive bonded joint and the moment of glass-steel contact are well predicted by the mechanical models.

Overall conclusion:

The research objectives are partly obtained. The first objective was finding a proper adhesive and getting insight into the in-plane structural behavior using both annealed float glass and heat strengthened glass. The adhesive was a key element in this research and will be a key element in further research. The advised adhesive by the manufacturer was at the moment of application the most proper adhesive available on the market. The structural acrylic adhesive behaves less stiff than the epoxy adhesive. Avoiding peak stresses in the right bottom corner of the glass pane, due to a sudden irregular stress distribution in the adhesive bonded joint because of the shear flexibility between the outside beam and the beadwork and accounting for material tolerances have been accomplished. The second objective was to adjust current mechanical models. The derived mechanical models describe the global in-plane behavior of the system very well. The third object was to get indicative insight into the behavior of in- and out-of-plane loaded glass panes. Indicative experiments where the system was loaded in- and out-of-plane showed large capacity to be loaded in- and out-of-plane.

Moreover, it can be concluded that the shear stiffness of the applied acrylic adhesive is not large enough to obtain the desired behavior of the system. The in-plane displacement of the right top corner of the system is too large causing the glass panes to fail due to glass-steel contact, without any audible or visible warnings. The desired failure mode of the system can be obtained by finding an adhesive which gives the system the ability to displace in-plane, further than the limited in-plane displacement of the right top corner (determined by the serviceability limit state) and fail due to exceeding the maximum principle (tension) stress in the right bottom corner of the glass pane accompanied with increasing horizontal in-plane load, before the moment of glass-steel contact occurs. Failure due to exceeding the maximum principle stresses in the right bottom corner of the system has shown, in experiments with joint type 2 based on the epoxy adhesive, to warn before failure by constant audible and visible cracking.

9 Recommendations

9.1 Glazing

The type of glass is crucial for the in-plane capacity of the system. The acrylic adhesive used in this research (section 3.1) adhered better to annealed float glass than to heat strengthened glass (section 4.8). Nevertheless, both glass types have to be tested in further research, because a system with a stiffer adhesive requires a higher representative flexural tension strength and a higher resistance against temperature changes in the glass pane.

9.2 Loading

Six experiments were carried out where the system with joint type two was exposed to a short term horizontal in-plane load. Two indicative experiments were carried out where the system was exposed to a short term in- and out-of-plane load. To understand the behavior of in- and out-of-plane loaded systems better, experiments which correspond to practice should be done. Further long term loads due geometrical imperfection of a building, cycle loads by wind and thermal loads are points of interest.

9.3 Adhesives

Regarding the results of the system it is advisable to combine joint type 1, performed with an adhesive with a very low stiffness, with joint type 2 performed with the acryl adhesive. At glass-steel contact the in-plane load is expected to be introduced gradually into the glass pane. Direct failure of the glass pane is expected to be postponed and the residual capacity of the system will become larger.

Glass panes produced according to section 2.2.1 have two different faces. The bottom face is called the tin side and contains some diffused tin molecules into the glass pane. The behavior of the adhesion of the adhesive on the two faces is not known and has to be investigated for both annealed float and heat strengthened glass panes.

Experiments to determine the uni-axial shear strength of the acrylic adhesive (section 3.1) were done with thick steel adherent shear tests. The relation of the relative shear stress with the relative in-plane displacement has been used in finite element analyses. As the acrylic adhesive showed different shear behavior when applied on annealed float and heat strengthened glass (section 4.8), the shear strength of adhesives in future research have to be determined in thick adherent shear tests using specimens where the adhesive adheres to glass and steel instead of steel to steel. Figure A.13 in appendix A.11 presents a proposal for new shear tests to get a better insight in the shear properties when steel is adhered to both annealed float and heat strengthened glass panes. This proposal gets closer to the real shear behavior of the adhesive and can explain the difference in the load-displacement curve of the system.

The acrylic adhesive compared to the epoxy adhesive affected the maximum principle stress distribution in the corners of the glass pane in a positive way. For the acrylic adhesive glass-steel contact is the failure mode of the system (section 5.7.3). The only problem is that the system does not warn before failure. A proper structural adhesive has to be found leading to failure of the system by exceeding the maximum principle stress in the corner of the glass pane, after a larger displacement of the right top corner than 1/500 of the height of the system and before the occurrence of glass-steel contact. Further requirements of the adhesive have to be a minimum applicable thickness of the adhesive bonded joint of 3 mm considering material tolerances and accounting for environmental conditions and mechanical properties at long-term duration.

Literature

- [Adams et al. 1997] Adams, R.D., Comyn, J., Wake W.C. (1997). Structural adhesive joints in engineering – second edition, Chapman & Hall, London, United Kingdom.
- [Adams and Peppiatt 1974] Adams, R.D., Peppiatt, N.A. (1974). Stress analysis of adhesively bonded lap joints, *Journal of Strain Analyses*, Vol 9, number 4, p.p. 185-196
- [Arenas et al. 2010] Arenas, J.M., Narbon, J.J., Alía, C. (2010). Optimum adhesive thickness in structural adhesives joints using statistical techniques based on Weibull distribution, *International Journal of Adhesion and Adhesives*, Vol 30, number 3, p.p. 160-165
- [Arnold et al. 2012] Arnold, A.; Neumann, L., Hochhauser, W. (2012), Stability of glued and embedded Glass Panes: Dunkerley straight Line as a conservative Estimate of superimposed buckling Coefficients in, ASC Report 01/2012, issued, Institute for Analysis and Scientific Computing, Vienna University of Technology, Vienna, Austria
- [ASTM D1002] ASTM D1002 (1983) Standard Test Method for Apparent Shear Strength of Single-Lap-Joint Adhesively Bonded Metal Specimens by Tension Loading (Metal-to-Metal), ASTM Committee D-14
- [Bedon and Amadio 2012] Bedon, C., Amadio, C., (2012) Buckling of flat laminated glass panels under in-plane compression or shear, *Engineering Structures* 36, 2012, p.p.185–197.
- [Brockmann et al. 2009] Brockmann, W., Geiß, P.L., Kligen, J., Schröder, B. (2009). Adhesive Bonding. Materials, Applications and Technology. Weinheim: WILEY-VCH Verlag GmbH & Co. KgaA
- [Chalkley and Chiu 1993] Chalkley, P.D., Chui, W.K. (1993). An improved method for testing the shear stress/strain behaviour of adhesives, *International Journal of Adhesion and Adhesives*, Vol 13, number 4, p.p. 237-242
- [Chiu and Jones 1992] Chiu, W. K., Jones, R. (1992). A numerical study of adhesively bonded lap joints, *International Journal of Adhesion and Adhesives*, Vol 12, number 4, p.p. 219-225
- [Crocombe 1989] Crocombe, A.D. (1989). Global yielding as a failure criterion for bonded joints, *International Journal of Adhesion and Adhesives*, Vol 9, number 3, p.p. 145-153
- [Da Silva et al. 2006] Da Silva, L.F.M., Rodrigues, T.N.S.S., Figueiredo, M.A.V., de Moura, M.F.S.F., Chousal, J.A.G. (2006). Effect of Adhesive Type and Thickness on the Lap Shear Strength, *Journal of*, Vol 82, number 11, p.p. 1091-1115
- [DIN 54 451:1978] DIN 54 451:1978 Schubspannungs- Gleitungsprüfung – Deutsches Institut für Normung, Berlin.
- [DIN EN 923] DIN EN 923:2008 Adhesives - Terms and definitions – Deutsches Institut für Normung, Berlin.
- [EN 572-1 2004] EN 572-1 (2004), Glass in building – Basic soda lime silicate glass products, part 1, Definitions and general physical and mechanical properties, CEN, Brussels, Belgium

- [EN 572-8 2004] EN 572-8 (2004), Glass in building – Basic soda lime silicate glass products, part 8, Supplied and final cut sizes, CEN, Brussels, Belgium
- [FEICA 2004] FEICA (2004). Bonding/Adhesives Textbook. [Electronic version]. FEICA Educational Material.
- [Fisher 2005] Fisher, W.L., (2005). Selection Of Engineering Materials And Adhesives, Taylor & Francis, Measurement Analysis Corporation, Torrance, California, USA
- [Gleich et al. 2001] Gleich, D.M., van Tooren, M.J.L., Beukers, A. (2001). Analysis and evaluation of bondline thickness effects on failure load in adhesively bonded structures, International Journal of Adhesion Science and Technology, Vol 15, number 9, p.p. 1091-1101
- [Grant et al. 2009] Grant, L.D.R., Adams, R.D., da Silva, L.F.M. (2009) Experimental and numerical analysis of single-lap joints for the automotive industry, International Journal of Adhesion and Adhesives, Vol 29, number 4, p.p. 405-413
- [Habenicht 2006] Habenicht, G. (2006), Kleben, Grundlagen, Technologien, Anwendungen, 5., erweiterte und aktualisierte Auflage, Springer-Verlag, Berlin, Germany
- [Haldimann et al. 2008] Haldimann, M., Luible, A., Overend, M. (2008), Structural use of Glass, Structural Engineering Documents 10, IABSE, Zurich, Switzerland.
- [Hess 2004] Hess, R (2004), Material Glass, Structural Engineering International, Vol. 14, number 2, p.p. 76-79, IABSE, Zurich, Switzerland
- [Huveners and Koggel 2006] Huveners, E.M.P.; Koggel, B.A. (2006). Tensile Shear Tests for the Determination of the Shear Strain Diagram of Several Adhesive Types, Report O-2006.11, Eindhoven University of Technology, Eindhoven, The Netherlands
- [Huveners 2009] Huveners, E.M.P. (2009). Circumferentially Adhesive Bonded Glass Panes for Bracing Steel Frames in Façades. PhD thesis. Eindhoven: Technische Universiteit Eindhoven.
- [Kaasschieter et al. 2008] Kaasschieter, C.C.J., Sluis van der, H.H., e.a. (2008). Lijmen van metalen. VM 87. Zoetermeer: Vereniging FME-CWM
- [Kadioglu et al. 2002] Kadioglu, F., Vaughn, L.F., Guild, F.J. and Adams, R.D. (2002). Use of thick adherent shear test for shear stress-strain measurements of stiff and flexible adhesives, Journal of Adhesion, Vol. 78, number 5, p.p. 355-381
- [Luible 2004] Luible, A. (2004), Stabilität von Tragelementen aus Glas, PhD thesis, EPFL, Thèse no 3014, Lausanne, Switzerland
- [Mocibob 2008] Mocibob, D. (2008), Glass Panel under Shear Loading – Use of Glass Envelopes in Building Stabilization, PhD thesis, EPFL, Thèse no 4185, Lausanne, Switzerland
- [NEN-EN 14869-2:2004] NEN-EN 14869-2:2004, Structural adhesives - Determination of shear behavior of structural bonds - Part 2:Thick adherends shear test, CEN, Brussels, Belgium

- [NEN-EN ISO 291] NEN-EN ISO 291 (1997), Plastics - Standard atmospheres for conditioning and testing, CEN/TC 249
- [NEN 2608-2:2007] NEN 2608-2:2007 nl, Glass in building - Part 2: Glazed installations non-vertical installed - Resistance against self-weight, wind load, snow load and isochore pressure - Requirements and determination method, NNI, Delft, the Netherlands
- [NEN 6702:2007] NEN 6702:2007 nl, Technical principles for building structures - TGB 1990 - Loadings and deformations, NNI, Delft, the Netherlands
- [NEN 6770:1997] NEN 6770:1997/A1:2005 nl, Technical Principles for Building Structures – TGB 1990 – Loadings and Deformations, NNI, Delft, the Netherlands
- [Schuler et al. 2004] Schuler, Ch.; Bucak, Ö.; Sackmann, V.; Gräf, H.; Albrecht, G. (2004), Time and Temperature Dependent Mechanical Behaviour and Durability of Laminated Safety Glass, Structural Engineering International, Vol. 14, number 2, p.p. 80-83, IABSE, Zurich, Switzerland
- [Sedlacek et al. 1999] Sedlacek, G.; Blank, K.; Laufs, W.; Güsgens, J. (1999), Glas im konstruktiven Ingenieurbau, Ernst und Sohn, Berlin, Germany
- [Sika ADPrep-5901] Sika ADPrep-5901 (2006). Sika ADPrep-5901 – Surface preparation agent for SikaFast adhesives. Version 03/2006, Sika Netherlands, Utrecht, The Netherlands
- [SikaFast-5215 2006] SikaFast-5215 (2006). SikaFast-5215 - Fast curing 2-C structural adhesive, designed for glass bonding. Version 04/2006, Sika Netherlands, Utrecht, The Netherlands
- [Specialchem 2010] Specialchem (2010). Adhesion theory. Retrieved October 10, 2010 from <http://www.specialchem4adhesives.com/resources/adhesionguide/index.aspx>
- [TNO Diana 2010] TNO Diana (2010). Diana Finite Element Analysis. User's Manual. Release 9.4.2. 1st edition. Delft: TNO Diana BV
- [Weller and Tashe 2008] Weller, B., Tasche, S. (2008). Strukturelles Kleben im Konstruktiven Glasbau. Stahlbau Spezial - Konstruktiver Glasbau, 2008, pp. 28-33.
- [Wellershoff 2006] Wellershoff, F. (2006), Nutzung der Verglasung zur Aussteifung von Gebäudehüllen, PhD thesis, Schriftenreihe – Stahlbau RWTH Aachen, Heft 57, Shaker Verlag, Aachen, Germany
- [Wigginton 1996] Wigginton, M. (1996), Glass in Architecture, Phaidon Press Limited, London, UK

Appendix A Determination of mechanical properties of the adhesive

A.1 Preparation bonded joint

Due to the fact that the quality of the bonded joint is affected by the ambient environment, such as temperature and relative humidity, the bonded joint will be prepared in two different manners under conditioned circumstances. The manufacturing temperature is room temperature (RT) and the temperature range lies between 18°C and 28°C in accordance with [NEN-EN ISO 291].

Treatment one consists of preparing the specimens using the general surface preparation agent for adhesively bonded systems recommended by the manufacturer. The application method consists of wiping the bonding area with a clean lint-free cloth or absorbent paper towel sparingly moistened with [Sika®ADPrep-5901]. Wiping the surface once is sufficient. The drying time is temperature dependant and for temperatures above 15°C it is approximate 1 minute. The open time is as long as 24 hours and during this time the bonding area is protected from dust and dirt. Using this method, cohesive failure within the adhesive layer is expected.

Treatment two consists of degreasing the specimens in an immersion bath with the organic solvent acetone (ACE). After immersing, the test specimens are rinsed by clean acetone.

The goal of testing specimens with these two preparation methods is to expose the influence on the shear strength of the bonded area. In practice builders can use another preparation method than is prescribed by engineers due to a lot of reasons, which can lead to much weaker bonding strengths than required. In figure A.1 the bonded joint is prepared and in figure A.2 the specimens are bonded together with the acrylic adhesive.

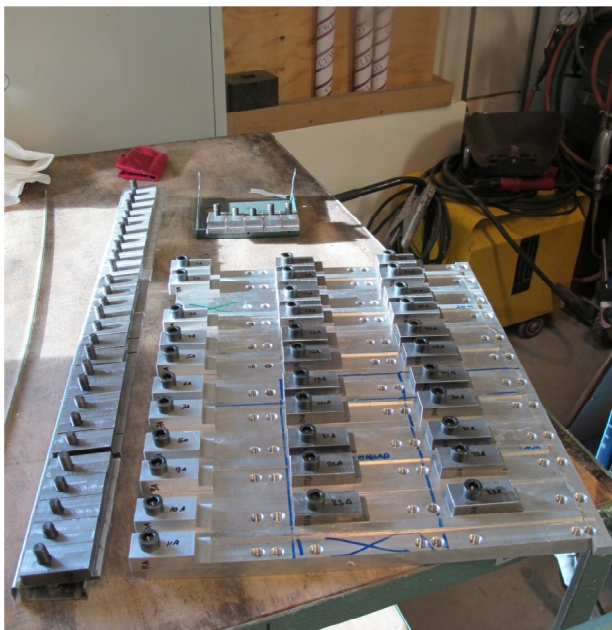


Figure A.1 Preparation of specimens.



Figure A.2 Adhesively bonded specimens.

The adhesive as described in section 3.1 is applied using a static mixer. The curing reaction of the two-component adhesive takes place after mixing at room temperature, without any need to apply pressure. The adherents must be fixed to avoid movement of the adhesive joints before the cure is complete. Figure A.3 shows how the specimens are bonded on the aluminum template.

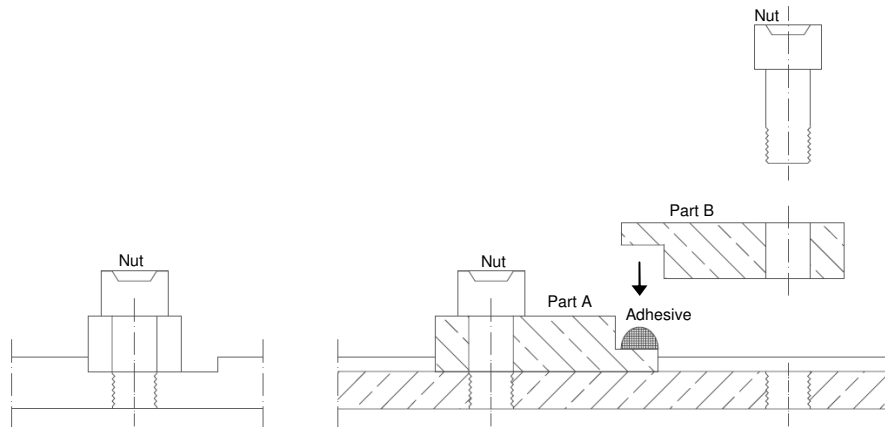


Figure A.3 Aluminum template to prepare the adhesively bonded specimens.

A.2 Storing specimens

After applying the adhesive, the uncured bonded joints of the specimens are stored in an environmental chamber for approximately 48 hours. After 15 minutes the adhesive has reached 80% of its strength according to the technical data sheet of the product. The storing room temperature and relative humidity are kept constantly, namely $RT = 23\text{ }^{\circ}\text{C}$ and $RH = 60\%$ respectively.

A.3 Testing conditions

The testing conditionings are equal for all specimens. However, to compare new test results with previous tests, the displacement velocity is adjusted from 0.5 mm/min to 2.5 mm/min , because the shear stress is influenced by this parameter. Tests of batch 1 are carried out with a displacement velocity of 2.5 mm/min in for comparison with [Huveners and Koggel 2006]. Batches 2 up to 6 are tested with a displacement velocity of 0.5 mm/min , according to [NEN-EN 14869-2:2004]. The testing temperature is room temperature, $RT = 23\text{ }^{\circ}\text{C}$ (see table A.1).

A.4 Coding specimens

To create a clear view of the circumstances in which the test are prepared and carried out, a wider range of abbreviations is used besides referring to the batch and sequence number. The test specimens are coded as follows:

BN-MAT-PREP-SN [ADH_ w_b _ t_b _RH_ T_0 _ T_t _DV]

In which:

- BN Batch number (1 up to 6);
- MAT Material type (Steel (ST) or Aluminum (ALU));
- PREP Type of preparation (ACE, SIK, according to section A.1);
- SN Sequence number (1 up to 5);
- ADH Type of adhesive (AC, according to section 3.1);
- w_b Bonded joint width;
- t_b Bonded joint thickness;
- RH Average relative humidity from manufacturing to testing [%];
- T_0 Manufacturing temperature of the specimen at day 0 [$^{\circ}\text{C}$]
- T_t Testing temperature [$^{\circ}\text{C}$]
- DV Displacement velocity [mm/min]

In section A.5 all the specimens with its properties are presented in table A.1

A.5 Oversight specimens

Table A.1 gives an overview of all test specimens with the corresponding codes. Of each batch at least 5 specimens were made and tested in the same constant circumstances. Tests of each batch are carried out in one day.

Table A.1 Batch number 1 up to 6.

Test Code	ADH	w_b [mm]	t_b [mm]	RH [%]	T_0 [°C]	T_t [°C]	DV [mm/min]
1-ALU-SIK-TEST	Acrylic adhesive	10	3	60	23	23	2.5
1-ALU-SIK-1	Acrylic adhesive	10	3	60	23	23	2.5
1-ALU-SIK-2	Acrylic adhesive	10	3	60	23	23	2.5
1-ALU-SIK-3	Acrylic adhesive	10	3	60	23	23	2.5
1-ALU-SIK-4	Acrylic adhesive	10	3	60	23	23	2.5
1-ALU-SIK-5	Acrylic adhesive	10	3	60	23	23	2.5
2-ALU-SIK-1	Acrylic adhesive	10	3	60	23	23	0.5
2-ALU-SIK-2	Acrylic adhesive	10	3	60	23	23	0.5
2-ALU-SIK-3	Acrylic adhesive	10	3	60	23	23	0.5
2-ALU-SIK-4	Acrylic adhesive	10	3	60	23	23	0.5
2-ALU-SIK-5	Acrylic adhesive	10	3	60	23	23	0.5
3-ST-SIK-TEST 1	Acrylic adhesive	10	3	60	23	23	0.5
3-ST-SIK-TEST 2	Acrylic adhesive	10	3	60	23	23	0.5
3-ST-SIK-1	Acrylic adhesive	10	3	60	23	23	0.5
3-ST-SIK-2	Acrylic adhesive	10	3	60	23	23	0.5
3-ST-SIK-3	Acrylic adhesive	10	3	60	23	23	0.5
3-ST-SIK-4	Acrylic adhesive	10	3	60	23	23	0.5
3-ST-SIK-5	Acrylic adhesive	10	3	60	23	23	0.5
4-ST-SIK-1	Acrylic adhesive	5	3	60	23	23	0.5
4-ST-SIK-2	Acrylic adhesive	5	3	60	23	23	0.5
4-ST-SIK-3	Acrylic adhesive	5	3	60	23	23	0.5
4-ST-SIK-4	Acrylic adhesive	5	3	60	23	23	0.5
4-ST-SIK-5	Acrylic adhesive	5	3	60	23	23	0.5
5-ST-ACE-1	Acrylic adhesive	5	3	60	23	23	0.5
5-ST-ACE-2	Acrylic adhesive	5	3	60	23	23	0.5
5-ST-ACE-3	Acrylic adhesive	5	3	60	23	23	0.5
5-ST-ACE-4	Acrylic adhesive	5	3	60	23	23	0.5
5-ST-ACE-5	Acrylic adhesive	5	3	60	23	23	0.5
6-ST-SIK-1	Acrylic adhesive	5	2	60	23	23	0.5
6-ST-SIK-2	Acrylic adhesive	5	2	60	23	23	0.5
6-ST-SIK-3	Acrylic adhesive	5	2	60	23	23	0.5
6-ST-SIK-4	Acrylic adhesive	5	2	60	23	23	0.5
6-ST-SIK-5	Acrylic adhesive	5	2	60	23	23	0.5

A.6 Measuring values

Geometry bonded joint

The specimens are manufactured with technical drawings (figure A.4). To draw conclusions on the results, the actual dimensions of the bonded joint and the bonded joint thickness have to be known.

The actual dimensions of the bonded joint are:

$$\text{Overlap length [mm]:} \quad l_b = \frac{1}{2}[c_1 - e_1 + c_2 - e_2]$$

$$\text{Overlap width [mm]:} \quad w_j = \frac{1}{2}[d_1 + d_2]$$

$$\text{Bonded joint thickness [mm]:} \quad t_b = \Pi_{\text{ave}} - a_1 - a_2$$

$$\text{Bonding area [mm]:} \quad A_b = l_b * w_b$$

In which:

$\Pi_a; \Pi_b$ [mm] is the thickness of part A and part B respectively;

Π_{ave} [mm] is the average overall thickness of the overlapping area;

$I_a; I_b$ [mm] is the adherent thickness of part A and part B respectively;

$c_1; c_2$ [mm] is the notch length of part A and part B respectively;

$d_1; d_2$ [mm] is the width of part A and part B respectively;

$e_1; e_2$ [mm] is the gap between part A and part B and between part B and A respectively.

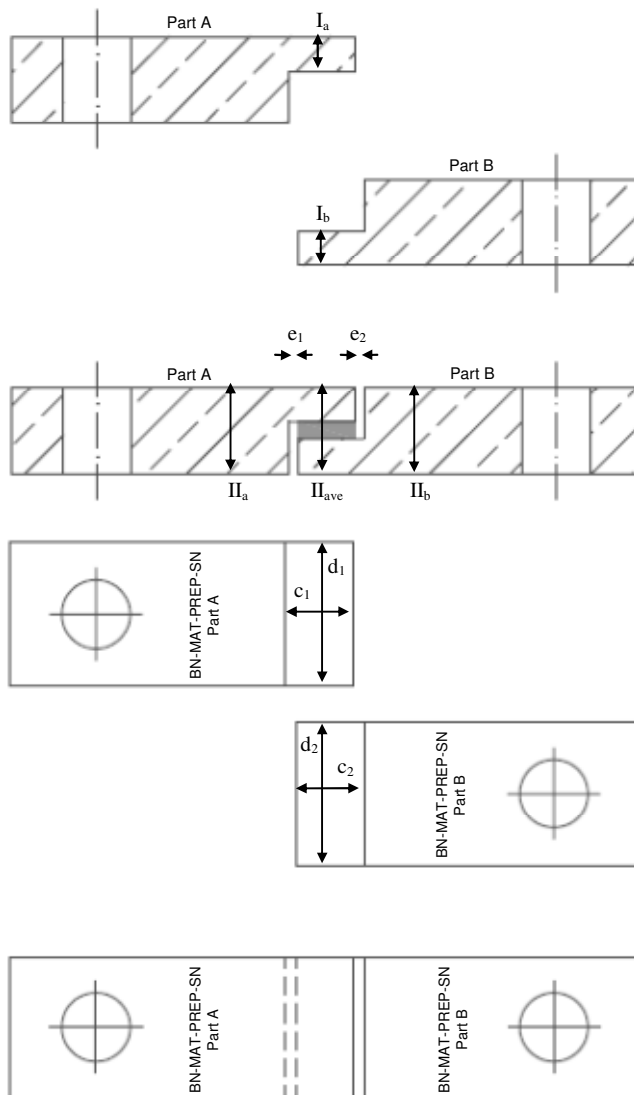


Figure A.4 Measuring geometry test specimens

Measuring during test

Appendix A.3 already mentioned that the test specimens are subjected to a continuously controlled displacement of 2.5 mm/min and 0.5 mm/min respectively. Due to a prevented elongation a tensile force is built up in the specimen. This tensile force is measured by the bench whereas the elongation of the test specimen is measured with two LVDT's (Linear Variable Differential Transformer) on both sides (figure 3.5 in section 3.1.2). This tensile force is then transformed through the bonded joint introducing an in plane shear force.

A.7 Results

In appendix A.8 the bonded joint thickness and bonded joint area of all specimens have been calculated depending on the actual geometry of the specimens. Theoretical the sides of the bonded joint, exposed to the surrounding air, have to be straight in line with the metal. If the bonded joint of the specimens visually does not clearly deviate from the theoretical straight bonded joint than the effective bonding area will be considered 100%.

Batch 1-ALU-SIK-.. [AC_10_3_60_23_23_2.5]

The results of batch 1-ALU-SIK-.. are shown in table A.2.

Table A.2 Results Batch 1-ALU-SIK-..

	Test	1	2	3	4	5
Failure mechanism	Cohesion: 100% Adhesion: -	Cohesion: 100% Adhesion: -	Cohesion: 100% Adhesion: -	Cohesion: 100% Adhesion: -	Cohesion: 100% Adhesion: -	Cohesion: 100% Adhesion: -
Effective bonding area	100%	± 110% !!	100%	100%	± 80% !!	100%
Status specimen	Valid	Invalid	Valid	Valid	Invalid	Valid

	Test	1	2	3	4	5
F_{max} [N]	1355	1846	1697	1776	1654	1804
Duration [s]	161.00	171.00	166.00	181.00	168.00	155.00
Average elongation [mm]	5.1455	5.0540	5.5939	6.0780	6.2823	5.4896
Elongation left (front) [mm]	5.4654	5.3614	6.1378	6.0254	6.6556	6.0123
Elongation right (back) [mm]	4.8256	4.7465	5.0499	6.1305	5.9090	4.9669
Bonded joint thickness [mm]	2.95	2.93	2.96	3.03	2.97	3.01

Two specimens of this batch can be considered invalid because of the big difference in test results. Specimen 1-ALU-SIK-1 had too big bonding area. The open space of this specimen (figure A.5) was filled with cured adhesive. The surplus on both sides was removed with a saw, so no there was no contact on de sides of the bonded joint. Due to inaccurate removal of the surplus (on the right in figure A.5), the bond width was bigger than 10 mm. For specimen 1-ALU-SIK-4 the opposite occurred (figure A.6). A metal strip to erase non cured adhesive was pulled too fast through the open space and removed too much adhesive. This causes the bonding area to be less than needed.

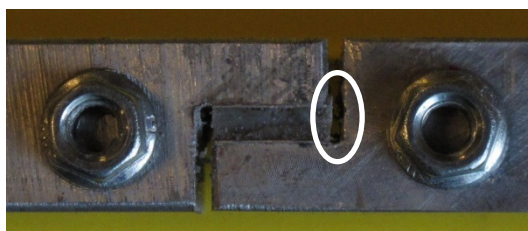


Figure A.5 Bonded joint width too much bonding area.



Figure A.6 Bonded joint with less bonding area.

The two invalid specimens are not taken into account determining the average formulae representing the shear stress, shear strain relation. The results of the shear tests shown in table A.2 are represented in figure A.7.

The discontinuity of the shear stress, strain relation of specimen 1-ALU-SIK-1 occurred after the test was stopped for a few seconds to get the photo camera. Due to the fact that creep immediately occurred, the test was preceded.

1-ALU-SIK-..

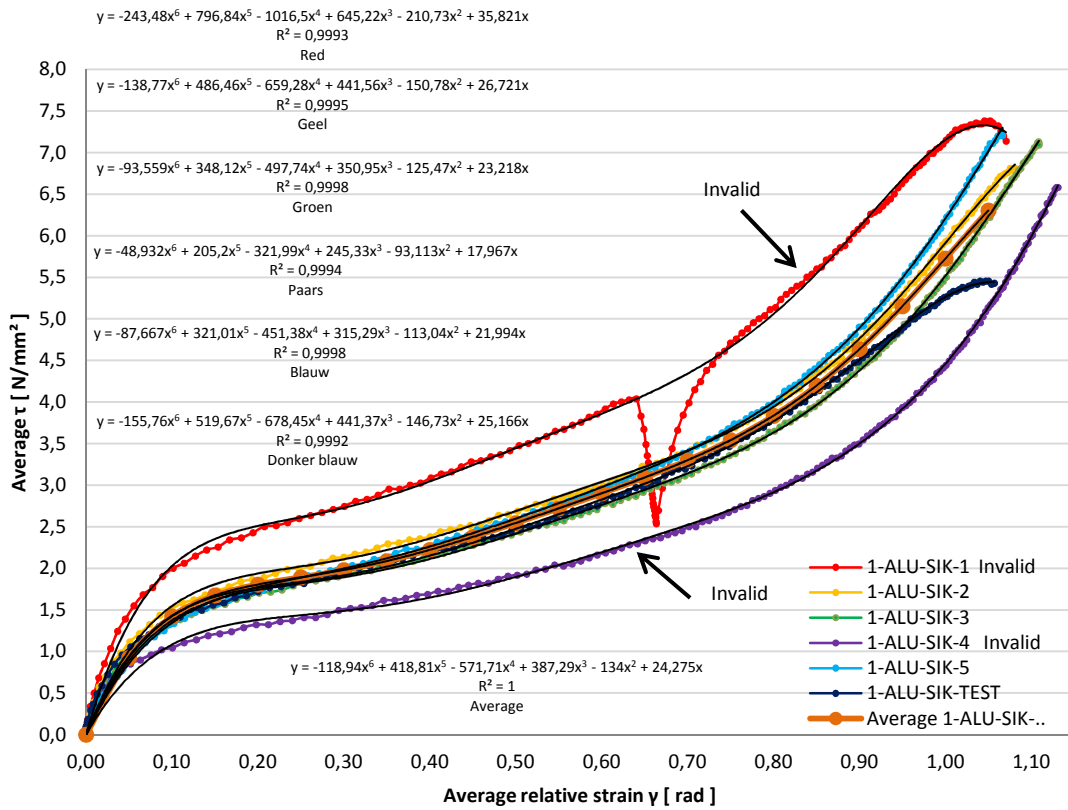


Figure A.7. Relation between the average shear stress and the average relative strain of batch 1.

Batch 2-ALU-SIK-.. [AC_10_3_60_23_23_0.5]

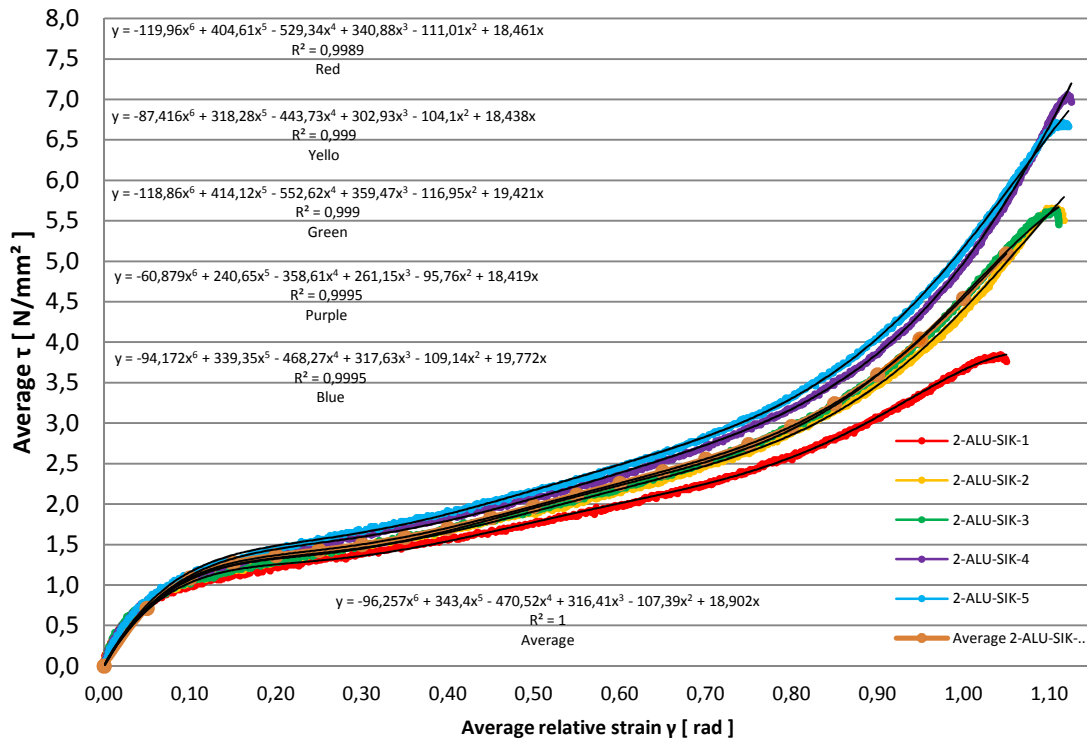
The results of batch 2-ALU-SIK-.. are shown in table A.3.

Table A.3 Results Batch 2-ALU-SIK-..

	1	2	3	4	5
Failure mechanism	Cohesion: 100% Adhesion: -	Cohesion: 100% Adhesion: -	Cohesion: 100% Adhesion: -	Cohesion: 100% Adhesion: -	Cohesion: 100% Adhesion: -
Effective bonding area	100%	100%	100%	100%	100%
Status specimen	Valid	Valid	Valid	Valid	Valid

	1	2	3	4	5
F _{max} [N]	952	1401	1401	1758	1663
Duration [s]	761	744	732	786	756
Average elongation [mm]	5.0977	5.8481	5.8740	6.0504	5.8725
Elongation left (front) [mm]	6.6897	6.044	5.8055	6.4354	5.9220
Elongation right (back) [mm]	3.5057	5.6522	5.9424	5.6653	5.8229
Bonded joint thickness [mm]	3.04	3.00	3.00	2.92	2.93

2-ALU-SIK-..



A.8. Relation between the average shear stress and the average relative strain of batch 2.

Batch 3-ST-SIK-.. [AC_10_3_60_23_23_0.5]

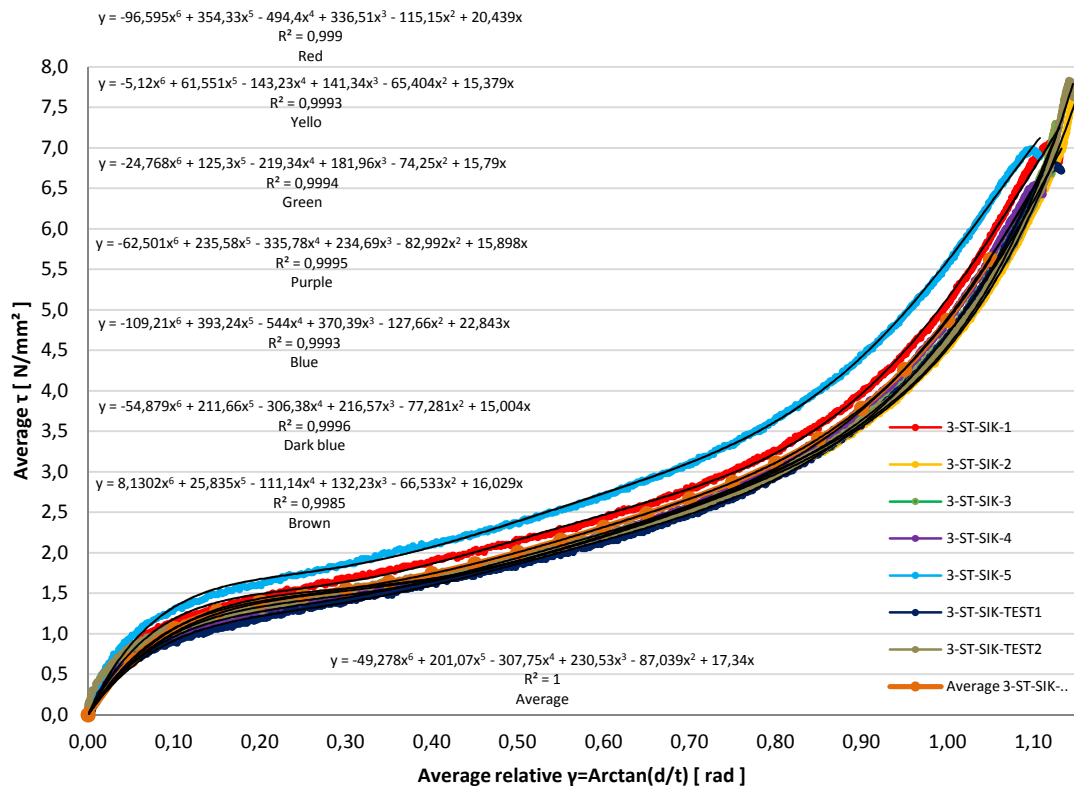
The results of batch 1-ALU-SIK-.. are shown in table A.4.

Table A.4 Results Batch 3-ST-SIK-..

	Test 1	Test 2	1	2	3	4	5
Failure mechanism	Cohesion: 100% Adhesion: -	Cohesion: 100% Adhesion: -	Cohesion: 100% Adhesion: -	Cohesion: 100% Adhesion: -	Cohesion: 100% Adhesion: -	Cohesion: 100% Adhesion: -	Cohesion: 100% Adhesion: -
Effective bonding area	100%	100%	100%	100%	100%	100%	100%
Status specimen	Valid	Valid	Valid	Valid	Valid	Valid	Valid

	Test 1	Test 2	1	2	3	4	5
F_{max} [N]	1685	1941	1761	1941	1825	1627	1736
Duration [s]	823	896	774	924	828	759	738
Average elongation [mm]	6.2247	6.5501	6.1527	6.5621	6.2770	5.9332	5.8390
Elongation left (front) [mm]	6.5944	7.0580	6.4675	6.9729	6.3578	5.8942	5.8535
Elongation right (back) [mm]	5.8550	6.0421	5.8378	6.1513	6.1962	5.9721	5.8245
Bonded joint thickness [mm]	2.98	3.00	2.99	2.95	3.00	3.01	3.00

3-ST-SIK-..



A.9. Relation between the average shear stress and the average relative strain of batch 3.

Batch 4-ST-SIK-.. [AC_5_3_60_23_23_0.5]

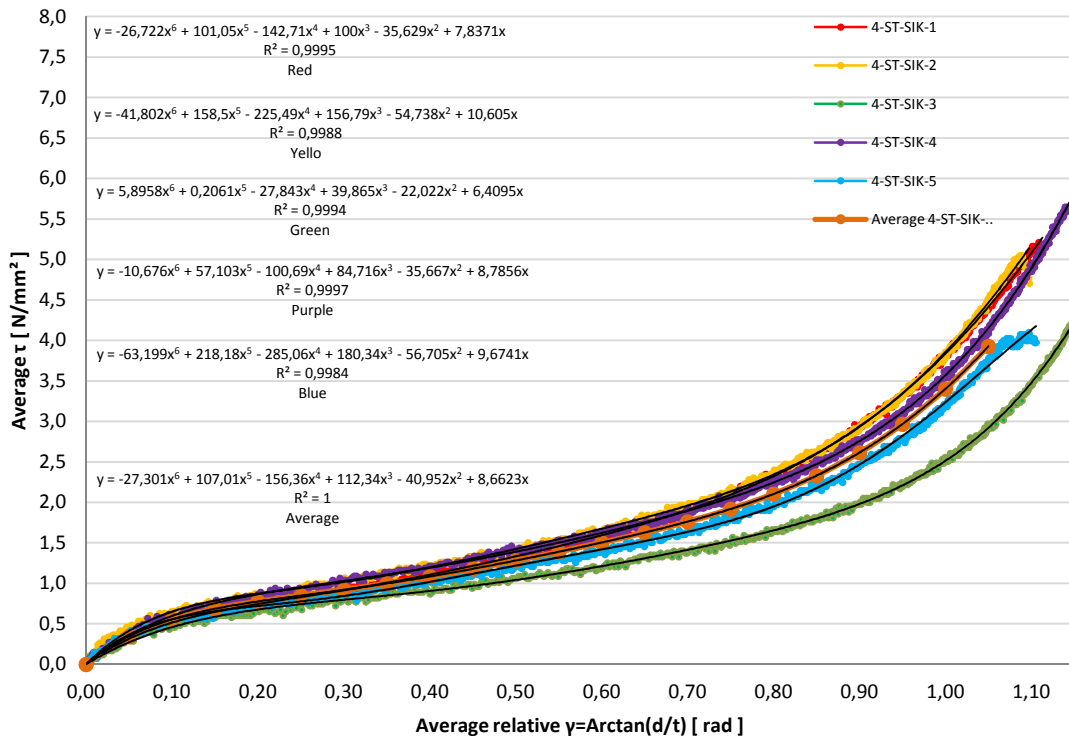
The results of batch 4-ST-SIK-.. are shown in table A.5.

Table A.5 Results Batch 4-ST-SIK-..

	1	2	3	4	5
Failure mechanism	Cohesion: 100% Adhesion: -	Cohesion: 100% Adhesion: -	Cohesion: 100% Adhesion: -	Cohesion: 100% Adhesion: -	Cohesion: 100% Adhesion: -
Effective bonding area	100%	100%	100%	100%	100%
Status specimen	Valid	Valid	Valid	Valid	Valid

	1	2	3	4	5
F _{max} [N]	650	635	644	696	507
Duration [s]	721	717	866	838	723
Average elongation [mm]	5.9215	5.8745	6.6937	6.4560	5.9080
Elongation left (front) [mm]	5.8257	6.1316	7.1518	7.0791	6.5602
Elongation right (back) [mm]	6.0173	5.6174	6.2355	5.8329	5.2557
Bonded joint thickness [mm]	2.95	3.09	2.78	2.94	3.03

4-ST-SIK-..



A.10. Relation between the average shear stress and the average relative strain of batch 4.

Batch 5-ST-ACE-.. [AC_5_3_60_23_23_0.5]

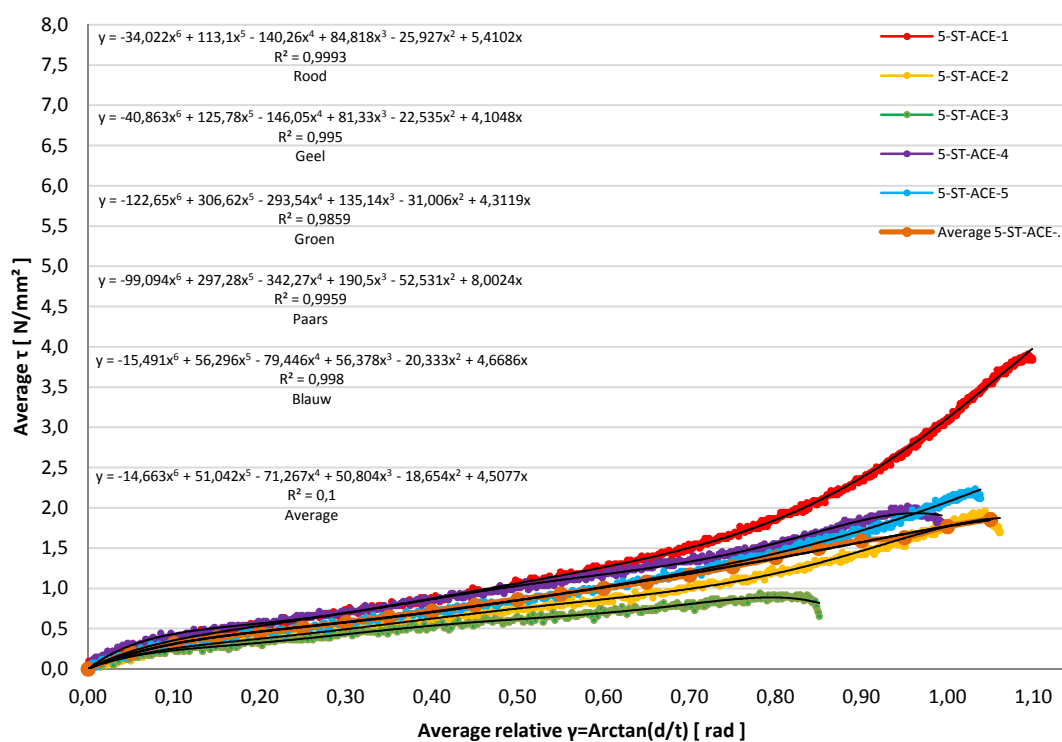
The results of batch 5-ST-ACE-.. are shown in table A.6.

Table A.6 Results Batch 5-ST-ACE-..

	1	2	3	4	5
Failure mechanism	Cohesion: 70% Adhesion: 30%	Cohesion: 20% Adhesion: 80%	Cohesion: - Adhesion: 100%	Cohesion: - Adhesion: 100%	Cohesion: - Adhesion: 100%
Effective bonding area	100%	100%	100%	100%	100%
Status specimen	Valid	Valid	Valid	Valid	Valid

	1	2	3	4	5
F_{max} [N]	485	244	119	250	287
Duration [s]	805	504	334	475	581
Average elongation [mm]	5.9771	4.2786	2.8982	4.1551	4.9369
Elongation left (front) [mm]	6.0872	5.0959	3.8401	4.3970	5.4500
Elongation right (back) [mm]	5.8670	3.4612	1.9562	3.9131	4.4237
Bonded joint thickness [mm]	3.1	2.5	2.9	3.0	3.0

5-ST-ACE-..



A.11. Relation between the average shear stress and the average relative strain of batch 5.

Batch 6-ST-SIK-.. [AC_5_2_60_23_23_0.5]

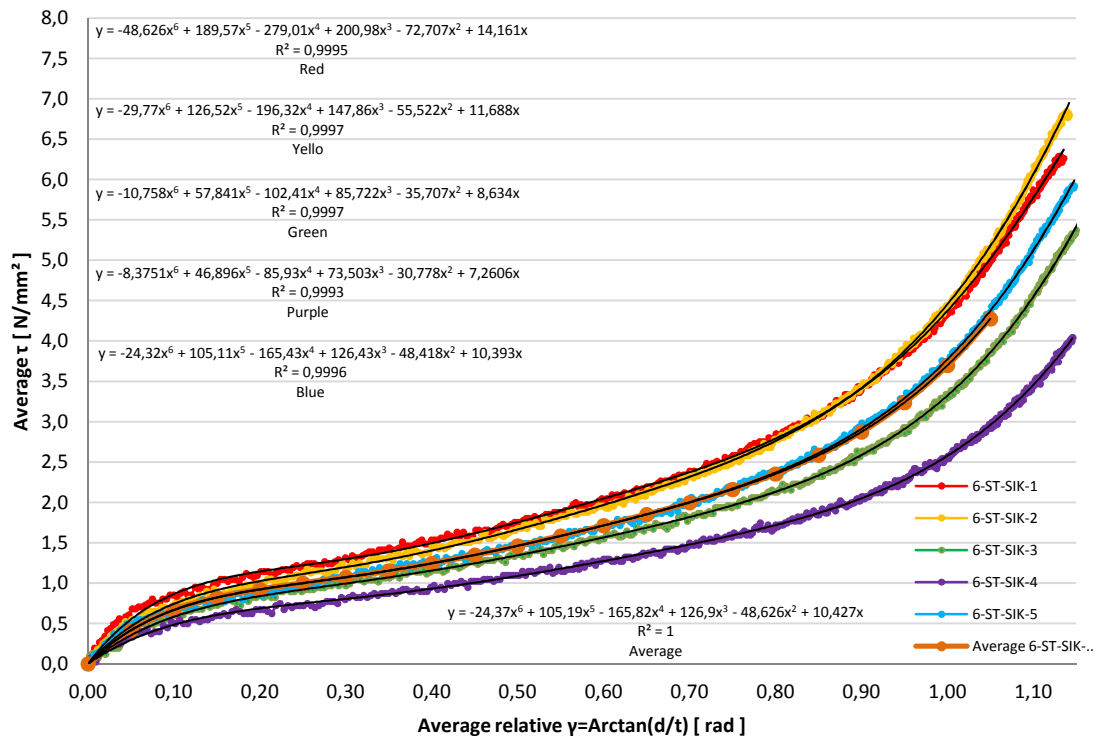
The results of batch 6-ST-SIK-.. are shown in table A.7.

Table A.7 Results Batch 6-ST-SIK-..

	1	2	3	4	5
Failure mechanism	Cohesion: 100% Adhesion: -	Cohesion: 100% Adhesion: -	Cohesion: 100% Adhesion: -	Cohesion: 100% Adhesion: -	Cohesion: 100% Adhesion: -
Effective bonding area	100%	100%	100%	100%	100%
Status specimen	Valid	Valid	Valid	Valid	Valid

	1	2	3	4	5
F _{max} [N]	787	833	678	525	742
Duration [s]	511	540	596	534	542
Average elongation [mm]	4.2334	4.3363	4.4455	4.4384	4.5215
Elongation left (front) [mm]	4.5243	4.4562	5.598	5.1399	4.8254
Elongation right (back) [mm]	3.9424	4.2163	3.2930	3.7369	4.2175
Bonded joint thickness [mm]	2.00	2.00	1.99	1.92	1.99

6-ST-SIK-..



A.12. Relation between the average shear stress and the average relative strain of batch 6.

A.8 Geometry of the bonded joint

Perfect bonded joint

	l_b [mm]	w_b [mm]	$Area_b$ [mm ²]	l_b [mm]	$Volume_b$ [mm ³]
A	10,00	25,00	250,00	3	750,00
B	10,00	25,00			

Data: 27-1-2011
Prepared: 13.00 - 14.00u.
Adhesively bonded: 14.15-15.00u.

Aluminum	Speed [mm/min]	Bonded joint thickness	
		3 [mm]	10 [mm]
1-ALU-SIK-..	2,5	3	10
2-ALU-SIK-..	0,5	3	10

	I	II	III	IV	V	l_b [mm]	w_b [mm]	$Area_b$ [mm ²]	l_b [mm]	$Volume_b$ [mm ³]	Testcode	difference percentage	
												$Area_b$	$Volume_b$
1A	11,40	6,09	15,17	24,95	59,75	9,90	24,95	248,40	2,95	731,55	1-ALU-SIK-TEST	-0,64%	-2,46%
1B	11,52	6,13	15,16	24,93	59,76	10,02	24,93						
2A	11,53	6,18	15,25	24,94	59,74	10,03	24,94	250,07	2,93	731,47	1-ALU-SIK-1	0,03%	-2,47%
2B	11,52	6,15	15,26	24,95	59,82	10,02	24,95						
3A	11,38	6,16	15,19	24,89	59,92	9,88	24,89	248,63	2,96	734,69	1-ALU-SIK-2	-0,55%	-2,04%
3B	11,55	6,12	15,28	25,01	59,75	10,05	25,01						
4A	11,50	6,05	15,19	24,95	59,82	10,00	24,95	249,10	3,03	753,53	1-ALU-SIK-3	-0,36%	0,47%
4B	11,48	6,11	15,18	24,92	59,73	9,98	24,92						
5A	11,57	6,06	15,13	24,99	59,92	10,07	24,99	251,30	2,97	745,10	1-ALU-SIK-4	0,52%	-0,65%
5B	11,57	6,13	15,18	24,92	59,75	10,07	24,92						
6A	11,48	6,03	15,17	25,03	59,83	9,98	25,03	248,95	3,01	748,10	1-ALU-SIK-5	-0,42%	-0,25%
6B	11,46	6,13	15,16	24,91	59,74	9,96	24,91						
7A	11,52	5,95	15,18	25,03	60,03	10,02	25,03	248,95	3,04	755,57	2-ALU-SIK-1	-0,42%	0,74%
7B	11,46	6,17	15,13	24,81	59,74	9,96	24,81						
8A	11,49	6,08	15,21	24,93	59,96	9,99	24,93	247,70	3,00	743,11	2-ALU-SIK-2	-0,92%	-0,92%
8B	11,45	6,11	15,17	24,76	59,74	9,95	24,76						
9A	11,47	6,04	15,16	24,98	59,66	9,97	24,98	249,60	3,00	747,55	2-ALU-SIK-3	-0,16%	-0,33%
9B	11,51	6,12	15,15	24,99	59,74	10,01	24,99						
10A	11,47	6,10	15,15	24,82	59,89	9,97	24,82	248,78	2,92	725,18	2-ALU-SIK-4	-0,49%	-3,31%
10B	11,52	6,13	15,14	24,96	59,73	10,02	24,96						
11A	11,40	6,08	15,21	24,94	59,83	9,90	24,94	247,63	2,93	725,56	2-ALU-SIK-5	-0,95%	-3,26%
11B	11,53	6,19	15,19	24,76	59,78	10,03	24,76						

Perfect bonded joint

	l_b [mm]	w_b [mm]	$Area_b$ [mm ²]	t_b [mm]	$Volume_b$ [mm ³]
A	10,00	25,00	250,00	3	750,00
B	10,00	25,00			

Data: 27-1-2011

Prepared: 13.00 - 14.00u.

Adhesively bonded: 14.15-15.00u.

Steel	Speed	Bonded joint thickness	Overlap
3-ST-SIK-..	0,5 [mm/min]	3 [mm]	10 [mm]

	I	II	III	IV	V	l_b [mm]	w_b [mm]	$Area_b$ [mm ²]	t_b [mm]	$Volume_b$ [mm ³]	Testcode	difference percentage	
												$Area_b$	$Volume_b$
12A	11,47	5,97	14,92	24,91	59,82	9,97	24,91	248,10	2,98	738,11	3-ST-SIK-TEST	-0,76%	-1,59%
12B	11,43	5,97	14,91	24,96	59,78	9,93	24,96						
13A	11,46	5,97	14,89	24,90	59,87	9,96	24,90	247,80	3,00	742,18	3-ST-SIK-TEST	-0,88%	-1,04%
13B	11,44	5,93	14,90	24,91	59,77	9,94	24,91						
14A	11,56	5,98	14,91	24,91	59,89	10,06	24,91	249,42	2,99	744,53	3-ST-SIK-1	-0,23%	-0,73%
14B	11,45	5,95	14,92	24,95	59,78	9,95	24,95						
15A	11,46	5,93	14,94	24,89	59,79	9,96	24,89	248,63	2,95	732,21	3-ST-SIK-2	-0,55%	-2,37%
15B	11,51	6,05	14,91	24,91	59,47	10,01	24,91						
16A	11,51	5,96	14,92	25,01	59,78	10,01	25,01	250,00	3,00	748,75	3-ST-SIK-3	0,00%	-0,17%
16B	11,49	5,96	14,91	24,99	59,80	9,99	24,99						
17A	11,46	5,97	14,93	24,93	59,84	9,96	24,93	248,50	3,01	747,99	3-ST-SIK-4	-0,60%	-0,27%
17B	11,48	5,94	14,91	24,92	59,80	9,98	24,92						
18A	11,47	5,97	14,91	24,95	59,71	9,97	24,95	248,58	3,00	745,73	3-ST-SIK-5	-0,57%	-0,57%
18B	11,46	5,94	14,91	24,94	59,79	9,96	24,94						

perfect bonded joint

	l_b [mm]	w_b [mm]	$Area_b$ [mm ²]	t_b [mm]	$Volume_b$ [mm ³]
A	5,00	25,00	125,00	2	250,00
B	5,00	25,00			
A	5,00	25,00	125,00	3	375,00
B	5,00	25,00			

Data: 27-1-2011

Prepared: 13.00 - 14.00u.

Adhesively bonded: 14.15-15.00u.

Steel	Speed	Bonded joint thickness	Overlap
6-ST-SIK-..	0,5 [mm/min]	2 [mm]	5 [mm]
4-ST-SIK-..	0,5 [mm/min]	3 [mm]	5 [mm]

	I	II	III	IV	V	l_b [mm]	w_b [mm]	$Area_b$ [mm ²]	t_b [mm]	$Volume_b$ [mm ³]	Testcode	difference percentage	
												$Area_b$	$Volume_b$
19A	6,56	5,97	13,98	25,01	59,78	5,06	25,01	125,20	2,00	249,77	6-ST-SIK-1	0,16%	-0,09%
19B	6,46	5,97	13,89	24,97	59,78	4,96	24,97						
20A	6,35	5,97	13,89	24,92	59,80	4,85	24,92	121,70	2,00	242,80	6-ST-SIK-2	-2,64%	-2,88%
20B	6,40	5,93	13,90	25,01	59,76	4,90	25,01						
21A	6,61	5,98	13,93	24,91	59,86	5,11	24,91	126,05	1,99	250,83	6-ST-SIK-3	0,84%	0,33%
21B	6,50	5,95	13,91	24,96	59,78	5,00	24,96						
22A	6,40	5,93	13,89	24,91	59,79	4,90	24,91	122,31	1,92	234,22	6-ST-SIK-4	-2,15%	-6,31%
22B	6,42	6,05	13,90	24,91	59,76	4,92	24,91						
23A	6,38	5,96	13,90	24,96	59,82	4,88	24,96	122,65	1,99	243,47	6-ST-SIK-5	-1,88%	-2,61%
23B	6,45	5,96	13,91	24,95	59,78	4,95	24,95						
24A	6,43	6,00	14,91	25,09	59,87	4,93	25,09	124,70	2,95	367,24	4-ST-SIK-1	-0,24%	-2,07%
24B	6,54	5,96	14,90	24,94	59,75	5,04	24,94						
25A	6,57	5,92	14,97	24,95	59,80	5,07	24,95	125,77	3,09	388,01	4-ST-SIK-2	0,62%	3,47%
25B	6,52	5,93	14,90	24,91	59,84	5,02	24,91						
26A	6,58	5,95	14,67	24,91	59,75	5,08	24,91	126,47	2,78	350,95	4-ST-SIK-3	1,18%	-6,41%
26B	6,57	6,05	14,88	24,93	59,82	5,07	24,93						
27A	6,39	5,97	14,74	24,91	59,79	4,89	24,91	123,20	2,94	361,61	4-ST-SIK-4	-1,44%	-3,57%
27B	6,50	5,92	14,91	24,92	59,77	5,00	24,92						
28A	6,46	5,94	14,75	24,95	59,93	4,96	24,95	123,58	3,03	374,44	4-ST-SIK-5	-1,14%	-0,15%
28B	6,45	5,86	14,91	24,93	59,79	4,95	24,93						

Perfect bonded joint													
			l_b	w_b	$Area_b$	t_b	$Volume_b$						
			[mm]	[mm]	[mm ²]	[mm]	[mm ³]						
Data: 27-1-2011													
Prepared: 13.00 - 14.00u.													
Adhesively bonded: 14.15-15.00u.													
	A		5,00	25,00	125,00	3	375,00						
	B		5,00	25,00									
Steel	Speed	Bonded joint thickness	Overlap										
5-ST-ACE-...	0,5 [mm/min]	2 [mm]	5 [mm]										
	I	II	III	IV	V	l_b	w_b	$Area_b$	t_b	$Volume_b$	Testcode	difference percentage	
						[mm]	[mm]	[mm ²]	[mm]	[mm ³]		$Area_b$	$Volume_b$
29A	6,38	5,91	14,90	25,09	59,81	4,88	25,09	124,02	3,09	383,24	5-ST-ACE-1	-0,78%	2,20%
29B	6,54	5,93	14,96	24,92	59,83	5,04	24,92						
30A	6,45	5,95	13,86	24,92	59,90	4,95	24,92	124,20	2,49	308,64	5-ST-ACE-2	-0,64%	-17,70%
30B	6,51	5,96	14,93	24,96	59,85	5,01	24,96						
31A	6,58	5,94	14,70	24,92	59,77	5,08	24,92	125,95	2,92	367,76	5-ST-ACE-3	0,76%	-1,93%
31B	6,53	5,94	14,90	24,91	59,78	5,03	24,91						
32A	6,50	5,95	14,76	24,91	59,80	5,00	24,91	123,70	2,95	364,92	5-ST-ACE-4	-1,04%	-2,69%
32B	6,43	5,93	14,90	24,92	59,80	4,93	24,92						
33A	6,60	5,96	14,89	25,01	59,76	5,10	25,01	128,20	2,95	378,20	5-ST-ACE-5	2,56%	0,85%
33B	6,64	5,99	14,91	25,07	59,80	5,14	25,07						

A.9 Sikafast 5215 technical datasheet

Industry

SikaFast[®]-5215

Fast curing 2-C structural adhesive, designed for glass bonding (Open time: 5 min.)

Technical Product Data

Properties	Component A SikaFast [®] -5215	Component B SikaFast [®] -5200
Chemical base	2-component ADP Acrylic	
Colour (CQP ¹⁾ 001-1)	White	Black
Colour mixed	Grey	
Cure mechanism	Polymerisation	
Density (CQP 006-4)	1,14 g/cm ³ approx.	1,46 g/cm ³ approx.
Mixing ratio	by volume by weight	
	10 : 1 10 : 1,28	
Consistency	Thixotropic paste	
Application temperature	+10° to +40°C (50° - 105°F)	
Open time ²⁾ (CQP 526-1), (static mixer) 23°C (73°F)	5 min. approx. (see diagram 1)	
Curing speed	See diagram 1	
Shore A hardness (CQP 023-1 / ISO 868)	90 approx.	
Shore D hardness	50 approx.	
Tensile strength ²⁾ (CQP 036-1 / ISO 527)	10 N/mm ² approx.	
Elongation at break ²⁾ (CQP 036-1 / ISO 527)	150% approx.	
Tensile-shear strength ²⁾ (CQP 546-1 / ISO 4587)	8 N/mm ² approx.	
Glass transition temperature (CQP 509-1 / ISO 4663)	52°C approx.	
Electrical resistance (CQP 079-2 / ASTM D 257-99)	1,6 x 10 ¹³ Ω cm approx.	
Service temperature (CQP 513-1)	-40° - +80°C (-40° - +175°F)	
Shelf life and storage ³⁾ (CQP 016-1)	12 months	

¹⁾ CSQP = Corporate Sika Quality Procedures ²⁾ 23°C (73°F) / 50% r.h.

³⁾ Stored at temperatures below 25°C (77°F) and not exposed to direct sun light

Description

SikaFast[®]-5215 is a fast curing, flexible 2-component adhesive system. It is based on ADP, Sika's polymer technology, derived from the acrylic chemistry.

Uncured SikaFast[®]-5215 is a pasty, non-sagging, non-flammable material which allows an easy and precise application.

SikaFast[®]-5215 is manufactured in accordance with ISO 9001 / 14001 quality assurance system and with the responsible care program.

Product Benefits

- Strength development within minutes after application
- Adhesion to a wide range of metals and plastics as well as glass with no or only limited substrate preparation
- High strength
- Gap filling, allowing for manufacturing tolerances (up to 3 mm)
- Flexible, Vibration damping
- Solvent and acid-free
- Easy mixing
- Low odour
- Approved NSF R2 (accidental food contact)

Areas of Application

The ADP technology offers a new generation of fast curing, flexible adhesives designed to substitute welding, riveting, clinching and other, mechanical fastening techniques. SikaFast[®]-5215 is suitable for structural and semi-structural bonding on a wide range of substrates in the assembly and trim shop, for high strength fastening of concealed joints on different types of substrates including glass, top coats, plastics, etc.



Cure Mechanism

SikaFast®-5215 contains the reactive monomer and SikaFast®-5200 (component B) acts as initiator. On mixing with a static mixer, the polymerisation reaction is started. SikaFast®-5215 offers a relatively long open time followed by fast curing which results in an optimal relation between application time and strength development to reach handling strength, see diagram (the curing time is slightly varying depending on ambient temperature). In spite of the quick strength build-up, premature exposure to stresses destroys the adhesive. Allow the adhesive to cure for 15 minutes (from mixing), before any load can affect the bond. Adjustment of the bonded parts is possible only within the open time (5 minutes from mixing).

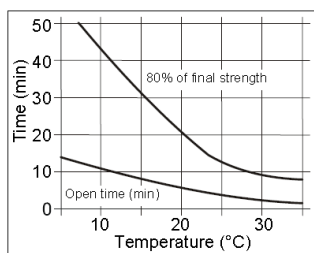


Diagram: Open time and curing speed for SikaFast®-5215

Chemical Resistance

For advice contact the Technical Service Department of Sika Industry.

Adhesion results

The following chart summarises lap-shear test results obtained with different substrates. These results are indications. Due to the diversity of substrates, preliminary tests are recommended. Be aware that the mechanical properties are temperature depending (values on request).

Adhesion table

Material		Value
Aluminium Al Mg3	C	8 N/mm ²
Steel St 32	C	8 N/mm ²
Stainless steel	C	8 N/mm ²
Galvanised steel	A	6 N/mm ²
UP-FRP	S	6 N/mm ²
Acrylic paint	S	6 N/mm ²
Glass	C	9 N/mm ²
ABS (Terulan)	C	6 N/mm ²
PVC (Köradur ES)	C	9 N/mm ²
Polycarbonate	S	8 N/mm ²

Table 1: Lap shear samples according to ISO 4587, bondline thickness. (1,5 mm)

Breaktype: Adhesive, Cohesive, Substrate

Method of Application

Surface preparation

Surfaces must be clean, dry and free from all traces of grease, oil and dust. Remove all loose particles or residues. Contaminated areas must be thoroughly cleaned before bonding. In combination with SikaFast®-5215 Sika strongly recommends the use of Sika® ADPrep-5901, the general surface preparation agent for Sika® ADP adhesive system.

Advice on specific applications is available from the Technical Service Department of Sika Industry.

Application

With a 2-C cartridge or pump at mixing ratio 10 : 1 through a static mixer. The open time can be slightly varied with adapted processing parameters (method on request). Consider that if applied in large masses, heat is generated by the exothermic reaction. To avoid excessive temperature the bond line thickness should not exceed 3 mm. For additional information and support in evaluation of the appropriate application equipment please contact our Sika System Engineering.

Removal

Excess material can best be removed before curing with a dry wipe. Uncured SikaFast®-5215 may be removed from tools and equipment with Sika® Remover-208 or a suitable solvent.

Once cured the material can only be removed mechanically.

Hands and exposed skin should be washed immediately using Sika® Handclean Towel or a suitable industrial hand cleaner and water. Do not use solvents!

Further Information

Copies of the following publications are available on request

- Material Safety Data Sheets
- SikaFast®-5000 Primer Chart

Packaging Information

Dual cartridge	50 ml
----------------	-------

Important

For information and advice regarding transportation, handling, storage and disposal of chemical products, users should refer to the actual Material Safety Data Sheets containing physical, ecological, toxicological and other safety-related data.

Note

The information, and, in particular, the recommendations relating to the application and end-use of Sika products, are given in good faith based on Sika's current knowledge and experience of the products when properly stored, handled and applied under normal conditions. In practice, the differences in materials, substrates and actual site conditions are such that no warranty in respect of merchantability or of fitness for a particular purpose, nor any liability arising out of any legal relationship whatsoever, can be inferred either from this information, or from any written recommendations, or from any other advice offered. The proprietary rights of third parties must be observed. All orders are accepted subject to our current terms of sale and delivery. Users should always refer to the most recent issue of the Australian version of the Product Data Sheet for the product concerned, copies of which will be supplied on request.



Sika Australia Pty Limited
 ABN 12 001 342 329

www.sika.com.au
 Tel: 1300 22 33 48

A.10 Sika ADPrep technical datasheet

Industry

Sika[®] ADPrep

Surface preparation agent for SikaFast[®] adhesives

Technical Product Data

Chemical base	Solvent-based surface preparation agent	
Colour (CQP ¹⁾ -001-1)	Transparent, clear	
Density (CQP006-3/ISO 2811-1)	0,8 kg/l approx.	
Viscosity ²⁾ (CQP029-3 / ISO 3219)	2 mPas approx.	
Flash point (CQP007-1/ISO 13736)	13°C	
Application temperature	+5°C to +35°C	
Application method	standard	Cloth, absorbent paper
	only on polyamide	Brush (thick layer)
Coverage	standard	50 ml/m ² approx.
	polyamide	100 – 200 ml/m ² approx.
Flash off time	> 15°C	1 min
(wipe on only)	< 15°C	3 min
Flash off time on polyamide	> 15°C	10 min
(applied with brush)	< 15°C	20 min
Max. flash off time	max.	24 h
Shelf life	12 months ³⁾	

¹⁾ CQP = Corporate Quality Procedures

²⁾ 23°C / 50% r.h.

³⁾ stored unopened at a dry cool place

Description

Sika[®] ADPrep is a cleaning and activating agent specifically formulated for the treatment of surfaces prior to application of SikaFast[®] adhesives.

Sika[®] ADPrep is manufactured in accordance with ISO 9001 / 14001 quality assurance system and with the responsible care program.

Areas of Application

Sika[®] ADPrep is used to pre-treat all substrates such as metals and plastics and to improve adhesion of SikaFast[®] adhesives on those substrates.

Method of Application

Surface Preparation

Wipe bond surfaces with a clean lint-free cloth or absorbent paper towel moistened with Sika[®] ADPrep. Apply Sika[®] ADPrep sparingly, and apply once only. Only in case of polyamide, apply Sika[®] ADPrep with a brush. Reseal container tightly after use. Apply SikaFast[®]-adhesives after the indicated flash off time, but latest after 24 hours.

Sika[®] ADPrep contains solvent, which may dull the surface finish of some freshly applied paints. Preliminary trials must be carried out. If Sika[®] ADPrep is accidentally applied or splashed onto adjacent surfaces, wipe off immediately with a clean, dry cloth.

For further information contact Sika Technical Service Industry.



Further Information

Copies of the following publications are available on request:

- Material Safety Data Sheets
- Primer Chart for SikaFast[®] adhesives
- General Guidelines for bonding with SikaFast[®] adhesives

Packaging Information

Bottle	250 ml
--------	--------

Important

For information and advice on the safe handling, storage and disposal of chemical products, users should refer to the current Material Safety Data Sheet containing physical, ecological, toxicological and other safety-related data.

Note

The information, and, in particular, the recommendations relating to the application and end-use of Sika products, are given in good faith based on Sika's current knowledge and experience of the products when properly stored, handled and applied under normal conditions. In practice, the differences in materials, substrates and actual site conditions are such that no warranty in respect of merchantability or of fitness for a particular purpose, nor any liability arising out of any legal relationship whatsoever, can be inferred either from this information, or from any written recommendations, or from any other advice offered. The proprietary rights of third parties must be observed. All orders are accepted subject to our current terms of sale and delivery. Users should always refer to the most recent issue of the Technical Data Sheet for the product concerned, copies of which will be supplied on request.



Further information available at:
www.sika.ch
www.sika.com

Sika Schweiz AG
 Industry
 Tüffenwies 16
 CH-8048 Zurich
 Switzerland
 Tel. +41 44 436 40 40
 Fax +41 44 436 45 30



Sika[®] ADPrep 2 / 2

A.11 Proposition new shear tests

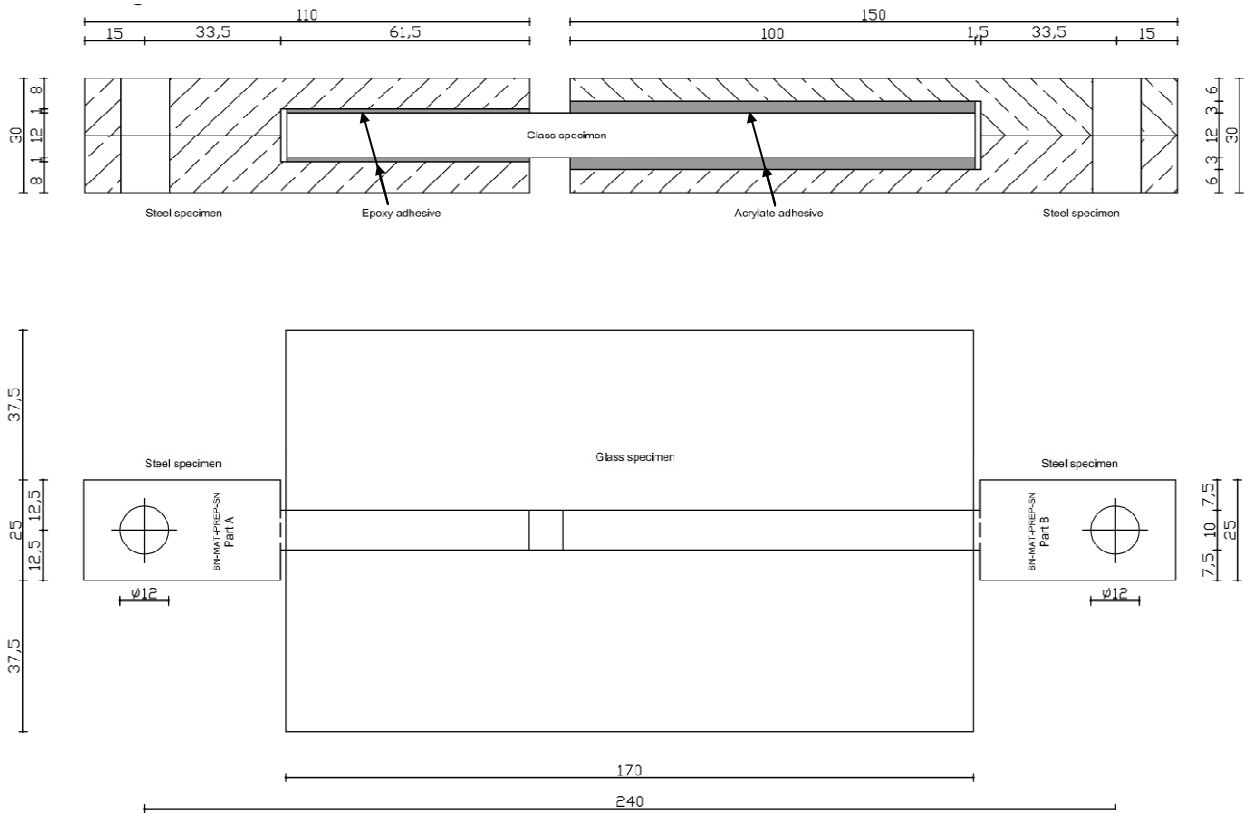


Figure A.13 Proposition of new uni-axial shear tests for further research.

Appendix B Supplementary data for the experiment

B.1 Dimensions of the steel frame

This appendix presents the parts of the system which are described in chapter 4. These parts are similar to those in the research of [Huveners 2009].

Table B1 Specification of the steel parts in the system.

Steel grade	S235
Bolt grade	10.9
H7	Diameter hole is 0.1 mm larger than the nominal diameter
h7	Diameter hole is 0.1 mm smaller than the nominal diameter
ZGB 30X36X30-W(INA)	Type of the applied sleeve-bearing bush used in the top and bottom transom with an internal diameter of 30 mm and an external diameter of 36 mm.

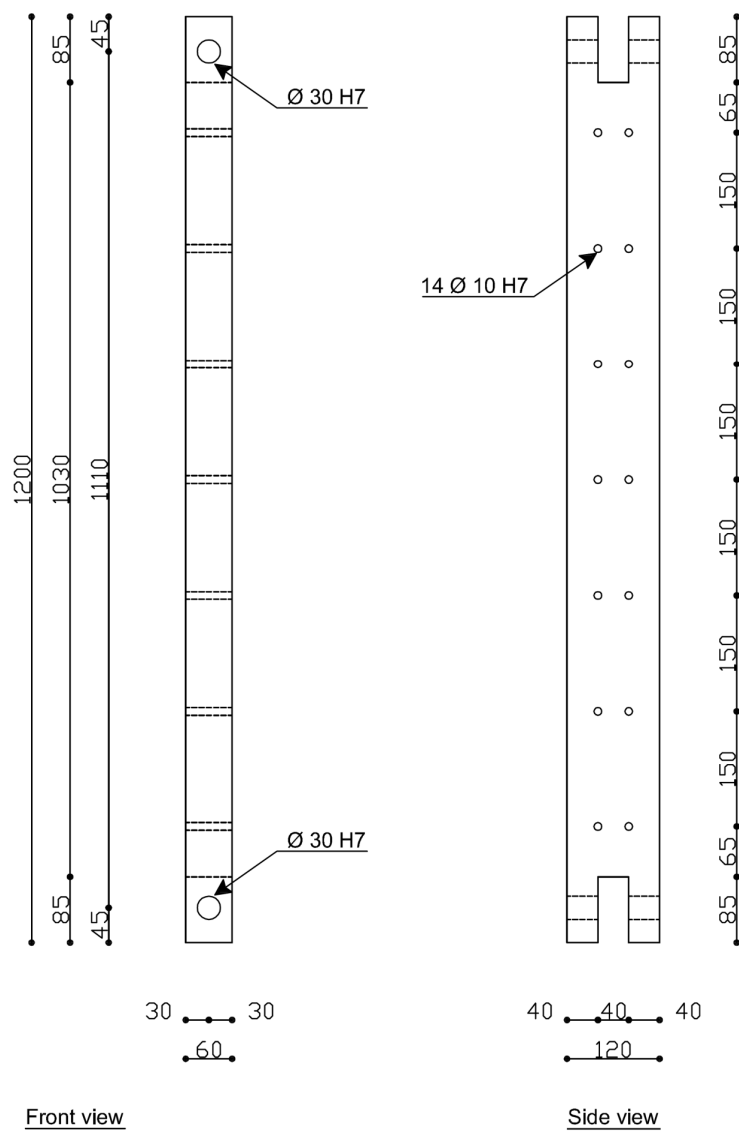
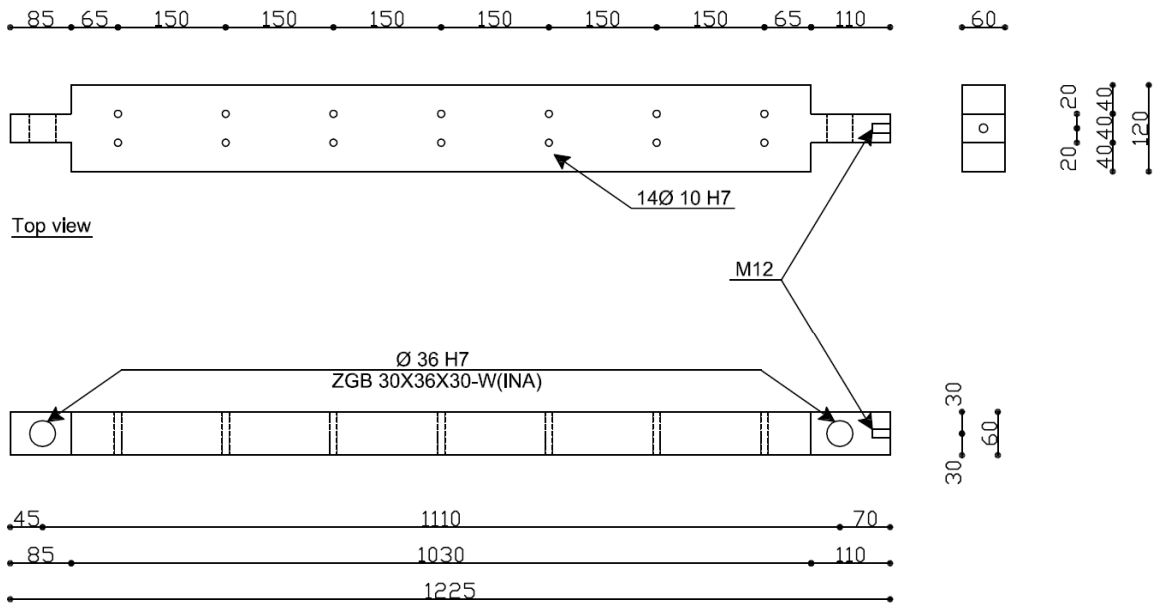


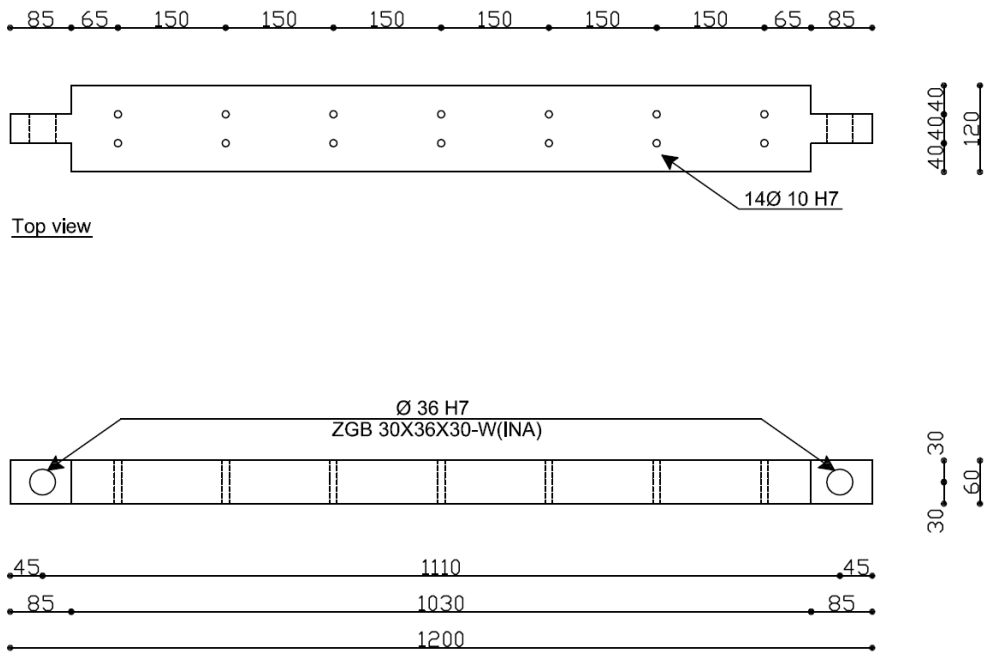
Figure B.1 Outside beam of the left and right mullion.



Top view

Front view

Figure B.2 Outside beam of the top transom.



Top view

Front view

Figure B.3 Outside beam of the bottom transom.

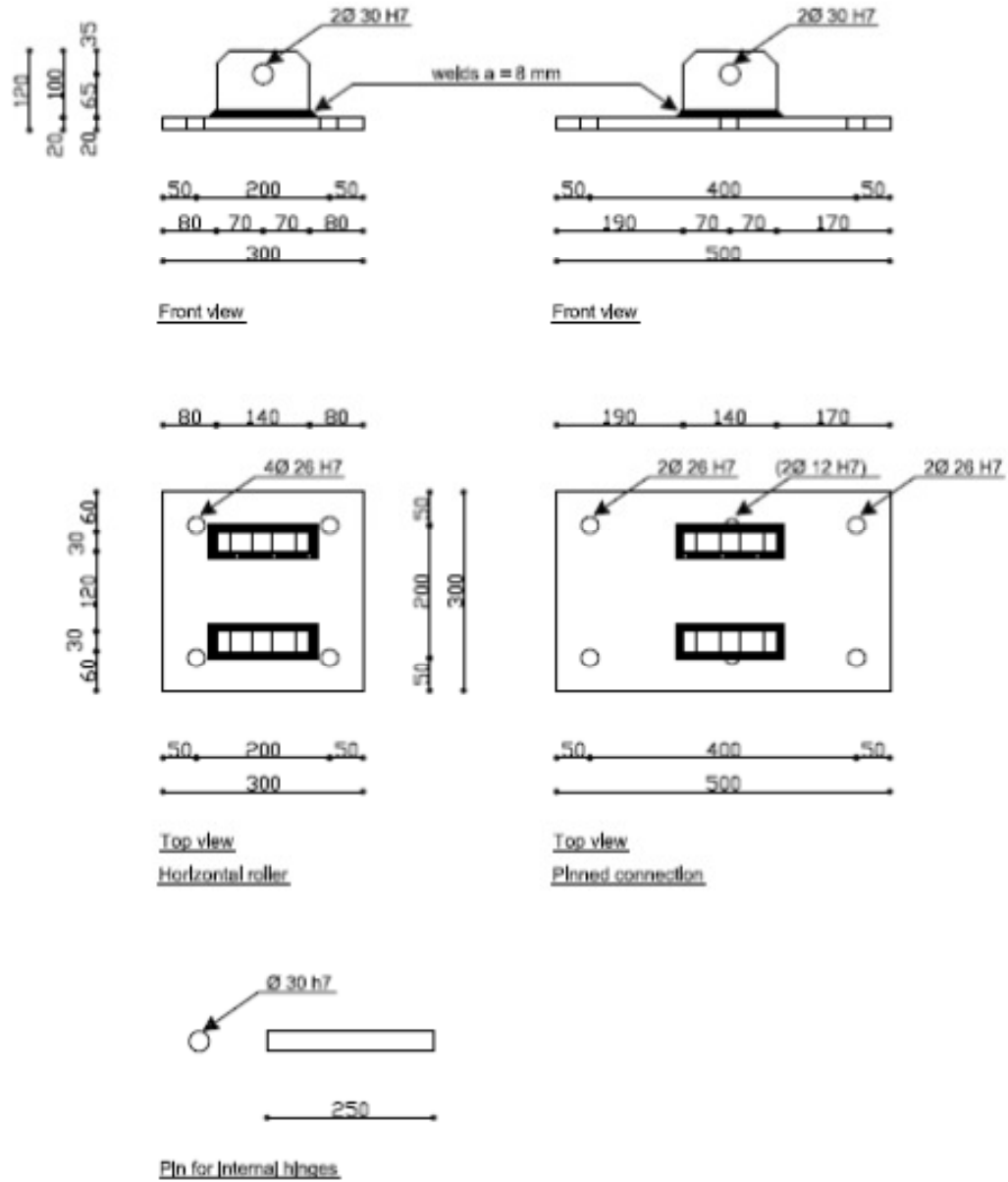


Figure B.4 Horizontal roller, pinned connection and the pin for the internal hinges.

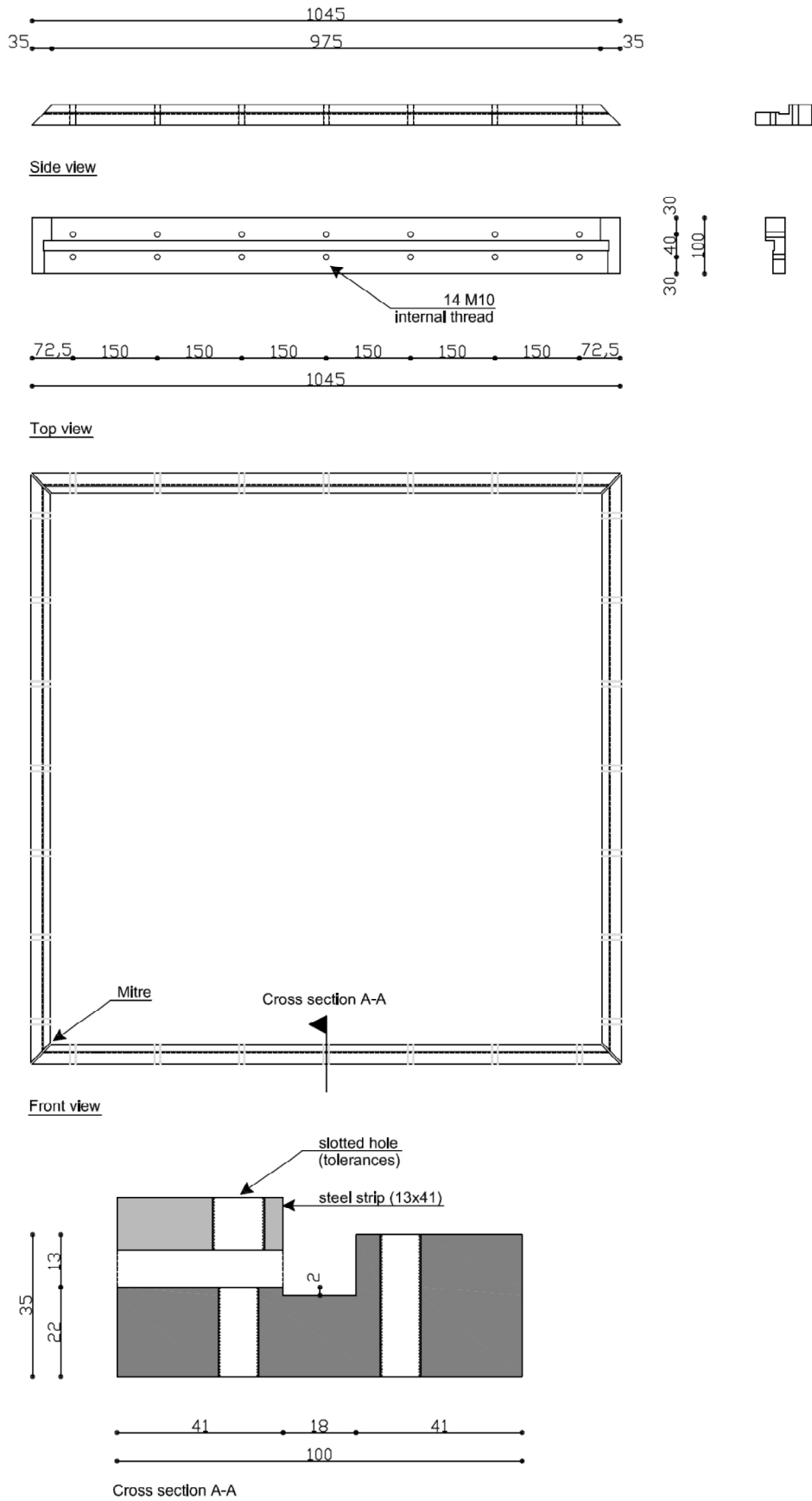


Figure B.5 Dimensions of the beadwork.

B.2 High-speed camera

To locate the point where failure of the glass pane exactly is introduced, a high speed camera is used during the experiments. The Redlake Motion Pro X3 high speed camera recorded 4000 images per second to catch the crack initiation and dispersion in the glass pane. The quality of the images was 100 x 100 dpi, enough to detect the crack behavior. Approximately four images are sufficient to follow the crack initiation and dispersion through the glass pane. At the moment when the observer of the glass pane heard a crack in the glass pane, a button was pressed. To capture the crack initiation and dispersion human audition and reaction time has to be considered. Each test took approximate 45 minutes and therefore the camera overwrote the old image of one second ago by a new image. After the button is triggered, the overwriting stops and 0.7 second (3000 images) before triggering and 0.3 second (1000 images) after triggering are saved. These images were saved on the computer. In one test maximum four seconds could be stored on the computer. These four seconds were split into four times one second, so the observer had four opportunities to capture cracks, based on audible and visible cracking of the glass pane.

B.3 Actual geometry of the glass pane

The actual geometry in terms of height, width and thickness of the glass panes according to figure 4.4 in section 4.4.1 are given in tables B.2 and B.3.

Table B.2 Glass pane thickness measurement (accuracy 0.05 mm).

Test	$t_{g;1}$	$t_{g;2}$	$t_{g;3}$	$t_{g;4}$	$t_{g;5}$	$t_{g;6}$	$t_{g;7}$	$t_{g;8}$	Average
ANG 1	12.10	12.10	12.10	12.05	12.00	12.05	12.05	12.05	12.06
ANG 2	12.10	12.05	12.10	12.05	12.05	12.10	12.05	12.05	12.07
ANG 3	12.05	12.05	12.05	12.05	12.10	12.05	12.05	12.05	12.06
HSG 1	11.90	11.90	11.90	11.90	11.95	11.95	11.90	11.90	11.91
HSG 2	11.91	11.91	11.93	11.92	11.92	11.88	11.92	11.92	11.91
HSG 3	11.91	11.90	11.91	11.91	11.91	11.91	11.90	11.91	11.91
ANG I+O	12.15	12.15	12.15	12.11	12.10	12.11	12.12	12.09	12.12
HSG I+O	11.90	11.91	11.91	11.91	11.92	11.91	11.90	11.91	11.91

Table B.3 Glass pane width and height measurement (accuracy 1.00 mm).

Test	$w_{g;1}$	$w_{g;2}$	$w_{g;1}$	$w_{g;2}$
ANG 1	1001	1000	1001	1000
ANG 2	1001	1001	1000	1000
ANG 3	1001	1001	1001	1000
HSG 1	1000	1001	1001	1000
HSG 2	1000	1000	1000	1000
HSG 3	1000	1001	1001	1000
ANG I+O	1000	1001	1001	1000
HSG I+O	1000	1000	1000	1000

The imperfections of the glass panes are measured using a measuring tool. The tool consisted out two supports on the left side and one support on the right, so the measurements could not be influenced by a rotated position of the measurement equipment in the middle (figure B.6). The distance between the supports was 200 mm. The out-of-plane imperfection per point is mapped with reference to the points on the left, right, below or above each point. The difference between to measurements gives a small change in distance (Δw). By adding, for example Δw of points 9 up to 11, the out-of-plane imperfection in the middle of the glass pane can be estimated. In table B.4 the measurement of each point is given. According to [Luible 2004] the maximum out-of-plane imperfection at the centre of the glass pane is the largest value of the length or the width of the glass pane divided by 2000. The initial out-of-plane imperfection never came close to 0.5 mm.

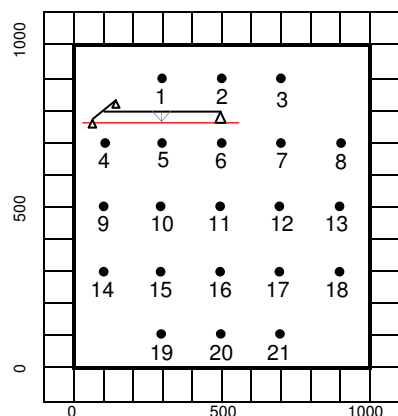


Figure B.6. Measurement- points and method for out-of-plane imperfections of glass panes.

Table B.4 Measurement of the glass pane curvature (accuracy 0.05 mm)

Point	ANG 1 In-plane	ANG 2 In-plane	ANG 3 In-plane	HSG 1 In-plane	HSG 2 In-plane	HSG 3 In-plane	ANG 1 In & out- of-plane	HSG 1 In & out- of-plane
1	-1,808	-1,753	-1,798	-1,693	-1,819	-1,848	-1,361	-1,160
2	-1,828	-1,789	-1,818	-1,698	-1,815	-1,838	-1,329	-1,069
3	-1,808	-1,775	-1,792	-1,721	-1,821	-1,848	-1,37	-1,135
4	-1,819	-1,890	-1,837	-1,818	-1,934	-1,829	-1,340	-1,218
5	-1,868	-1,804	-1,871	-1,819	-1,929	-1,838	-1,351	-1,249
6	-1,852	-1,789	-1,850	-1,819	-1,907	-1,832	-1,316	-1,250
7	-1,871	-1,774	-1,869	-1,810	-1,940	-1,821	-1,39	-1,211
8	-1,841	-1,770	-1,831	-1,803	-1,952	-1,801	-1,404	-1,208
9	-1,831	-1,722	-1,842	-1,810	-1,882	-1,811	-1,301	-1,191
10	-1,835	-1,726	-1,839	-1,797	-1,847	-1,786	-1,321	-1,179
11	-1,829	-1,747	-1,831	-1,754	-1,812	-1,747	-	-1,1996
12	-1,837	-1,766	-1,835	-1,799	-1,852	-1,766	-1,324	-1,204
13	-1,810	-1,816	-1,842	-1,773	-1,860	-1,816	-1,323	-1,216
14	-1,887	-1,821	-1,819	-1,897	-1,958	-1,821	-1,343	-1,318
15	-1,861	-1,778	-1,851	-1,863	-1,917	-1,798	-1,327	-1,262
16	-1,864	-1,846	-1,872	-1,853	-1,894	-1,816	-1,333	-1,263
17	-1,876	-1,826	-1,882	-1,837	-1,957	-1,826	-1,314	-1,311
18	-1,867	-1,807	-1,870	-1,840	-1,963	-1,807	-1,333	-1,279
19	-1,834	-1,838	-1,819	-1,734	-1,809	-1,858	-1,308	-1,204
20	-1,810	-1,829	-1,820	-1,669	-1,787	-1,859	-1,341	-1,147
21	-1,839	-1,863	-1,829	-1,751	-1,889	-1,853	-1,304	-1,118

B.4 Application of the adhesive and preparation of the experiment

In this section the preparation of the adhesive bonded joint according to joint type two is described. The encircled numbers in figure B.7. indicate the step order and are explained below.

Step 1

The first step consisted of burning of the biggest part of the adhesive from the groove and the strip of the beadwork. To remove small adhesive remainders an abrasive wheel was used which made the bonding area smooth. After the beadwork was assembled within the frame, the bonding area was cleaned with a clear cloth to remove dust and grease. The last part of step one consists of wiping the bonding area using a clean lint-free cloth or absorbent paper and sparingly moistened with the preparation agent recommended by the manufacturer (appendix A.10). According to the supplier, wiping the surface once was sufficient to increase adhesion. After this was done, touching the bonding area with greasy attributed e.g. fingers, was not permitted.

Step 2

The space between the groove of the top transom and the bottom transom consist of 15 mm + 980 mm + 15 mm and is equal to the left and right mullion. The length and width of the glass pane is 1000 mm. Small rubbery spacers with a cross section 18 mm x 7 mm and a length of 10 mm were placed on the groove at one third on each side of the bottom transom. The weight of the glass pane deforms the rubber spacers about 2 mm.

Step 3

A special made foam tape with a cross section of 18 mm x 5 mm was attached at the groove of the mullions and transoms except at the positioning of the two spacers.

Step 4

The glass pane, already prepared with strain gauges, was placed with suction cups into the test set-up, and the rubbery spacers were pushed in due the dead weight of the glass pane. The thickness of the spacers became 5 mm. The applied foam tape covered the edges of the glass pane and guaranteed the width of the adhesive bonded joint. The foam tape was easy to push in (by hand) and had no structural contribution to the in-plane stiffness of the frame. The rubbery spacers to carry the dead weight of the glass pane during the curing procedure of the adhesive were permanent, because removing could lead to damage of the glass pane.

Step 5

The thickness of the adhesive bonded joint on the back of the glass pane was guaranteed by pushing it against 3 mm thick spacers of Polyvinyl Chloride (PVC) or hardboard made from timber.

Step 6

The steel strips with slotted holes were set on the front of the glass pane against 3 mm thick spacers and bolted to the frame. This guaranteed the thickness of the adhesive bonded joint on the front of the glass pane. If the gaps on both sides of the glass pane were equally measured the spacers could be removed.

Step 7

After the handgun was prepared, the end of the nozzle was placed in front of the gap and straightforwardly but slowly filled the gap with the adhesive from corner to corner.

Step 8

Applying the adhesive with the handgun was not sufficient to create a smooth and tight bonded joint with a width of 10 mm. The gap was filled for almost 100% but to guarantee the bonded joint width, the adhesive was pushed in using a spatula. By doing so, any present air bubbles were pushed out. To create a smooth and tight bonded joint, the spatula was used to wipe off the surplus. The adhesive cured very fast and after 15 minutes in the ambient temperature of the laboratory it had already 80% of its strength.

After each test, the beadwork including the steel strip were dismantled and placed on a movable bench for cleaning. The preparation for the new test started with step 1 to 8.

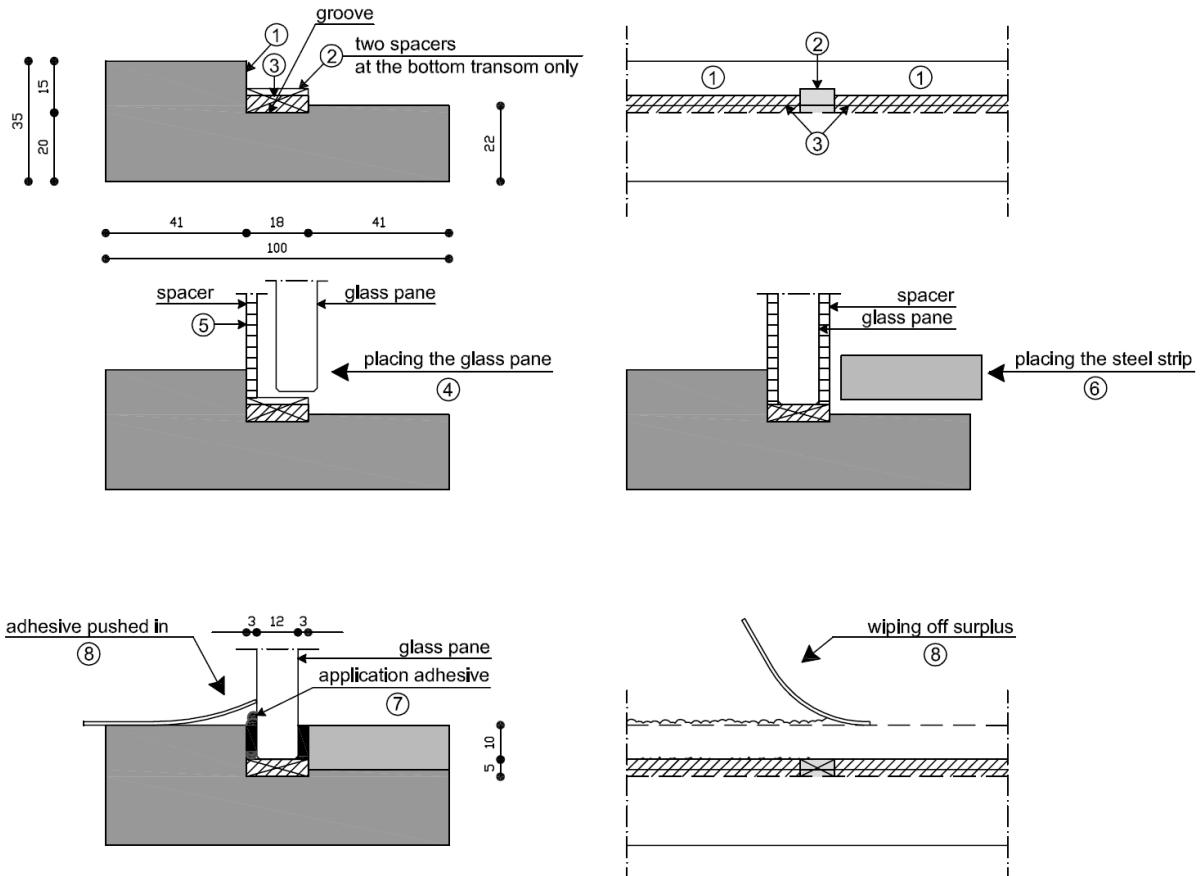


Figure B.7 Preparation of the adhesive bonded joint for joint type two in eight steps.

Table B.5 presents the time schedule for the preparation of the experiments. In order to avoid variations in strength properties of the adhesive bonded joint due to varying cure cycles, a fixed time schedule was adopted for preparation of the test. After the adhesive was applied, the bonded joint cured for three days.

Table B.5 Time schedule for preparation of each experiment

Day	Action
Tuesday	Removal of broken glass Dismantling the beadwork including the steel strip Burning of the adhesive
Wednesday	Cleaning the bonded joint surface with an abrasive wheel Assembly of the beadwork onto outside beam of the system
Thursday	Preparing strain gauges on the glass pane Geometry measurement of the glass pane Surface preparation (Appendix A1) Positioning of the glass pane into the frame Application of the adhesive
Friday	Undisturbed curing
Saturday	Undisturbed curing
Sunday	Undisturbed curing
Monday	Preparing the measuring equipment Full-scale experiment on the system.

B.5 Principles stresses in the glass pane

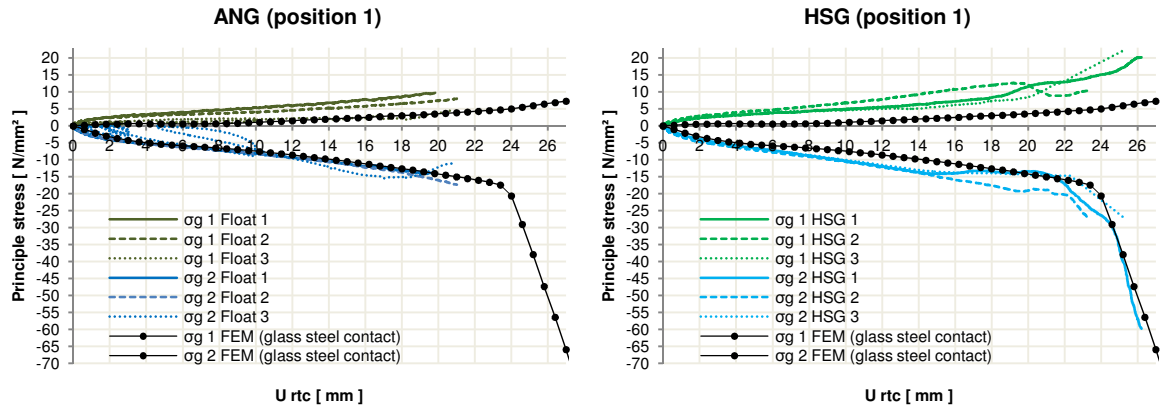


Figure B.8 (ANG left and HSG right) Comparison of the relation between the principle stress at position 1 and the horizontal in-plane displacement of the RTC of the FE simulation (black bolt dots) and the experiments (continuous, dashed and dotted green and blue lines).

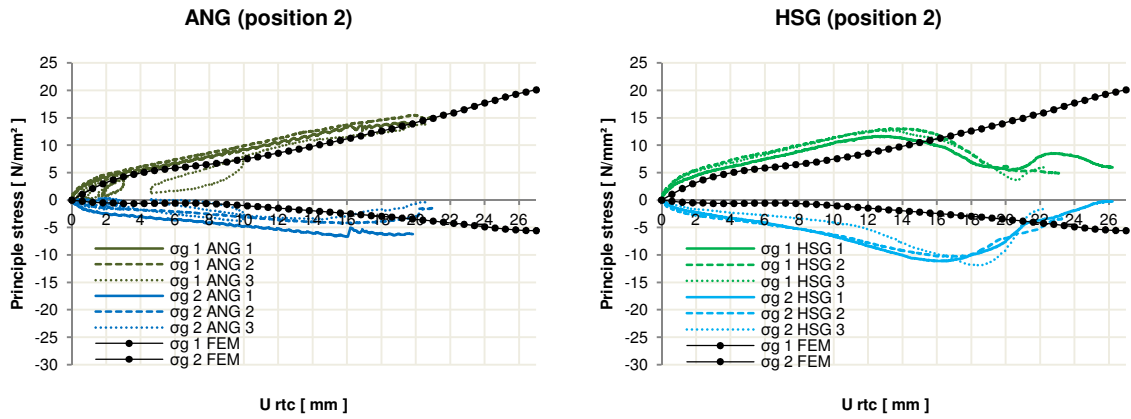


Figure B.9 (ANG left and HSG right) Comparison of the relation between the principle stress at position 2 and the horizontal in-plane displacement of the RTC of the FE simulation (black bolt dots) and the experiments (continuous, dashed and dotted green and blue lines).

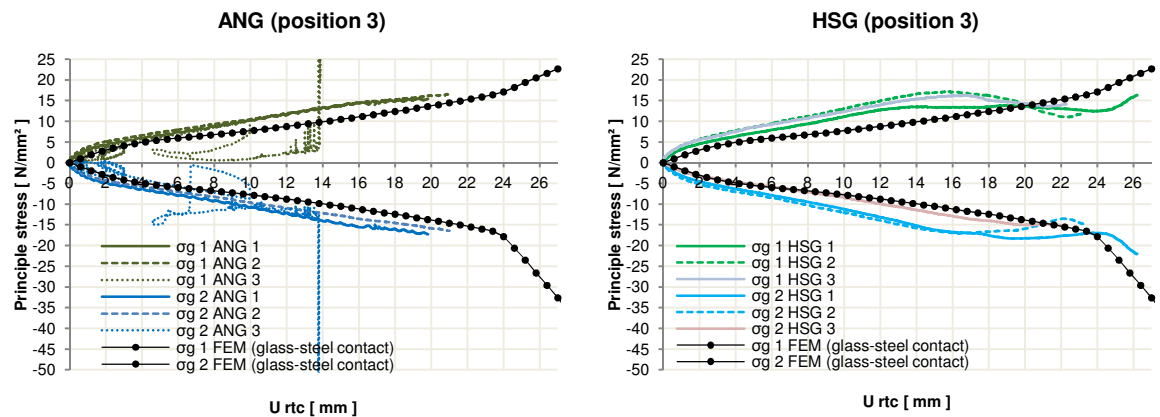


Figure B.10 (ANG left and HSG right) Comparison of the relation between the principle stress at position 3 and the horizontal in-plane displacement of the RTC of the FE simulation (black bolt dots) and the experiments (continuous, dashed and dotted green and blue lines).

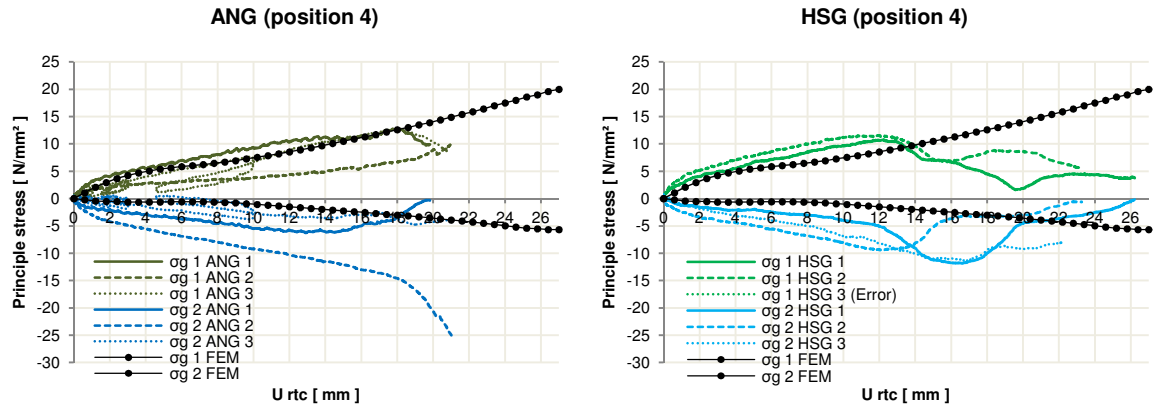


Figure B.11 (ANG left and HSG right) Comparison of the relation between the principle stress at position 4 and the horizontal in-plane displacement of the RTC of the FE simulation (black bolt dots) and the experiments (continuous, dashed and dotted green and blue lines).

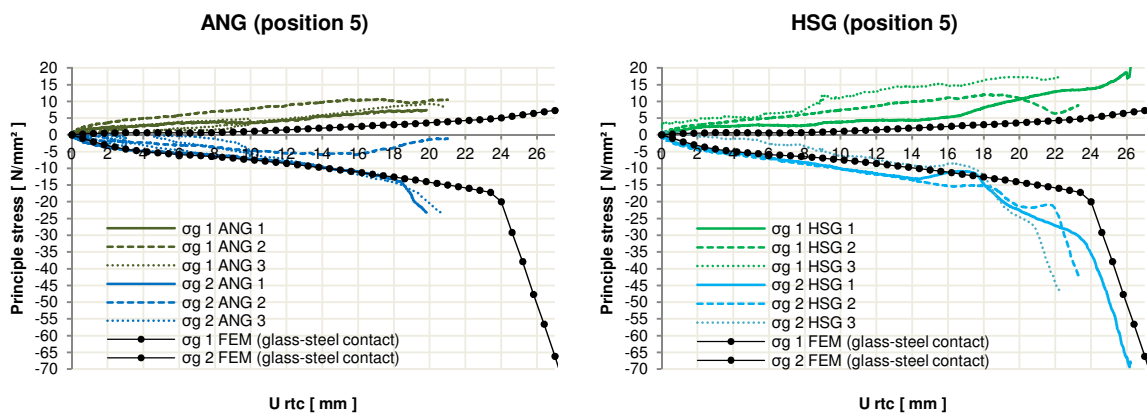


Figure B.12 (ANG left and HSG right) Comparison of the relation between the principle stress at position 5 and the horizontal in-plane displacement of the RTC of the FE simulation (black bolt dots) and the experiments (continuous, dashed and dotted green and blue lines).

Appendix C Example input iDiana

FEMGEN MODEL: GNLFNL-12MM-SIKA-1
 ANALYSIS TYPE: Structural 3D

'UNITS'
 LENGTH MM
 TIME SEC
 TEMPER KELVIN
 FORCE N

'COORDINATES'
 1 0.0000E+00 0.0000E+00 0.0000E+00
 2 5.0000E+00 0.0000E+00 0.0000E+00
 3 1.0000E+01 0.0000E+00 0.0000E+00

.....

 17744 1.0090E+03 1.0550E+03 3.0150E+00
 17745 1.0270E+03 1.0550E+03 3.0150E+00
 17746 1.0550E+03 1.0550E+03 3.0151E+00

'ELEMENTS'
 CONNECTIVITY
 1 L12BE 1 2
 2 L12BE 2 3
 3 L12BE 3 4

 367 L12BE 367 368
 368 L12BE 368 369
 369 L12BE 369 187
 370 CL12I 370 374 371 372 375 373
 371 CL12I 371 386 376 373 391 381
 372 CL12I 376 387 377 381 392 382

.....

 495 CL12I 865 876 866 870 881 871
 496 CL12I 866 877 867 871 882 872
 497 CL12I 867 884 629 872 885 883
 498 CQ40S 1 2 3 899 887 902 886 898
 499 CQ40S 3 4 5 900 888 903 887 899
 500 CQ40S 5 6 7 901 889 904 888 900

.....

 633 CQ40S 1271 1297 1282 1300 1285 1303 1272 1277
 634 CQ40S 1282 1298 1283 1301 1286 1304 1285 1300
 635 CQ40S 1283 1299 1284 1302 1287 1305 1286 1301
 636 CL12I 894 916 895 1306 1310 1307
 637 CL12I 895 917 896 1307 1311 1308
 638 CL12I 896 918 897 1308 1312 1309

.....

 679 CL12I 1272 1303 1285 1391 1396 1393
 680 CL12I 1285 1304 1286 1393 1397 1394

681	CL12I	1286 1305 1287 1394 1398 1395
682	CQ40S	1306 1310 1307 1408 1400 1411 1399 1407
683	CQ40S	1307 1311 1308 1409 1401 1412 1400 1408
684	CQ40S 1	308 1312 1309 1410 1402 1413 1401 1409
.....		
.....		
.....		
1113	CQ40S	2623 2649 2634 2652 2637 2655 2624 2629
1114	CQ40S	2634 2650 2635 2653 2638 2656 2637 2652
1115	CQ40S	2635 2651 2636 2654 2639 2657 2638 2653
1116	CL12I	2246 2268 2247 2658 2662 2659
1117	CL12I	2247 2269 2248 2659 2663 2660
1118	CL12I	2248 2270 2249 2660 2664 2661
.....		
.....		
.....		
1159	CL12I	2624 2655 2637 2743 2748 2745
1160	CL12I	2637 2656 2638 2745 2749 2746
1161	CL12I	2638 2657 2639 2746 2750 2747
1162	CQ40S	2658 2662 2659 2760 2752 2763 2751 2759
1163	CQ40S	2659 2663 2660 2761 2753 2764 2752 2760
1164	CQ40S	2660 2664 2661 2762 2754 2765 2753 2761
.....		
.....		
.....		
1581	CQ40S	3939 3965 3950 3968 3953 3971 3940 3945
1582	CQ40S	3950 3966 3951 3969 3954 3972 3953 3968
1583	CQ40S	3951 3967 3952 3970 3955 3973 3954 3969
1584	CL12I	3565 3586 3564 3974 3978 3975
1585	CL12I	3564 3585 3563 3975 3979 3976
1586	CL12I	3563 3584 3562 3976 3980 3977
.....		
.....		
.....		
1627	CL12I	3955 3973 3954 4061 4064 4062
1628	CL12I	3954 3972 3953 4062 4065 4063
1629	CL12I	3953 3971 3940 4063 4066 4059
1630	CQ40S	3977 3980 3976 4076 4068 4079 4067 4075
1631	CQ40S	3976 3979 3975 4077 4069 4080 4068 4076
1632	CQ40S	3975 3978 3974 4078 4070 4081 4069 4077
.....		
.....		
.....		
2061	CQ40S	5291 5317 5302 5320 5305 5323 5292 5297
2062	CQ40S	5302 5318 5303 5321 5306 5324 5305 5320
2063	CQ40S	5303 5319 5304 5322 5307 5325 5306 5321
2064	CL12I	4917 4938 4916 5326 5330 5327
2065	CL12I	4916 4937 4915 5327 5331 5328
2066	CL12I	4915 4936 4914 5328 5332 5329
.....		
.....		
.....		
2107	CL12I	5307 5325 5306 5413 5416 5414
2108	CL12I	5306 5324 5305 5414 5417 5415
2109	CL12I	5305 5323 5292 5415 5418 5411
2110	CQ40S	5329 5332 5328 5428 5420 5431 5419 5427
2111	CQ40S	5328 5331 5327 5429 5421 5432 5420 5428
2112	CQ40S	5327 5330 5326 5430 5422 5433 5421 5429
.....		
.....		

```

.....
2391 CQ40S      870 881 871 6219 6031 6041 6030 6218
2392 CQ40S      871 882 872 6220 6032 6042 6031 6219
2393 CQ40S      872 885 883 6221 6053 6055 6032 6220
2394 CQ48I      1617 1626 1623 1793 1792 1794 1788 1790 6222 6226 6223 6228
                6225 6229 6224 6227
2395 CQ48I      1623 1647 1632 1800 1795 1805 1792 1793 6223 6240 6230 6245
                6235 6250 6225 6228
2396 CQ48I      1632 1648 1633 1801 1796 1806 1795 1800 6230 6241 6231 6246
                6236 6251 6235 6245

.....
.....
.....
2647 CQ48I      6975 6990 6980 7004 7001 7003 7000 7002 3391 3394 3390 3392
                3229 3234 3230 3393
2648 CQ48I      7156 7161 7158 7162 7157 7160 7155 7159 6142 6155 6153 6154
                6054 6057 6037 6147
2649 CQ48I      7296 7306 7130 7145 7135 7313 7312 7314 3485 3487 3474 3479
                3369 3389 3386 3486
2650 CHX60      6222 6226 6223 6228 6225 6229 6224 6227 7466 7465 7467 7468
                372 375 373 7463 7462 7464 758 761
2651 CHX60      6223 6240 6230 6245 6235 6250 6225 6228 7465 7488 7490 7467
                373 391 381 7474 7469 7479 7462 7463
2652 CHX60      6230 6241 6231 6246 6236 6251 6235 6245 7488 7487 7491 7490
                381 392 382 7475 7470 7480 7469 7474

.....
.....
.....
4695 CHX60      13869 13920 13870 14069 738 748 737 14068 17691 17692 17745
                17744 7290 7300 7291 7305 7295 7310 7294 7304
4696 CHX60      13870 13921 13871 14070 739 749 738 14069 17692 17684 17741
                17745 7291 7301 7130 7306 7296 7311 7295 7305
4697 CHX60      13871 14007 605 627 625 756 739 14070 17684 17709 17746
                17741 7130 7145 7135 7313 7312 7314 7296 7306

```

MATERIALS

```

/ 2650-4697 / 1
/ 370-497 / 2
/ 2394-2517 2642-2645 / 3
/ 2518-2641 2646-2649 / 4
/ 1-92 94-369 498-635 682-1115 1162-1583 1630-2063 2110-2393 / 5
/ 636-681 1116-1161 1584-1629 2064-2109 / 6
/ 93 / 7

```

GEOMETRY

```

/ 370-497 / 1
/ 774-909 1254-1381 1722-1857 2202-2329 / 2
/ 910-977 1382-1445 1858-1925 2330-2393 / 3
/ 682-773 1162-1253 1630-1721 2110-2201 / 4
/ 636-681 1116-1161 1584-1629 2064-2109 / 5
/ 498-635 978-1115 1446-1583 1926-2063 / 6
/ 2-91 94-185 187-276 278-369 / 7
/ 1 186 / 9
/ 92 277 / 10
/ 93 / 8

```

'MATERIALS'

```

1 YOUNG 7.000000E+04
  POISON 2.300000E-01
2 DSTIF 10E-9 10E-9

```

```

3  DSTIF  13.53      4.51
   SIGDIS -13.53 -8.0 0.0 0.0 13.53 8.0
   TAUDIS -1E-6 -30 -1E-6 -11 -3 -9 -5 -7.5 -6.9 -6.5 -7 -6.25 -6.8 -6
      -6.5 -5.75 -6.1 -5.5 -5.7 -5.25 -5.34 -5 -5 -4.75 -4.66 -4.5
      -4.36 -4.25 -4.1 -4 -3.8 -3.75 -3.55 -3.5 -3.3 -3.25 -3.06 -3
      -2.82 -2.75 -2.6 -2.5 -2.4 -2.25 -2.2 -2 -2.06 -1.75 -1.93 -1.5
      -1.82 -1.25 -1.7 -1 -1.53 -0.75 -1.26 -0.5 -0.79 -0.25 0 0
      0.79 0.25 1.26 0.5 1.53 0.75 1.7 1 1.82 1.25 1.93 1.5 2.06 1.75
      2.2 2 2.4 2.25 2.6 2.5 2.82 2.75 3.06 3 3.3 3.25 3.55 3.5
      3.8 3.75 4.1 4 4.36 4.25 4.66 4.5 5 4.75 5.34 5 5.7 5.25 6.1 5.5
      6.5 5.75 6.8 6 7 6.25 6.9 6.5 5 7.5 3 9 1E-6 11 1E-6 30
4  DSTIF  13.53      4.51
   SIGDIS -13.53 -8.0 0.0 0.0 13.53 8.0
   TAUDIS -1E-6 -30 -1E-6 -11 -3 -9 -5 -7.5 -6.9 -6.5 -7 -6.25 -6.8 -6
      -6.5 -5.75 -6.1 -5.5 -5.7 -5.25 -5.34 -5 -5 -4.75 -4.66 -4.5
      -4.36 -4.25 -4.1 -4 -3.8 -3.75 -3.55 -3.5 -3.3 -3.25 -3.06 -3
      -2.82 -2.75 -2.6 -2.5 -2.4 -2.25 -2.2 -2 -2.06 -1.75 -1.93 -1.5
      -1.82 -1.25 -1.7 -1 -1.53 -0.75 -1.26 -0.5 -0.79 -0.25 0 0
      0.79 0.25 1.26 0.5 1.53 0.75 1.7 1 1.82 1.25 1.93 1.5 2.06 1.75
      2.2 2 2.4 2.25 2.6 2.5 2.82 2.75 3.06 3 3.3 3.25 3.55 3.5
      3.8 3.75 4.1 4 4.36 4.25 4.66 4.5 5 4.75 5.34 5 5.7 5.25 6.1 5.5
      6.5 5.75 6.8 6 7 6.25 6.9 6.5 5 7.5 3 9 1E-6 11 1E-6 30
5  YOUNG      2.100000E+05
   POISON     3.000000E-01
6  DSTIF      1.000000E+06  10
7  spring     2.73E+5

```

'GEOMETRY'

```

1  CONFIG     MEMBRA
   THICK      1.200000E+01
2  THICK      1.800000E+01
3  THICK      3.400000E+01
4  THICK      1.900000E+01
5  CONFIG     MEMBRA
   THICK      1.500000E+01
6  THICK      3.000000E+00
7  RECTAN     6.000000E+01  1.180000E+02
8  AXIS       0.000000E+00  1.000000E+00  0.000000E+00
9  RECTAN     60          180
   HINGE PHIZ1
10 RECTAN     60          180
   HINGE PHIZ2

```

'GROUPS'

ELEMEN

```
1  PANE       / 2650-4697 /
```

NODES

```
2  PANE_N     / 372 373 375 381-385 391-395 401-405 411-415 421-425
              431-435 441-445 451-455 461-465 471-475 481-485 491-495
              497 499 500 503 505-509 515-519 525-529 535-539 545-549
              555-559 565-569 575-579 585-589 595-599 605-609 615-619
              625 627 629 630 633 635-639 645-649 655-659 665-669
              675-679 685-689 695-699 705-709 715-719 725-729 735-739
              745-749 756 758 761 763-767 773-777 783-787 793-797
              803-807 813-817 823-827 833-837 843-847 853-857 863-867
              873-877 884 6222-17746 /
```

ELEMEN

```
3  GJB2       / 370-401 /
```

NODES

```
4  GJB2_N     / 370-499 /
```


ELEMEN
5 GJR2 / 402-433 /
NODES
6 GJR2_N / 497 500-628 /
ELEMEN
7 GJT2 / 434-465 /
NODES
8 GJT2_N / 625 629-757 /
ELEMEN
9 GJL2 / 466-497 /
NODES
10 GJL2_N / 372 629 758-885 /
ELEMEN
11 GJB3 / 2394-2425 /
NODES
12 GJB3_N / 1617 1623 1626 1632-1636 1647-1651 1657-1661 1672-1676
1682-1686 1697-1701 1707-1711 1722-1726 1732-1736
1747-1751 1757-1761 1772-1776 1778 1781 1788 1790
1792-1887 6222-6384 /
ELEMEN
13 GJR3 / 2426-2455 2643 2645 /
NODES
14 GJR3_N / 2968 2969 2973 2979-2983 2994-2998 3004-3008 3019-3023
3029-3033 3044-3048 3054-3058 3069-3073 3079-3083
3094-3098 3104-3108 3119-3123 3125 3128-3226 6359
6364 6374 6380-6534 6668 6682 6692-6694 /
ELEMEN
15 GJT3 / 2456-2487 /
NODES
16 GJT3_N / 4285 4291 4294 4300-4304 4315-4319 4325-4329 4340-4344
4350-4354 4365-4369 4375-4379 4390-4394 4400-4404
4415-4419 4425-4429 4440-4444 4446 4449 4456 4458
4460-4555 6514 6519 6529 6535-6694 /
ELEMEN
17 GJL3 / 2488-2517 2642 2644 /
NODES
18 GJL3_N / 5636 5637 5641 5647-5651 5662-5666 5672-5676 5687-5691
5697-5701 5712-5716 5722-5726 5737-5741 5747-5751
5762-5766 5772-5776 5787-5791 5793 5796-5894 6222-6229
6535-6542 6695-6841 /
ELEMEN
19 GJB1 / 2518-2549 /
NODES
20 GJB1_N / 1894 1900 1903 1909-1913 1924-1928 1934-1938 1949-1953
1959-1963 1974-1978 1984-1988 1999-2003 2009-2013
2024-2028 2034-2038 2049-2053 2055 2058 2065 2067
2069-2164 6842-7004 /
ELEMEN
21 GJR1 / 2550-2579 2647 2649 /
NODES
22 GJR1_N / 3229 3230 3234 3240-3244 3255-3259 3265-3269 3280-3284
3290-3294 3305-3309 3315-3319 3330-3334 3340-3344
3355-3359 3365-3369 3380-3384 3386 3389-3487 6975
6980 6990 7000-7154 7296 7306 7312-7314 /
ELEMEN
23 GJT1 / 2580-2611 /

NODES

24 GJT1_N / 4562 4568 4571 4577-4581 4592-4596 4602-4606 4617-4621
4627-4631 4642-4646 4652-4656 4667-4671 4677-4681
4692-4696 4702-4706 4717-4721 4723 4726 4733 4735
4737-4832 7130 7135 7145 7155-7314 /

ELEMEN

25 GJL1 / 2612-2641 2646 2648 /

NODES

26 GJL1_N / 5897 5898 5902 5908-5912 5923-5927 5933-5937 5948-5952
5958-5962 5973-5977 5983-5987 5998-6002 6008-6012
6023-6027 6033-6037 6048-6052 6054 6057-6155 6842-6849
7155-7162 7315-7461 /

ELEMEN

27 BOTTOM / 1-93 498-977 /

NODES

28 BOTTOM_N / 1-94 370 371 374 376-380 386-390 396-400 406-410
416-420 426-430 436-440 446-450 456-460 466-470
476-480 486-490 496 498 886-2237 /

ELEMEN

29 RIGHT / 94-185 978-1445 /

NODES

30 RIGHT_N / 93 95-186 501 502 504 510-514 520-524 530-534 540-544
550-554 560-564 570-574 580-584 590-594 600-604 610-614
620-624 626 628 2238-3553 /

ELEMEN

31 TOP / 186-277 1446-1925 /

NODES

32 TOP_N / 186-278 631 632 634 640-644 650-654 660-664 670-674
680-684 690-694 700-704 710-714 720-724 730-734 740-744
750-755 757 3554-4905 /

ELEMEN

33 LEFT / 278-369 1926-2393 /

NODES

34 LEFT_N / 1 187 279-369 759 760 762 768-772 778-782 788-792
798-802 808-812 818-822 828-832 838-842 848-852 858-862
868-872 878-883 885 4906-6221 /
35 TOPPANE / 6842-6845 6850 6855 6875 6880 6900 6905 6925 6930
6950 6955 6975 6980 7000 7001 7005 7010 7030 7035
7055 7060 7080 7085 7105 7110 7130 7135 7155-7158
7167 7172 7192 7197 7217 7222 7242 7247 7267 7272
7296 7312 7319 7324 7344 7349 7369 7374 7394 7399
7419 7424 14177 14277 14377 14477 14577 14782 14882
14982 15082 15182 15387 15487 15587 15687 15787 15992
16092 16192 16292 16392 16597 16697 16797 16897 16997 /

36 GROUP1 / 1 /

37 GROUP2 / 93 /

38 GROUP3 / 186 /

39 GROUP4 / 187 /

ELEMEN

40 GROUP5 / 1-93 370-401 498-977 2394-2425 2518-2549 2650-4697 /

NODES

41 GROUP5_N / 1-94 370-500 503 505-509 515-519 525-529 535-539
545-549 555-559 565-569 575-579 585-589 595-599
605-609 615-619 625 627 629 630 633 635-639 645-649
655-659 665-669 675-679 685-689 695-699 705-709
715-719 725-729 735-739 745-749 756 758 761 763-767
773-777 783-787 793-797 803-807 813-817 823-827
833-837 843-847 853-857 863-867 873-877 884 886-2237
6222-17746 /

ELEMEN

42 GROUP6 / 94-185 402-433 978-1445 2426-2455 2550-2579 2643 2645
2647 2649-4697 /

NODES

43 GROUP6_N / 93 95-186 372 373 375 381-385 391-395 401-405 411-415
421-425 431-435 441-445 451-455 461-465 471-475
481-485 491-495 497 499-630 633 635-639 645-649
655-659 665-669 675-679 685-689 695-699 705-709
715-719 725-729 735-739 745-749 756 758 761 763-767
773-777 783-787 793-797 803-807 813-817 823-827
833-837 843-847 853-857 863-867 873-877 884 2238-3553
6222-17746 /

ELEMEN

44 GROUP7 / 186-277 434-465 1446-1925 2456-2487 2580-2611 2650-4697 /

NODES

45 GROUP7_N / 186-278 372 373 375 381-385 391-395 401-405 411-415
421-425 431-435 441-445 451-455 461-465 471-475
481-485 491-495 497 499 500 503 505-509 515-519
525-529 535-539 545-549 555-559 565-569 575-579
585-589 595-599 605-609 615-619 625 627 629-758
761 763-767 773-777 783-787 793-797 803-807 813-817
823-827 833-837 843-847 853-857 863-867 873-877
884 3554-4905 6222-17746 /

ELEMEN

46 GROUP8 / 278-369 466-497 1926-2393 2488-2517 2612-2642 2644
2646 2648 2650-4697 /

NODES

47 GROUP8_N / 1 187 279-369 372 373 375 381-385 391-395 401-405
411-415 421-425 431-435 441-445 451-455 461-465
471-475 481-485 491-495 497 499 500 503 505-509
515-519 525-529 535-539 545-549 555-559 565-569
575-579 585-589 595-599 605-609 615-619 625 627
629 630 633 635-639 645-649 655-659 665-669 675-679
685-689 695-699 705-709 715-719 725-729 735-739
745-749 756 758-885 4906-17746 /

ELEMEN

48 GJ1 / 2518-2641 2646-2649 /

NODES

49 GJ1_N / 1894 1900 1903 1909-1913 1924-1928 1934-1938 1949-1953
1959-1963 1974-1978 1984-1988 1999-2003 2009-2013 2024-2028
2034-2038 2049-2053 2055 2058 2065 2067 2069-2164 3229 3230
3234 3240-3244 3255-3259 3265-3269 3280-3284 3290-3294
3305-3309 3315-3319 3330-3334 3340-3344 3355-3359 3365-3369
3380-3384 3386 3389-3487 4562 4568 4571 4577-4581 4592-4596
4602-4606 4617-4621 4627-4631 4642-4646 4652-4656 4667-4671
4677-4681 4692-4696 4702-4706 4717-4721 4723 4726 4733
4735 4737-4832 5897 5898 5902 5908-5912 5923-5927 5933-5937
5948-5952 5958-5962 5973-5977 5983-5987 5998-6002 6008-6012
6023-6027 6033-6037 6048-6052 6054 6057-6155 6842-7461 /

ELEMEN

50 GJ2 / 370-497 /

NODES

51 GJ2_N / 370-885 /

ELEMEN

52 GJ3 / 2394-2517 2642-2645 /

NODES

53 GJ3_N / 1617 1623 1626 1632-1636 1647-1651 1657-1661 1672-1676
 1682-1686 1697-1701 1707-1711 1722-1726 1732-1736 1747-1751
 1757-1761 1772-1776 1778 1781 1788 1790 1792-1887 2968 2969
 2973 2979-2983 2994-2998 3004-3008 3019-3023 3029-3033
 3044-3048 3054-3058 3069-3073 3079-3083 3094-3098 3104-3108
 3119-3123 3125 3128-3226 4285 4291 4294 4300-4304 4315-4319
 4325-4329 4340-4344 4350-4354 4365-4369 4375-4379 4390-4394
 4400-4404 4415-4419 4425-4429 4440-4444 4446 4449 4456
 4458 4460-4555 5636 5637 5641 5647-5651 5662-5666 5672-5676
 5687-5691 5697-5701 5712-5716 5722-5726 5737-5741 5747-5751
 5762-5766 5772-5776 5787-5791 5793 5796-5894 6222-6841 /

ELEMEN

54 LIJM / 2595 2596 2529 2538 2626 2627 2569 2560 2467 2476 2409 2410 2498
 2507 2440 2441 /

ELEMEN

55 POSITIE1 / 2711 2732 2851 2872 3735 3756 3875 3896 /

ELEMEN

56 POSITIE2 / 2811 2832 2951 2972 3835 3856 3975 3996 /

ELEMEN

57 POSITIE3 / 3081 3102 3221 3242 4105 4126 4245 4266 /

ELEMEN

58 POSITIE4 / 3351 3372 3491 3512 4375 4396 4515 4536 /

ELEMEN

59 POSITIE5 / 3451 3472 3591 3612 4475 4496 4615 4636 /

'SUPPORTS'

/ 93 94 186 / TR 1
 / 1 94 / TR 2
 / 1-2167 2238-3487 3554-4835 4906-6155 / TR 3

'LOADS'

CASE 1

DEFORM

186 TR 1 -0.300000E+02

'DIRECTIONS'

1 1.000000E+00 0.000000E+00 0.000000E+00
 2 0.000000E+00 1.000000E+00 0.000000E+00
 3 0.000000E+00 0.000000E+00 1.000000E+00

'END'